

Design of Inclined Loaded Drilled Shafts in High-Plasticity Clay Environment

Technical Report 0-6146-1

Conducted for

Texas Department of Transportation

P.O. Box 5080

Austin, Texas 78763

May 2011



The University of Texas at Arlington

URL: <http://tti.tamu.edu/documents/0-6146-1.pdf>

1. Report No. FHWA/TX-11/0-6146-1		2. Government Accession No.		3. Recipient's Catalog No.	
4. Title and Subtitle DESIGN OF INCLINED LOADED DRILLED SHAFTS IN HIGH-PLASTICITY CLAY ENVIRONMENT				5. Report Date November 2010 Published: May 2011	
				6. Performing Organization Code	
7. Author(s) Anand J. Puppala, Thornchaya Wejrungsikul, Richard S. Williammee, Thomas (Tom) Witherspoon, and Laureano Hoyos				8. Performing Organization Report No. Report 0-6146-1	
9. Performing Organization Name and Address Department of Civil Engineering The University of Texas at Arlington Arlington, Texas 76019				10. Work Unit No. (TRAIS)	
				11. Contract or Grant No. Project 0-6146	
12. Sponsoring Agency Name and Address Texas Department of Transportation Research and Technology Implementation Office P. O. Box 5080 Austin, Texas 78763-5080				13. Type of Report and Period Covered Technical Report: November 2008–August 2010	
				14. Sponsoring Agency Code	
15. Supplementary Notes Project performed in cooperation with the Texas Department of Transportation and the Federal Highway Administration. Project Title: Design of Short, Laterally Loaded Drilled Shafts in High Plasticity Clay URL: http://tti.tamu.edu/documents/0-6146-1.pdf					
16. Abstract Drilled shaft foundations are principally used to support many structures such as bridge piers, towers, buildings, transmission towers, and roadway cable barriers. This research focuses on the use of drilled shafts in the cable median barrier systems which play an important role in protecting people's lives due to cross-over collisions on highways. During December 2006 to February 2007, several failures of 3-cable median barrier (TL-3) were observed in Kaufman County near Dallas without any traffic-related vehicular impacts. Preliminary investigation of failures showed that failed drilled shafts were located in high plasticity clay. Causes of failures are attributed to cold temperature induced shrinkage in the cables that increased in the tension in them, soil saturation due to long periods of rainfall and small sizes of drilled shafts used. Various sizes of drilled shafts were established and constructed in an environment similar to the one in which foundation distress was observed. Geotechnical sampling and laboratory testing were performed, and a new test setup for the application of an inclined tensile loading on drilled shafts was designed to simulate the loading under real field conditions. The capacities of different sizes of drilled shafts from field test were tested and measured under this setup. Once good simulation was obtained, the models are used for various foundation dimensions and various undrained shear strengths of soils which, in turn, provided results that are used in the development of foundation design charts. Additionally, construction guidelines and recommendation for periodic maintenance are provided in this report.					
17. Key Word Drilled Shaft, Deep Foundation, High-Plasticity Clay, Cable Barriers, Lateral Load, Uplift, Inclined Load			18. Distribution Statement No restrictions. This document is available to the public through NTIS: National Technical Information Service Alexandria, Virginia 22312 http://www.ntis.gov		
19. Security Classif. (of this report) Unclassified		20. Security Classif. (of this page) Unclassified		21. No. of Pages 242	22. Price

DESIGN OF INCLINED LOADED DRILLED SHAFTS IN HIGH-PLASTICITY CLAY ENVIRONMENT

by

Anand J. Puppala, Ph.D., PE
Professor
The University of Texas at Arlington

Thornchaya Wejrungsikul, MECE, EIT
Graduate Research Assistant
The University of Texas at Arlington

Richard S. Williammee, MSCE, PE
Former Graduate Student
The University of Texas at Arlington

Thomas (Tom) Witherspoon, Ph.D., PE
Consulting Engineer

and

Laureano Hoyos, Ph.D., PE
Associate Professor
The University of Texas at Arlington

Project 0-6146
Report 0-6146-1

Project Title: Design of Short, Laterally Loaded Drilled Shafts in High-Plasticity Clay

Performed in cooperation with the
Texas Department of Transportation
and the
Federal Highway Administration

November 2010
Published: May 2011

The University of Texas at Arlington
Arlington, Texas 76019

DISCLAIMER

The contents of this report reflect the views of the authors/principal investigators who are responsible for the facts and the accuracy of the data presented herein. The contents do not necessarily reflect the views or policies of the Federal Highway Administration (FHWA) or the Texas Department of Transportation (TxDOT). This report does not constitute a standard, specification, or regulation.

The United States Government and the State of Texas do not endorse products or manufacturers. Trade or manufacturers' names appear here solely because they are considered essential to the object of this report.

ACKNOWLEDGMENTS

This study was supported by the Texas Department of Transportation (TxDOT) under Research Project No. 0-6146. The authors acknowledge the following individuals and companies:

- Dr. Nicasio Lozano, Project Director for his guidance and help.
- The local Texas vendors that participated in the construction and testing: Texas Shafts, McKinney Drilling of Ft. Worth, Auger Drilling, and Schutte Drilling for providing their services to this research project at no cost.
- Mr. Clayton Stephens for his enthusiasm and support during the construction phase.
- Mr. Joel Taylor and Mr. David Hall of S & W Foundations for their assistance during the construction and testing phases.

TABLE OF CONTENTS

LIST OF FIGURES	IX
LIST OF TABLES	XIII
EXECUTIVE SUMMARY	1
CHAPTER 1 INTRODUCTION.....	3
PROBLEM STATEMENT AND OBJECTIVES.....	4
CHAPTER 2 LITERATURE REVIEW.....	7
MEDIAN BARRIERS USED IN TEXAS.....	7
OVERVIEW OF VARIOUS FACTORS INFLUENCING THE FAILURES.....	9
<i>High Plasticity Clays</i>	<i>10</i>
<i>Temperature Effect</i>	<i>12</i>
UPLIFT CAPACITY OF DEEP FOUNDATIONS SUBJECTED TO INCLINED LOADS	15
UPLIFT CAPACITY OF DEEP FOUNDATIONS IN EXPANSIVE SOILS.....	17
LATERAL LOAD ANALYSIS METHODS	19
<i>Broms' Method</i>	<i>20</i>
<i>Equivalent Cantilever Method.....</i>	<i>23</i>
<i>Characteristic Load Method (CLM).....</i>	<i>24</i>
<i>p-y Method (Non-Linear Analysis)</i>	<i>29</i>
<i>Strain Wedge Model.....</i>	<i>31</i>
<i>Comparison of Lateral Load Analysis (Broms' Method and p-y Method)</i>	<i>33</i>
LATERAL LOAD TESTS ON DRILLED SHAFTS.....	35
<i>Conventional Load Test.....</i>	<i>36</i>
<i>Osterberg Load Cell Test.....</i>	<i>37</i>
<i>Statnamic Load Test.....</i>	<i>37</i>
SUMMARY	38
CHAPTER 3 SITE SELECTION AND LABORATORY STUDIES	39
SITE SELECTION	39
<i>Soil Sampling and Laboratory Testing.....</i>	<i>39</i>
<i>Soil Suction Measurement by Pressure Plate and Filter Paper Techniques</i>	<i>51</i>
SHEAR STRENGTH PARAMETER TESTS (DIRECT SHEAR AND UNCONSOLIDATED-UNDRAINED TEST).....	59
<i>Direct Shear Tests.....</i>	<i>60</i>
<i>Unconsolidated-Undrained or UU Triaxial Tests</i>	<i>61</i>
<i>Unsaturated Case</i>	<i>62</i>
<i>Saturated Case.....</i>	<i>67</i>
SUMMARY	71
CHAPTER 4 CONSTRUCTION OF DRILLED SHAFTS AND INCLINED LOAD TEST DESIGN.....	73
DESIGN OF FIELD TEST SETUP	73
<i>Design of Test and Reaction Shafts</i>	<i>73</i>
CONSTRUCTION TEST SETUP.....	78
<i>Construction Process.....</i>	<i>79</i>
<i>Field Quality Control Checks—Concrete.....</i>	<i>86</i>
FIELD TESTING AND DATA ACQUISITION	88
SUMMARY	92

CHAPTER 5 LOAD TESTS AND ANALYSIS OF TEST RESULTS	93
FAILURE OBSERVATIONS	93
DATA AND ANALYSIS.....	95
<i>Load Data</i>	95
<i>Hydraulic Load Gage</i>	96
LATERAL DISPLACEMENT DATA.....	97
<i>Inclinometer and MEMS-SAA Displacement Plots</i>	97
<i>MEMS-SAA Comparison Plots (Summer versus Winter)</i>	101
SUMMARY OF TEST RESULTS.....	103
CHAPTER 6 DESIGN/CONSTRUCTION GUIDELINES OF DRILLED SHAFTS	
IN HIGH PI CLAYS.....	107
ANALYSIS APPROACH	107
<i>Uplift Force Models</i>	108
<i>Finite Element Modeling (FEM Model)</i>	113
DEVELOPMENT OF DESIGN CHARTS	116
<i>Example Illustrating the Use of the Design Chart</i>	127
CONSTRUCTION GUIDELINE AND RECOMMENDATION	129
CHAPTER 7 SUMMARY AND CONCLUSIONS.....	131
REFERENCES.....	135
APPENDIX A: DESIGN AND CONSTRUCTION GUIDELINES FOR SHAFTS	
SUPPORTING TRAFFIC BARRIERS (PRODUCT 1)	143
APPENDIX B: DISTRICT SURVEY ANALYSIS.....	159
APPENDIX C: MANUFACTURER DESIGN PLAN SHEET	169
APPENDIX D: CONCRETE MIX DESIGNS.....	173
APPENDIX E: AS-BUILT DRAWING FOR LOAD TEST SETUP.....	177
APPENDIX F: LOAD CELL CALIBRATION REPORT	191
APPENDIX G: LATERAL LOAD TEST RESULTS.....	195
APPENDIX H: DETAIL OF RECOMMENDATION FOR CONCRETE PAD	
USED ON TOP OF DRILLED SHAFTS AT THE END OF CABLE	
BARRIER SYSTEMS	223

LIST OF FIGURES

Figure 1.1. Typical Foundation Failures of 3-Cable Median Barriers Built on Expansive Soils.....	4
Figure 2.1. Photos of Various Barriers Used in Texas and the US (Alberson 2006).	8
Figure 2.2. Connection Details of Cables to Drilled Shafts for the Gibraltar TL-3 Barrier System.....	8
Figure 2.3. Plasticity Chart for Indicating Minerals in Soil (Mitchell 1976; Holtz and Kovacs 1981).	11
Figure 2.4. Behavior of a Post in Frost Heaving (Penner and Burn 1970).	14
Figure 2.5. Forces of Anchors under Inclined Loads (Meyerhof 1973a; 1980).	15
Figure 2.6. Uplift Coefficients for a Rigid Rough Shaft (Meyerhof 1973a).	16
Figure 2.7. Results of $Q_{u(\alpha)}$ with Different Degree of Load Inclinations (α) and L/D (Ubanyionwu 1985).	17
Figure 2.8. Deep Foundation Movements in Expansive Soil.	18
Figure 2.9. Schematic for a Laterally Loaded Pile in a Cohesive Soil (Broms 1964).	22
Figure 2.10. Design Chart for Short Piles in Cohesive Soils (Broms 1964b).	23
Figure 2.11. Cantilever Idealization of Pile: (a) Fixed Head; (b) Pinned Head (Abendroth et al. 1989).	24
Figure 2.12. Deflection Curves of (a) Ground line Shear and (b) Ground line Moment for Clay (Duncan et al. 1994).	25
Figure 2.13. Load-Moment Curves (Duncan et al. 1994).	27
Figure 2.14. Parameters A_m and B_m (Matlock and Reese 1961).	28
Figure 2.15. Physical Model of a Deep Foundation under a Lateral Load.	30
Figure 2.16. Basic Strain Wedge in Uniform Soil (Ashour et al. 1998).	32
Figure 2.17. Linearized Deflection Pattern (Ashour et al. 1998).	32
Figure 2.18. Comparison of SW, LPILE, and Field Data for Free- and Fixed-Head Piles in Clays at the Sabine River (Ashour et al. 2002).	33
Figure 2.19. Comparison of Lateral Load Analysis in Stiff Clay.	34
Figure 2.20. Comparison of Lateral Load Analysis in Soft Clay.	35
Figure 2.21. Comparison of Lateral Load Analysis in Cohesionless Soil.	35
Figure 2.22. Test Setup for a Conventional Load Test.	36
Figure 2.23. Osterberg Load Cell for the Lateral Load Test.	37
Figure 2.24. Test Setup for a Statnamic Test.	38
Figure 3.1. Test Site Located on IH 20 and Rose Hill Road.	39
Figure 3.2. Soil Sampling and Density Measurement by Using Nuclear Gauge.	40
Figure 3.3. Typical Standard Compaction Curve.	41
Figure 3.4. Standard Compaction Curve and Point of Field Density of Layer 2.	42
Figure 3.5. Standard Proctor Compaction Curve and Point of Field Density of Layer 3.	42
Figure 3.6. Three-Dimensional Swell Test.	44
Figure 3.7. Vertical Swell Strain Results for Soil Layer 2 at Three Different Moisture Contents and Field Density Conditions.	45
Figure 3.8. Radial Swell Strain Results for Soil Layer 2 at Three Different Moisture Contents and Field Density Conditions.	45
Figure 3.9. Volumetric Swell Strain Results for Soil Layer 2 at Three Different Moisture Contents and Field Density Conditions.	46

Figure 3.10. Vertical Swell Strain Results for Soil Layer 3 at Three Different Moisture Contents and Field Density Conditions.	46
Figure 3.11. Radial Swell Strain Results for Soil Layer 3 at Three Different Moisture Contents and Field Density Conditions.	47
Figure 3.12. Volumetric Swell Strain Results for Soil Layer 3 at Three Different Moisture Contents and Field Density Conditions.	47
Figure 3.13. Schematic Drawing of Pressure Plate Apparatus (Soil-Moisture Equipment Corp. 2003).	52
Figure 3.14. Contact and Noncontact Filter Paper Methods for Measuring Matric and Total Suction, Respectively (Al-Khafaf and Hanks 1974).	53
Figure 3.15. Weighing Balance Used in Measuring the Weight of the Filter Papers.	53
Figure 3.16. Calibration Suction-Water Content Curves for Filter Papers.	54
Figure 3.17. Pressure Plate Testing.	56
Figure 3.18. Filter Paper Testing.	56
Figure 3.19. SWCC for Soil in Layer 1.	57
Figure 3.20. SWCC for Soil in Layer 2.	57
Figure 3.21. SWCC for Soil in Layer 3.	58
Figure 3.22. SWCC for Soil in Layer 4.	58
Figure 3.23. SWCC for Soil in Layer 5.	59
Figure 3.24. The Direct Shear Test Setup and Compacted Silty Sand Used in the Test.	60
Figure 3.25. Shear Strength versus Effective Normal Stress for the Silty Sand.	60
Figure 3.26. Shear Stress versus Horizontal Displacement for the Silty Sand.	61
Figure 3.27. The Failed Specimen Performed by Triaxial Test.	62
Figure 3.28. Mohr's Circle at Failure for 10, 25, and 40 Psi Confining Pressure of Soil Layer 2.	62
Figure 3.29. Triaxial Plot for 10, 25, and 40 Psi Confining Pressure of Soil Layer 2.	63
Figure 3.30. Mohr's Circle at Failure for 10, 25, and 40 Psi Confining Pressure of Soil Layer 3.	63
Figure 3.31. Triaxial Plot for 10, 25, and 40 Psi Confining Pressure of Soil Layer 3.	64
Figure 3.32. Mohr's Circle at Failure for 10, 25, and 40 Psi Confining Pressure of Soil Layer 4.	64
Figure 3.33. Triaxial Plot for 10, 25, and 40 Psi Confining Pressure of Soil Layer 4.	65
Figure 3.34. Mohr's Circle at Failure for 10, 25, and 40 Psi Confining Pressure of Soil Layer 5.	65
Figure 3.35. Triaxial Plot for 10, 25, and 40 Psi Confining Pressure of Soil Layer 5.	66
Figure 3.36. Mohr's Circle at Failure for 10, 25, and 40 Psi Confining Pressure of Soil Layer 2 in Saturated Case.	67
Figure 3.37. Triaxial Plot for 10, 25, and 40 Psi Confining Pressure of Soil Layer 2 in Saturated Case.	67
Figure 3.38. Mohr's Circle at Failure for 10, 25, and 40 Psi Confining Pressure of Soil Layer 3 in Saturated Case.	68
Figure 3.39. Triaxial Plot for 10, 25, and 40 Psi Confining Pressure of Soil Layer 3 in Saturated Case.	68
Figure 3.40. Mohr's Circle at Failure for 10, 25, and 40 Psi Confining Pressure of Soil Layer 4 in Saturated Case.	69

Figure 3.41. Triaxial Plot for 10, 25, and 40 Psi Confining Pressure of Soil Layer 4 in Saturated Case.....	69
Figure 3.42. Mohr's Circle at Failure for 10, 25, and 40 Psi Confining Pressure of Soil Layer 5 in Saturated Case.	70
Figure 3.43. Triaxial Plot for 10, 25, and 40 Psi Confining Pressure of Soil Layer 5 in Saturated Case.....	70
Figure 4.1. Plan View of Design Test Setups.....	73
Figure 4.2. Typical Plan Views of Test Setup.....	77
Figure 4.3. Typical Elevation Views of Test Setup.....	78
Figure 4.4. Plan View of As-Built Test Setups.....	79
Figure 4.5. Construction of the First Reaction Shaft Rebar Cage.....	79
Figure 4.6. Construction of a Test Shaft Rebar Cage.....	80
Figure 4.7. Construction of Casings.....	80
Figure 4.8. Drilling of Reaction Shaft Holes.....	81
Figure 4.9. Channel Steel Tied to Steel Rebar Cage.....	81
Figure 4.10. Setting the Steel Rebar Cages.....	82
Figure 4.11. Pouring Concrete and Final Shaft.....	83
Figure 4.12. Reaction Shaft Construction.....	83
Figure 4.13. Dywidag Construction.....	84
Figure 4.14. Sonotube Installations.....	84
Figure 4.15. Taking Initial Inclinometer Readings.....	85
Figure 4.16. Test Shaft Inclinometer Installation.....	85
Figure 4.17. Concrete Cylinder Specimens with Capping Compound.....	86
Figure 4.18. The 400 kip Tinius Olsen Tensile and Compression Machine Used for Testing.....	87
Figure 4.19. Compressive Strength Test Setup and Failed Concrete Specimen.....	88
Figure 4.20. MEMS Probe System.....	89
Figure 4.21. Dywidag System Parts.....	89
Figure 4.22. Dywidag Tensioning System.....	90
Figure 4.23. Dywidag Bar System.....	90
Figure 4.24. Hydraulic Piston Setup for Tensioning.....	90
Figure 4.25. Hydraulic Tensioning System.....	91
Figure 4.26. Test Shaft Loading.....	91
Figure 4.27. Collecting Inclinometer Readings.....	92
Figure 4.28. Collection of Inclinometer, MEMS Probe, and Elevation Survey Readings.....	92
Figure 5.1. General Test Shaft Failure.....	94
Figure 5.2. Field Adjustment to Eliminate Yielding Steel Channels.....	95
Figure 5.3. Comparisons between Measured and Actual Applied Loads.....	96
Figure 5.4. Actual Force Applied versus Time Period.....	97
Figure 5.5. Test Shaft (1 ft [0.3 m] Diameter × 6 ft [1.8 m] Depth) (Summer Condition).....	98
Figure 5.6. Test Shaft (1 ft [0.3 m] Diameter × 6 ft [1.8 m] Depth) Displacement Data.....	100
Figure 5.7. MEMS-SAA Plots for Summer and Winter Condition (Dry and Wet Season).....	101
Figure 5.8. Test Shaft Displacements in Summer Condition.....	102
Figure 5.9. Test Shaft Displacement in Winter Condition.....	103
Figure 5.10. Failures of Test Shafts from Inclined Loading Tests.....	105

Figure 6.1. Example of Comparison between Field Test Results and LPILE Model of the 2 ft (0.6 m) Diameter × 6 ft (3 m) Depth.	111
Figure 6.2. Comparisons between Ultimate Load of Field Results and Models (Deflection–0.5 in.).....	112
Figure 6.3. Model Developed in FEM Model.....	114
Figure 6.4. Stress in Shaft after Loading.	114
Figure 6.5. Stress in the Surrounding Soil after Loading.	115
Figure 6.6. Comparison among Field Test Result, FEM Model by ABAQUS Program and LPILE Model of the 2 ft (0.6 m) Diameter × 6 ft (3 m) Depth.....	116
Figure 6.7. Design Chart on Field Results for Finding the Appropriate Size of Drilled Shaft in the Cable Barrier Systems by Using 0.5 in. Lateral Deflection Criterion.	117
Figure 6.8. Design Chart Based on Field Results for Finding the Appropriate Size of Drilled Shaft in the Cable Barrier Systems by Using 1.0 in. Lateral Deflection Criterion.	118
Figure 6.9. Flow Chart for Choosing the Design Chart for Bottom Layer Consideration.	120
Figure 6.10. An Example of LPILE Results under Different Undrained Shear Strengths.	121
Figure 6.11. Flow Chart for Choosing the Design Chart for 1 Bottom Layer Consideration.	122
Figure 6.12. Design Chart A with 0.5 in. Deflection Criteria (δ).	122
Figure 6.13. Design Chart A with 1.0 in. Deflection Criteria (δ).	123
Figure 6.14. Design Chart B with 0.5 in. Deflection Criteria (δ).	123
Figure 6.15. Design Chart B with 1.0 in. Deflection Criteria (δ).	124
Figure 6.16. Design Chart C with 0.5 in. Deflection Criteria (δ).	124
Figure 6.17. Design Chart C with 1.0 in. Deflection Criteria (δ).	125
Figure 6.18. Design Chart D with 0.5 in. Deflection Criteria (δ).	125
Figure 6.19. Design Chart D with 1.0 in. Deflection Criteria (δ).	126
Figure 6.20. Example of Using the Design Chart.....	128
Figure 6.21. Details of Concrete Pad Placed on the Top of the Drilled Shaft at the End of Cable Barrier Systems.....	129

LIST OF TABLES

Table 2.1. Expansive Soils Identification (Wiseman et al. 1985).....	12
Table 2.2. Values of n_h for Cohesionless Soils, kip/ft ³ (kN/m ³) (after Terzaghi 1955).....	21
Table 2.3. Values of K_s for Cohesive Soils, kip/ft ³ (kN/m ³).	21
Table 2.4. Minimum Penetrations for Clay of Drilled Shafts for the Characteristic Load Method (Duncan et al. 1994).	29
Table 3.1. Basic Soil Properties.....	40
Table 3.2. Standard Proctor Compaction Test Results.	43
Table 3.3. Three-Dimensional Volumetric Swell Strain Test Results.....	48
Table 3.4. Volumetric Shrinkage Strain Results.....	50
Table 3.5. Swell Pressure Test Results.	51
Table 3.6. Direct Shear and Unconsolidated-Undrained Test Results for Unsaturated Cases.	66
Table 3.7. Unconsolidated-Undrained Test Results for Saturated Case.....	71
Table 4.1. Predicted Lateral Deflection of Drilled Shafts at the Ground Surface.	75
Table 4.2. Predicted Percent Differences in Lateral Movements of Reaction Shaft and Test Shaft.	75
Table 4.3. Compressive Strength Test Results.	88
Table 5.1. Examples of Maximum Lateral Movement in the Influence Zone Due to the Load Applied to the Shafts.	100
Table 5.2. Summary of Loads at Lateral Movements of 0.50 in., 0.75 in., and at Failure.	104
Table 6.1. Summary of Ultimate Uplift Results Compared with the Models.....	109
Table 6.2. Summary of Ultimate Lateral Results Compared with the Models at 0.5 in.....	112
Table 6.3. Calibration Factor at Different Lateral Deflection.	113
Table 6.4. Example of Undrained Shear Strength for Choosing the Design Chart.	127

EXECUTIVE SUMMARY

Drilled shaft foundations are principally used to support many structures such as bridge piers, towers, buildings, transmission towers, and roadway cable barriers. The main characteristics of drilled shafts are the ability of load transfer to the stronger layers in the vertical axis and ability of lateral movement resistance. This research focuses on the use of drilled shafts in the cable median barrier systems which play an important role in protecting people's lives due to cross-over collisions on highways.

Certain foundation problems were detected when drilled shafts are used to connect all the cables of the cable barrier systems. During December 2006 to February 2007, several failures of 3-cable median barrier (TL-3) were observed in Kaufman County near Dallas without any traffic-related vehicular impacts. Preliminary investigation of failures showed that failed drilled shafts were located in high plasticity clay. Causes of failures are attributed to cold temperature induced shrinkage in the cables that increased in the tension in them, soil saturation due to long periods of rainfall and smaller sizes of drilled shafts used. In order to mitigate these failures, a research study is performed to study the inclined load capacities of the drilled shafts and determine the sizes that work for the low temperature conditions in high PI clayey soil.

Various sizes of drilled shafts were chosen and constructed in a clayey soil environment similar to the one in which foundation distress was observed. Geotechnical sampling and laboratory testing were performed which showed different soil layer types including high plasticity clayey soil near the ground surface. Soil strength properties for unsaturated (field condition) and saturated conditions are determined and used in the analysis of field test results.

A new test setup for the application of an inclined tensile loading on drilled shafts was designed to simulate the loading under real field condition, which is different from the conventional load tests. The capacities of different sizes of drilled shafts from field test were tested and measured under this setup and load tests were conducted until the failure. Test results were validated with the uplift capacity and lateral capacity analyses models. Once good simulation was obtained, the models are used for various hypothetical foundation dimensions and various undrained shear strengths of soils which in turn provided results that are used in the development of foundation design charts. Additionally, construction guidelines and recommendation for periodic maintenance are provided.

CHAPTER 1

INTRODUCTION

Drilled shafts and piles are structural members placed in the ground and used to transfer loads from a structure to the foundation soil or resist lateral movements of structural objects. Drilled shafts are deep foundations where fluid concrete and steel rebar is placed in the drilled hole, whereas precast steel or concrete piles are mostly driven into the ground. In the construction process, drilled shafts can be constructed with or without casing or use slurry to protect the drilled hole walls from soil collapse which is dependent on the groundwater table and soil condition. Drilled shaft foundations were originally developed to support heavy buildings in many cities such as Chicago, Cleveland, Detroit, and London (O'Neill and Reese 1999). In Texas, the Department of Transportation (TxDOT) first used drill shafts in 1950 to build a bridge in the San Angelo District (McClelland 1996). Since then, drilled shafts have become one of the design alternatives of foundation systems used throughout the State to include the coastal areas of Texas (O'Neill and Reese 1999).

Drilled shafts have been used in many civil engineering applications such as foundations of high-rise buildings and bridge/retaining wall columns. The advantages of drilled shafts over pile foundations are outlined below, are proven, and have been used in design and construction for many years.

- Drilled shafts provide significantly less ground vibrations and damage to nearby structures.
- The bell-shaped tip of the drilled shaft can resist the uplift pressures.
- They have high resistance to both axial and lateral loads.
- They are economical by avoiding the usage of heavy pile caps.

Principally, lateral loads influence drilled shafts from earth pressures, current forces from flowing water, wind loads and wave forces in some unusual instances (O'Neil and Reese 1999). Examples of the structures where lateral forces have an effect on the drilled shafts are bridge abutments, offshore platforms, and transmission towers (Reese et al. 1977). Additionally, overhead-sign structures, high mast illumination systems, and median barriers are required to be supported on or by drilled shaft foundations.

In this study, the drilled shafts supporting ends of three-cable (3-cable) median barrier systems are considered for inclined load design. The loads taken into account are derived from the sustained pretension lateral load due to anchorage of the cables, thermal stresses in the cable

due to temperature fluctuations (expansion and contraction), and loads coming from vehicular impacts.

PROBLEM STATEMENT AND OBJECTIVES

The use of median cable barrier systems within the highway facilities are to eliminate or greatly mitigate cross-over collisions due to high traffic volumes, highway congestion, and driver error. TxDOT extensively used 3-cable type median barriers along many highways including one along Interstate Highway 20 (IH 20) and US Highways 80 and 175 (US 80 and US 175) in Kaufman County, Texas. Construction of these barriers was accomplished from July 2006 to February 2007. Figure 1.1 shows the failures of end foundation systems supporting a 3-cable barrier system constructed in an expansive soil area. The foundation failure is affecting the safety features of the barrier system.



IH 20 Westbound Sta. 903+00
Plan Sheet 45



IH 20 Westbound Sta. 973+44
Plan Sheet 61

TxDOT Control-Section-Job (CSJ): 0495-01-052

Figure 1.1. Typical Foundation Failures of 3-Cable Median Barriers Built on Expansive Soils.

The photos shown in Figure 1.1 demonstrate excessive lateral movements and uprooting of the foundations. A review of the causes of these failures yielded the following observations (Personal communication with Ms. Jan Heady, PE, TxDOT Dallas District):

- Kaufman County, where the drilled shaft foundation failures were recorded, had experienced low temperatures, including a few ice storms, from December 2006 to February 2007.
- Two of the median barrier systems in which each cable was connected to one 18 in. (0.46 m) diameter by 5 ft (1.5 m) deep drilled shaft.

- Cable barriers in which three cables were connected to one end drilled shaft has experienced the distress in the field as drilled shaft was uprooted from the original position.

Median barrier system failures are not acceptable due the potential liabilities incurred with any failure of these systems. It is imperative to understand the cause(s) of these inclined loaded drilled shaft failures—and design practical foundation systems in high PI clays to eliminate future failures. Therefore, to understand the possible causes of failures of the drilled shafts and methods to mitigate the failures, the following research objectives are developed:

- Investigate the mechanisms that cause failure of laterally loaded drilled shafts in highly plastic clay environments.
- Design and construct test drilled shafts with various dimensions and subject them to loading similar to the one that might have resulted in the existing failures shown in Figure 1.1 in the actual field environment.
- Develop a new or modified foundation design system based on the analyses of test results from the field load tests using both analytical and computational modeling of both the foundation and surrounding soil environment.
- Provide alternative design approaches including modification of soils at shallow depths (≥ 5 ft [1.5 m]) that will lead to no failures of the anchor shafts for the median barrier foundation systems.

This research report provides a comprehensive description of various issues related to the hypothetical failure mechanisms in traffic barrier systems listed above. The next few chapters describe the literature review, experimental program, field testing program, and analyses of results and development of design charts for new foundation systems.

CHAPTER 2 LITERATURE REVIEW

MEDIAN BARRIERS USED IN TEXAS

Cable barrier systems are used to prevent cross-over collisions by capturing and maintaining errant vehicles in their direction of travel. A cable barrier system requires appropriate clearance in the lateral direction as it will deflect when struck. This deflection will quickly and effectively reduce the impact forces transmitted to the vehicle occupants, greatly increasing their survival chances. The Texas Department of Transportation (TxDOT) provides a positive median barrier when the distance between the striped edge is 30 ft or less. Cable barrier systems cost \$70k + per mile compared to \$300k+ per mile for concrete traffic barriers. Hence, they have been increasingly used in a majority of the states (Alberson 2006). In general, there are six major types of barriers being used in the United States as given below and shown in Figure 2.1:

- U.S. Generic Low Tension.
- Safence.
- Gibraltar (Cable Barrier System).
- Brifen (Wire Rope Safety Fence-WRSF).
- Nucor Marion (U. S. High Tension).
- Trinity (Cable Safety System-CASS).

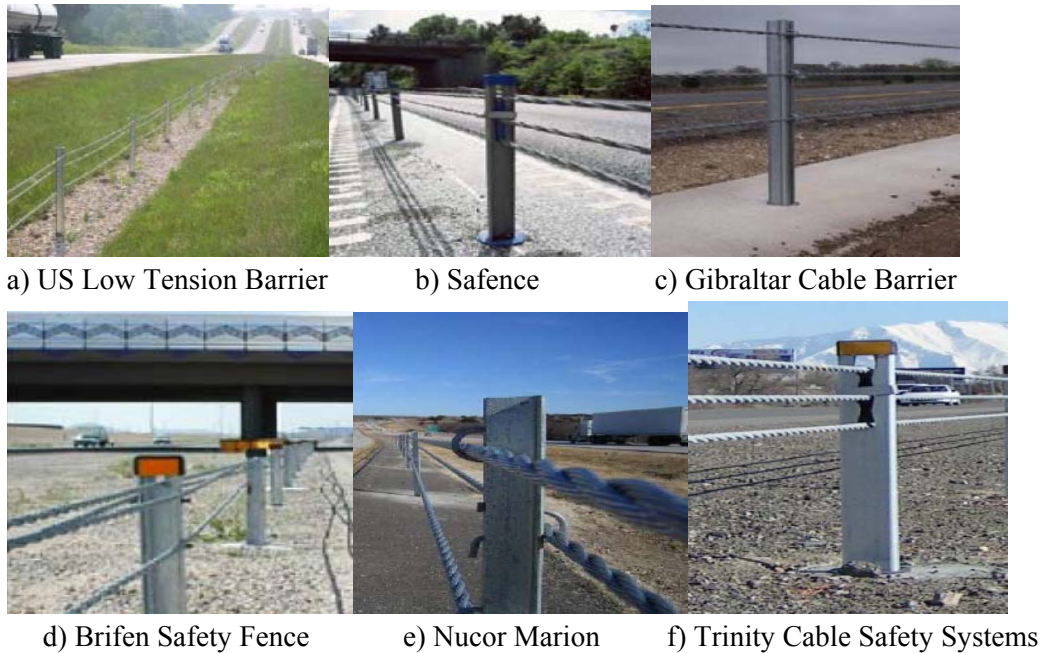


Figure 2.1. Photos of Various Barriers Used in Texas and the United States (Alberston 2006).

From the six typical systems shown in Figure 2.1, except for the first system (U.S. Low Tension), the other five systems are classified in the high-tension cable group. Each system has a unique post design, cable placement, and end treatment. All of these cable barrier system posts were founded on concrete drill shafts with sockets for ease of repair and maintenance. These barriers were installed for lengths of more than 600 miles (Alberston 2006).

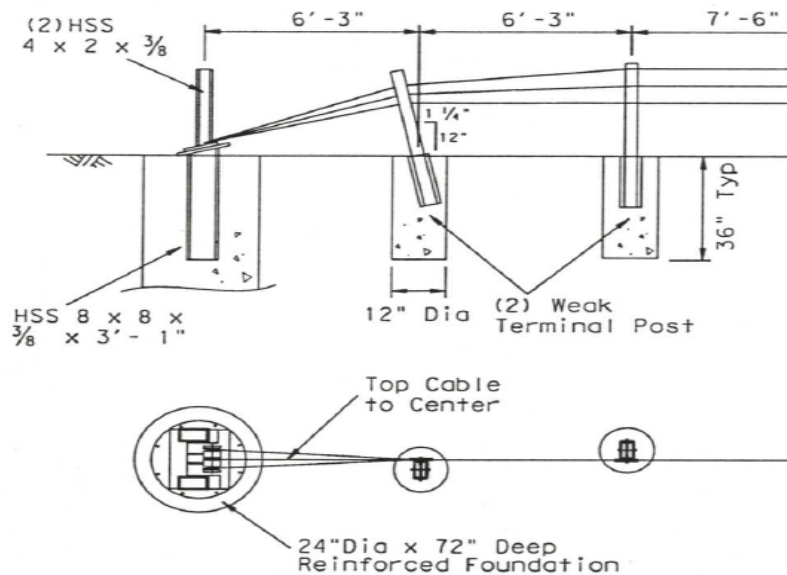


Figure 2.2. Connection Details of Cables to Drilled Shafts for the Gibraltar TL-3 Barrier System.

OVERVIEW OF VARIOUS FACTORS INFLUENCING THE FAILURES

Median barriers are used to prevent cross-over collisions due to high traffic volumes, highway congestion, and driver error (Albin et al. 2001). In the state of Texas, the two types of median barrier systems currently in use are concrete traffic and 3-cable. According to AASHTO's report on cable median barriers, these have been in use in 47 of the 50 U.S. states. (Albin et al. 2001). According to AASHTO's technology implementation group, the state of Texas has more than 600 miles of 3-cable median barriers and has invested approximately \$157 million on this technology.

With the heavy implementation of these systems across the state in a short amount of time, a vast majority of the installations have relied on the individual manufacturer recommendations. In light of the failures shown in Figure 1.1 in the previous chapter, end treatment designs have been adequate in all but a few of the installations. This project addresses the need for better engineering and design methods to account for all types of cable barrier systems in all soil types across the state.

Many or all of the systems use a drilled shaft for the end treatment to which the three cables are attached. This end treatment provides an anchor on each end of the median barrier runs against which the cables can be tightened to provide the manufacturers' tension requirements. Since drilled shafts are highly resistant against lateral loads in most soil types, drilled shaft foundations have become the primary foundation system for these cable barrier systems (TL-3 and TL-4 types). The drilled shaft foundations function satisfactorily in non-expansive soils; however, cable barrier systems have some foundation failure issues in expansive soils including drilled shaft concrete to soil loss of contact and foundation uprooting. Therefore, it is hypothesized that these failures are primarily due to a combination of several factors summarized below.

- Foundation soils, where the problems were observed, are high plasticity clays (predominantly CH type) exhibiting an expansive nature. Cyclic movements of the expansive soil also contributed to the lateral load on the drilled shafts. Due to these volumetric movements, the soil around the base of the foundation is softened with time due to moisture changes and lateral forces from the tensioned cables, and ultimately caused the foundation failures.

- Tension developed in the cables due to severe temperature changes observed during this period might have induced higher tensile stresses in the cables. These tensile stresses, along with high vehicular impact forces, would have added risk to the foundation failures.
- Another factor contributing to the failure of the foundation could be attributed to the cables connected to a single drilled shaft. Since all three cables were connected to a single drilled shaft, the amount of lateral pull might have exceeded the design value.
- A final possible reason for these failures could be the length of the drill shaft. As mentioned earlier, the drilled shafts were only 3–6 ft (0.91 m–1.83 m) deep, which is the depth for short shafts. The shorter length of these foundations could not develop sufficient frictional resistance required to withstand the amount of lateral pull generated as a result of the aforementioned factors.

In summary, the failures of the foundation drill shafts of the 3-cable median barrier systems are influenced by many factors including high plasticity clays, temperature, and length of the drilled shafts. These contributing factors are further discussed in the following sections.

High Plasticity Clays

One of the reasons for the failure of these drilled shafts subjected to lateral loading is the expansive and high plasticity nature of the clayey soils. According to the Unified Soil Classification System (USCS), particle size of fine-grained soil smaller than 0.002 mm is classified as clay. The cohesion and plasticity of clays are very significant in their engineering behavior. For this research project, the focus will be on expansive soils. Expansive soils exhibit swell-shrink characteristics due to moisture fluctuations and have been a problem to civil engineering infrastructures including roads and foundations from ancient times (Nelson and Miller 1992). In the United States, expansive soils are abundant in Texas, Colorado, Wyoming, and California (Chen 1988). Damage from the swell and shrink behavior of these soils costs about \$6 to \$11 billion per year (Nuhfer et al. 1993). One of the earlier National Science Foundation (NSF) studies reported that the damage to structures caused by expansive soils, particularly to light buildings and pavements, is more than any other natural disaster, including earthquakes and floods (Jones and Holtz 1973). Petry and Armstrong (1989) noted that it is always advisable to stabilize expansive clay soils during construction of a facility rather than

leaving the soils unstable which would need remediation at a future date. It is more economical to address the problem immediately rather than performing the remedial treatments later.

Many minerals combine naturally to form soils. The type or amount of clay minerals can significantly influence soil properties such as swelling, shrinkage, and plasticity. Examples of expansive clays include high plasticity index (high PI) clays, overconsolidated (OC) clays rich with montmorillonite and bentonite minerals, and shales. Soils containing significant quantities of the minerals such as bentonite, illite, and attapulgite are characterized by strong swell or shrinkage properties. Kaolinite is relatively non-expansive (Johnson and Stroman 1976). The heaving mineral montmorillonite has an expanding lattice and can undergo large amounts of swelling when hydrated. Soils rich with these minerals can be found in many places all over the world especially in the arid and semi-arid regions (Hussein 2001). In this research, North Texas is a semi-arid region. The plasticity index (PI) and liquid limit (LL) chart was developed to simplify the classification of the type of minerals in the soil as shown in Figure 2.3 (Mitchell 1976; Holtz and Kovacs 1981). However, this technique is not accurate enough to satisfactorily identify the soil minerals for this project because the soil can consist of many different clay minerals.

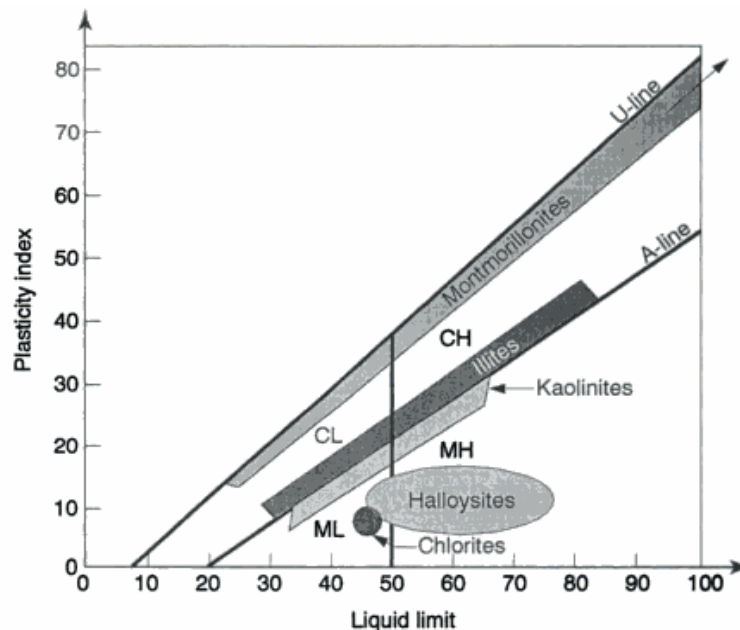


Figure 2.3. Plasticity Chart for Indicating Minerals in Soil (Mitchell 1976; Holtz and Kovacs 1981).

According to Wiseman et al. (1985), the following factors can be used to classify a soil as problematic or not:

- Soil type that exhibits considerable volume change with changes of moisture content.
- Climatic conditions such as extended wet or dry seasons.
- Changes in moisture content (climatic, man-made or vegetation).
- Light structures that are very sensitive to differential movement.

A summary of various methods for identifying the expansive nature of soils can be found in Puppala et al. (2004). Expansive soils can be identified by using the following plasticity-based index tests and the magnitudes of their test results are shown in Table 2.1.

Table 2.1. Expansive Soils Identification (Wiseman et al. 1985).

Index Test	Non-Problematic	Problematic
Plasticity Index	<20	>32
Shrinkage Limit	>13	<10
Free Swell (%)	<50	>100

Foundations to support the civil infrastructure often extend beyond the active depths of these clays. In Texas, active clay depths range from 2 ft (0.61 m) to 12 ft (3.66 m) or more, creating very problematic and expensive remediation.

Temperature Effect

In Texas, the temperature between summer and winter has varied from -13°F (-25°C) in winter to 120°F (45°C) in summer, considered to be a very wide range. As discussed before, failure of the drilled shafts of the 3-cable median barriers occurred during low winter temperatures. Low temperatures cause thermal stresses due to contraction in the steel cable and frost heave in the soil due to ice lens. Therefore, the difference in temperature between the low and high temperatures can have a measurable influence on the barrier systems' performance.

Cables

A change in temperature can cause material expansion or contraction. Temperature can significantly influence material properties such as yield strength and modulus of elasticity (Craig 1999). Generally, expansion or contraction of homogeneous materials is linearly related to temperature increase or decrease in all directions (Hibbeler 2008).

Thermal strain can be expressed as the following equation:

$$\epsilon_x = \epsilon_y = \epsilon_z = \alpha \Delta T \quad (1)$$

where $\epsilon_{x,y,z}$ = thermal strain.

α = coefficient of thermal expansion (COTE).

ΔT = is the change in temperature.

To find the elongation in the member, the following expression can be used:

$$\Delta T_{xT} = (\alpha \Delta T)L_x, \Delta T_{yT} = (\alpha \Delta T)L_y, \Delta T_{zT} = (\alpha \Delta T)L_z \quad (2)$$

where $\Delta T_{xT,yT,zT}$ = the elongation in the x, y, and z directions.

The coefficient of thermal expansion, α , is the thermal property of a material. It can be determined by measuring the change in dimensions of the material when applying a change in temperature. COTE is expressed in strain per degree of temperature unit. For instance, α in the U.S. customary unit is $1/^\circ\text{F}$ (the reciprocal of degree Fahrenheit), with α in 'SI' units as $1/^\circ\text{K}$ (the reciprocal of degree Kelvin) or $1/^\circ\text{C}$ (the reciprocal of degree Celsius). For determining the elongation of materials due to temperature decrease, the change in temperature (ΔT) in Eq. 2 is negative. The elongation is a function of the length of the cable that will be connected to the foundation. In the barrier systems, the lengths of two or three cables that are connected to the drilled shafts are practically close to each other and hence the length of the cable do not influence the failure of the foundation.

Soils

In soils, the temperature variation can cause fluctuations in moisture content of the soil. These moisture fluctuations can cause swell-shrink behavior if the given soil is expansive in nature. During summer (high temperatures), soil moisture evaporates, leading to shrinkage of the soil. In rainy season, the soil moisture increases, leading to swelling of these expansive soils. Studies on the effects of frost and heaving, which can cause damage to pavements and

foundations, have been conducted by many researchers such as Casagrande (1932), Kaplar (1970), Penner and Burn (1970), and Yong and Warkentin (1975). In the expansion of the volume of water when it freezes, there is about a 10 percent increase in volume. Damage from frost in the soil is due to the formation of ice lens, leading to frost heave. Originally, frost heave was considered when freezing of water in the soil occurred. However, the vertical displacement of the frost heaving phenomenon can be greater than the expansion that occurs when ice freezes. Day (2006) stated that there are many cases where damage or deterioration from the expansion of water is not evidently shown until the frost is melted; therefore, it might be very difficult to summarize damage or deterioration caused from frost heave. For foundations, Penner and Burn (1970) studied movements in the soil resulting from ice lens expansion. The results showed that when soil under a foundation freezes, soil expansion due to ice lens growth can be transmitted to the structure as shown in Figure 2.4; this process is called “adfreezing.” However, adfreeze strength studies could not provide the exact uplift values for all foundation materials such as concrete, wood, and steel in various soil types. In this research, the probability that frost heave occurred is very low because ice lens expansion needs to occur in very low temperatures for a long period which is atypical in the Dallas area.

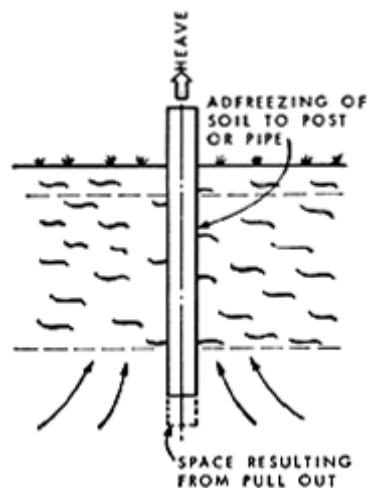


Figure 2.4. Behavior of a Post in Frost Heaving (Penner and Burn 1970).

UPLIFT CAPACITY OF DEEP FOUNDATIONS SUBJECTED TO INCLINED LOADS

The primary function of a deep foundation system is to transfer the axial and lateral loads to the foundation soil. Deep foundations, in particular drilled shafts or piers, are often used to support various structures including median barriers. In some cases, deep foundations are designed to resist uplift loads, such as foundations for transmission towers and high mast illumination poles in expansive soils. The uplift capacity of a shaft under vertical and inclined anchors was studied by Meyerhof (1973a,b; 1980). He presented the semi-empirical relationship to estimate the ultimate uplift capacity of rigid shafts in clay under inclined load as shown in Figure 2.5. The behavior of foundations under oblique loads depends, to a considerable extent, on the deformation characteristics of both the foundation and the soil. In addition, the failure mechanism becomes more complicated because of the foundation being unsymmetrical and three-dimensional in nature.

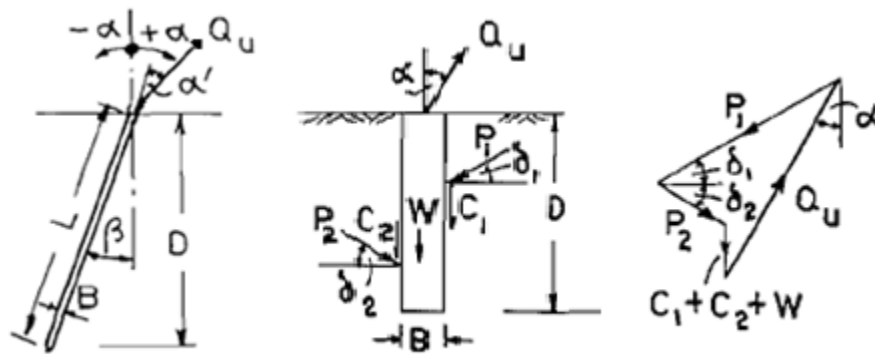


Figure 2.5. Forces of Anchors under Inclined Loads (Meyerhof 1973a; 1980).

From Figure 2.5 above, the ultimate load can be estimated from the force using the semi-empirical equation expressed as:

$$Q_u = \left(cK_c'D + \frac{\gamma D^2 K_b'}{2} \right) B + W \cos \alpha \quad (3)$$

where Q_u = the net ultimate capacity of the piles.

D = the depth.

K'_b = the uplift coefficient based on the angle of internal friction shown in Figure 2.6.

K'_c = the uplift coefficient given by $K'_c = 1 + 0.08 \frac{D}{B}$ with a maximum value of 3 for horizontal tension (Meyerhof and Adams 1968).

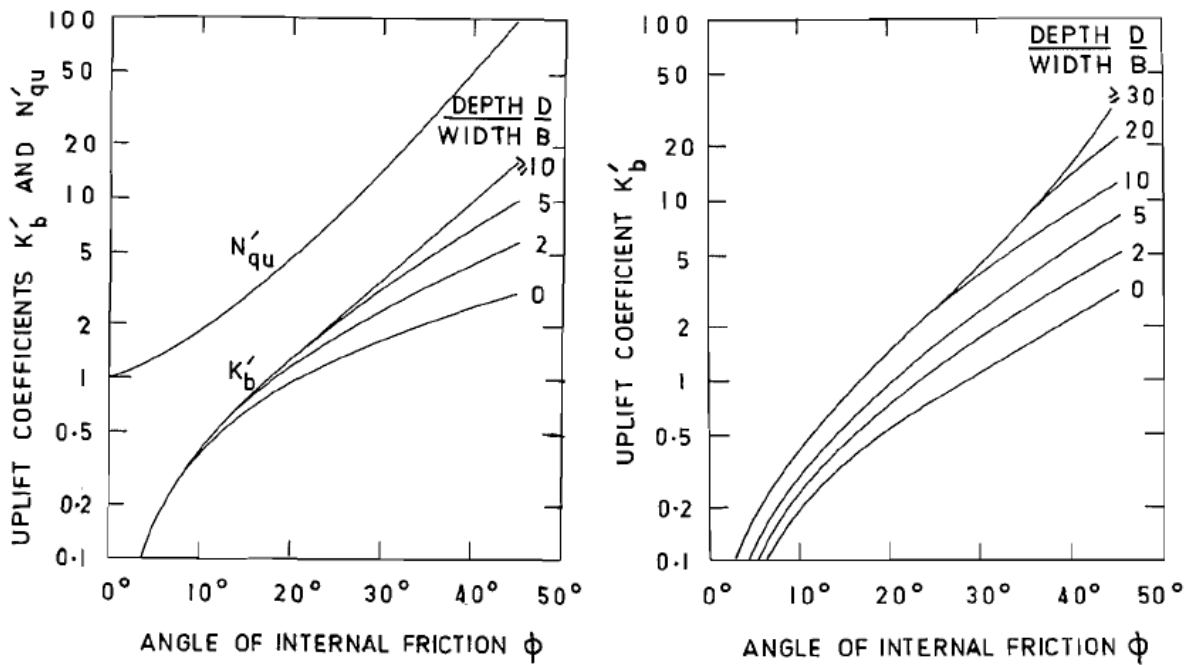
$K'_c = \pi$ in saturated clay ($\phi = 0^\circ$).

W = the weight of the shafts.

c = the cohesion force.

γ = the unit weight of the soil.

B = the width (diameter) of the shaft.



a) Vertical uplift coefficient

b) Horizontal uplift coefficient

Figure 2.6. Uplift Coefficients for a Rigid Rough Shaft (Meyerhof 1973a).

Meyerhof (1973a) developed the relation between vertical and horizontal pulling resistance, Q_v and Q_h , respectively, through a series of model tests. The expression for the ultimate bearing capacity (Q_u) due to an obliquely loaded tension is:

$$\left(\frac{Q_{u(\alpha)} \cos \alpha}{Q_v}\right) + \left(\frac{Q_{u(\alpha)} \sin \alpha}{Q_h}\right)^2 = 1 \quad (4)$$

where Q_h and Q_v are given by Eq. 4 with $\alpha = 90^\circ$ and $\alpha = 0^\circ$, respectively.

α = the angle of the inclined force with the horizontal axis ($^\circ$).

In 1985, Ubanyionwu compared his study with Meyerhof's equation by using a laboratory model test in which a 1 in. (25.4 mm) diameter pile was vertically installed in an 18 in. × 18 in. × 30 in. (457.2 mm × 457.2 mm × 762 mm) box compacted with clay. In these studies, the density of the compacted clay was maintained at 128.81 lb/ft³ (20.25 kN/m³) and the degree of saturation was equal to 97.9 percent, which was close to a 100 percent saturated soil. Also, the piles were pulled out at different angles (0°–90°). The result of these experiments provided good agreement with the semi-empirical equation developed by Meyerhof (1973a). Figure 2.7 compares the laboratory test data with the theoretical data.

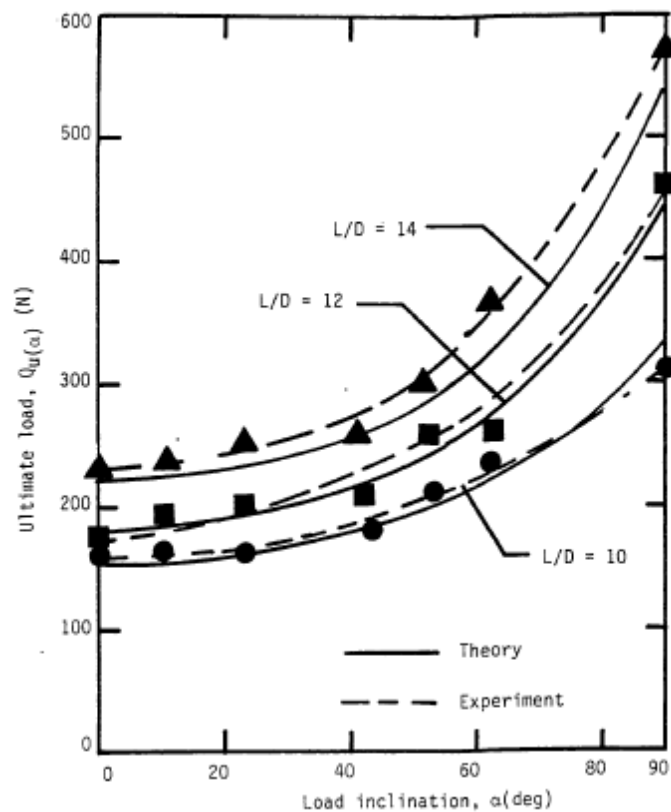


Figure 2.7. Results of $Q_{u(\alpha)}$ with Different Degree of Load Inclinations (α) and L/D (Ubanyionwu 1985).

UPLIFT CAPACITY OF DEEP FOUNDATIONS IN EXPANSIVE SOILS

Generally, capacity of piles or shafts is the combination of end bearing and skin friction resistance. However, design of deep foundations in expansive soil is different from design in non-expansive soil conditions. If these shafts are not designed and constructed effectively, the

damage from the horizontal and vertical soil expansion can be very high. When these movements are excessive, shafts can be uplifted as shown in Figure 2.8. The uplift of shafts occurs when the uplift force is greater from the swelling pressure of the soil than the resistance force of the shaft from the skin friction.

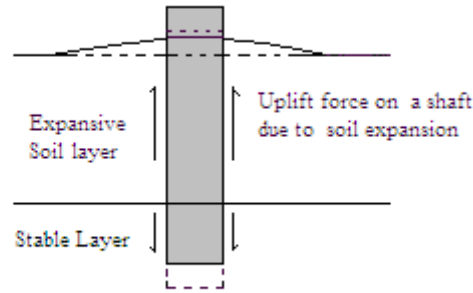


Figure 2.8. Deep Foundation Movements in Expansive Soil.

Many researchers have studied the uplift capacity of piles from the viewpoint of temperature, moisture content, and active depth (Westman 1993). O'Neill and Poormoayed (1980) developed an equation for computing the value of f_{max} in the zone of expansion as shown in Eq. 5.

$$f_{max} = \varphi \sigma'_{ho} \tan \delta_r \quad (5)$$

where φ = a correlation coefficient.

σ'_{ho} = the horizontal swell pressure at the depth where f_{max} is computed.

δ_r = the effective residual of the interface friction between concrete and expansive soil.

In the previous equation, it is assumed that the expansion process happens slowly so that excess positive or negative pore water pressures are not developed. Also, they recommended a value of $\varphi = 1.3$; however, the universal value of φ has not been established. Then, Cameron and Walsh (1981) described a study of small diameter timber piles driven to various depths in an expansive soil profile monitored through wet and dry seasons. In the field, the active depth of expansive soil was between 4.92 and 6.56 ft (1.5 and 2.0 m). After monitoring for five years, they observed maximum seasonal ground surface movements of 2.56 in (65 mm). They also observed that the piles driven to the active depth recorded movements between 15–32 percent of the ground surface movement. However, piles installed between the 6.56 and 8.20 ft (2 and

2.5 m) depth were effective in resisting the ground movements. Then Duffy and Charania (1984) developed a modified oedometer-type test to facilitate the design of piled foundations in expansive soils, which models the interaction between a pile and a swelling clay as the clay is exposed to water. Later, numerical simulations of piles in expansive soils were developed by Justo et al. (1984), Mohamedzein et al. (1999), and Sinha and Poulos (1999). Westman (1993) studied different variables that affect pier uplift in expansive soil and formulated the following equation from numerical models to measure the vertical displacement of the pier head where the load applied was calculated:

$$Y = \frac{e^{0.3575 T^{1.61}}}{D^{1.17} L^{0.831} f_s^{0.760} C^{1.61}} \quad (6)$$

where Y = the vertical displacement of the pier head (ft).

S = the swell pressure of the expansive soil (ksf).

T = the thickness of the expansive soil (ft).

D = the depth to center of the expansive soil (ft).

L = the structural load applied to the pier head (ksf).

f_s = the interface friction between the pier and the soil.

C = the cohesion of the expansive soil (ksf).

Al-Saoudi and Salim (1998) studied the movements of the heads of the model piles which were embedded in the expansive soils. The results showed that the movements of the heads of the piles were less than the movements at the soil surface. Chapel and Nelson (1998) conducted the test using bored concrete piles and helical screw plate anchors for lightweight construction in expansive soils, and concluded that both the piles and anchors performed satisfactorily when installed below the active depth.

LATERAL LOAD ANALYSIS METHODS

The application of lateral load to a drilled shaft results in lateral deflection that, in turn, causes a lateral soil reaction. Lateral load, which is greater than lateral resistance of the drilled shafts, can lead to excessive deformation of the shafts, soil failure around the shafts, and

structural failure. The factors such as maximum bending moment and shear force in the embedded drilled shaft are also important, depending to a large extent on the reaction provided by the soil. Consequently, the main objectives of designing the shaft are to determine the necessary diameter and penetration depth of the drilled shaft, mechanical properties of the concrete and steel rebar to resist bending and shear, and determine the deformations or stiffness of the drilled shaft to assess the performance of the structure.

In the analysis of laterally loaded drilled shafts, there are many common design methods available, such as “Broms’ Method,” “Equivalent Cantilever Method,” “Characteristic Load Method,” the “p-y Method,” and “Strain Wedge Model.” These methods deal with the non-linear system of soil response (Reese et al. 1977) which will be described later.

Broms’ Method

The lateral capacity of a shaft had been initially studied by Brinch Hansen (1961). Later, Broms (1964a, 1964b, 1965) developed the test to determine the ultimate lateral capacity of deep foundations in homogeneous soil deposits that are purely cohesive and cohesionless. Broms constituted the analysis by considering the distribution of the shear resistance with the depth, the short-rigid piles, long-flexible piles, and fixed and free-head cases separately. In addition, he gave the criterion for dividing shafts into two groups that are short-rigid and long-flexible piles, which is the ratio between embedded length of shafts and stiffness factor as given below:

$$\text{Short-Rigid Pile: } \frac{L}{T} \text{ or } \frac{L}{R} \leq 2$$

$$\text{Long-Flexible Pile: } \frac{L}{T} \geq 4 \text{ or } \frac{L}{R} \geq 3.5$$

where T and R are termed as the stiffness factors. In the case of NC clays, T is used and for OC Clays, R is used in the assessments of short and long piles.

These factors account for the modulus of elasticity (E) and the moment of inertia (I) of the pile and soil modulus (the compressibility of the soil) which depends on the depth of influence area, width of pile, and type of soil. For normally consolidated (NC) clays and cohesionless soils, the modulus of the soil is assumed to increase with the depth linearly, and the stiffness factor can be expressed as:

$$T = \left[\frac{EI}{n_h} \right]^{1/5} \quad \text{in length units} \quad (7)$$

where E = the modulus of elasticity of the pile material.

I = the moment of inertia of the pile section.

n_h = the coefficient of modulus variation.

For normally consolidated clay, $n_h = 2,228-4,774$ pcf (350–750 kN/m³). For soft organic silt, $n_h = 950$ pcf (150 kN/m³). For granular soil, n_h can be seen in Table 2.

Table 2.2. Values of n_h for Cohesionless Soils, kip/ft³ (kN/m³) (after Terzaghi 1955).

Type of Sand	Loose	Medium	Dense
Dry or moist sand	15.91 (2500)	47.74 (7500)	127.32 (20,000)
Submerged sand	8.91 (1400)	31.83 (5000)	76.39 (12,000)

For overconsolidated clays, the modulus is assumed to be constant with the depth, so the stiffness factor is shown as:

$$R = \left[\frac{EI}{KD} \right]^{1/5} \quad \text{in length units} \quad (8)$$

where D is the diameter or width of pile.

K is $K_s/1.5$ (where K_s is subgrade modulus reaction (kN/m³ or (kg/m³)), or

K is $n_h \times x/D$ where x is the depth of the soil considered.

According to Terzaghi (1955), K_s values of cohesive soils are listed in Table 3 below.

Table 2.3. Values of K_s for Cohesive Soils, kip/ft³ (kN/m³).

Consistency	Stiff	Very Stiff	Hard
Unconfined Strength, psf (kN/m ²)	208.85–417.71 (10–20)	417.71–835.42 (20–40)	≥835.42 (40)
Recommended K_s	171.88 (27,000)	343.76 (54,000)	687.52 (108,000)

In this case, the short, free-headed piers in the cohesive soils are considered which corresponds with the 3-cable median barriers. Eqs. 9, 10, and 11 are expressed below. In addition, the schematic of the deflected shape, passive soil reaction, and moment diagram in cohesive soils can be seen in Figure 2.9.

$$f = \frac{H_u}{9c_u D} \quad (9)$$

where f = the length of pile required to develop the passive soil reaction.

H_u = the ultimate lateral capacity of the pile.

c_u = the undrained cohesion.

D = the diameter or width of the pile.

$$M = H_u(e + 1.5B + 0.5f) \quad (10)$$

where M = the moment in the pile at the point of fixity.

e = the unsupported length of the pile.

$$2.25Dc_u \left[L - \frac{H_u}{9c_u D} \right]^2 = H_u \left[e + 1.5D + \frac{H_u}{18c_u D} \right] \quad (11)$$

where L = the embedded length of the pile.

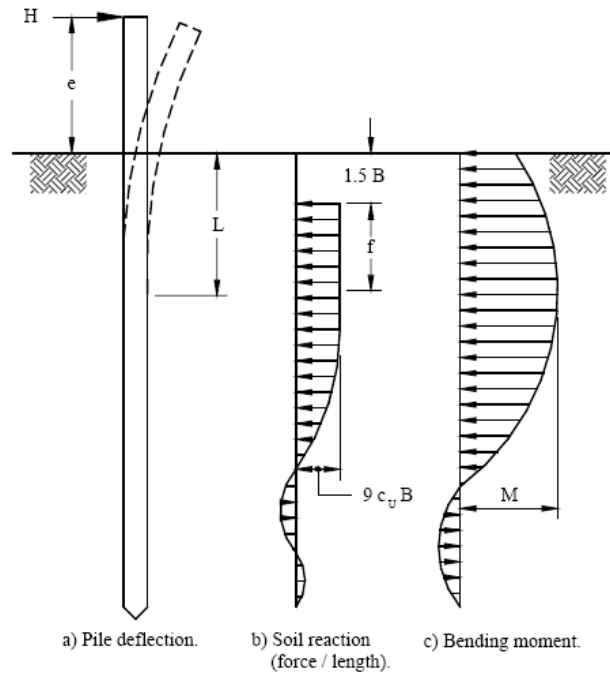


Figure 2.9. Schematic for a Laterally Loaded Pile in a Cohesive Soil (Broms 1964).

Eq. 9 can be solved by trial and error for the Q_{hu} value. However, Broms simplified this method by using the graph shown in Figure 2.10 below to calculate Q_{hu} .

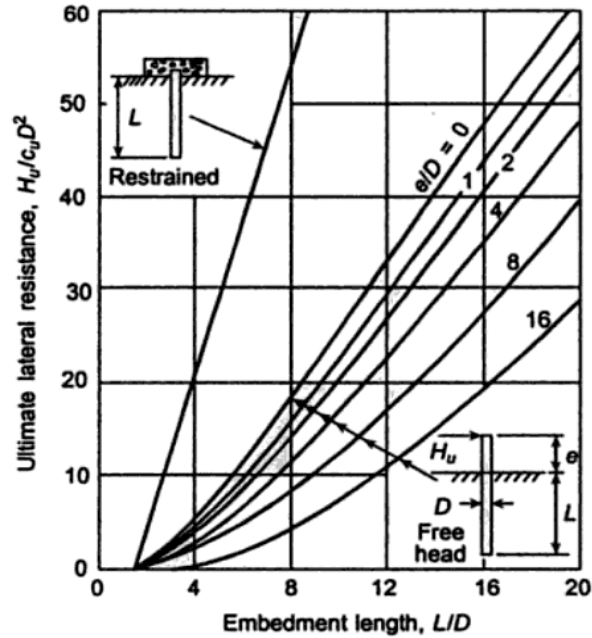


Figure 2.10. Design Chart for Short Piles in Cohesive Soils (Broms 1964b).

Equivalent Cantilever Method

Davisson and Robinson (1965) determined the elastic forces and moments in piles using the Equivalent Cantilever Method. After that, Greimann et al. (1987) refined this design method based on Rankine's equation for inelastic buckling. Abendroth et al. (1989) evolved this method further for designing piles of integral bridges due to the fact that the previous method provided very conservative results. They idealized the piles through the cantilever model as shown in Figure 2.11. The method was based on analytical and finite element studies. The drilled shaft was replaced by an equivalent cantilever beam in order to simplify the analysis. However, Robinson et al. (2006) observed that the results from the analyses of the cantilevered columns with an "equivalent" length did not match the magnitudes of maximum moments, lateral pile top displacements, or buckling behavior from non-linear lateral analysis.

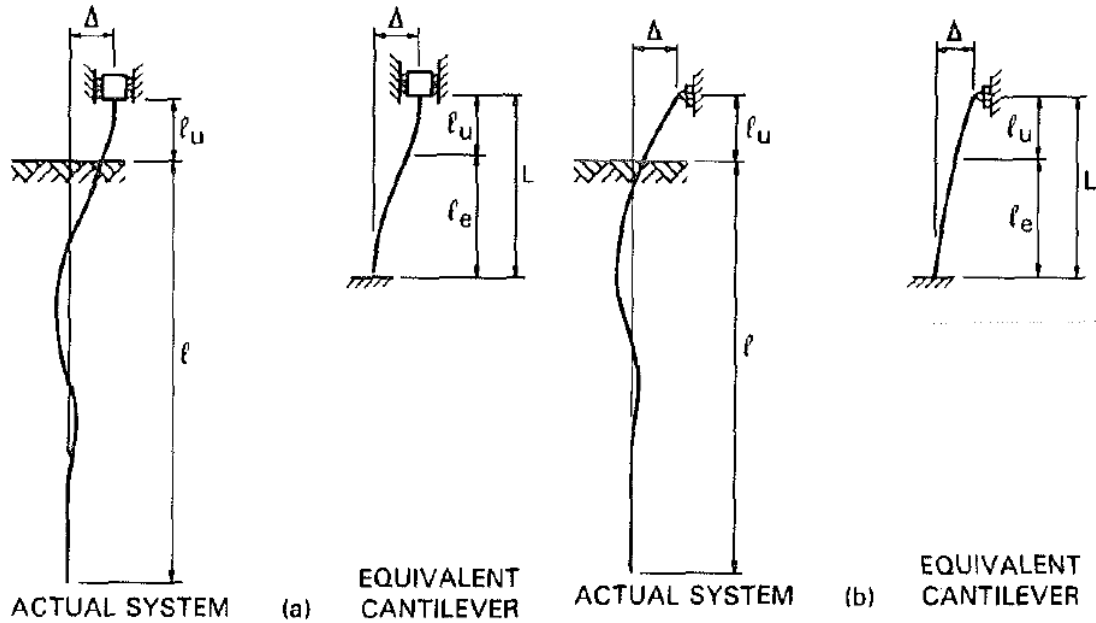


Figure 2.11. Cantilever Idealization of Pile: (a) Fixed Head; (b) Pinned Head (Abendroth et al. 1989).

Characteristic Load Method (CLM)

Duncan et al (1994) proposed a method based on parametric analysis of numerous p-y curves. The significance of this method over the equivalent cantilever method is that it can deal with non-linearity of the soil behavior. The non-linear behavior of pile foundations subjected to lateral loads is due to two factors. The first factor is non-linearity of the load-deflection behavior of the soil around the pile, and the second one is load transfer from the upper part of the pile to the greater depth resulting in an increase of the moment from the load at the top of the shaft. In addition, the authors stated that this method can be used to determine:

- Ground line deflections due to ground line shears for fixed shaft condition.
- Ground line deflections due to moment applied at the ground line.
- Maximum bending moment within the shaft.
- Position of the maximum moment.

The relationships of the characteristic load method (CLM) were formed by using the dimensionless variables to represent a wide range of real conditions as given below:

For clay,

$$P_c = 7.34D^2(E_p R_I) \left[\frac{S_u}{E_p R_I} \right]^{0.68} \quad (12)$$

$$M_c = 3.86D^2(E_p R_I) \left[\frac{S_u}{E_p R_I} \right]^{0.46} \quad (13)$$

where P_c = the characteristic or normalizing shear load.

M_c = the characteristic or normalizing bending moment.

D = the width or diameter of the pile or drilled shaft.

E_p = the modulus of elasticity of the pile or drilled shaft.

R_I = the ratio of moment of inertia (I_p / I_r) = ratio of moment of inertia of the pile or drilled shaft (I_p) to the moment of inertia of a solid circular cross section (I_r).

S_u = the undrained shear strength of undisturbed samples of clay.

From these equations, the shear and moment loads are determined at the ground line or ground surface. After determining the variables P_c and M_c , the solution parameters can be obtained with the help of various curves, which are ground line shear and ground line moment deflection curves as presented in Figure 2.12.

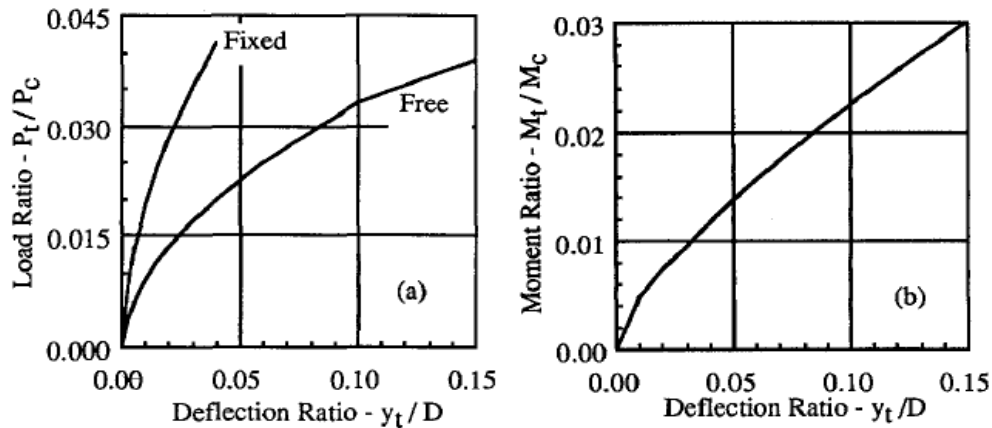


Figure 2.12. Deflection Curves of (a) Ground line Shear and (b) Ground line Moment for Clay (Duncan et al. 1994).

To compute the ground shear deflection (y_{tpm}) and the ground moment deflection (y_{tmp}) for use in Eq. 14, the following steps are performed:

Step 1—Divide the ground line load (P_t) by the characteristic shear load (P_c) and the moment (M_t) by the characteristic bending moment (M_c). P_c and M_c are calculated from Eqs. 12 and 13 above.

Step 2—Using the graphs shown in Figure 2.12 (a) and (b) above, determine the deflection ratios for the ground line shear (y_{tp}/D) (Graph a) and for the ground line moment (y_{tm}/D) (Graph b). Multiply the drilled shaft diameter (D) by the shear and moment Deflection Ratios to obtain the ground line deflection (y_t) if only y_t for each property is desired.

Step 3—Using the same deflection ratio from the ground line moment (y_{tm}/D), determine the ground line shear (P_m) by entering this value on the horizontal axis in Graph a, extend this value vertically to the curve, project a horizontal line from this point to the y-axis, and read the value as P_m/P_c . Using the same deflection ratio from the ground line shear (y_{tp}/D), determine the ground line moment (M_p) in the same manner as described for P_m using Graph b.

Step 4—For the ground line shear, add P_t and P_m , divide by P_c , and enter this value in Graph a. Project a horizontal line to the curve, and then project a vertical line down to the x-axis. Read the value and record as y_{tpm}/D . For the ground line moment, add M_t and M_p , divide by M_c , and enter this value in Graph b. Project a horizontal line to the curve, and then project a vertical line down to the x-axis. Read the value and record as y_{tmp}/D . Divide y_{tpm}/D and y_{tmp}/D by D to obtain y_{tpm} and y_{tmp} , respectively.

Step 5—Finally, compute the lateral deflection ($y_{t \text{ combined}}$) by using the following equation:

$$y_{t \text{ (combined)}} = 0.5(y_{tpm} + y_{tmp}) \quad (14)$$

To find the maximum moment in this method in a free- or fixed-head drilled shaft and if the only load applied is a ground line shear, Figure 2.13 can be used.

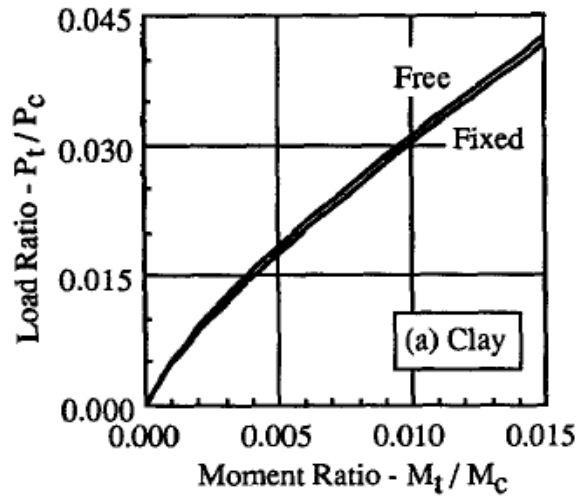


Figure 2.13. Load-Moment Curves (Duncan et al. 1994).

However, if the moment and shear are both applied, the lateral deflection, $y_{t(combined)}$, is determined as mentioned above and then the characteristic length (T) is found from the following equation:

$$y_{t(combined)} = \frac{2.43P_t}{E_p I_p} T^3 + \frac{1.62M_t}{E_p I_p} T^2 \quad (15)$$

The next step is to calculate the bending moment of the drilled shaft by using the following equation:

$$M_z = A_m P_t T + B_m M_t \quad (16)$$

where M_z = the moment at depth z .

A_m, B_m = the dimensionless moment coefficient, which is obtainable from the graph below.

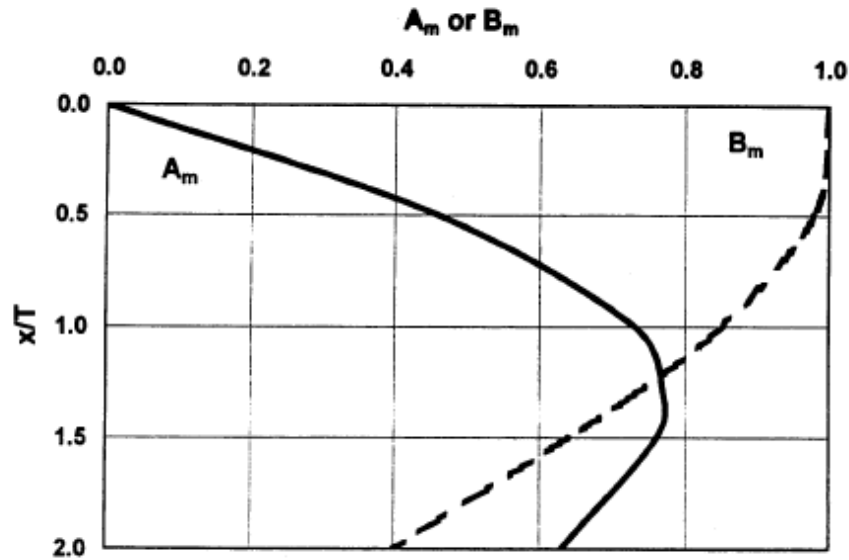


Figure 2.14. Parameters A_m and B_m (Matlock and Reese 1961).

Although the characteristic load method was developed from the p-y method, it is not generally used as the p-y method. There are some limitations of this CLM method which are outlined below (O'Neil and Reese 1999):

- Piles and drilled shafts must be long enough so their behavior is not affected to any significant degree by their length, which depends on the relative thickness of the piles or shafts to the stiffness of the soil. Thus, Duncan et al. (1994) provided the minimum drilled shaft penetrations to fit with this method. However, in case that a shaft is shorter than the length mentioned in Table 4, the ground line will be underestimated and the maximum bending moment will be overestimated. In addition, the minimum penetration depth is influenced by the cyclic loading emanating from seismic, environmental (temperature or moisture induced) and other events and the presence of free water.
- It is founded on generally uniform soil conditions; also, it has not been used when shafts are founded in the rock sockets.
- The effect of axial loads on the bending moment is not taken into account.
- The shear could not be analyzed directly.
- The non-linear bending in the drilled shaft is not considered in this method. Thus, if there are some cracks at the depth of the maximum moment, the ground line deflection will be underestimated.

Table 2.4. Minimum Penetrations for Clay of Drilled Shafts for the Characteristic Load Method (Duncan et al. 1994).

Type of Soil	Criterion	Minimum Length
Clay	$E_p R_l / S_u = 100,000$	6D
Clay	$E_p R_l / S_u = 300,000$	10D
Clay	$E_p R_l / S_u = 1,000,000$	14D
Clay	$E_p R_l / S_u = 3,000,000$	18D

p-y Method (Non-Linear Analysis)

This method is more generally used to analyze a drilled shaft subjected to lateral loading due to its versatility, including the distributed load along the shaft caused by flowing water or creeping soil, non-linear bending characteristics, cracked concrete pier sections, layered soils, and non-linear soil response. This method is recommended for use with the most critical foundations. The p-y model was first developed using the response of a single shaft subjected to lateral loads (Reese and Matlock 1956). McClelland and Focht (1958) developed the p-y model based on the results of a lateral load test on a 24 in. (610 mm) diameter pile embedded to a depth of 75 ft (23 m) in a normally consolidated (NC) clay in the Gulf of Mexico. After that, many researchers including Matlock and Ripperger in 1958, Matlock in 1970, Reese et al. in 1975, Reese and Welch in 1975, and Bhushan et al. in 1979 have improved this method. Later, Reese (1984, 1986) reported comprehensive information on laterally loaded piles and drilled shafts design in a Federal Highway Administration (FHWA) document which has been broadly accepted.

The fundamental aspect of this method is to develop the p-y curves representing the true behavior of soils by considering the non-linearity of the soil modulus. This is based on a numerical solution of a physical model for the laterally loaded, deep foundation based on the soil along the unit length of shafts and replaced with a series of mechanisms surrounding the shaft as shown in Figure 2.15. At different depths of drill shaft, the resisting force per unit length of the shaft (soil reaction) (p) performs as the non-linear function of the lateral deflection (y).

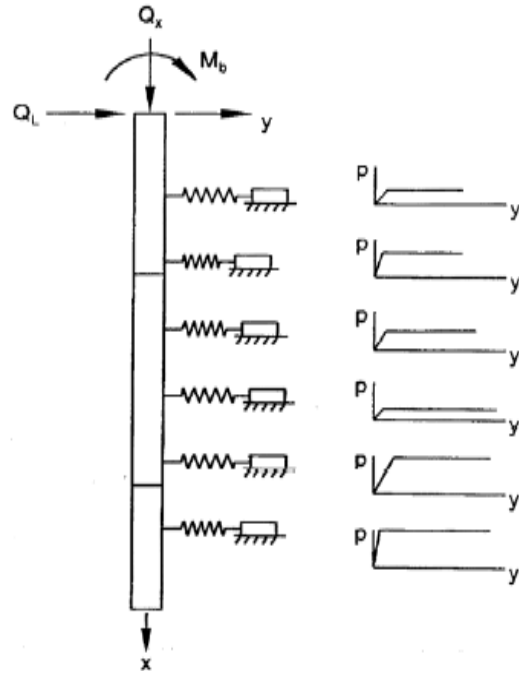


Figure 2.15. Physical Model of a Deep Foundation under a Lateral Load.

The methods representing the p-y curves are cited after presenting the governing equations. The drilled shaft is treated as a beam column with lateral soil support. The general behavior of a drilled shaft under a combination of lateral and axial loading can be obtained by solving the differential equation given below (Hetenyi 1946):

$$EI \frac{d^4 y}{dx^4} + Q \frac{d^2 y}{dx^2} - p - w = 0 \quad (17)$$

where Q = the axial load on the shaft.

y = the lateral deflection of the shaft at a point x along the length of the shaft.

p = the lateral soil reaction per unit length.

EI = the flexural rigidity of the drilled shaft.

w = the distributed load along the length of the shaft.

In addition, the equations that are produced from derivatives are necessary in design as shown below. For transverse shear (V),

$$EI \frac{d^3 y}{dx^3} + Q \frac{dy}{dx} = V \quad (18)$$

For bending moment in the drilled shaft (M),

$$EI \frac{d^2y}{dx^2} = M \quad (19)$$

For the slope of the deflection diagram (S),

$$\frac{dy}{dx} = S \quad (20)$$

For the slope of secant to any p-y curve or soil modulus (E_s)

$$E_s = \frac{p}{y} \quad (21)$$

After substituting E_s (Eq. 21) into the main equation (Eq. 17), the results show that there are finite difference terms depending on a number of nodes along the drilled shafts, which the p-value at each node is equal to $E_s \cdot y$. Thus, y-values are the unknown parameters in this problem. Generally, y-values depend on soil stiffness. The deeper the embedment depth, the higher the vertical stresses which induce an increase in the soil stiffness. Also, the lateral movement from the piles will additionally increase the stress in the soil.

Even though the bending moment, shear force, and other design aspects of the drilled shafts are computed from the finite difference forms of the equations above, computer-generated solutions such as LPILE^{plus} and other software programs are efficient, time saving, and create an opportunity for investigating the influence of a large number of parameters with minimum difficulty.

In the present research, the researchers propose to analyze the drill shaft load test results using the p-y method-based software such as the ‘L-Pile’ program. Other methods including the ‘Characteristic Load Method’ and ‘Broms’ Method’ will also be considered if the soil conditions at the test site location match with the assumptions used in these methods.

Strain Wedge Model

The Strain Wedge (SW) Model, developed in 1996 by Ashour et al. (1998), improved upon Reese’s (1977) Beam on Elastic Foundation (BEF) pile response parameters and his realization of limitations of the p-y curves (1983) for soil continuity and pile properties. The SW method added the capability to analyze piles in multiple soil layers to include sand and clay. Additionally, the method allowed the effect of pile head conditions (free- or fixed-head) to be included in the analysis.

118The method uses a 3-D passive soil wedge that is formed in front of a laterally loaded pile that accounts for stress-strain-strength parameters. The SW model is interdependent on the BEF model through the horizontal soil strain, ϵ , the horizontal soil stress change, $\Delta\sigma_h$, and the nonlinear variation in the Young's modulus, E .

Figure 2.16 shows a diagram of the soil wedge. Figure 2.17 shows the deflection pattern of the pile, which is assumed to be linear. Each layer's soil properties encountered in the field can be applied in this model and used to more accurately determine the effect to the soils from lateral loading on the pile.

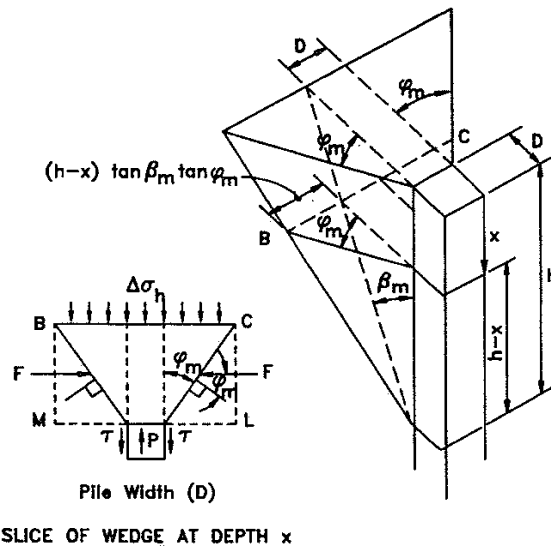


Figure 2.16. Basic Strain Wedge in Uniform Soil (Ashour et al. 1998).

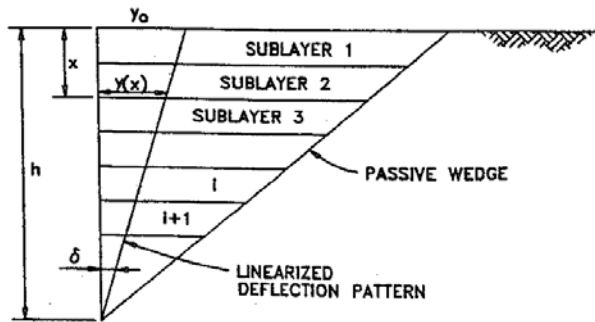


Figure 2.17. Linearized Deflection Pattern (Ashour et al. 1998).

The horizontal strain in the soil is the most influential parameter in the model. In normally consolidated clay, the effective unit weight, the Plasticity Index, effective friction angle, undrained shear strength, and soil strain at 50 percent stress level are used in the

calculation of the modulus of subgrade reaction, E , and representing the secant slope at any point on the p-y curve.

Wedge thicknesses are created based on soil types. But additional wedges can be created if a soil layer is determined to be too thick and possibly affect the calculations. Additionally, a wedge can be created for a fixed-head pile and included in the calculations. This greatly assists in replacing the conditions in such programs as COM624 and LPILE that consider p-y curves to be unique. Soil and pile variations have a dramatic effect upon the response of soils and their p-y curves as shown by actual field tests in Figure 2.18.

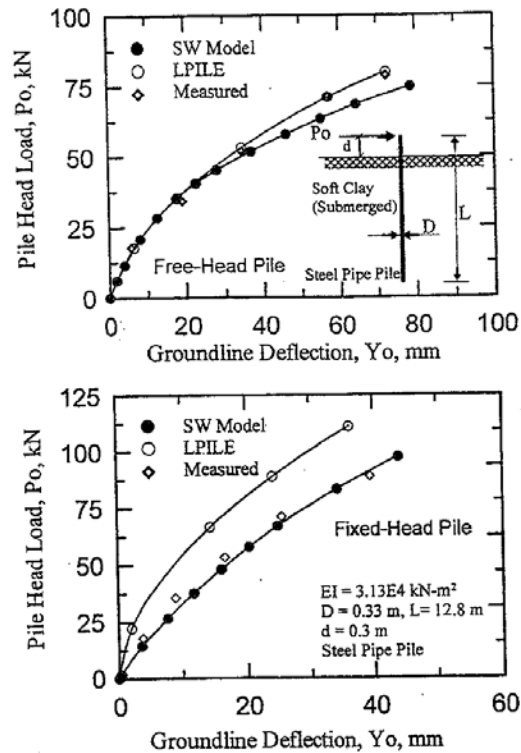


Figure 2.18. Comparison of SW, LPILE, and Field Data for Free- and Fixed-Head Piles in Clays at the Sabine River (Ashour et al. 2002).

Comparison of Lateral Load Analysis (Broms' Method and p-y Method)

Klaiber et al. (2004) compared the results between the Broms' Method and the p-y Method, and reported that the p-y Method (the non-linear method) can be used in more complex soil conditions and provides more accurate results of the moment distribution along the depth of piers whereas the Broms' Method (the linear method) does not take into account the redistribution of loads below the point of fixity. They also compared both methods by using

different soils, stiff clay (SPT blow count of $N = 25$), soft clay (SPT blow count of $N = 2$), and cohesionless soil (SPT blow count of $N = 25$), with different magnitudes of lateral loads by changing the backwall height. In short, the Broms' Method is more conservative in predicting stiff clays than the p-y Method as shown in Figure 2.19. For soft clays, the Broms' Method is less conservative than the p-y Method as shown in Figure 2.20. For cohesionless soils, both methods yield more or less the same results (Figure 2.21).

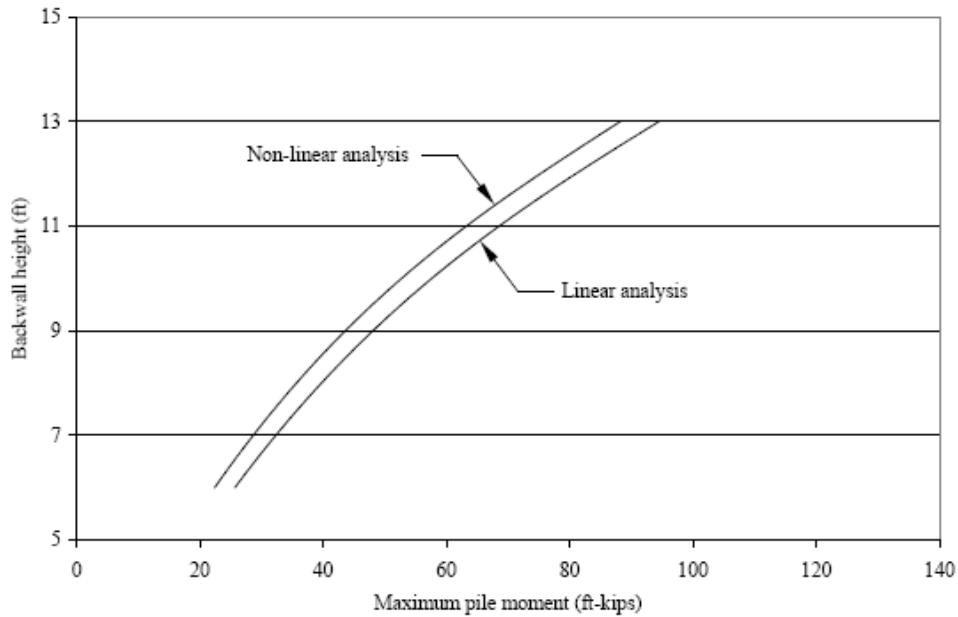


Figure 2.19. Comparison of Lateral Load Analysis in Stiff Clay.

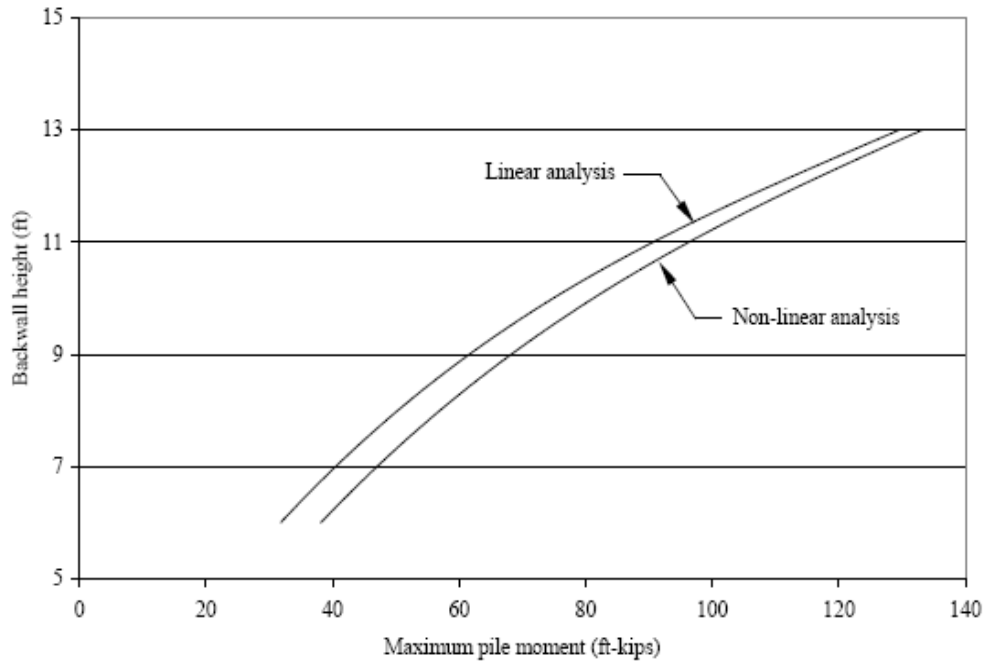


Figure 2.20. Comparison of Lateral Load Analysis in Soft Clay.

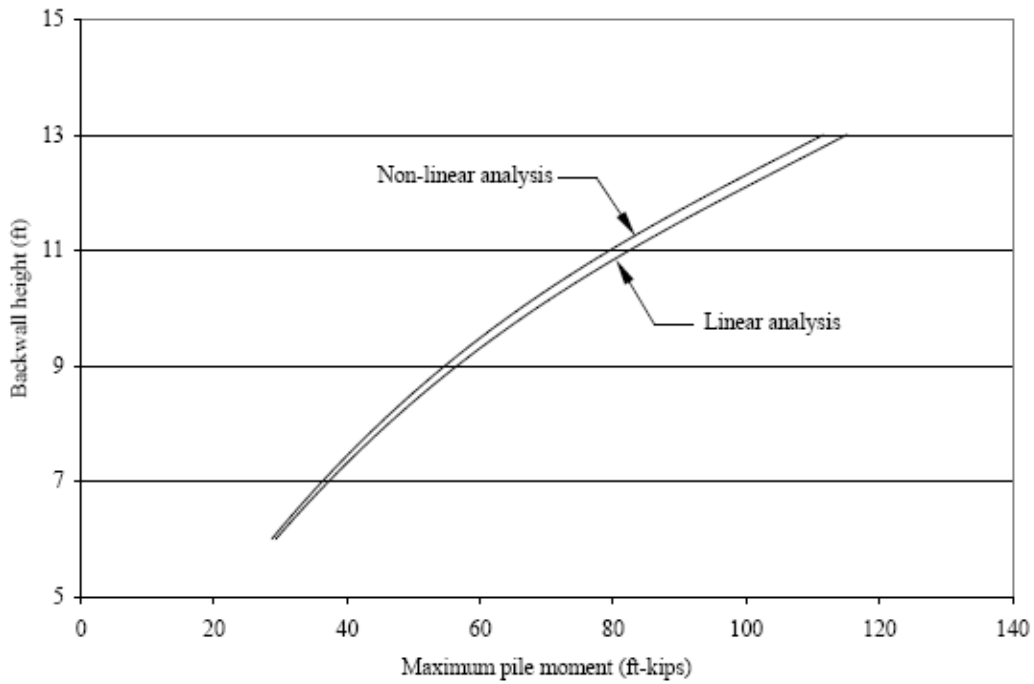


Figure 2.21. Comparison of Lateral Load Analysis in Cohesionless Soil.

LATERAL LOAD TESTS ON DRILLED SHAFTS

The performance of drilled shafts in different types of soils with the derivation of the p-y curve are able to be evaluated with different types of the tests, which leads to more accurate

designs of drilled shafts (O’Neil and Reese 1999). Standard lateral load tests for drilled shafts are described in the FHWA IP-84-11 report and ASTM D 3966 (ASTM 2007). The most common types of lateral load tests that are conducted on drilled shafts are the Conventional Load Test, Osterberg Load Cell Test, and the Statnamic Load Test. A brief description of these test methods is given below.

Conventional Load Test

In the Conventional Load Test, a test shaft of known diameter is placed between two reaction shafts which are mounted with a reaction frame. The load is gradually applied by this reaction frame to the test shaft. Hydraulic jacks are placed on the test shaft on a leveled steel plate. Figure 2.22 shows a typical Conventional Load Test setup.

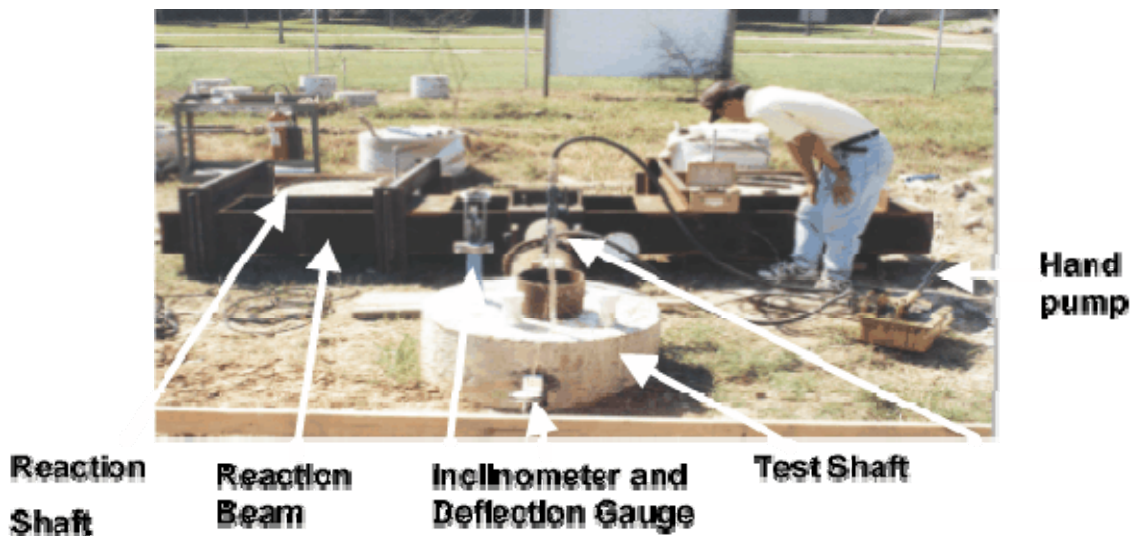


Figure 2.22. Test Setup for a Conventional Load Test.
 (Source: <http://www.fhwa.dot.gov/infrastructure/tccc/tutorial/shafts/fhcha10.htm>)

In this test, the test shaft is pulled away from the two reaction shafts and the readings are taken using the dial gauge fitted to the test shaft. From Figure 2.22, the inclinometer which has been cast into the drilled shafts along the centroidal axis is used to measure the deflection of the shafts. As a result, the p-y curves can be obtained from the loading tests directly if the bending moment is considered as a function of the lateral loads and depth (Welch and Reese 1972; Dunnavant and O’Neill 1989). The disadvantage of this method is that it is very expensive compared to other testing methods. However, a set number of reaction shafts are installed with

an “I” beam framework bolted to the reaction piers. The number of test shafts can be increased since they will be of a smaller magnitude and depth compared to the reaction shafts.

Osterberg Load Cell Test

The Osterberg Load Cell, or O-cell, named after its inventor, Dr. Jorj O. Osterberg, has radically changed the way foundation load tests are designed, performed and interpreted. This test can be performed on high capacity shafts at low costs unlike the conventional load testing. Engineers need to rely on the information obtained from the load tests conducted on smaller test shafts. In this method, the Osterberg load cell is installed within the drilled shaft during its construction as shown in Figure 2.23. The cell is mounted on a reaction socket, which is made of two sockets, and these sockets are jacked apart with the help of hydraulics to duplicate the effect of lateral loading. Lateral displacement is measured by using LVDTs connected between the plates. The lateral load applied can be calculated by dividing the load in the cell by the length of the socket.



Figure 2.23. Osterberg Load Cell for the Lateral Load Test.
(Source: <http://www.loadtest.co.uk/Loadtest%20Ltd/downloads.htm>)

Statnamic Load Test

Drilled shafts are also tested by mounting Statnamic devices horizontally adjacent to the shaft (O’Neill et al. 1990; Rollins et al. 1997). In this test, lateral loads are applied on the shaft with the help of a propellant, which is accelerated to generate heavy masses (Figure 2.24). This type of test is more economical when there are no reaction frames. Also, the type of loading that

is applied is impact loading. McVay (2003) had conducted a study to collect a database of statnamic tests and conventional tests on drilled shafts and driven piles in different soil and rock conditions and established resistance factors for load and resistance factors design (LRFD) for statnamic tests.



Figure 2.24. Test Setup for a Statnamic Test.

(Source: <http://www.fhwa.dot.gov/infrastructure/tccc/tutorial/shafts/fhcha10.htm>)

Lateral load tests were conducted by several researchers in non-expansive soils and a few of these results are discussed in tasks outlined in the work plan. Houston et al. (2004) conducted lateral load tests to assess the performance of drilled shafts installed in cemented sands. In the case of high plasticity clays, limited test results are available.

SUMMARY

This chapter provided a comprehensive review of various aspects that are crucial for proposed research. Sections describing expansive soils, lateral load analysis and load tests are described in detail. The next chapter describes few of the earlier tasks including site selection and laboratory tests performed on the site soils.

CHAPTER 3 SITE SELECTION AND LABORATORY STUDIES

SITE SELECTION

During the site selection process, two sites were proposed. The first site was IH 20 and Rose Hill Road, and the second one was IH 20 and FM 2578. Several criteria, such as high plasticity characteristics of the CH soil at Site 1 or cable barrier foundations that experienced distress problems at Site 2, were considered in the selection process. However, the most important criterion was if the area would have enough space to work on the field tests. Comparing the two sites, the first location met the criteria much better than the second one. Therefore, the test site located on IH 20 and Rose Hill Road located in Kaufman County, Texas, was selected as shown in Figure 3.1.

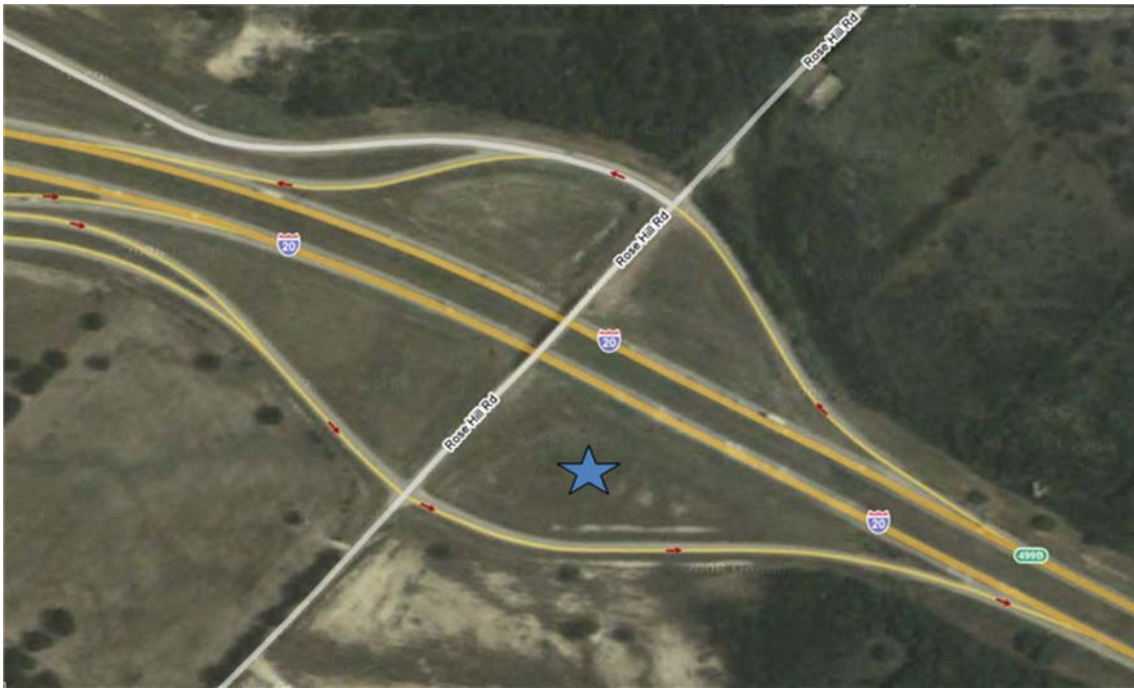


Figure 3.1. Test Site Located on IH 20 and Rose Hill Road.

Soil Sampling and Laboratory Testing

For identifying properties of the soil, field open pit sampling was performed by using a backhoe. Nuclear gauge tests were also performed at the site to determine both the density and moisture content of the soil in field conditions, as shown in Figure 3.2.



Figure 3.2. Soil Sampling and Density Measurement by Using Nuclear Gauge.

Basic Soil Properties Tests

The collected soil samples at various elevations were subjected to a variety of laboratory physical tests including specific gravity, Atterberg (ASTM D4318-05, 2003), and linear shrinkage bar tests (Tex-107-E, 2002). All the soils are considered as fine-grained soils, as more than 50 percent of the soils are passing through the sieve No.200. Classification of types of the soils from the field was performed by using the Unified Soil Classification System (USCS) method. Table 3.1 shows the results of the basic soil properties.

Table 3.1. Basic Soil Properties.

Depth, ft (m)	LL	PL	PI	SL	% Linear Shrinkage	Classification
0.0–1.0 (0.0–0.3)	N.A.	N.A.	N.A.	N.A.	0.00	Silty Sand
1.0–3.0 (0.3–0.9)	77	18	59	10	12.07	CH
3.0–5.0 (0.9–1.5)	47	20	28	14	8.40	CL
5.0–10.0 (1.5–3.0)	41	20	21	15	2.62	CL
> 10.0 (> 3.0)	33	21	12	17	2.10	CL

Atterberg test results are also presented in the same table. From the test results presented in the table, it can be concluded that the soil at 1 to 3 ft (0.3 to 0.9 m) depth has the highest plasticity index (PI) value. The second highest PI value is measured for the soil strata located at 5–10 ft (1.5–3 m) depth interval. The soil encountered in third layer has a PI value equal to 28, and the linear shrinkage strain is 8.4 percent, which is considered high.

Standard Proctor Compaction Tests

Proctor compaction tests were performed on the field soil samples to establish compaction relationships. These results are presented here for general discussions and not used for any laboratory compactions for soil specimens. The optimum moisture content (OMC) of the soil is the water content at which the soil is compacted to a maximum dry density condition. Water contents at 95 percent of maximum dry density conditions that are dry of OMC and wet of OMC were selected for testing and are shown in Figure 3.3 below. In addition, Figures 3.4 and 3.5 show the standard compaction for Layers 2 and 3. Table 3.2 summarizes the values obtained from the laboratory testing.

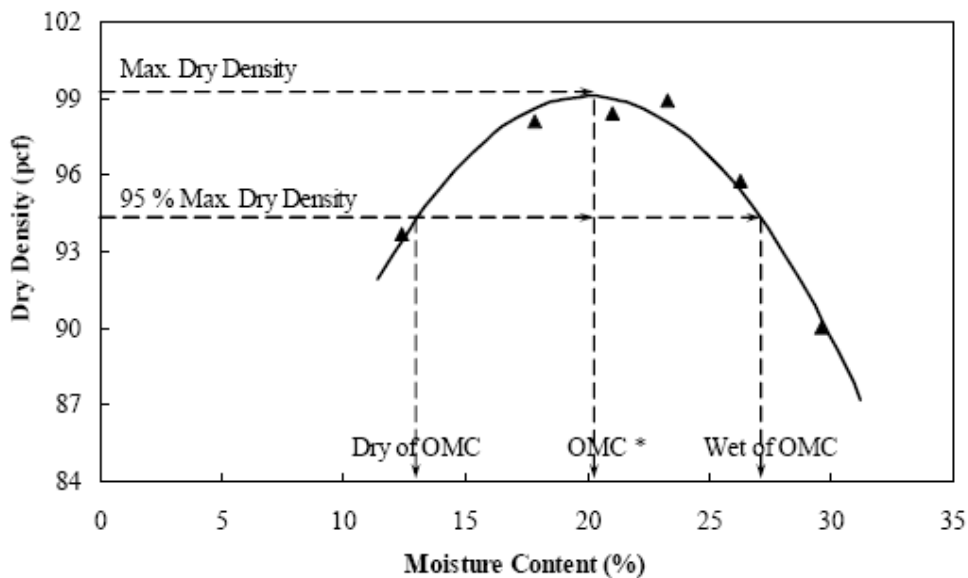


Figure 3.3. Typical Standard Compaction Curve.

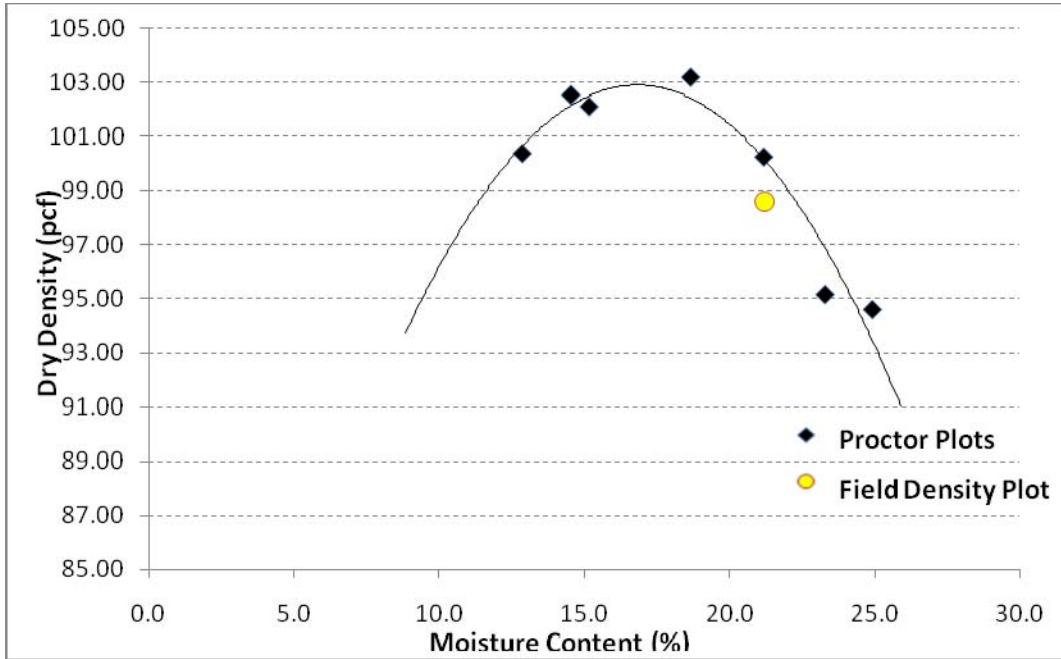


Figure 3.4. Standard Compaction Curve and Point of Field Density of Layer 2.

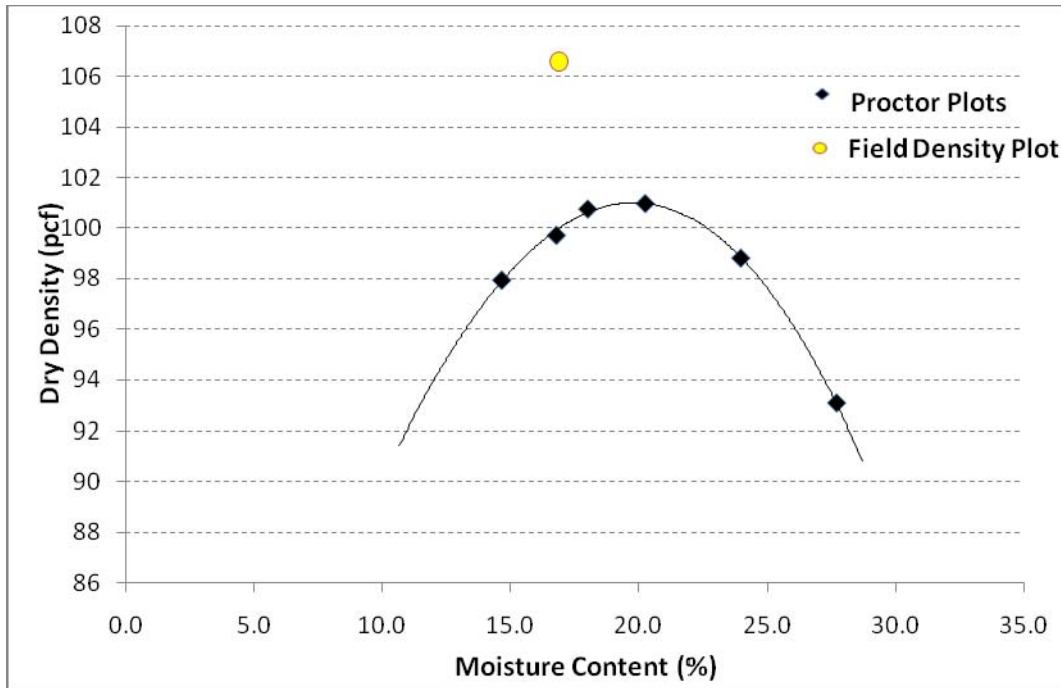


Figure 3.5. Standard Proctor Compaction Curve and Point of Field Density of Layer 3.

Table 3.2. Standard Proctor Compaction Test Results.

		Layer 2 1.0–3.0 ft (0.3–0.9 m)	Layer 3 3.0–5.0 ft (0.9–1.5 m)
Moisture Content (%)	Wet OMC	22.80	26.05
	OMC	16.80	19.80
	Dry OMC	10.91	13.02
Dry Density (pcf)	Wet OMC	97.76	95.95
	OMC	102.90	101.0
	Dry OMC	97.76	95.95

Note: OMC—Optimum Moisture Content in %

From Table 3.2, the second and third soil layers exhibit the highest dry density equal to 102.90 and 101.0 pcf, respectively. It is noted that all three compaction moisture content conditions, wet of OMC, OMC, and dry of OMC, are used as reference moisture contents for the engineering tests performed in this research. Soils in the field undergo moisture content fluctuations during the seasonal changes; hence, it is important to determine the properties of soils over a wider range of moisture contents expected in the field. Such properties will be needed for numerical modeling of the field load tests on drilled shafts as a part of the analysis task.

The Three Dimensional (3-D) Swell Tests

The three-dimensional free swell test provides a reasonable representation of the soil maximum volumetric swell potentials (Punthutaecha 2006). All the specimens of 4.0-in. diameter and 4.6 in. height were placed between two porous stones (Figure 3.6a), wrapped in a rubber membrane, and was then subjected to soaking by inundating it with water from both ends. The specimen was monitored for the vertical and radial swell movements until there was no considerable movement. In this research, soil specimens were prepared at three different moisture content conditions, which are dry of optimum, optimum and wet of optimum moisture content conditions (Figure 3.6b). In addition, one specimen was prepared at the same density and moisture condition as measured in the field. The results of the 3D swell tests can be seen in Figures 3.7 to 3.11 and in Table 3.3.



Radial Measurement



Test Setup of 3D Swell Test (Dry OMC, OMC, and Wet OMC [left to right])

Figure 3.6. Three-Dimensional Swell Test.

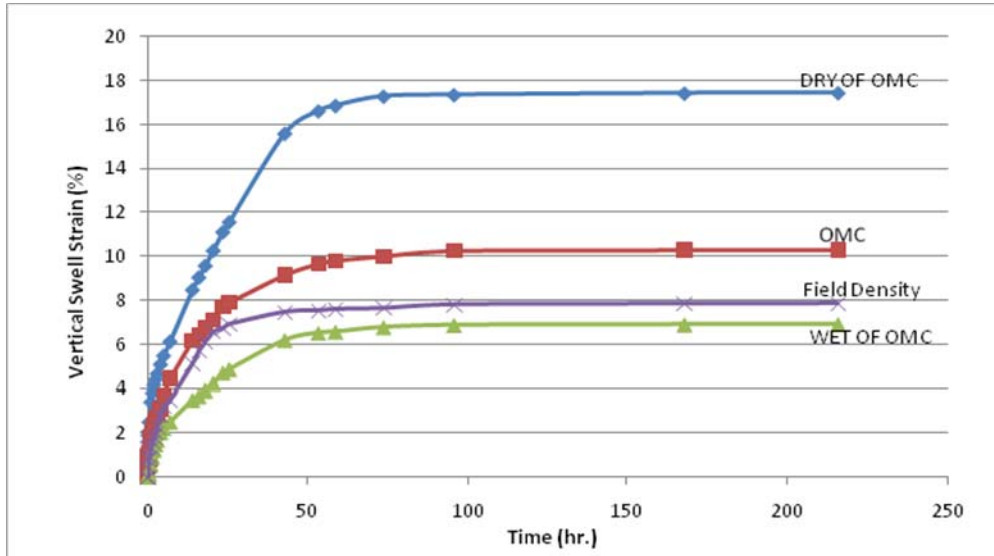


Figure 3.7. Vertical Swell Strain Results for Soil Layer 2 at Three Different Moisture Contents and Field Density Conditions.

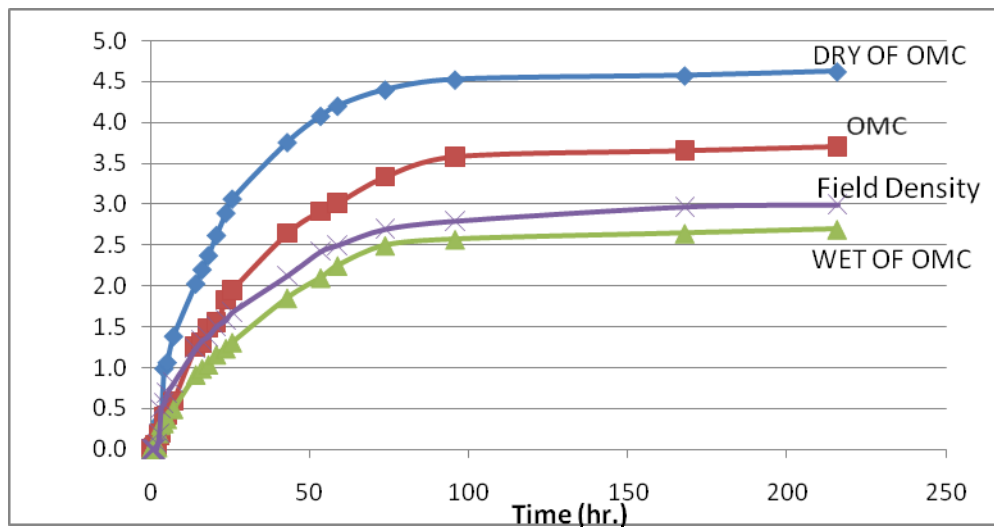


Figure 3.8. Radial Swell Strain Results for Soil Layer 2 at Three Different Moisture Contents and Field Density Conditions.

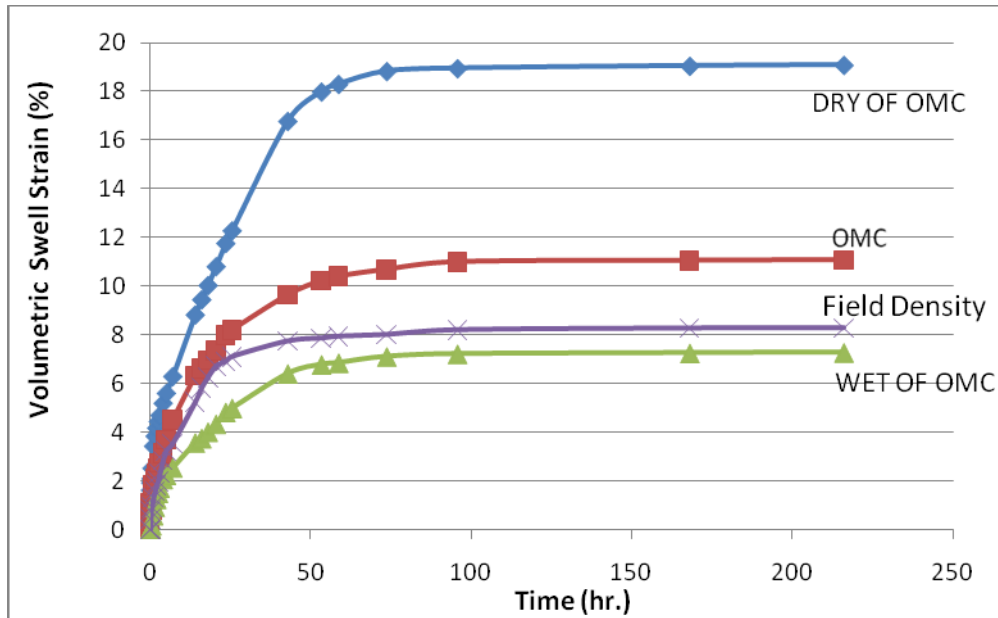


Figure 3.9. Volumetric Swell Strain Results for Soil Layer 2 at Three Different Moisture Contents and Field Density Conditions.

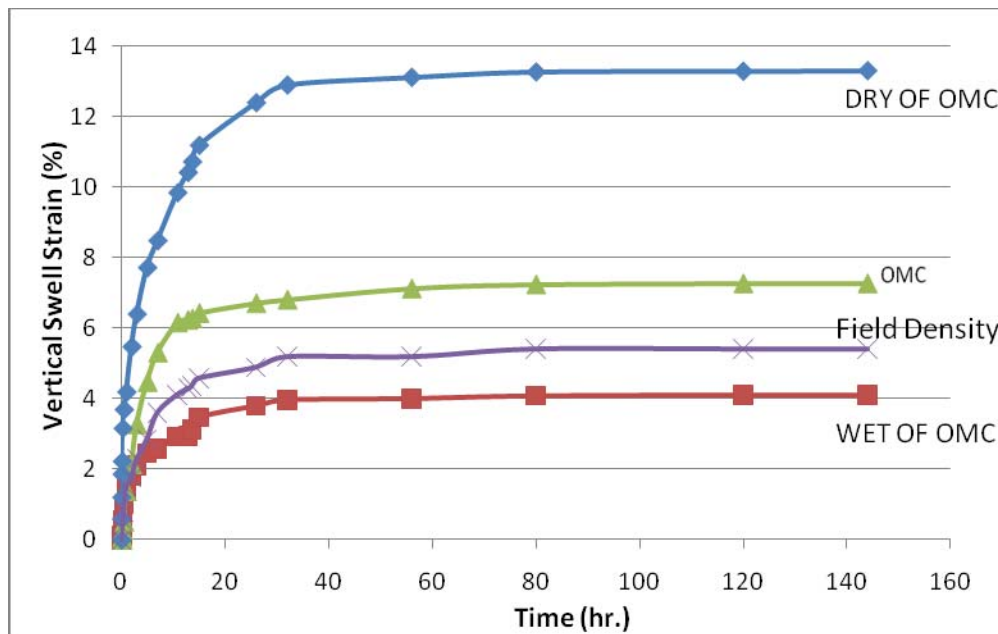


Figure 3.10. Vertical Swell Strain Results for Soil Layer 3 at Three Different Moisture Contents and Field Density Conditions.

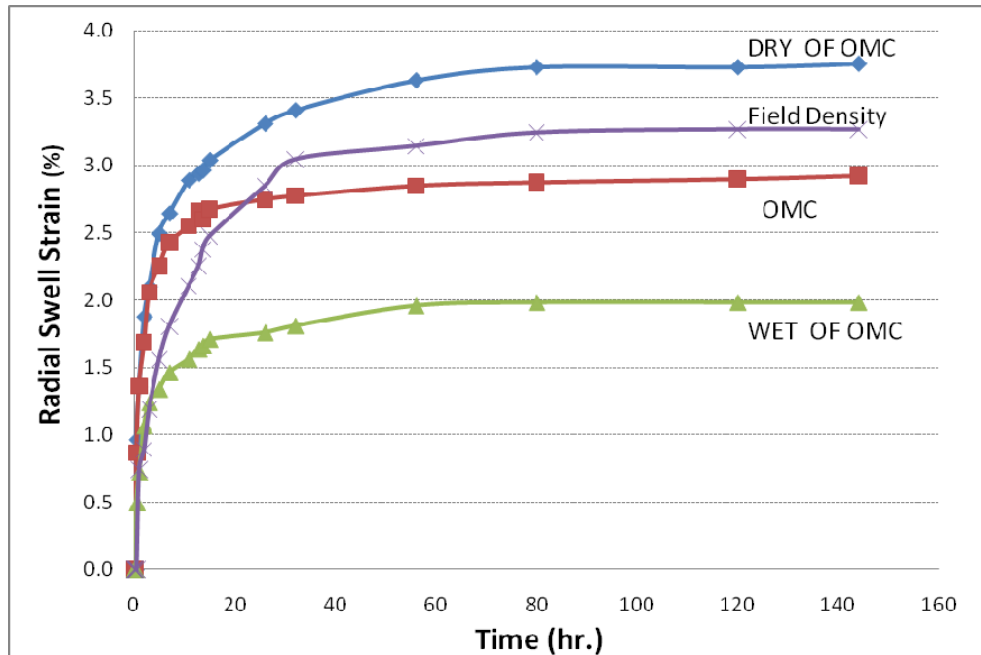


Figure 3.11. Radial Swell Strain Results for Soil Layer 3 at Three Different Moisture Contents and Field Density Conditions.

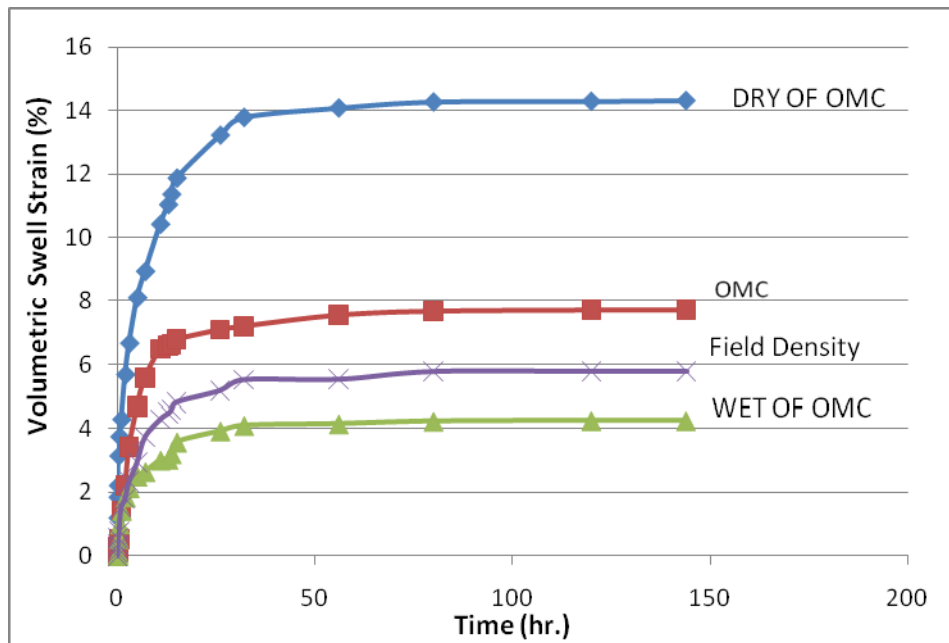


Figure 3.12. Volumetric Swell Strain Results for Soil Layer 3 at Three Different Moisture Contents and Field Density Conditions.

Table 3.3. Three-Dimensional Volumetric Swell Strain Test Results.

Moisture Condition	Swell Strain (%)	
	Soil Layer 2 1.0–3.0 ft (0.9–1.5 m)	Soil Layer 3 3.0–5.0 ft (1.5–3.0 m)
95% Dry of OMC		
Vertical	17.44	13.30
Radial	4.63	3.73
Volumetric	19.09	14.32
OMC		
Vertical	10.29	7.28
Radial	3.71	2.87
Volumetric	11.07	7.71
95% Dry of OMC		
Vertical	6.90	4.10
Radial	2.69	1.98
Volumetric	7.28	4.26
Field Density		
Vertical	7.83	7.28
Radial	3.00	3.24
Volumetric	8.28	5.77

Based on these results and those shown in Table 3.1, it can be concluded that both second and third layers have high swelling potential. The soil encountered between the 1.0 and 3.0 ft (0.9–1.5 m) depths of Layer 2 has a volumetric swell strain (for the OMC condition) value more than 10 percent and this value indicates a high degree of expansion potential as per the problematic volumetric swell characterizations that Chen (1988) mentioned. In addition, the soils encountered between the 3.0 and 5.0 ft (1.5 to 3.0 m) depths (i.e., Layer 3) exhibited a plasticity index or PI value of 28, a linear shrinkage strain of 8.4 percent, and a volumetric swell strain of 7.7 percent. Again, these values indicate that this soil layer is a problematic expansive soil layer as per the soil characterizations reported by Chen (1988).

Volumetric Shrinkage Strain Tests

This test was developed at the University of Texas in Arlington (UTA) because of the limitations in the linear shrinkage bar test. The cylindrical compacted soil specimens were subjected to a drying process, after which the researchers measured the volumetric, axial, and

radial shrinkage strains. There are several advantages of the volumetric shrinkage test over conventional linear shrinkage bar test, namely:

- Reduced interference of boundary conditions on the shrinkage.
- Allowance of a larger amount of soil to be tested.
- Better simulation of the compaction states of the moisture content—dry density conditions.

This method was published in an ASTM geotechnical testing journal (Puppala et al. 2004), signifying the importance of this method being accepted by the researchers and practitioners.

Volumetric shrinkage tests were conducted to measure the decrease in the total volume of the soil specimens due to the loss of moisture content from the predetermined initial moisture content to a completely dry state. Three different initial moisture contents (dry of optimum, optimum, and wet of optimum) were used as the initial compaction conditions. Tests were conducted as per the procedure outlined in Puppala et al. (2004). Specimen preparations were performed by mixing the air-dried clay with an appropriate amount of water added to achieve the designed water contents, compacting the soil specimens in 2.26 in. (57 mm) diameter by 5 in. (127 mm) high molds, and measuring the initial height of the specimens. The specimens were cured in the molds at room temperature for 12 hours and then transferred to an oven at a temperature of 220°F (104°C) for 24 hours. The researchers then manually measured the average height and radial of the shrunken soil specimens; the test results are shown in Table 3.4.

Table 3.4. Volumetric Shrinkage Strain Results.

Moisture Condition	Shrinkage Strain (%)	
	Soil Layer 2 1.0–3.0 ft (0.9–1.5 m)	Soil Layer 3 3.0–5.0 ft (1.5–3.0 m)
95% Dry of OMC		
Vertical	1.93	1.34
Radial	1.70	1.19
Volumetric	5.24	3.68
OMC		
Vertical	3.01	1.87
Radial	1.97	1.73
Volumetric	6.79	5.22
95% Wet of OMC		
Vertical	4.37	2.91
Radial	2.19	2.58
Volumetric	8.51	7.85

Overall, these test results indicate that the present soils undergo large volumetric shrinkage strains when subjected to drying. Such strains are expected to induce problematic soil conditions in the field during drought type situations.

Swell Pressure Tests

Swell pressure tests were also conducted on all soil samples using a 1-D consolidation setup and Test Method ASTM D 4546-96 titled “Standard Test Methods for One-Dimensional Swell or Settlement Potential of Cohesive Soils.” These results were used in the estimation of uplift forces. According to Sridharan et al. (1986) and Fredlund and Rahardjo (1993), the swell pressure tests are performed by measuring maximum loads or pressures at which these soils do not exhibit any volume change. Once the sample stops expanding, the pressure at that time is considered as the maximum swell pressure. In the specimen preparation phase, soil specimens were compacted to have the same density and moisture content in the field. Also, the specimens were kept in the moisture room at least 24 hours to make the moisture inside the specimens homogeneous before the tests. Swell pressure test results are presented in terms of ksf (kilopounds per square foot) values as shown in Table 3.5.

Table 3.5. Swell Pressure Test Results.

Soil Sample	Swell Pressure, ksf (kPa)
Soil Layer 2 (1–3 ft)	1.28 (61.2)
Soil Layer 3 (3–5 ft)	0.49 (23.3)

From Table 3.5, the swelling pressures of Layer 2 are higher than those of Layer 3. This is in agreement with the Plasticity Index of these clays. Overall, the swell pressure values measured for Layers 2 and 3 are considerable to potentially pose a problem in the field.

Soil Suction Measurement by Pressure Plate and Filter Paper Techniques

Soil suction measurements were measured on the soils at different compaction moisture content conditions in order to establish a Soil Water Characteristic Curves (SWCCs) for all soil types. The main reason for considering the SWCCs is to include these results for estimating the shear strength properties of unsaturated soil conditions in the real field conditions.

The SWCC describes a unique relationship between matric suction and moisture content of soils. In unsaturated soil mechanics, the SWCC is used directly and indirectly to interpret soil strength, permeability and volume change related characteristics (Fredlund et al. 1994). The curve depends on the size and distribution of the pore structures in the soils, which control the permeability and amount of volume changes expected in the soil (Fredlund et al. 1994). The water content defines the amount of water contained in the soil pores, which can be expressed as gravimetric water content, w , volumetric water content, θ , or degree of saturation, S . There are many types of methods using filter paper, Tempe cell, and pressure plate to measure SWCCs of unsaturated soils. In this study, both pressure plate and filter paper methods were used to generate the SWCC results over a wide range soil suctions expected in the field.

Pressure Plate Method

A pressure plate consists of a pressure vessel with a saturated high-air entry ceramic disk as shown in Figures 3.12 and 3.13. In the test, the applied pressure cannot exceed the air entry value of the disk. The air will not be able to pass through the saturated high-air entry disk (HAE), which means the matric suction does not go beyond the air entry value of the disk (Aung et al. 2001). In applying pressure, air is supplied within the pressure vessel and the lower part of the

high-air entry disk which is connected to a burette of water under atmospheric pressure. As shown, a small water reservoir is formed below the plate using an internal screen and a neoprene diaphragm. The water reservoir is vented to the atmosphere through an outflow tube located on top of the plate, thus allowing the air pressure in the vessel and the water pressure in the reservoir to be separated across the air-water interfaces bridging the saturated pores of the HAE material (Lu and Likos 2004). Therefore, the applied matric suction can be represented from this test by the applied air pressure subtracted from the atmospheric pressure from the water below the disk. The test was stopped when the outflow of the water connected from the tube ceased. The pressure vessel was opened and the water content of one or more of the specimens was measured, generating one point on the soil-water characteristic curve. The current pressure plate device at UTA is limited in that it can only measure matric suction up to 1,000 kPa.

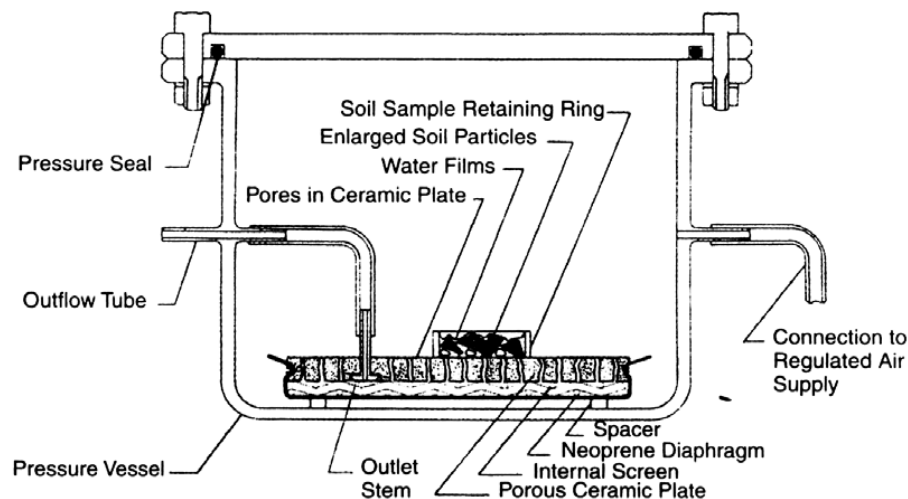


Figure 3.13. Schematic Drawing of Pressure Plate Apparatus (Soil-Moisture Equipment Corp. 2003).

Filter Paper Method

The Filter Paper method is based on the principle that the relative humidity inside the container will be controlled by the soil water content and suction. The Filter Paper method can evaluate both matric and total suction (total suction is a summation of matric suction and osmotic suction). For total suction, a filter paper (Whatman No. 42) is suspended on a perforated disk in the headspace above the specimen and below the container lid such that the moisture transfer occurs in the vapor phase. The equilibrium amount of water absorbed by the filter paper is a function of the pore-air relative humidity and the corresponding total soil suction. For matric

suction, a filter paper (Whatman No. 42) located between two separator papers is contacted directly with water from the soil specimen so that the equilibrium can be achieved by exchanging vapor moisture between the soil and the filter paper (see Figure 3.14). The soil sample and filter paper are allowed to equilibrate for a period of at least seven days at a constant temperature of $25^{\circ} \pm 1^{\circ}\text{C}$.

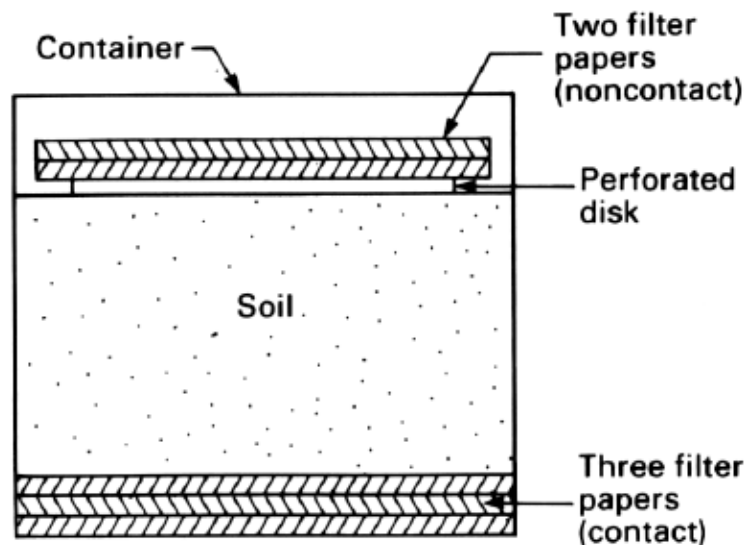


Figure 3.14. Contact and Noncontact Filter Paper Methods for Measuring Matric and Total Suction, Respectively (Al-Khafaf and Hanks 1974).

After equilibrium has been reached, the suction in the filter paper will be the same value as that in the soil. At the end of the equilibrium period, the filter paper is rapidly removed and its water content was determined by precise weighing (± 0.0001 g) before and after oven drying.



Figure 3.15. Weighing Balance Used in Measuring the Weight of the Filter Papers.

Calibration of the Filter Paper Test

The filter paper is used as passive sensors to determine the matric and total suctions by absorbing moisture which evaluates the soil suction by using filter paper calibration curves or equations. The calibration curve for this test depends on a specific filter paper (e.g., Whatman No.42 or Schleicher and Schnell, No. 589), which can be found by measuring the water content of the filter paper when it reaches equilibrium with a salt solution having a known osmotic suction (Fredlund and Rahardjo 1993; Marinho and Oliveira 2006; Power et al. 2008). Therefore, in order to create SWCCs, several water content points from filter papers (w_f) should be used to determine the corresponding suctions by substituting them into the equations shown below and creating a graph of filter paper water content (%) against their corresponding suction values (kPa). Many matric suction equations already exist for the Whatman No. 42 filter paper; hence, this method was used to determine high suction values. Based on the ASTM D5298-03, the two most commonly used filter papers are the Whatman No. 42 and the Schleicher and Schnell 589. Figure 3.16 shows the calibration curves for both types of filters.

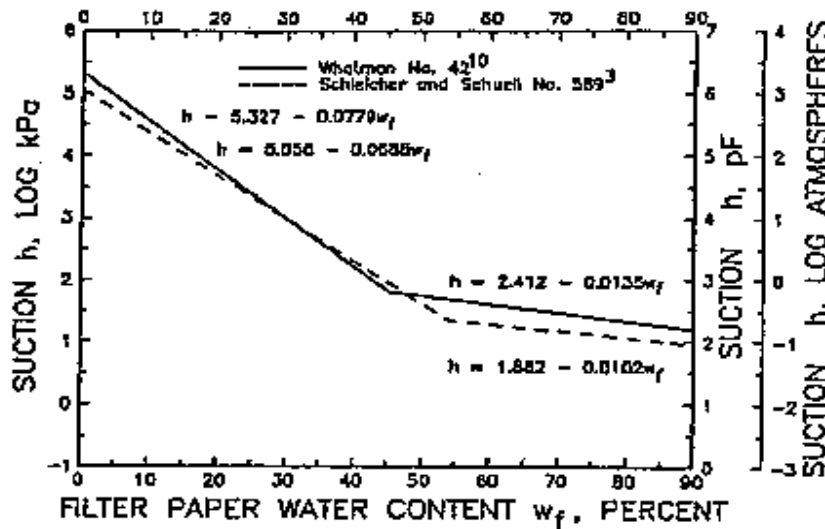


Figure 3.16. Calibration Suction-Water Content Curves for Filter Papers.

Researchers used the matric suction calibration curve using the Whatman No. 42 filter papers for this study. The equations of the matric suction calibration curve for the Whatman No. 42 filter paper are:

$$\log h = 5.327 - 0.0779w_f, \quad \text{for } w_f < 45.3\% \quad (22)$$

$$\log h = 2.412 - 0.0135w_f, \quad \text{for } w_f \geq 45.3\% \quad (23)$$

Specimen Preparation

All the specimens used in the Filter Paper test were prepared at the same density and moisture content as well as in saturated states. In this research, two specimens were used for establishing the SWCCs. For the saturated specimens, Figure 3.17 shows the Pressure Plate test that was used. For the unsaturated but field moist specimens, the Filter Paper test was conducted as shown in Figure 3.18. The pattern of specimen preparation that Perez (2009) developed was used in this research. Perez (2009) showed that the advantages of this pattern results in a drastic reduction of specimens required for one SWCC by being able to get the exact moisture of a soil specimen from the drying process, and being able to use undisturbed soil samples.

For the filter paper specimen preparation, soil specimens are extruded from the field sampler and then cut perpendicular to the field specimen. After that, the specimens are wrapped in plastic paper. Three papers are set into the bottom of the container, the soil specimen placed directly on top of these three papers, a perforated disk is placed on top of the soil specimen, two more papers placed on top of the disk, and the lid screwed onto the container. The lid is then sealed around the interface of the lid and container to minimize water vapor evaporation out of the container. All the steps of the specimen preparation can be seen in Figure 3.18. The specimens are kept in the container under constant temperature for 7–10 days. After that, the filter papers are rapidly removed from the container and immediately weighed as described above.

Limitations of the current pressure plate device at UTA restrict the measurement of the matric suction up to only 1,000 kPa. The Filter Paper method can be used over a wide range of suctions up to approximately 10^6 kPa (150,000 psi). Therefore, the Filter Paper method was used to measure the soil suction that had a range more than 1,000 kPa. Thus, both the Pressure Plate and Filter Paper methods were employed in the development of a complete SWCC of the soils used in this study.



Figure 3.17. Pressure Plate Testing.



Figure 3.18. Filter Paper Testing.

The combined test results from the Pressure Plate and Filter Paper methods are presented in the form of SWCCs as shown in Figures 3.19–3.23 for all five soils from the different layer considered in this study as shown in Table 3.1.

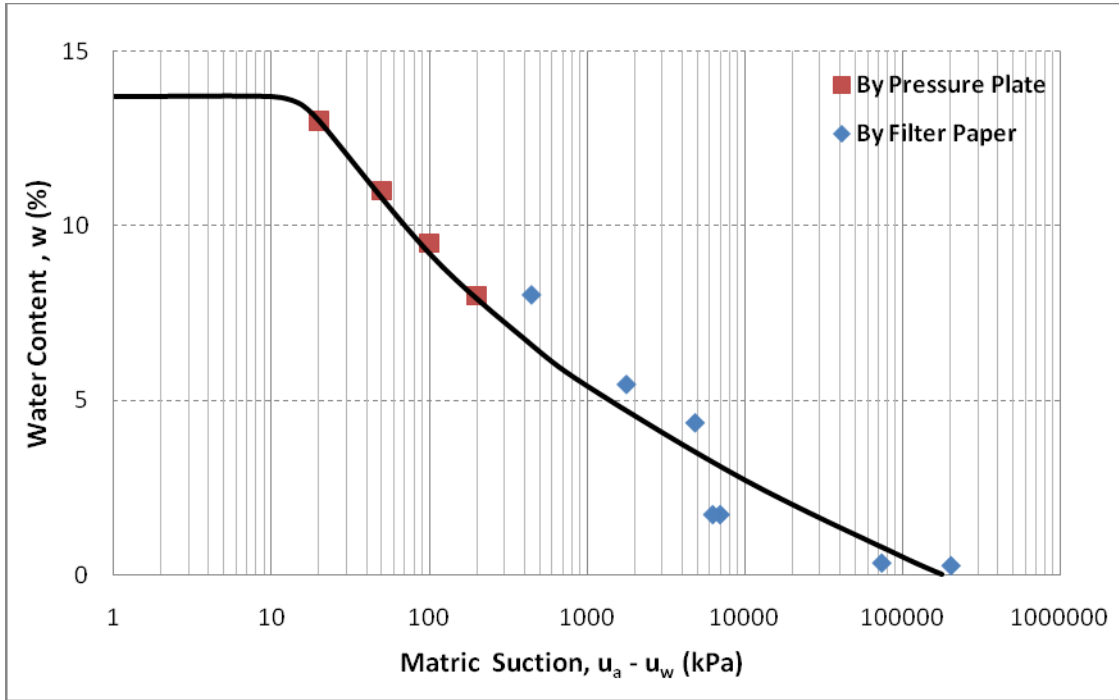


Figure 3.19. SWCC for Soil in Layer 1.

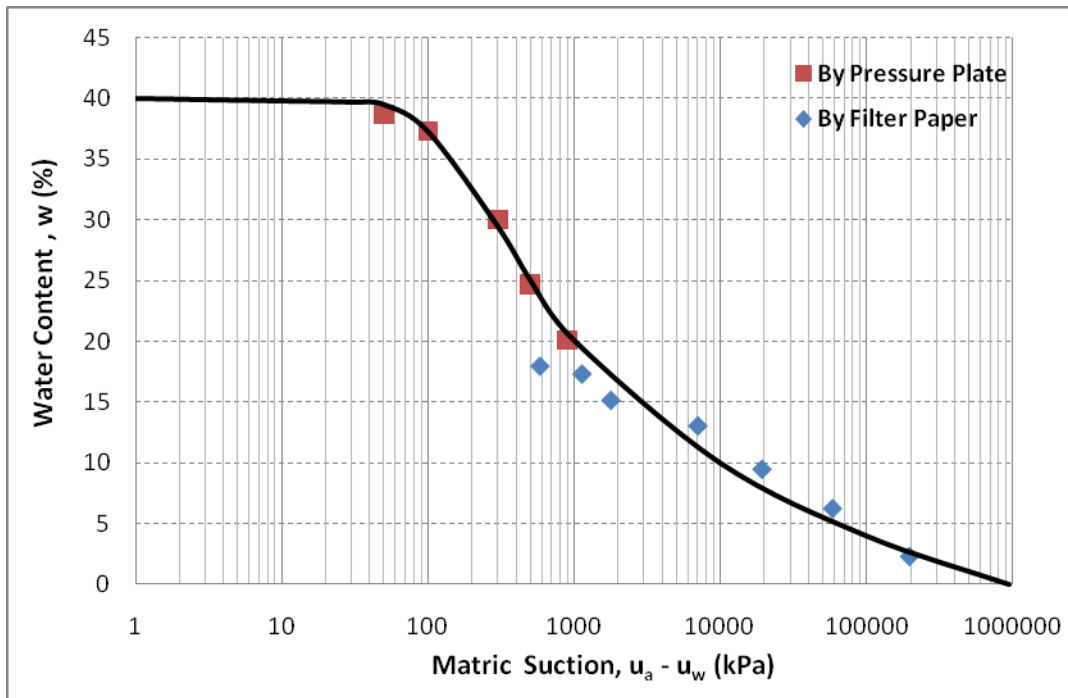


Figure 3.20. SWCC for Soil in Layer 2.

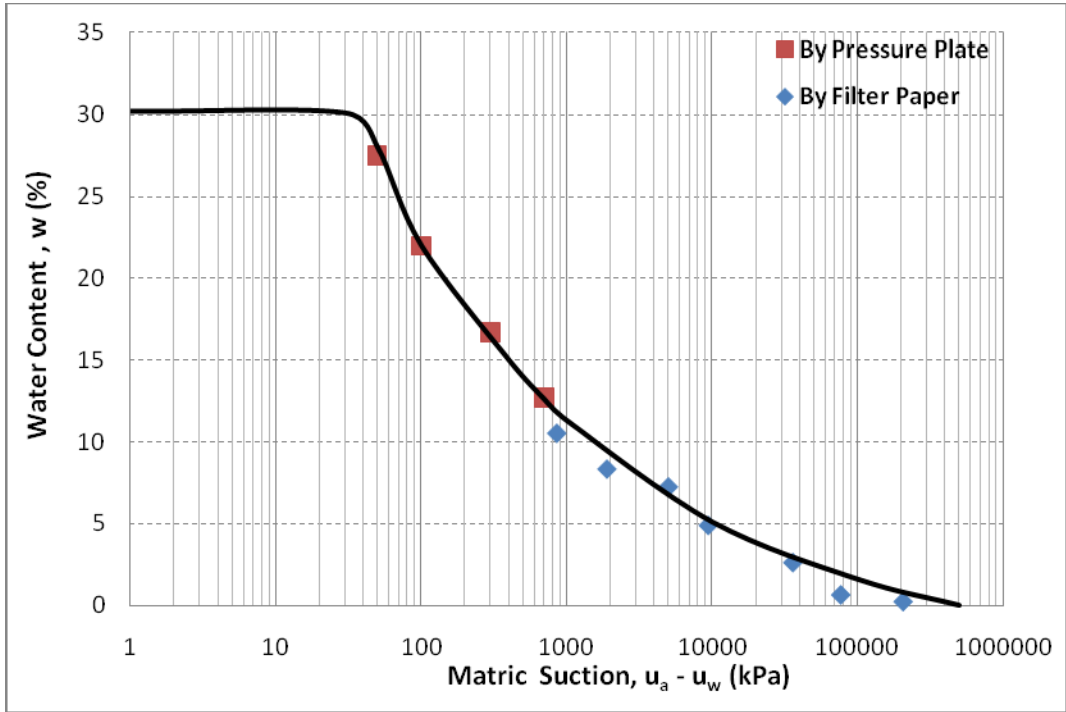


Figure 3.21. SWCC for Soil in Layer 3.

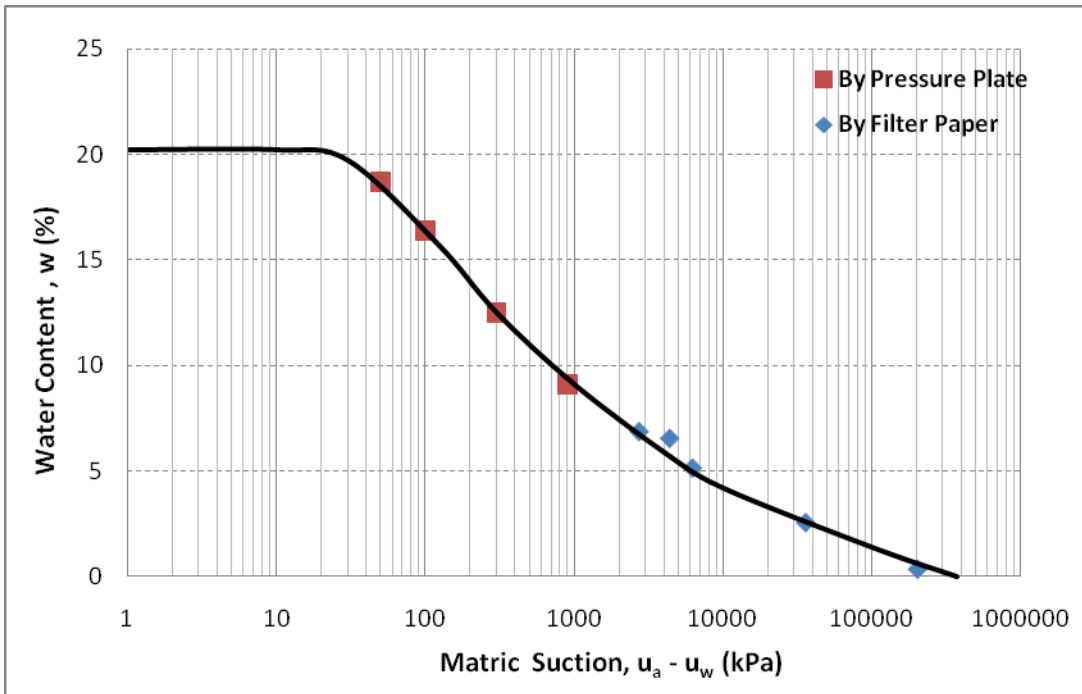


Figure 3.22. SWCC for Soil in Layer 4.

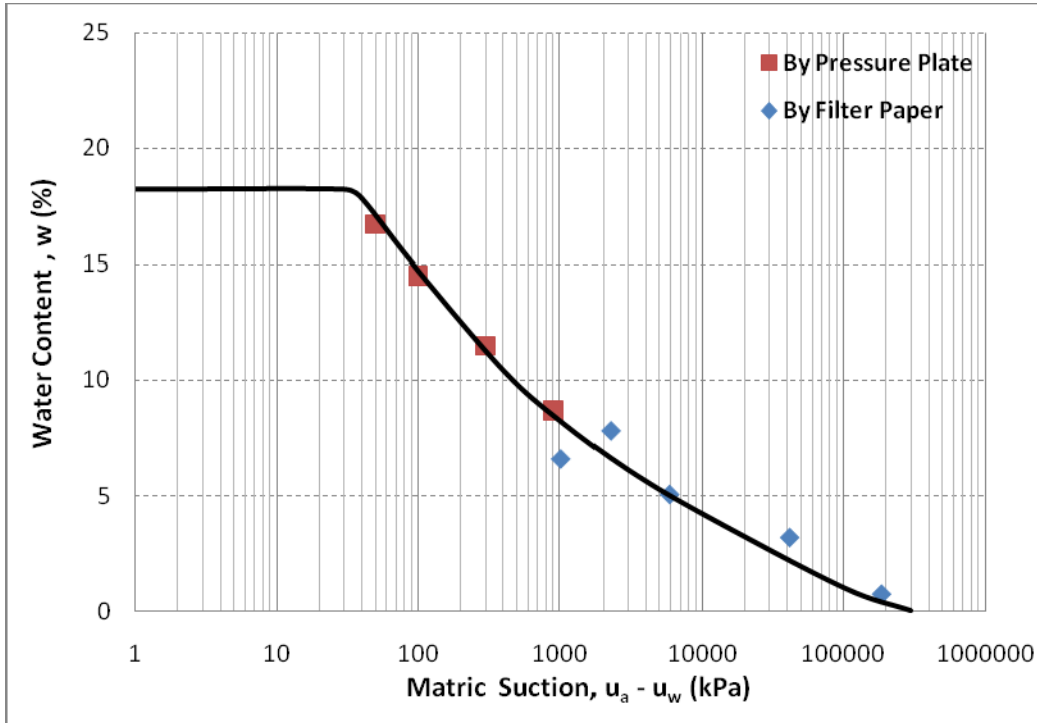


Figure 3.23. SWCC for Soil in Layer 5.

In this suction testing, soil in Layer 2 is CH while the rest of the soils are CL as shown in Table 3.1. The SWCCs of all five types of soils exhibited similar shapes. The only noticeable difference is the saturated moisture content (at zero suction) between CL and CH for soil from layer 3, 4, 5 versus layer 2, which has saturated moisture content much lower than the soil from layer 2. This lower value indicates less ability to hold up water or moisture, which means that they do not undergo large swelling when hydrated.

SHEAR STRENGTH PARAMETER TESTS (DIRECT SHEAR AND UNCONSOLIDATED-UNDRAINED TEST)

Both direct shear and UU triaxial tests were conducted to determine the shear strength and stress-strain relationships of the soils. These results are used to model the foundation tests using the field conditions close to the failures that have been occurring. To find cohesion, c , and angle of internal friction, ϕ for both silty sand and clayey soil, two tests—Direct Shear and Triaxial tests—were conducted to determine these parameters. Both test methods are summarized below.

Direct Shear Tests

This experiment is a simple method for finding shear stress and friction angle of soils. Researchers performed this test using the ASTM D 3080-98 method. Generally, the specimen can be cubical or cylindrical. The shape conducted in this test was cylindrical. Normal forces used for the Direct Shear test were 2000, 4000, and 8000 psf. The specimen tested was the silty sand located in the first layer (0–3 ft). For specimen preparation, all three specimens were prepared at the same density and moisture content as measured in the field. Figure 3.24 shows the equipment and soil specimen used in the test.



Figure 3.24. The Direct Shear Test Setup and Compacted Silty Sand Used in the Test.

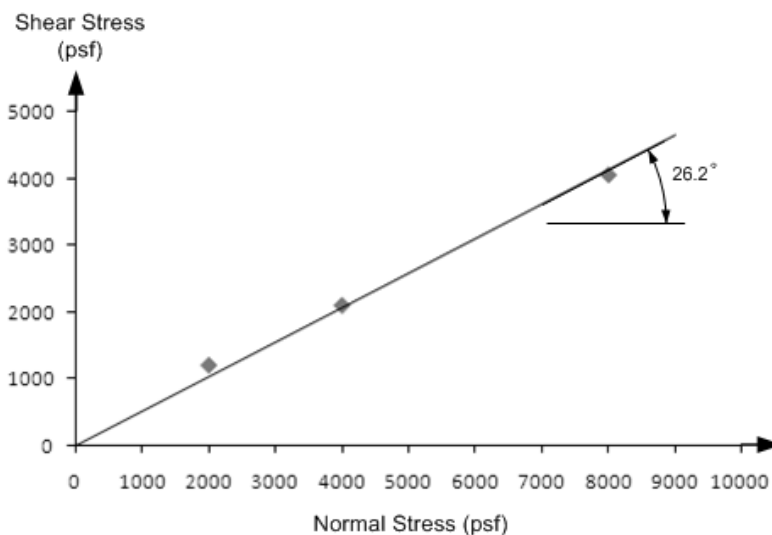


Figure 3.25. Shear Strength versus Effective Normal Stress for the Silty Sand.

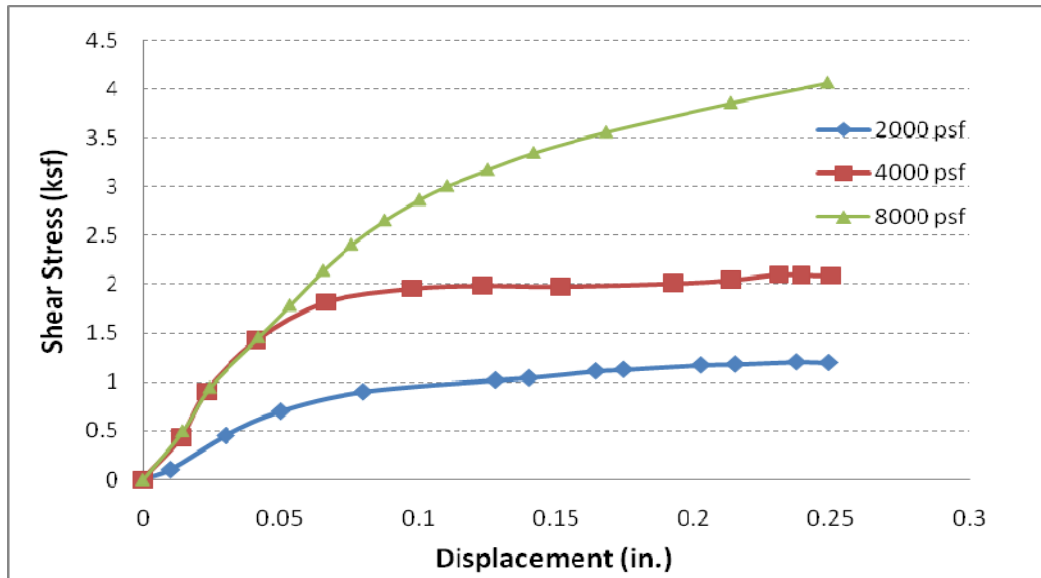


Figure 3.26. Shear Stress versus Horizontal Displacement for the Silty Sand.

Unconsolidated-Undrained or UU Triaxial Tests

The unconsolidated-undrained test is used to find shear strength parameter (c and ϕ). This test was performed using Test Method ASTM D 2850-95 (2003), titled “Standard Test Method for Unconsolidated-Undrained Triaxial Compression Test on Cohesive Soils.” The test procedure requires the placement of a cylindrical specimen sealed by the rubber membrane in the triaxial chamber and applying confining pressure by not allowing water to dissipate from the specimen. After that, the specimen is tested by increasing the axial (vertical) stress. Figure 3.27 shows the failed specimen. Tests were performed in two case scenarios. The first one is unsaturated case. In this case, all the specimens are prepared at the same density and having the same moisture content as in the field. After preparation, the specimens were cured in the moisture room for seven days to make the moisture inside specimen be homogeneous. For the second case, researchers used saturated soil specimens. All the specimens are prepared at the same density and moisture content as in the first. However, when the specimens have been compacted, these are kept in the water for two weeks to saturate the whole specimens.



Figure 3.27. The Failed Specimen Performed by Triaxial Test.

Unsaturated Case

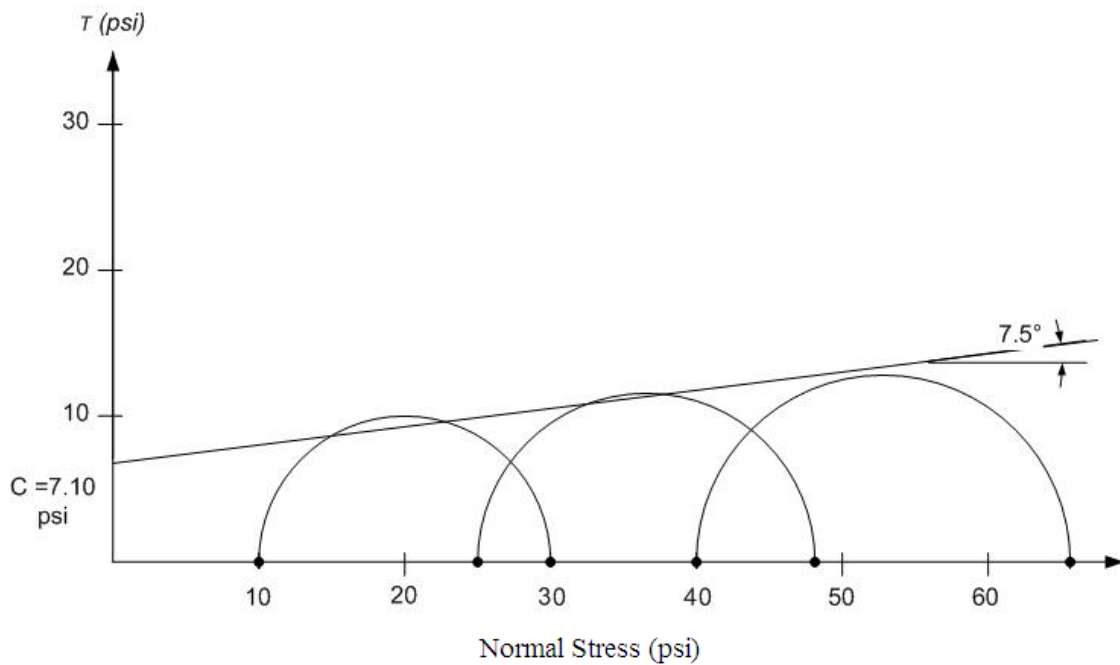


Figure 3.28. Mohr's Circle at Failure for 10, 25, and 40 Psi Confining Pressure of Soil Layer 2.

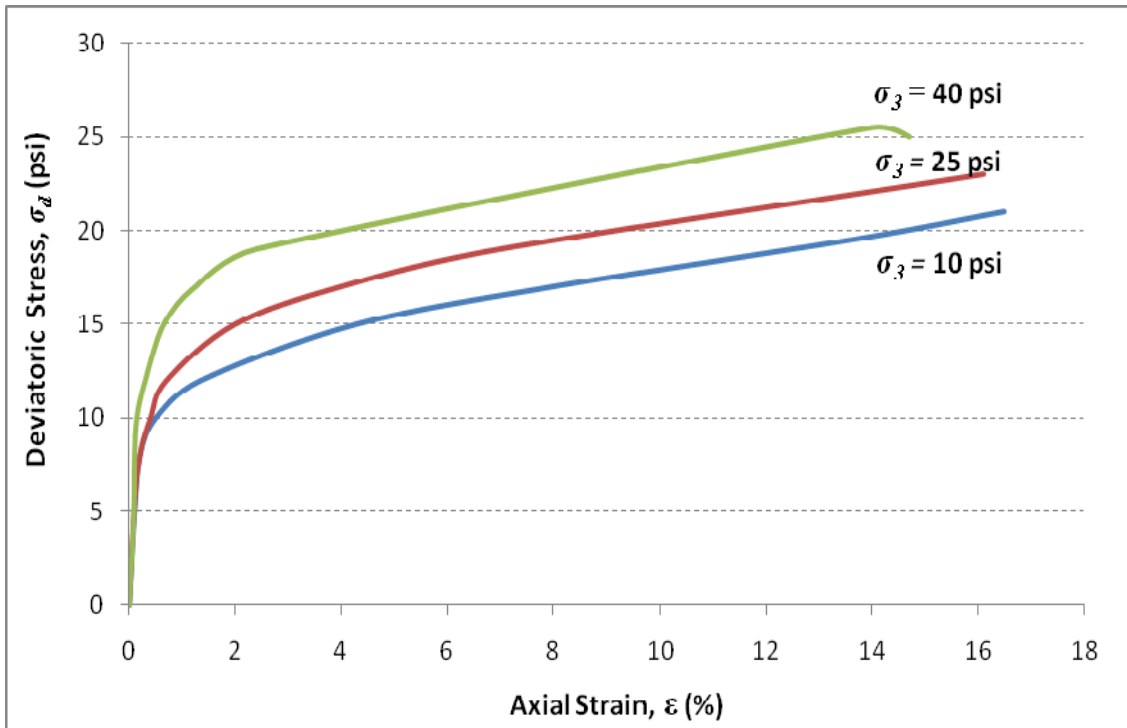


Figure 3.29. Triaxial Plot for 10, 25, and 40 Psi Confining Pressure of Soil Layer 2.

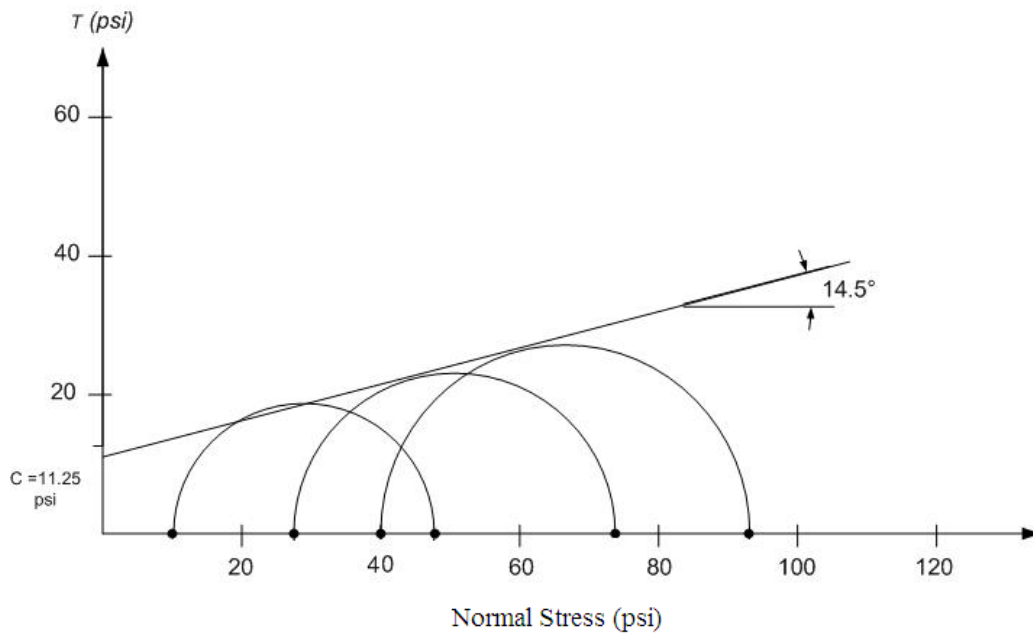


Figure 3.30. Mohr's Circle at Failure for 10, 25, and 40 Psi Confining Pressure of Soil Layer 3.

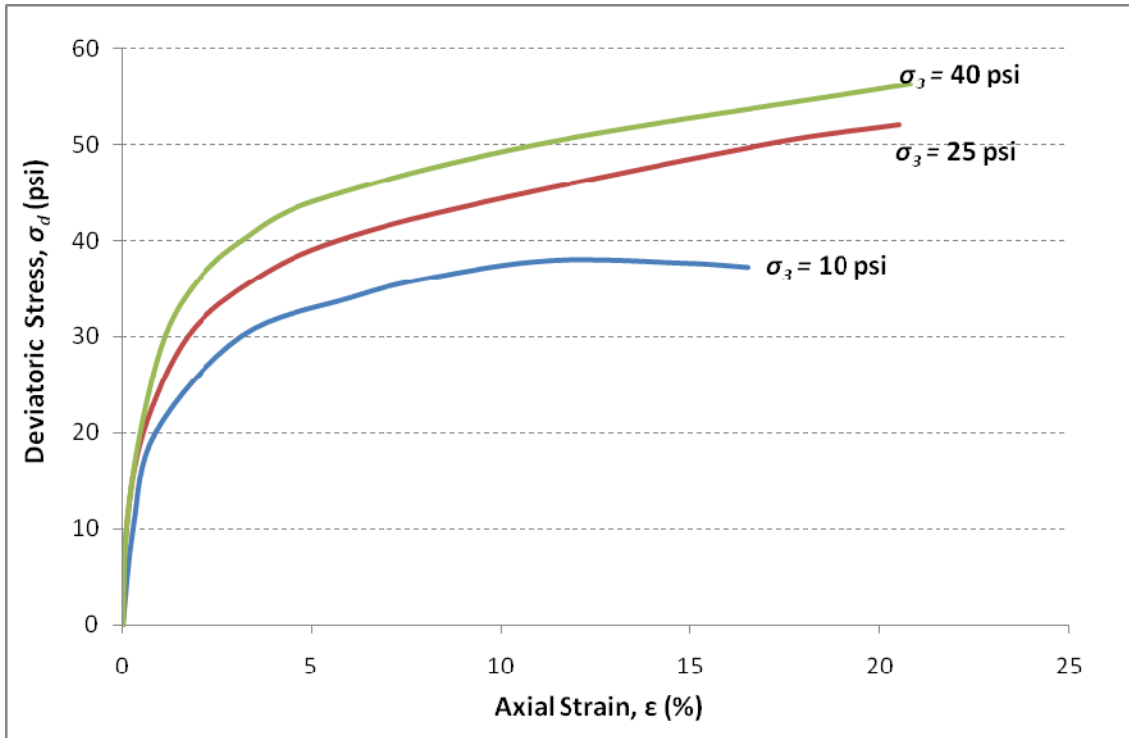


Figure 3.31. Triaxial Plot for 10, 25, and 40 Psi Confining Pressure of Soil Layer 3.

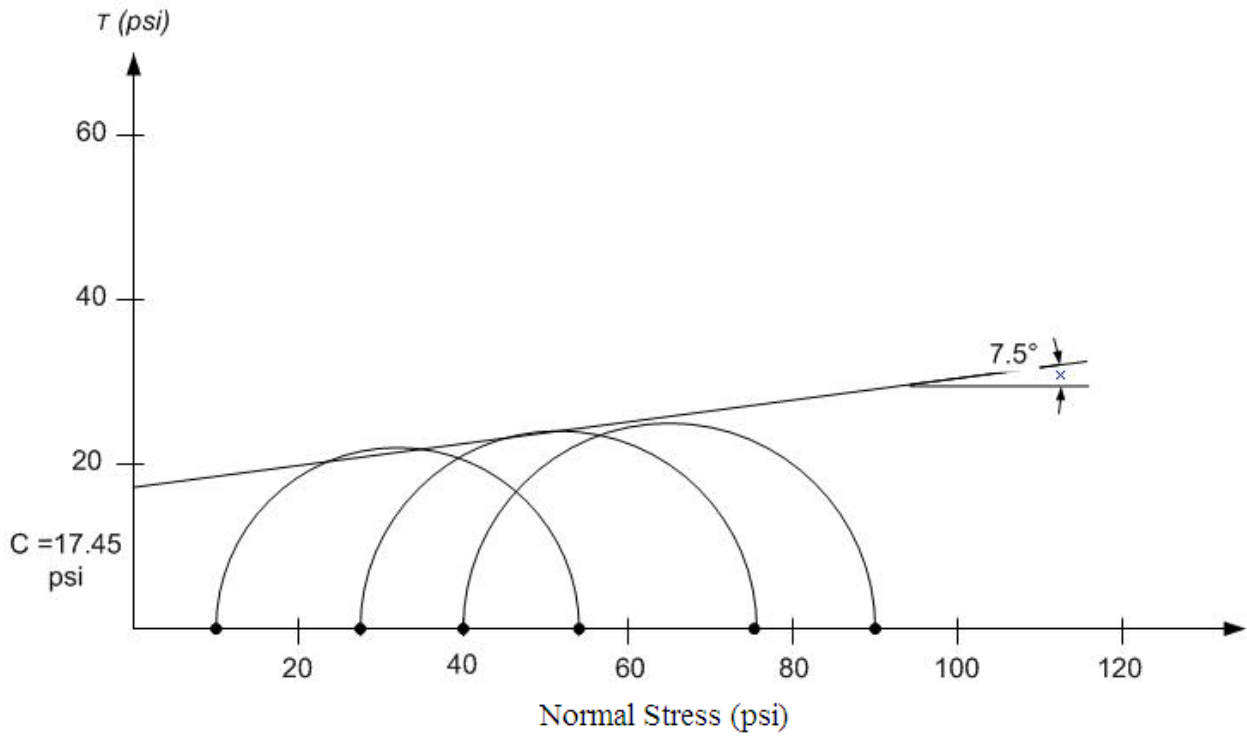


Figure 3.32. Mohr's Circle at Failure for 10, 25, and 40 Psi Confining Pressure of Soil Layer 4.

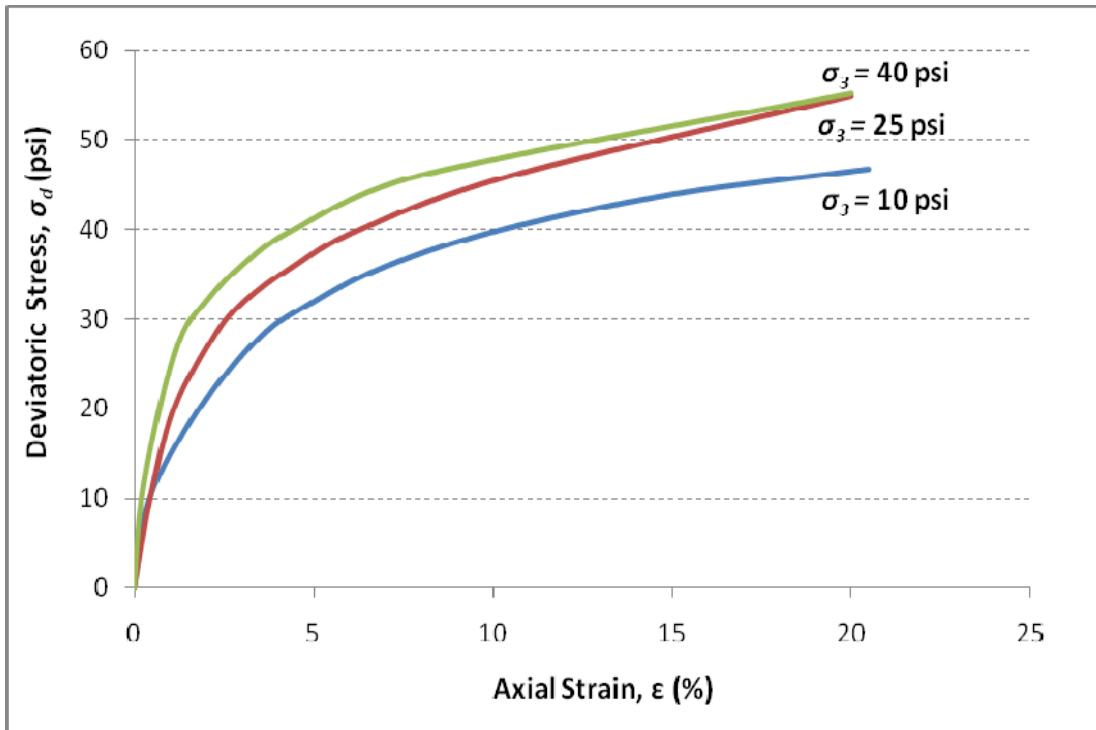


Figure 3.33. Triaxial Plot for 10, 25, and 40 Psi Confining Pressure of Soil Layer 4.

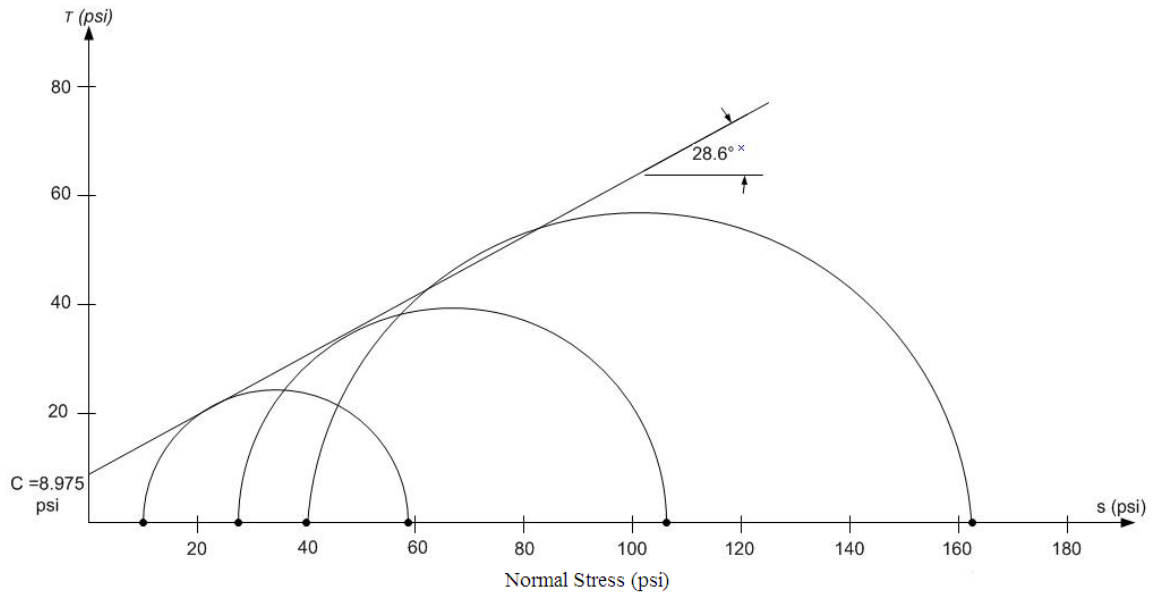


Figure 3.34. Mohr's Circle at Failure for 10, 25, and 40 Psi Confining Pressure of Soil Layer 5.

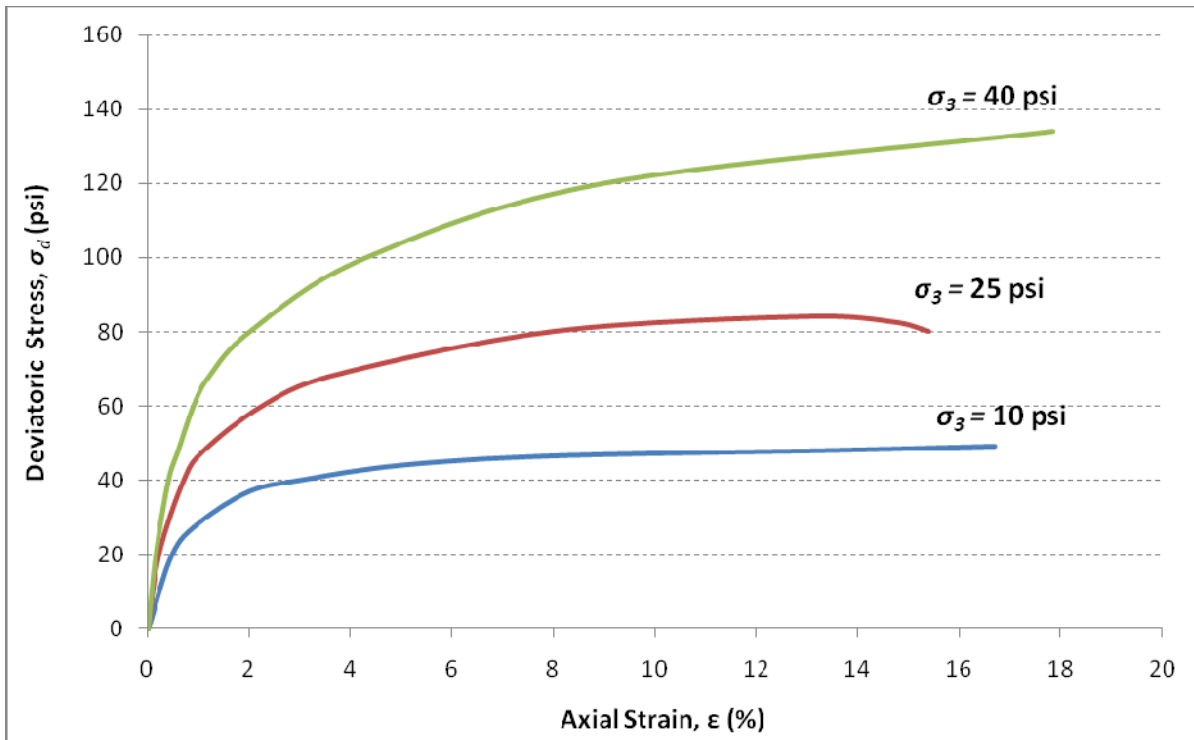


Figure 3.35. Triaxial Plot for 10, 25, and 40 Psi Confining Pressure of Soil Layer 5.

Table 3.6 summarizes the test results from the Direct Shear and Unconsolidated-Undrained Triaxial tests for soils tested in unsaturated conditions.

Table 3.6. Direct Shear and Unconsolidated-Undrained Test Results for Unsaturated Cases.

Depth (ft)	Total Density (pcf)	Cohesion, c (psi)	Friction, ϕ , (°)
0–1.0	110.38	0	26.2
1.0–3.0	119.54	7.10	7.5
3.0–5.0	124.57	11.25	14.5
5.0–10.0	137.87	17.45	7.5
> 10.0	125.27	8.98	28.6

Saturated Case

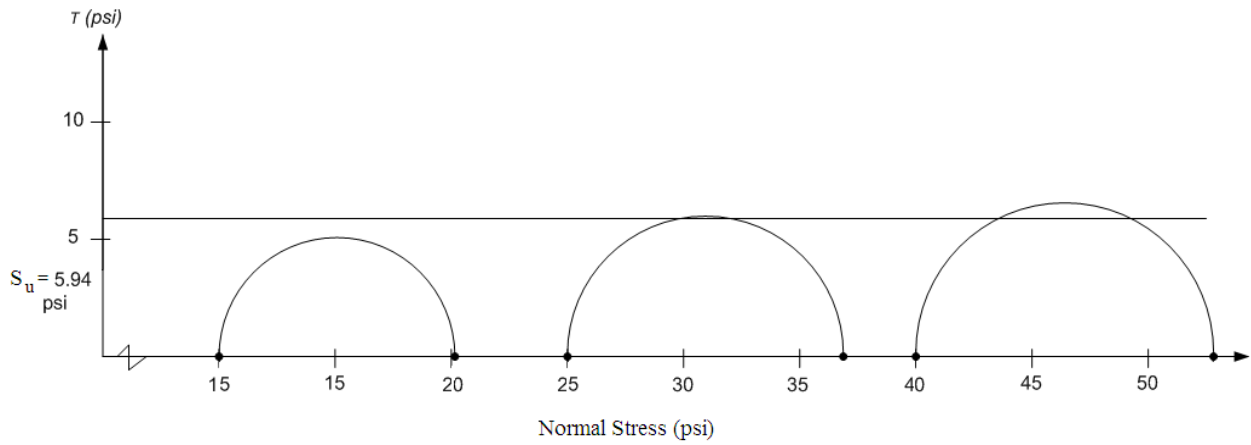


Figure 3.36. Mohr's Circle at Failure for 10, 25, and 40 Psi Confining Pressure of Soil Layer 2 in Saturated Case.

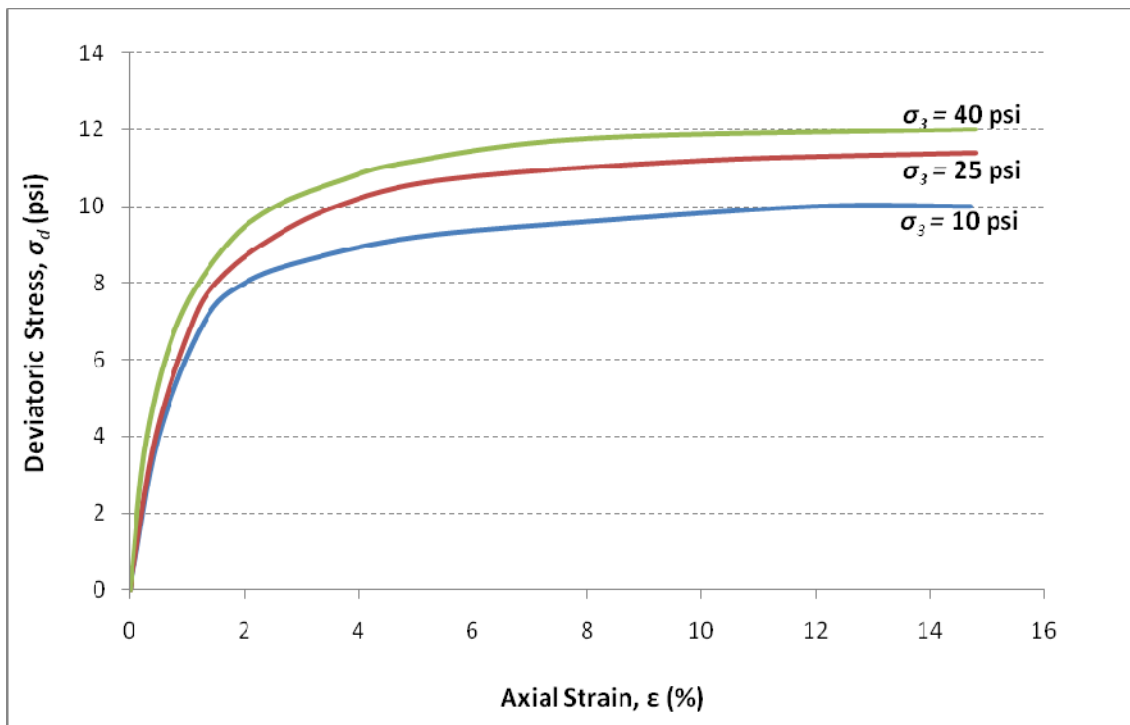


Figure 3.37. Triaxial Plot for 10, 25, and 40 Psi Confining Pressure of Soil Layer 2 in Saturated Case.

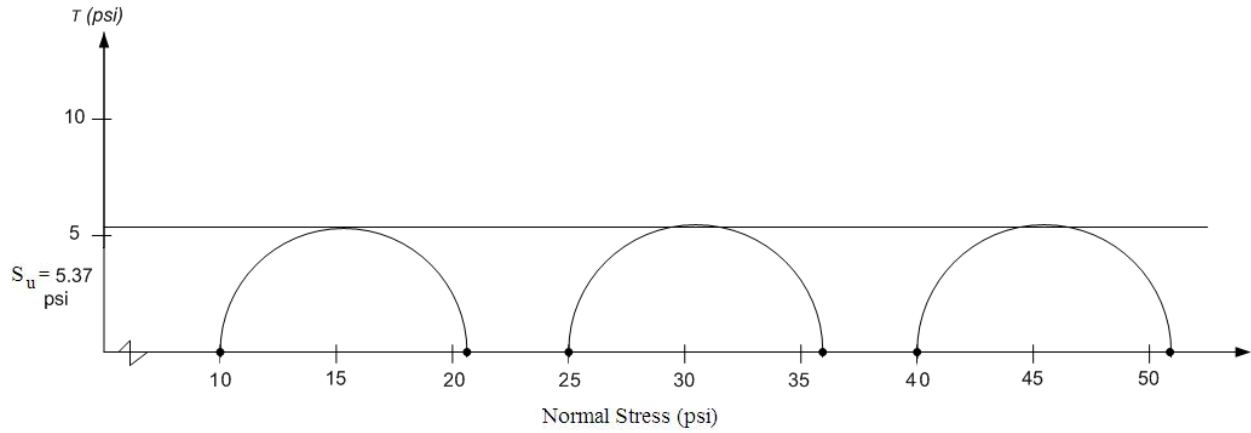


Figure 3.38. Mohr's Circle at Failure for 10, 25, and 40 Psi Confining Pressure of Soil Layer 3 in Saturated Case.

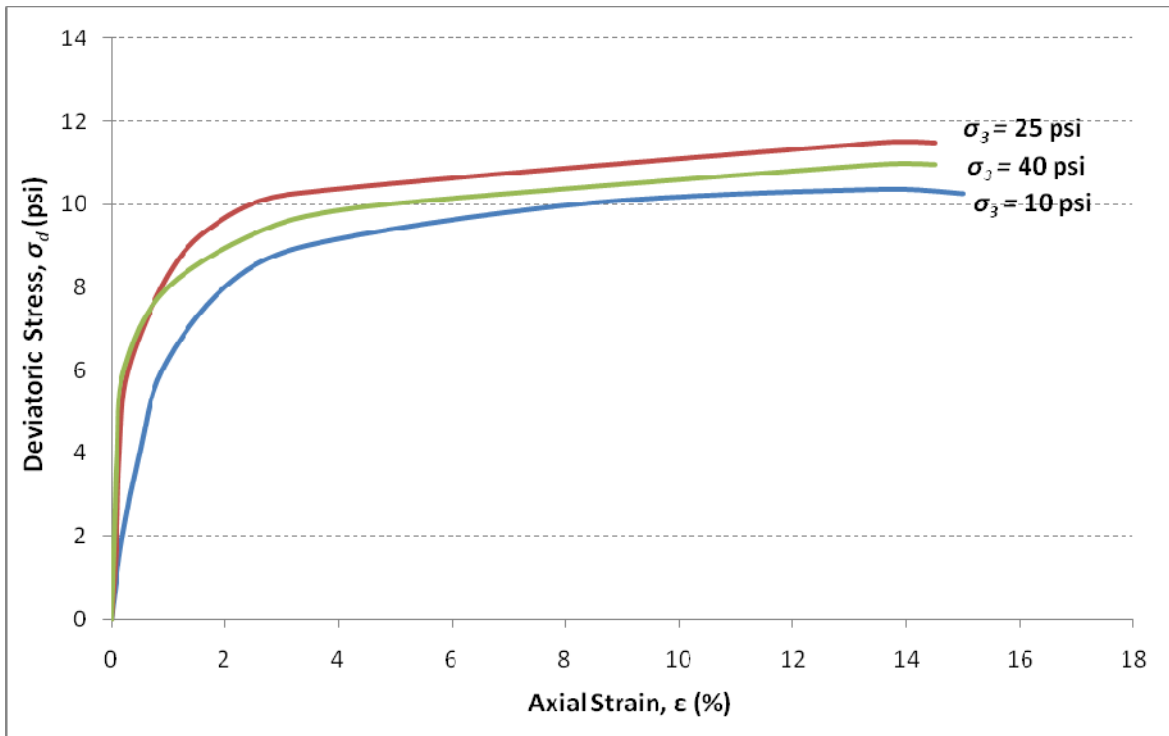


Figure 3.39. Triaxial Plot for 10, 25, and 40 Psi Confining Pressure of Soil Layer 3 in Saturated Case.

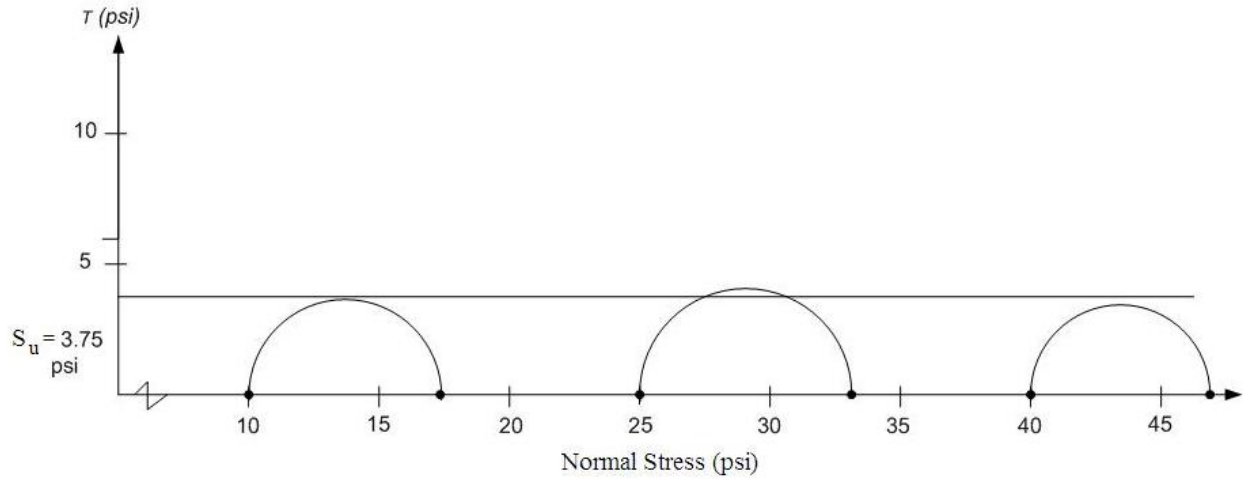


Figure 3.40. Mohr's Circle at Failure for 10, 25, and 40 Psi Confining Pressure of Soil Layer 4 in Saturated Case.

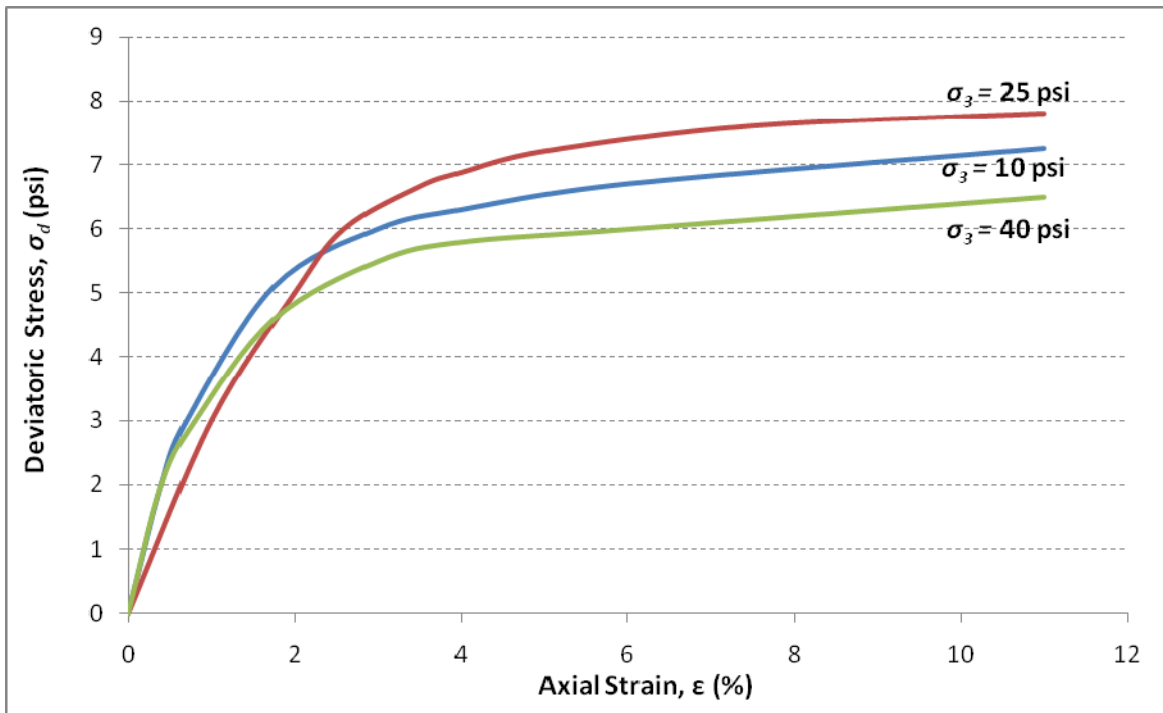


Figure 3.41. Triaxial Plot for 10, 25, and 40 Psi Confining Pressure of Soil Layer 4 in Saturated Case.

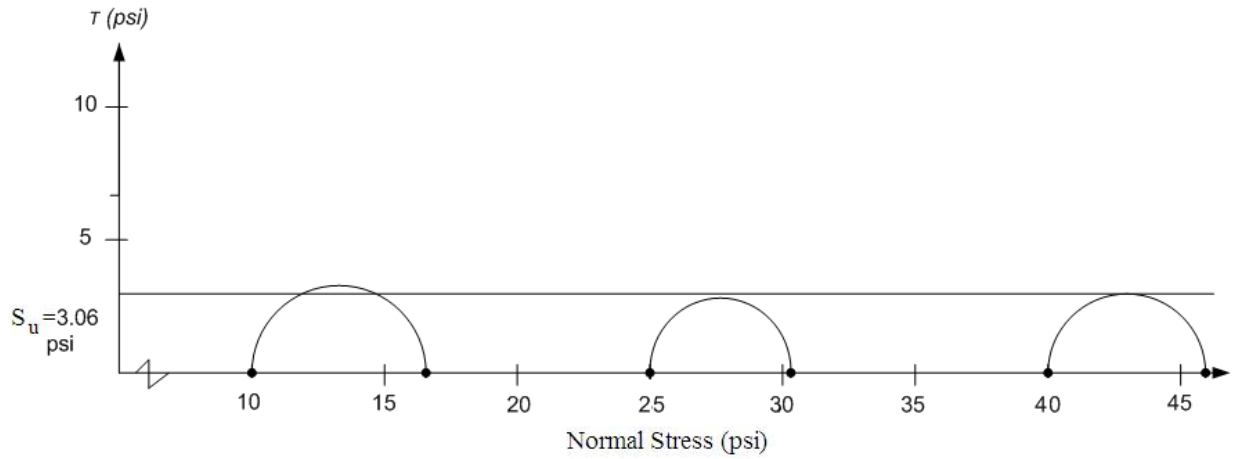


Figure 3.42. Mohr's Circle at Failure for 10, 25, and 40 Psi Confining Pressure of Soil Layer 5 in Saturated Case.

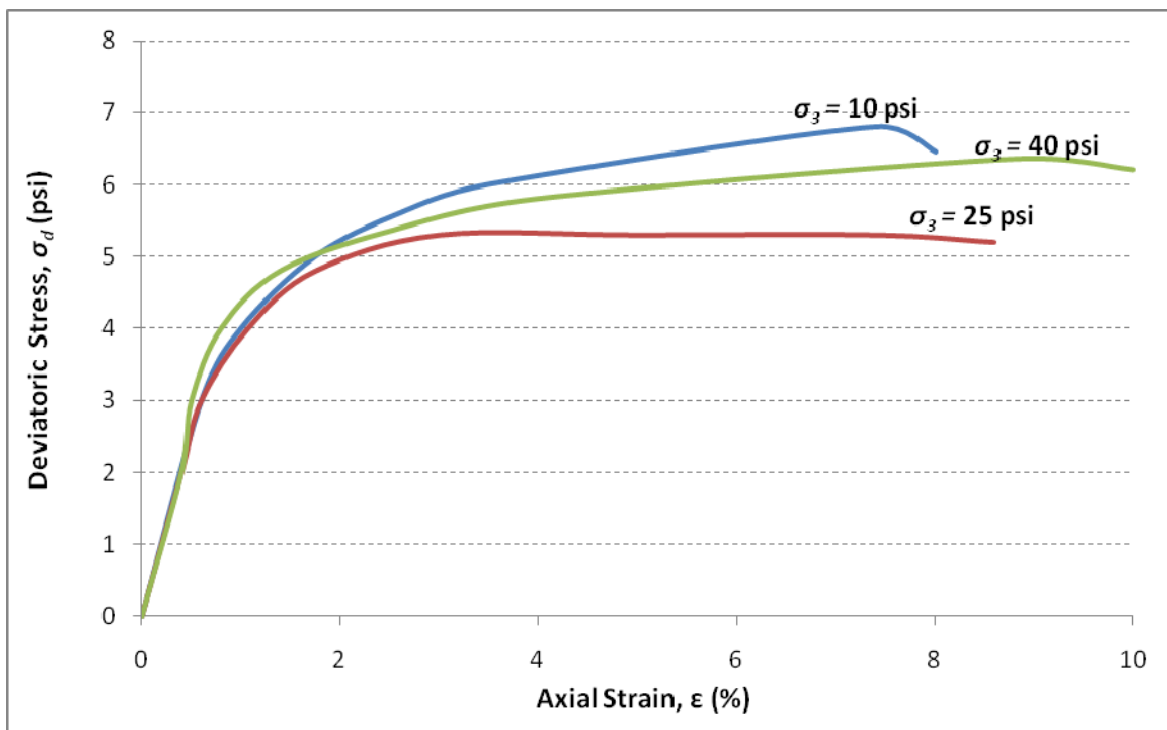


Figure 3.43. Triaxial Plot for 10, 25, and 40 Psi Confining Pressure of Soil Layer 5 in Saturated Case.

Table 3.7 summarizes the test results from the Direct Shear and Unconsolidated-Undrained Triaxial tests.

Table 3.7. Unconsolidated-Undrained Test Results for Saturated Case.

Depth (ft)	Water Content, w (%)	Total Density (pcf)	Undrained Shear Strength, S_u (psi)
1.0–3.0	32.3	119.54	5.97
3.0–5.0	26.3	124.57	5.37
5.0–10.0	19.2	137.87	3.75
> 10.0	17.1	125.27	3.06

SUMMARY

This chapter describes the site details, soil sampling and laboratory tests performed to determine plasticity, swell, and strength properties of various soil strata of the field site. UU triaxial tests were performed to determine the shear strength properties at full saturation to compaction moisture content conditions. Chapter 4 describes the field load testing program.

CHAPTER 4 CONSTRUCTION OF DRILLED SHAFTS AND INCLINED LOAD TEST DESIGN

DESIGN OF FIELD TEST SETUP

UT Arlington performed the design of the drilled shaft load test system. This involved the development of a field setup that would very closely imitate the cable barrier systems TxDOT currently used in the field. The design plan layout, as shown in Figure 4.1, was designed to have the three test sets completely separated from each other to eliminate any chance of influence from any test performed at an adjoining set.

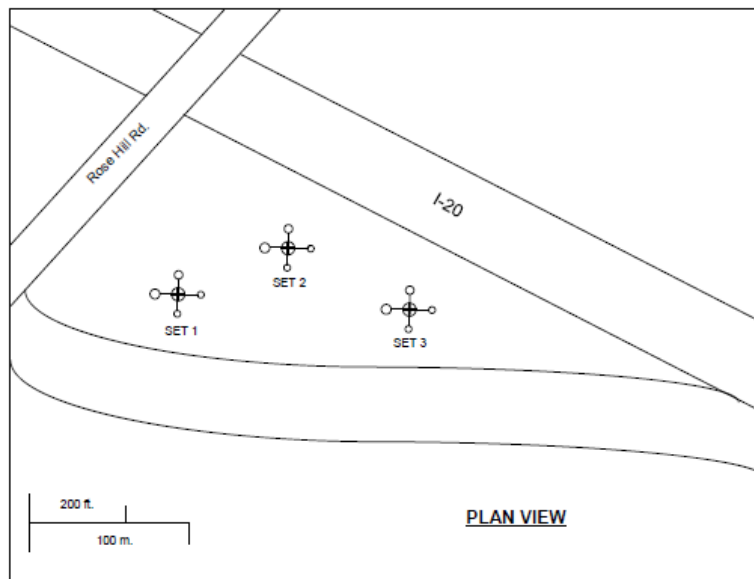


Figure 4.1. Plan View of Design Test Setups.

One full test set system was comprised of one reaction shaft and four test shafts with the clear distance between the reaction shaft and the test shafts at 20 ft (6.1 m). The angle of force acting toward the test shafts was set at 16.1° to copy the angle of the currently installed cable barrier systems. This is one of the few Inclined Load field tests performed in the country based on a thorough Literature Review.

Design of Test and Reaction Shafts

Originally, the dimensions of the drilled shafts that failed in the field were 2 ft (0.6 m) in diameter and 6 ft (1.8 m) deep. To determine the most effective size(s) of drilled shafts to be

required in project plans for expansive soil environments, three different test shaft diameter sizes of 1 ft (0.3 m), 2 ft (0.6 m), and 3 ft (0.9 m), and three different lengths of 6 ft (1.8 m), 10 ft (3.0 m) and 14 ft (4.3 m) were designed. Additionally, the three reaction shafts were designed to be 3 ft (0.9 m) and 4 ft (1.2 m) in diameter and 35 ft (10.7 m) deep.

In lateral load testing, the distance between the test shafts and the reaction shaft is a very important parameter. Stress created in the soil around the reaction shaft during the test can influence the results of the test shafts. A clear distance between each test shaft and the reaction shaft of 20 ft (6.1 m) was selected based on Test Method ASTM D 3966–90, Standard Test Method for Piles under Lateral Loads.

One of the important steps for this testing was to design each reaction shaft such that the loading sequence followed in the procedure would not influence the test results of the test shafts. The reaction shafts are used as foundations to subject the tensile loads to the long Dywidag bar that, in turn, simulates the tension mobilized in the three-cable barrier system. To reiterate, the angle of force acting toward the test shafts was set at 16.1° . The reaction shaft must be rigid enough to resist significant movements during load testing that in no way would affect the test shaft reactions. As a result, L-PILE software was used to compare probable loads expected in the shafts.

Table 4.1 shows predicted results of deflection of all test shafts using the forces calculated from thermal- and swell-induced forces in winter and summer conditions. Based on the analyzed lateral displacements on all shafts, the percent differences in surface lateral movements were determined and are included in Table 4.2.

Table 4.1. Predicted Lateral Deflection of Drilled Shafts at the Ground Surface.

Shaft Number (Diameter × Length)	Deflection at ground surface (in.) (Winter Time)	Deflection at ground surface (in.) (Summer Time)
1 (1 ft × 6 ft)	N.A.	1.26
2 (1 ft × 10 ft)	1.03	0.30
3 (1 ft × 14 ft)	0.91	0.32
4 (2 ft × 6 ft)	N.A.	0.79
5 (2 ft × 10 ft)	0.51	0.15
6 (2 ft × 14 ft)	0.28	0.09
7 (3 ft × 6 ft)	N.A.	0.75
8 (3 ft × 14 ft)	0.22	0.06
Reaction Shafts (Diameter × Length)	Deflection at ground surface (in.) (Winter Time)	Deflection at ground surface (in.) (Summer Time)
3 ft × 35 ft depth	0.10	0.04
4 ft × 35 ft depth	0.05	0.02

Note: N.A. means the deflection of the pile head was high due to the computed deflection being larger than the allowable deflection limit.

From Table 4.1, it was concluded that the first reaction shaft, 3 ft (0.9 m) diameter and 35 ft (10.7 m) deep, can be used with the test shafts of 6 ft (1.8 m) depths. This becomes possible due to the high computed lateral deflections of the short test shafts when compared with small lateral deflection experienced by the reaction shaft. Hence, it was concluded that while performing the lateral load tests, all the test shafts would not be influenced by the movements of the reaction shafts.

Table 4.2. Predicted Percent Differences in Lateral Movements of Reaction Shaft and Test Shaft.

Shaft Number (Diameter × Depth)	Percent difference of lateral movement (%) in Winter		Percent difference of lateral movement (%) in Summer	
	Reaction Shaft 1	Reaction Shaft 2	Reaction Shaft 1	Reaction Shaft 2
1 (1 ft × 6 ft)	N.A.	N.A.	2.8	1.6
2 (1 ft × 10 ft)	9.3	5.1	11.7	6.5
3 (1 ft × 14 ft)	10.5	5.7	11.1	6.2
4 (2 ft × 6 ft)	N.A.	N.A.	4.5	2.5
5 (2 ft × 10 ft)	18.8	10.2	24.3	13.5
6 (2 ft × 14 ft)	33.6	18.3	39.1	21.7
7 (3 ft × 6 ft)	N.A.	N.A.	4.7	2.6
8 (3 ft × 14 ft)	44.0	24.0	56.3	31.3

Note: N.A. means the deflection of the pile head could not be analyzed due to the computed deflection being larger than the allowable deflection limit.

For the larger reaction shaft, 4 ft (1.2 m) diameter and 35 ft (10.7 m) deep, it was also concluded that the load tests could be conducted on test shafts of 10 ft (3.0 m) and 14 ft (4.3 m) depth. This is determined from the predicted percent differences in the lateral deflections which varied from a low of 5 percent to 24 percent, with the high value computed for the winter test condition. For Test Shaft 8 (3 ft [0.9 m] × 14 ft [4.3 m]), the percent difference is slightly high for summer test conditions. Hence, load tests need to be interpreted by considering the influence of the reaction test set movements on the test results.

From the analyzed predictions above, test shafts in the winter condition have higher lateral deflections and bending moments than for the summer condition. Cable tensions in the summer conditions are lower than the winter conditions and the uplift force in the summer season (dry season) are also low, resulting in less deflection values than predicted for the winter conditions.

The field load test system included a means of applying the inclined load plus measuring the lateral load and deflections of the drilled shafts. Figures 4.2 and 4.3 present the overall system, which show the schematics of plan and elevation views of the three test sets and how each one is different from the other two. Appendix A shows the steel rebar reinforcement plans for the test and reaction shafts that were used.

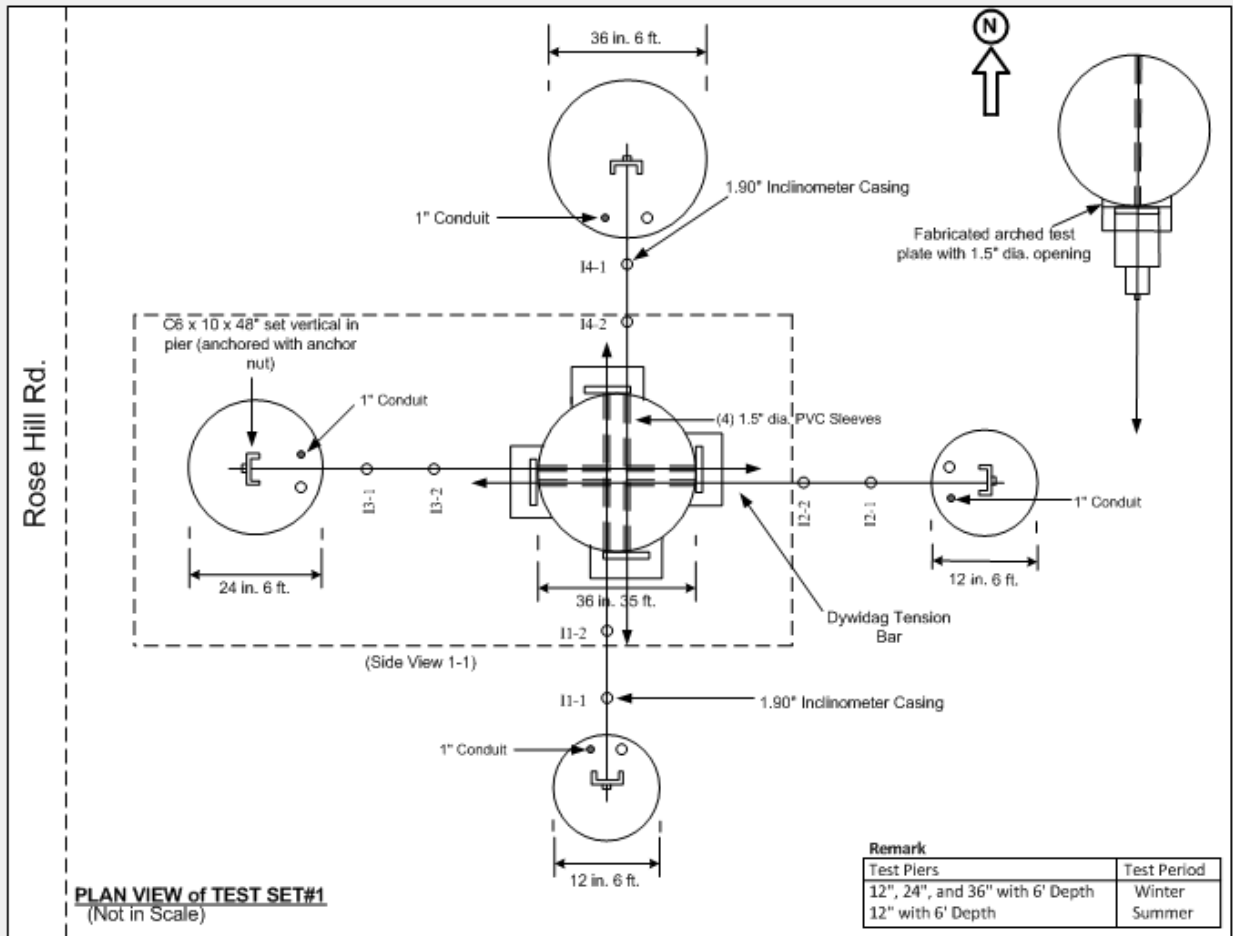


Figure 4.2. Typical Plan Views of Test Setup.

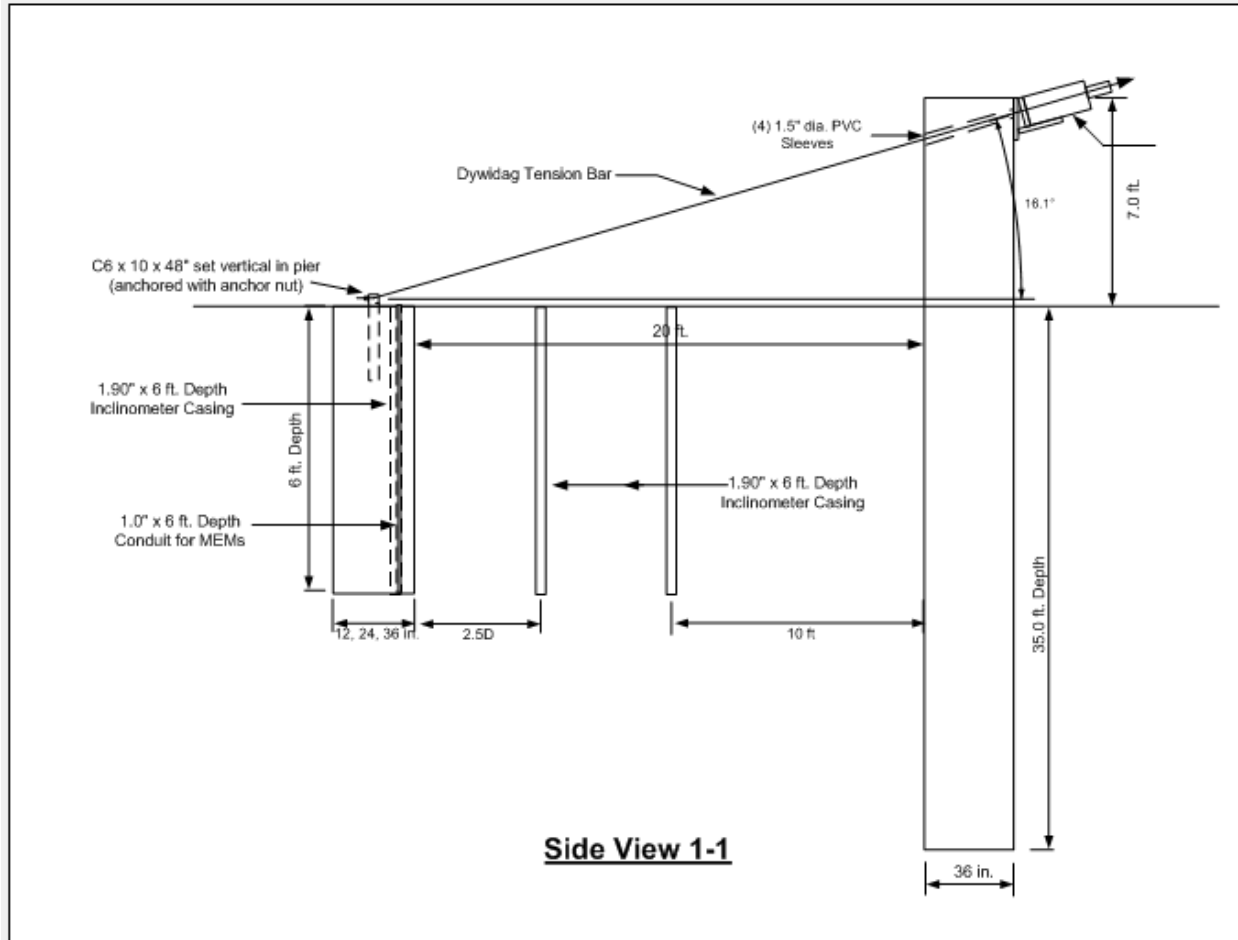


Figure 4.3. Typical Elevation Views of Test Setup.

CONSTRUCTION TEST SETUP

The drilled shaft installation plan was not constructed according to design, but was modified in the field to accommodate the speed of construction with the available equipment. Figure 4.4 shows the final test sets that were constructed. The required spacing between the test and reaction shafts were retained per the design requirements and were not expected to influence the loading nor the final results.

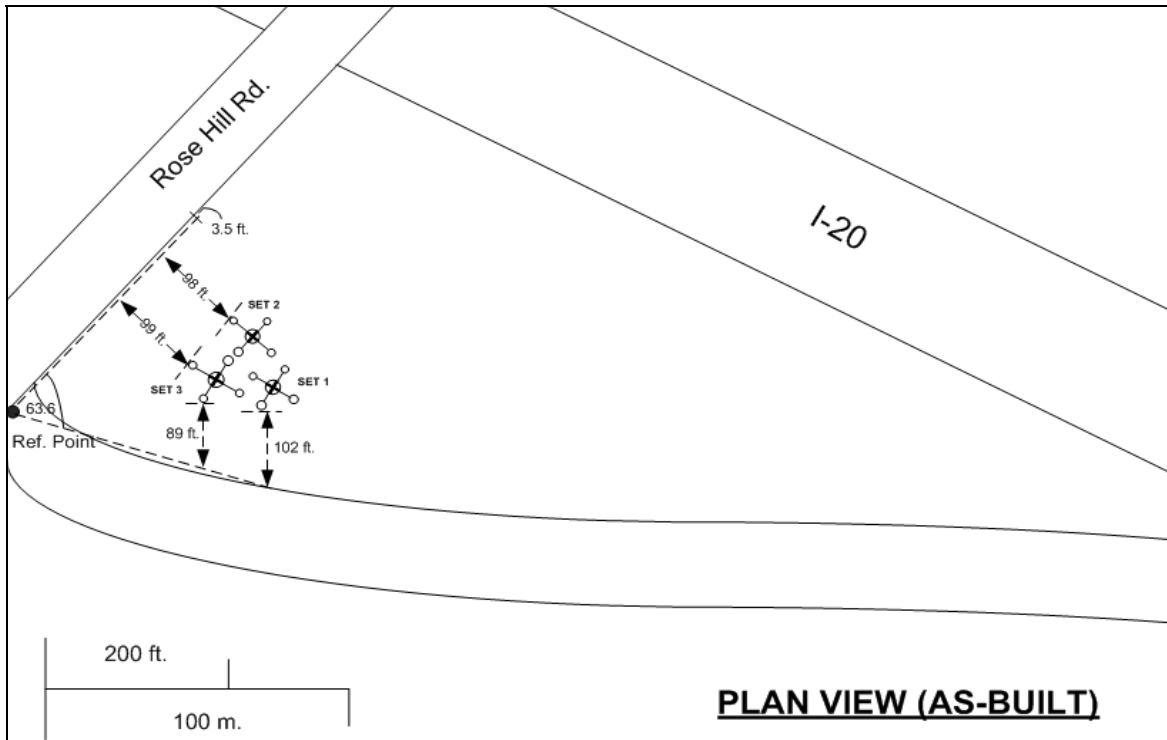


Figure 4.4. Plan View of As-Built Test Setups.

Construction Process

Construction commenced at the test site on Monday, June 8, 2009. The first task was to tie the steel rebar into the circular shapes used in typical drill shaft construction. Two separate crews began tying the steel; one crew built and tied the three reaction shafts (Figure 4.5), while a second crew built and tied the 12 test shafts (Figure 4.6). Different sized vertical rebars and spiral rebars were used to hold the cages together. This was accomplished on June 8 and 9, 2009.



Figure 4.5. Construction of the First Reaction Shaft Rebar Cage.



Figure 4.6. Construction of a Test Shaft Rebar Cage.

Inclinometer casing (2.75 in. [70 mm] dia.) was measured, cut, and tied onto the steel cages prior to installation for use by Slope Indicator’s DigiTilt Measurement System. Additionally, 1.25 in. (32 mm) PVC pipe was measured, cut, and tied to the steel cages for use by the MEMS sensor system for in-place deformation data collection during loading application (see Figure 4.7).



(a) Inclinometer Casings (Blue)



(b) MEMS Casing (White)

Figure 4.7. Construction of Casings.

The drilling for reaction shaft holes was started on June 9. The first drilled hole encountered slight sloughing or caving of the in-situ soil at about the 18–20 ft (5.0–6.1 m) depth (Figure 4.8). No casing was used due to lack of bore hole data. Extra care was taken by slowing the drilling operation; as a result, soil caving did not occur in the other two reaction shafts.



Figure 4.8. Drilling of Reaction Shaft Holes.

While drilling operations were ongoing, steel rebar cages were prepared; both inclinometer (blue casings) and MEMS instrumentation (white casings) were attached to these cages. Also, steel channels were connected into the test shaft cages (Figure 4.9), which were used to attach the Dywidag bars to the reaction shaft to perform the load testing.



Figure 4.9. Channel Steel Tied to Steel Rebar Cage.

Each steel rebar cage was carefully lifted into a vertical position (refer to Figure 4.10), moved into position over each drilled hole, and then carefully lowered into the hole until they were approximately 3 in. (76 mm) above the bottom of the hole. A gravel concrete mix was then poured into each hole until the drilled hole was completely filled to the groundline (Figure 4.11). Concrete materials supplied by Texas Industries Inc. (TXI) and the mix design details was Self-Consolidating Concrete or SCC. It is a highly flowable, non-segregating concrete mix that can spread into place and fill the formwork without using mechanical vibration. The code used to order the concrete was P40PSIN. In the concrete design, the Water/Cement Ratio was 0.459 with

a slump of 6 in. (150 mm) or more. Concrete materials and the mix design details are shown below. The material proportions per 1 CY of mix are:

- Water 30 gal.
- Cement 451 lb.
- Pea Gravel 1800 lb.
- Sand 1479 lb.
- Flyash 113 lb.

Admixtures:

- Water Reducing Admixtures (Type A)–MIRA 85 16.9 oz.



Figure 4.10. Setting the Steel Rebar Cages.



Figure 4.11. Pouring Concrete and Final Shaft.

For the three reaction shafts, the steel rebar cages were extended above the groundline to their designed height prior to the application of a cardboard sonotube and concrete. Cardboard sonotube was used to extend the concrete reaction shafts 7 ft (2.1 m) and 7.5 ft (2.3 m) above the groundline (Figure 4.12) to provide the proper angles and lengths of the Dywidag bars in direct proportion to those used by the median cable barrier system manufacturers.



(a) Setting Sonotube casing for Reaction Shaft



(b) 7 and 7.5 ft (2.1 and 2.3 m) Tall Sonotube Casing for Reaction Shaft

Figure 4.12. Reaction Shaft Construction.

PVC pipes measuring 2 in. (50 mm) in diameter were cut and placed through the sonotube walls at the proper angles (Figure 4.13) to allow the future tensioning of the Dywidag system by connecting it to the test shafts. The angle of placement (16.1°) of the PVC pipes matches the angles of the cables connected to the drilled shafts in the field. The same gravel mix TXI supplied that was used for the drilled shafts was also used to fill in around the steel rebar up to the top of each piece of sonotube to create the reaction shafts (Figure 4.14).



(a) Installing the PVC Pipe



(b) Check of Angle for Dywidag Bars

Figure 4.13. Dywidag Construction.



(a) Pouring Concrete in Sonotubes



(b) Final View of Test Setup Area

Figure 4.14. Sonotube Installations.

Initial inclinometer data were collected on Monday, June 15, six days after installation of all the reaction and test shafts (Figure 4.15).



Figure 4.15. Taking Initial Inclinometer Readings.

Nineteen additional inclinometers were installed between the reaction and test shafts on August 14, 2009. The holes were drilled with a 3.5 in. (90 mm) auger powered by a small generator and turned with a hydraulic-driven chuck as shown in Figure 4.16.



(a) Auger and Drill Stem



(b) Drilling Operation

Figure 4.16. Test Shaft Inclinometer Installation.

Thirteen days were allowed to elapse before any inclinometer readings were taken to allow the concrete mix to solidify. Initial inclinometer readings were taken on August 27, 2009. Additionally, the sonotube casing for the easternmost reaction shaft was removed, exposing the concrete. The sonotube on the other two reaction shafts was removed on September 5, 2009.

Field Quality Control Checks—Concrete

In construction, it is necessary to have quality control checks to validate that the structures in the field perform as predicted in the Design phase. For this research project, checks on the concrete were performed by randomly collecting samples from different concrete trucks that provided the concrete for the reaction and test shafts. A total of five cylinder specimens were made. Three samples were collected and specimens made from each reaction shaft and the other two samples were randomly collected and specimens made from the test shafts. The dimensions of the cylindrical specimens was 6 in. (150 mm) diameter and 12 in. (300 mm) long as specified in Test Method ASTM C31/C31M–09, Standard Practice for Making and Curing Concrete Test Specimens in the Field.

After making the cylinders, all specimens were left in the field for approximately two days to allow them to field cure and minimize damage during transportation back to the laboratory. All five specimens were cured in lime water for an additional 26 days. After completion of the standard 28 days, the specimens were taken out of the water. All specimens were capped on the top and bottom with sulfur compound prior to breaking. This provided a 100 percent contact between the base and loading plates and the surfaces of the concrete cylinders as required by Test Method ASTM C617 - 09a, Standard Practice for Capping Cylindrical Concrete Specimens and as shown in Figure 4.17.



Figure 4.17. Concrete Cylinder Specimens with Capping Compound.

A Tinius Olsen compression tester was used to break the specimens in compression as required by Test Method ASTM C39 / C39M - 05e2, Standard Test Method for Compressive Strength of Cylindrical Concrete Specimens. The testing machine primarily performs compressive strength testing and has a capacity of about 400 kips for both compression and tension (Figure 4.18). The target compressive strength of the concrete based on the mix design was 4000 psi. In providing the load to the specimens, they were individually placed between the base and the loading plates and the loading was applied and manually controlled at a rate of 300 lb/sec until the specimens failed as shown in Figure 4.19.

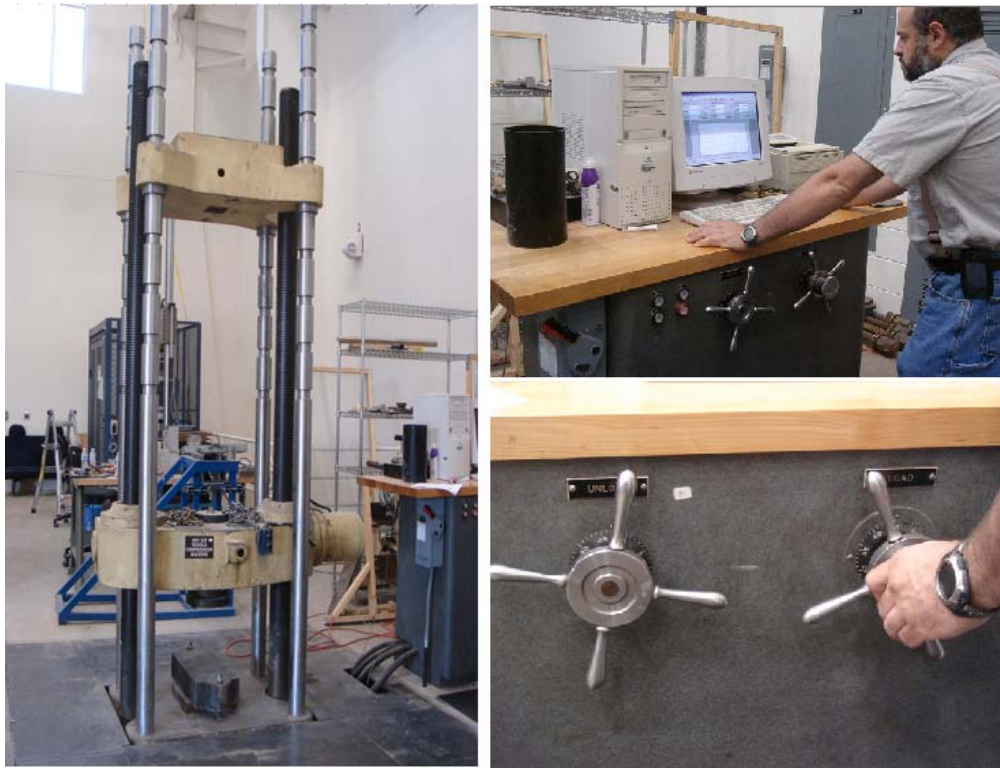


Figure 4.18. The 400 kip Tinius Olsen Tensile and Compression Machine Used for Testing.



Figure 4.19. Compressive Strength Test Setup and Failed Concrete Specimen.

The results and interpretations are automatically collected by the test software and these test results are summarized and shown in Table 4.3.

Table 4.3. Compressive Strength Test Results.

Specimen No.	Peak Stresses (psi) at 28 days
1	4075
2	4037
3	3972
4	4116
5	4033

From the results, the average compressive strength of all five specimens is equal to 4046.6 psi with a Standard Deviation (SD) equal to 53.54 psi. Although one specimen broke at a compressive strength lower than 4000 psi, it was more than 90 percent of the design concrete strength of 3600 psi and was deemed acceptable.

FIELD TESTING AND DATA ACQUISITION

Field testing and acquisition of inclinometer and MEMS data was performed on September 30, 2009. The Dywidag bars were delivered as well as the hydraulic piston system for applying the tension load on the Dywidag bar. One test shaft for each reaction shaft was tested.

Inclinometer and MEMS probe data was acquired during the incremental loading. An elevation survey was also continuously performed at each incremental load to measure surface changes.

One test per test set was performed on each test drilled shaft with inclined reaction applied using a hydraulic system placed against the reaction shaft. For the test shafts, both inclinometer and MEMS sensors measured lateral movements. In addition, the final vertical movement of the reaction shafts was measured at the center both before and after the start of each test by using standard survey equipment. Figures 4.20–4.28 provide details of the field testing for the summer season condition.



Figure 4.20. MEMS Probe System.



(a) Dywidag Bars



(b) Dywidag Bar Retaining Nut

Figure 4.21. Dywidag System Parts.



(a) Hydraulic Piston Shelf



(b) Hydraulic Piston and Pump

Figure 4.22. Dywidag Tensioning System.



(a) Dywidag Bar in Place for Testing



(b) Retaining Nut Attached to Test Shaft Steel Channel

Figure 4.23. Dywidag Bar System.



(a) Installing the Hydraulic Piston

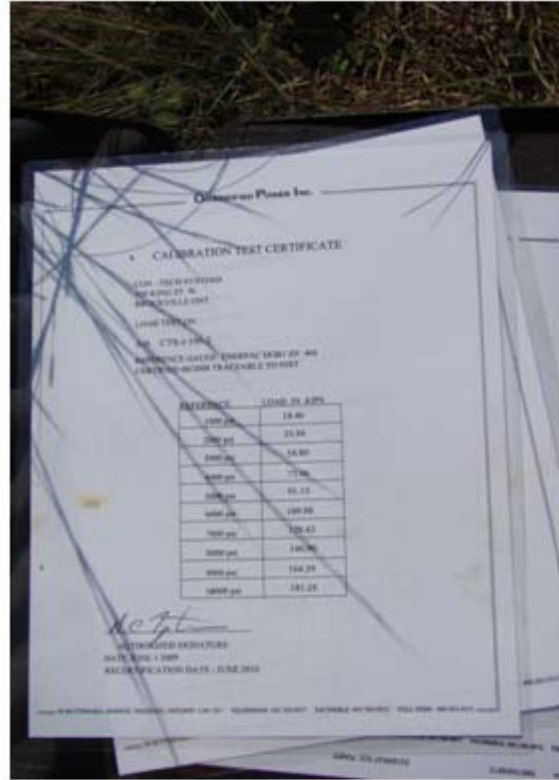


(b) Hydraulic Piston and Retaining Nut

Figure 4.24. Hydraulic Piston Setup for Tensioning.



(a) Tensioning System Setup



(b) Hydraulic Pump Calibration Records

Figure 4.25. Hydraulic Tensioning System.



(a) Applying Tensioning Loads



(b) Test Shaft Deflection Due to Loading

Figure 4.26. Test Shaft Loading.



(a) Test Shaft



(b) Mid-Point

Figure 4.27. Collecting Inclinometer Readings.

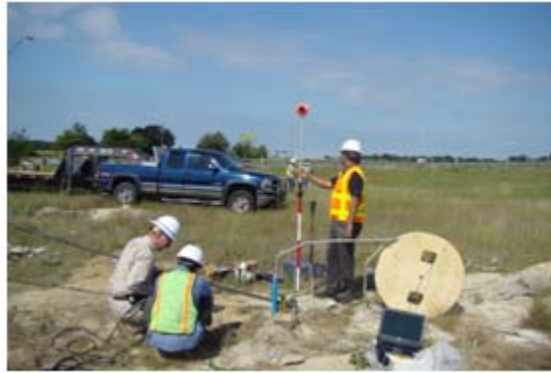


Figure 4.28. Collection of Inclinometer, MEMS Probe, and Elevation Survey Readings.

SUMMARY

This chapter describes details of the design of load test setup and construction of the system. Also, instrumentation details for capturing load-deformation responses of the test shafts are mentioned.

CHAPTER 5

LOAD TESTS AND ANALYSIS OF TEST RESULTS

A total of 12 test shafts were subjected to load tests with three tested in the summer condition and the other nine tested in the winter condition. The summer condition load testing was conducted in early September in dry soils and with daytime temperatures close to 104°F (40°C). The winter condition load testing was conducted in early February between unusually high rainfall amounts and a 24-hr record 12-inch snow storm producing totally saturated soil conditions similar to those created in the Winter of 2006–2007 in which the original shafts were distressed.

FAILURE OBSERVATIONS

Several different failure mechanisms were observed during testing. As shown in Figure 5.1a, the concrete at the ground surface actually cracked. Figures 5.1b and 5.1c show separation of the concrete for the test shaft from the adjoining soil. This indicates movement of the test shaft toward the reaction shaft.



Cracked Concrete



(b) Soil-Test Shaft Separation (Distance)



(c) Soil-Test Shaft Separation (Depth)

Figure 5.1. General Test Shaft Failure.

Figure 5.2a shows yielding and imminent failure of the steel channel in a test shaft. This was of great concern to the testers' safety and was corrected with the addition of a steel plate to reinforce the steel channel (Figure 5.2b), allowing the shaft to fail rather than the channel.



(a) Steel Channel Yielding



(b) Extra Plate Added

Figure 5.2. Field Adjustment to Eliminate Yielding Steel Channels.

DATA AND ANALYSIS

Load Data

Transfer of the load from the appropriate reaction shaft to each test shaft was accomplished thru a Dywidag high tension steel bar. It was necessary to measure the load during and after each test to measure any losses from friction or other factors of the bar passed through a PVC pipe in each reaction shaft. Strain gage instrumentation, explained in an earlier section, was used to collect the applied tensile stresses at the top of each test shaft. The actual results were calculated using the modulus of elasticity of the Dywidag bar steel. Figure 5.3 presents the applied tensile load by the hydraulic system and the measured tensile load from the strain gage on the bar of three tested shafts of different diameters. In all three cases, the loads at the top of the test shaft are about 92 percent to 93 percent of the applied load, thus indicating no major loss of loads applied by the hydraulic system.

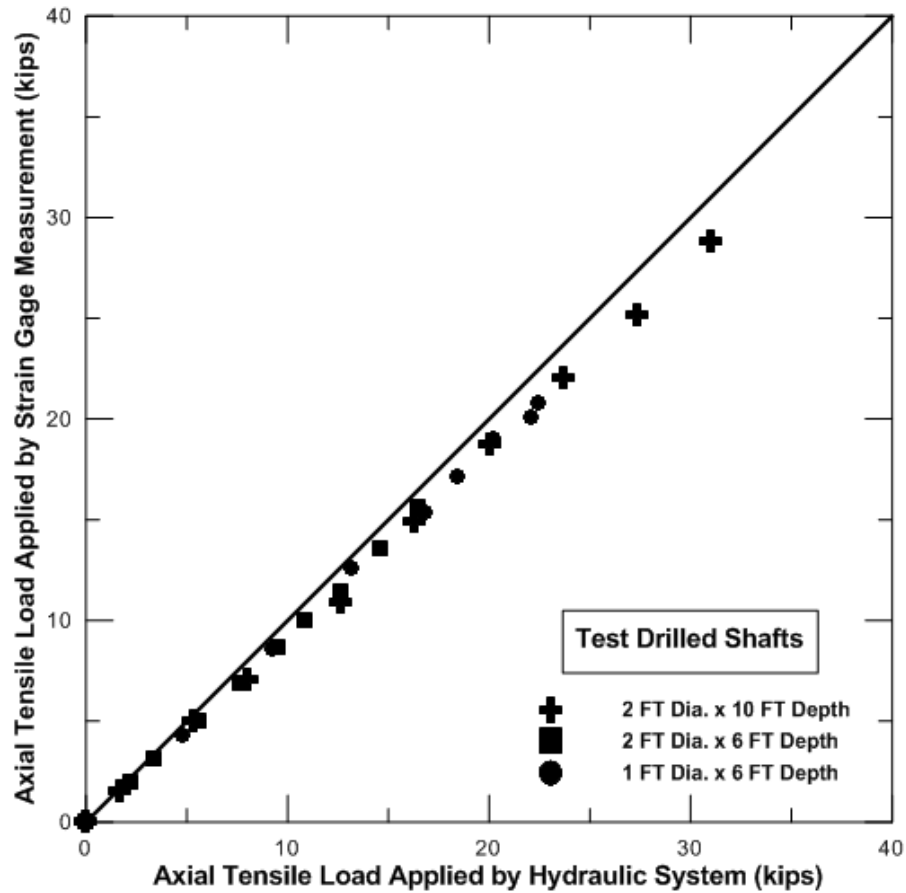
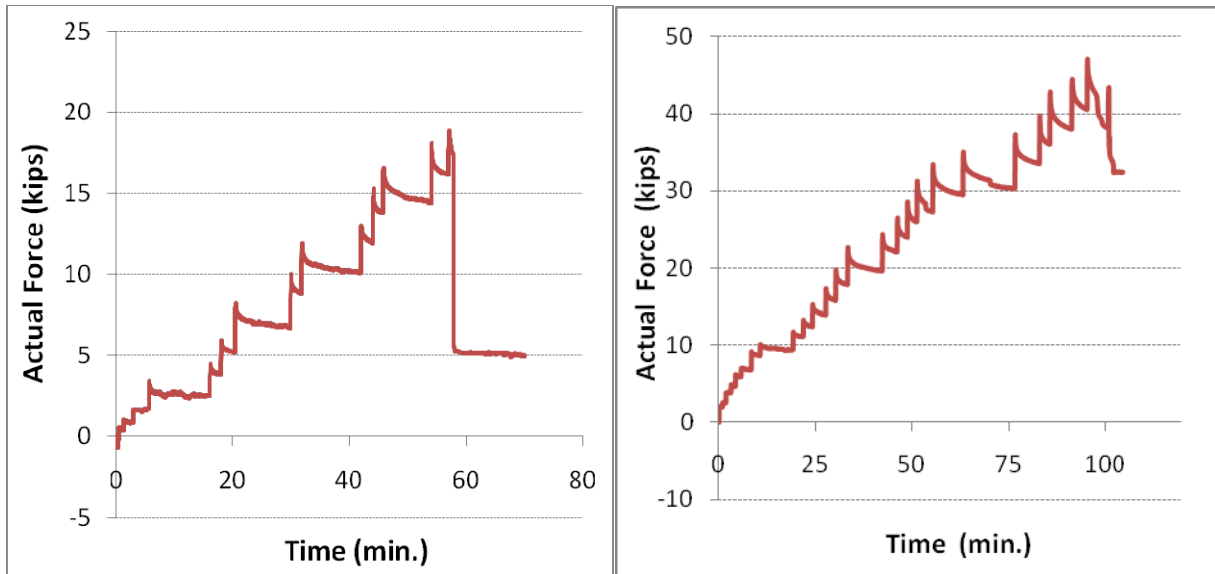


Figure 5.3. Comparisons between Measured and Actual Applied Loads.

Hydraulic Load Gage

The maximum capacity values were computed by recording the values read directly from the strain gage and applying the calibration curve conversion. The actual loads applied to the Dywidag bars versus the time of application for each load are shown in Figures 5.4a to 4b, which are representatives of the 1 ft (0.3 m) dia. × 10 ft (3.0 m) depth shaft and the 2 ft (0.6 m) dia. × 10 ft (3.0 m) depth shaft. The extended horizontal portions of the graphs are the loads at which the inclinometer readings were taken. This validates the calibration of the hydraulic piston application system.



(a) 1 ft (0.3 m) diameter × 10 ft (3.0 m) depth

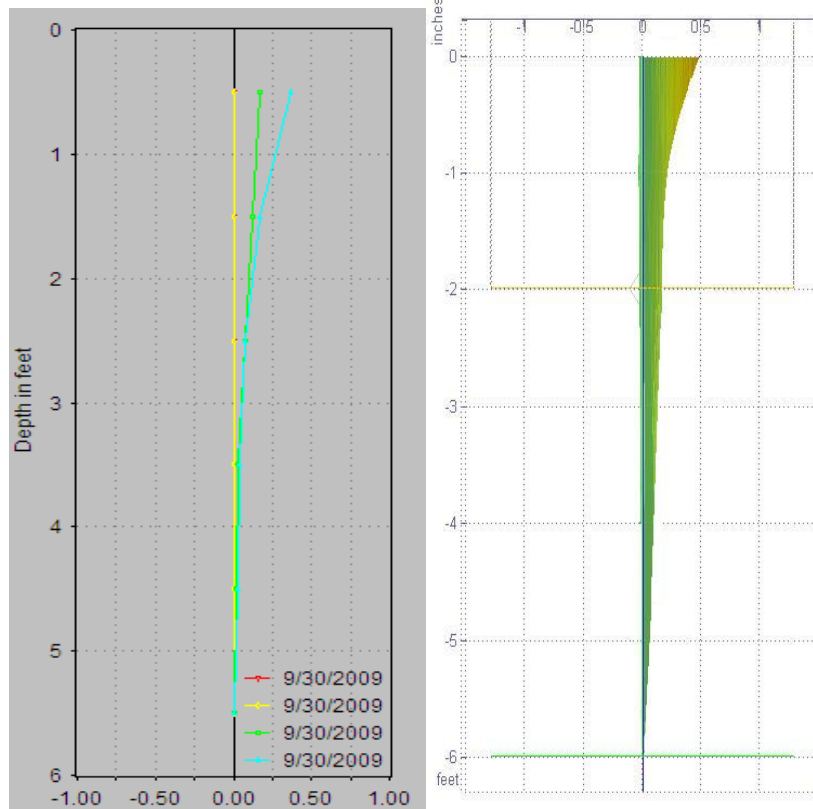
(b) 2 ft (0.6 m) diameter × 10 ft (3.0 m) depth

Figure 5.4. Actual Force Applied versus Time Period.

LATERAL DISPLACEMENT DATA

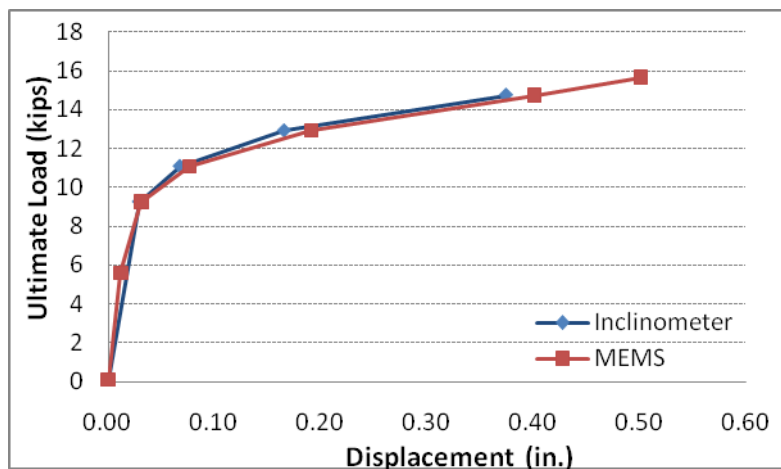
Inclinometer and MEMS-SAA Displacement Plots

Both inclinometer and MEMS-SAA readings were collected during testing on each test shaft. The inclinometer displacement data was collected at certain incremental loads while the MEMS-SAA data was continuously read and stored through a laptop computer used onsite. Figure 5.5 shows the plots created from the field collected data for both the inclinometer and MEMS-SAA systems, and Appendix G shows the rest of the graph results.



(a) Inclinometer

(b) MEMS-SAA



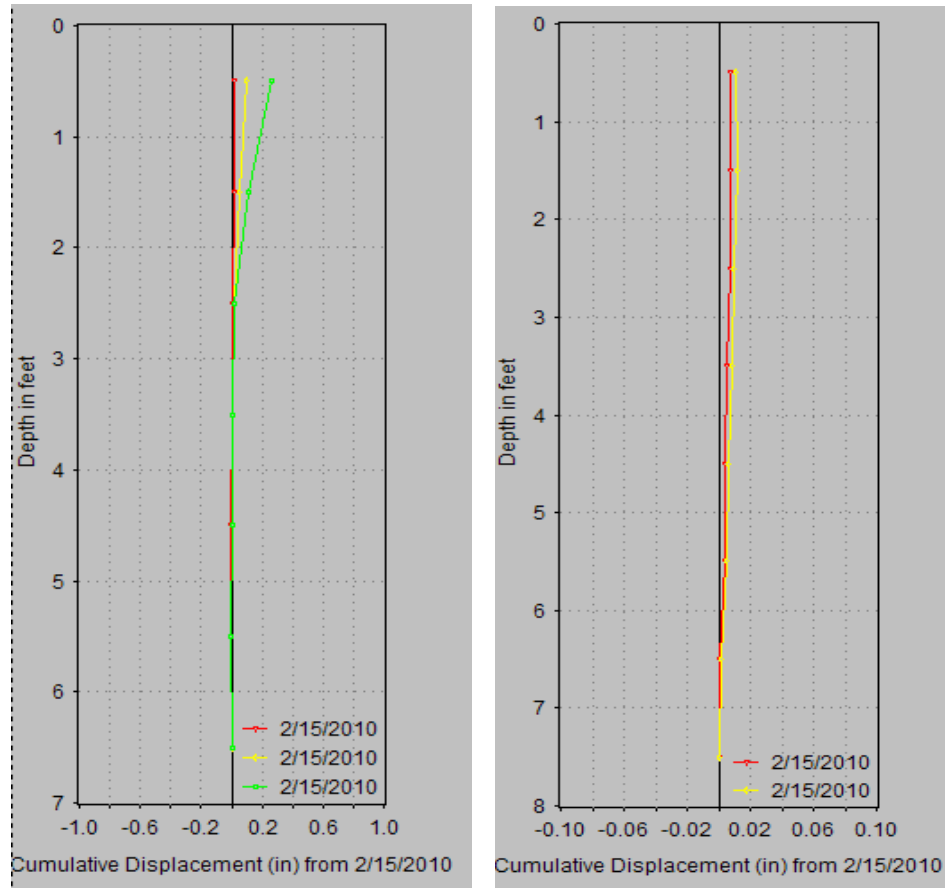
(c) Ultimate Load versus Displacement Comparison

Figure 5.5. Test Shaft (1 ft [0.3 m] Diameter × 6 ft [1.8 m] Depth) (Summer Condition).

The graphs illustrate that the MEMS-SAA data are close to the inclinometer displacement data. Additionally, the MEMS-SAA provided continuous real-time data showing the continuous increase in the lateral displacements under each load increment. Another benefit of using the

MEMS-SAA system was realized in the final loading increment. The MEMS-SAA probe, with its flexibility, was able to capture the ultimate load and displacement profile. With the inclinometer, this measurement was unable to perform as the probe could not be inserted into the failed test shaft as the casing was distorted. This is a significant advantage between the inclinometer and the MEMS-SAA when the load tests were conducted from the start of initial loading until the final failure of the deep foundation system. The measurements of entire load test results has provided valuable information which resulted in future and further research and investigations with the MEMS-SAA system. Therefore, for the rest of this analysis, displacement results will be reviewed using the MEMS-SAA data, where applicable, in lieu of the inclinometer data.

To see the influence on the reaction and test shafts, researchers measured the inclinometer casings located between the reaction and test shafts after selected loads were applied. For the 0.3 m (1 ft [0.3 m]) test shafts, additional inclinometer readings were taken at the periphery of two diameter point of the test shaft and mid-point locations from the test shaft to the reaction shaft as shown in Figure 5.6. Table 5.1 summarizes the maximum lateral movement in the influence zone between the reaction and test shafts due to the load applied.



(a) Inclinometer at 2D of Test Shaft (b) Inclinometer at the Middle of Test Shaft and Reaction Shaft

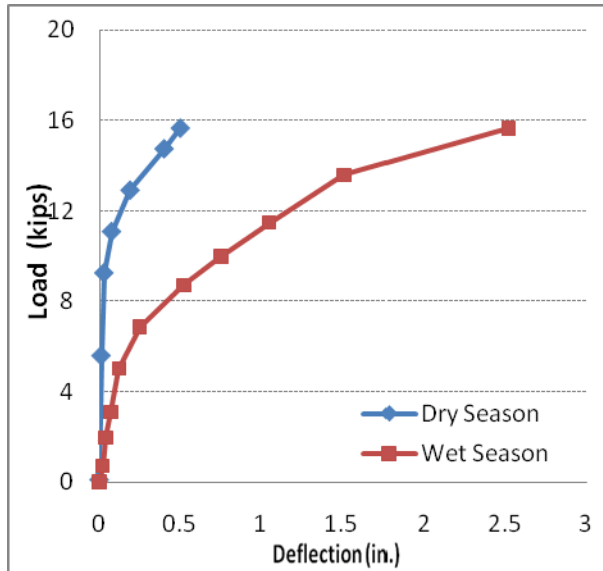
Figure 5.6. Test Shaft (1 ft [0.3 m] Diameter × 6 ft [1.8 m] Depth) Displacement Data.

Table 5.1. Examples of Maximum Lateral Movement in the Influence Zone Due to the Load Applied to the Shafts.

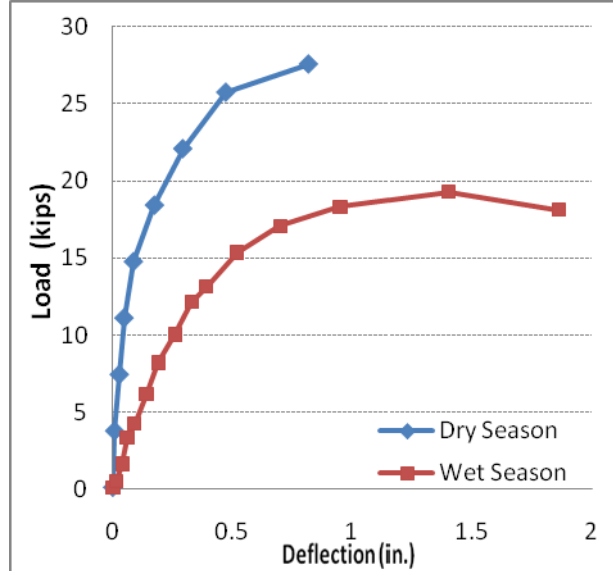
Test Set	Dimension Diameter × Depth ft × ft (m × m)	Lateral Movement at 2 Times Diameters from Test Shaft in. (mm)	Lateral Movement at Midpoint between Reaction and Test Shaft in. (mm)
1	1 × 6 (0.3 × 1.8)	0.27 (6.9)	0.016 (0.40)
2	1 × 10 (0.3 × 3)	0.12 (3.0)	0.017 (0.43)
2	2 × 10 (0.6 × 3)	N.A.	0.018 (0.46)

MEMS-SAA Comparison Plots (Summer versus Winter)

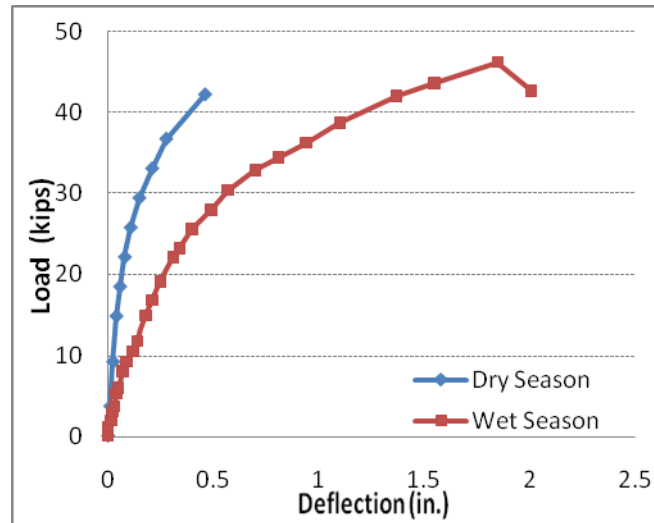
From the continuous data that the MEMS-SAA system had collected, the data recorded during the summer condition (dry season) and the winter condition (wet season) for the three test shaft sizes are plotted in Figures 5.7a through 5.7c.



(a) 1 ft (0.3 m) diameter × 6 ft (1.8 m) depth



(b) 1 ft (0.3 m) diameter × 10 ft (3.0 m) depth



(c) 2 ft (0.6 m) diameter × 10 ft (3.0 m) depth

Figure 5.7. MEMS-SAA Plots for Summer and Winter Condition (Dry and Wet Season).

In these figures, the results show that there was larger deflection (along the axis of the shaft) and displacement of the test shafts in the winter condition when the soil was totally saturated than in the summer condition. Also, the failure results of the test shafts (Figure 5.7)

showed a brittle failure mode in the summer condition while the test shafts in the winter condition showed a semi-flexible failure mode. From Figure 5.7, for the same lateral deflections, the drilled shafts tested in the summer condition provided higher capacities.

Figures 5.8 and 5.9 show the photos of the distressed drilled shaft during load tests. Larger deflections were recorded during winter load testing than in the summer load testing. Majority of the drilled shafts experienced large lateral deformation evident in the gaps between shaft and the adjacent soil. In one case, researchers observed foundation cracking due to concrete material failure. Hence, one can conclude that large movements of soils around the shaft contributed to the failures of drilled shafts.



Figure 5.8. Test Shaft Displacements in Summer Condition.



Figure 5.9. Test Shaft Displacement in Winter Condition.

SUMMARY OF TEST RESULTS

Table 5.2 summarizes the ultimate inclined load at failure and inclined loads at the specific displacements; 0.5 in. (12.5 mm) or 0.75 in (19.0 mm) for both the summer and winter conditions. These results are analyzed for the development of design charts and tables for drilled shafts subjected to inclined loads.

Table 5.2. Summary of Loads at Lateral Movements of 0.50 in., 0.75 in., and at Failure.

	Shaft No.	Diameter ft (m)	Depth ft (m)	Measured Load in kips (kN)		
				@0.50 in. (12.5 mm)	@0.75 in. (19.0 mm)	@ Failure (Ultimate Load)
Winter	1	1 (0.3)	6 (1.8)	8.4 (37.2)	9.6 (42.6)	15.0 (66.9)
	2	1 (0.3)	10 (3.0)	15.1 (67.2)	16.9 (75.2)	17.4 (77.5)
	3	1 (0.3)	14 (4.2)	15.0 (47.6)	18.5 (61.8)	26.0 (115.8)
	4	2 (0.6)	6 (1.8)	12.6 (56.1)	14.8 (65.8)	19.9 (88.5)
	5 ^A	2 (0.6)	10 (3.0)	-	-	27.7 (123.2)
	6	2 (0.6)	10 (3.0)	26.9 (119.7)	32.1 (142.6)	41.0 (182.2)
	7	2 (0.6)	14 (4.2)	41.6 (185.0)	Failed Already	41.6 (185.0)
	8	3 (0.9)	6 (1.8)	14.9 (66.1)	17.8 (79.0)	22.5 (123.9)
	9 ^B	3 (0.9)	14 (4.2)	-	-	35.6 (158.2)
Summer	1	1 (0.3)	6 (1.8)	15.0 (66.9)	-	15.0 (66.9)
	2	1 (0.3)	10 (3.0)	25.0 (111.2)	26.1 (116.1)	26.5 (117.7)
	3	2 (0.6)	10 (3.0)	40.5 (180.3)	-	40.5 (180.3)

Note: ^A denotes concrete material failure and ^B denotes excessive channel section yielding

Figure 5.10 shows the typical failures of the test shafts due to inclined loading at different views. It was clear from these pictures that the test setup and field tests conducted were able to capture the failure pattern that transpired in the original drilled shaft foundations built to support the cable barrier systems.



(a)



(b)

Figure 5.10. Failures of Test Shafts from Inclined Loading Tests.

All of the test shafts were tested under static inclined tension loading. The data were analyzed to formulate acceptable design methods for drilled shafts under inclined tensile loads. The conclusions based on the lateral load results and analyses are shown in the following:

- The designed test setup was successfully constructed and used to apply inclined load tests on various sized drilled shafts. Tests provided results that are well within the trends expected for different test shafts of different dimensions.

- The design of the reaction shaft dimensions and spacing between the reaction and test shafts proved to be sound as the field observations. Test results showed no effects of yielding or lateral movement in the reaction shafts.
- The drilled shafts tested in the summer and winter conditions showed major variations in their load versus displacement behaviors. The test shafts in the winter condition exhibited lower ultimate inclined load capacities and experienced larger lateral and vertical movements. The major contributor to differences in the summer (dry) and winter (wet) test conditions was the nature of the high-plasticity clay creating the uplift forces due to soil expansion as the moisture content increased. Also, the load-displacement pattern of drilled shafts in the winter condition showed semi-brittle response, whereas the same displacements of the test shafts in the summer condition is close to rigid brittle pattern.
- The percent loss of the tensile loads applied at the reaction shafts and the loads experienced at the test shafts is less than 10 percent, indicating that there was no major friction loss during load testing of the test shafts.
- The load-deformation patterns, whose deformations of test shafts were recorded during the MEMS-SAA probe, matched with those recorded with the inclinometer system. The major advantage of the MEMS-SAA system was that it provided a complete load-displacement data collection process including the final inclined load, ultimate load at the test shaft, and the corresponding lateral displacement. This is possible due to the use of the in-place and flexible MEMS-SAA probe, which was able to provide a complete loading profile at the same time allowing users to retrieve the unit after the test.
- The recorded failures of all test shafts matched with the original distressed shafts visually observed in the winter of 2006–2007. This match indicated that this field inclined load testing was successful in simulating the loading mechanisms that transpired in the original distressed shafts.

The next chapter presents numerical and analytical modeling of the present test results.

CHAPTER 6

DESIGN/CONSTRUCTION GUIDELINES OF DRILLED SHAFTS IN HIGH PI CLAYS

ANALYSIS APPROACH

To generate the design charts, it is necessary to analyze the present test results with existing numerical and analytical models. Since the applied load has both lateral and vertical uplift type force components, the present test results are separated into two of the force components. The present test conditions are then simulated with the available lateral load and vertical uplift load analyses methods to predict the lateral load and uplift loads. Saturated soil layer properties are used in this analysis. The load predictions are compared with the field load test results. Necessary modifications to the analyses are developed as a part of this analysis. Later, the modified models for uplift capacity and lateral load predictions are used to determine the inclined loads for various shaft dimensions and soil conditions. These results are used to develop the design charts that can be used to design the foundations to support the median cable barrier systems. Designs are developed for worst case scenarios, i.e., simulating below freezing temperatures in the environment and full saturation in soils, including all of the soil properties and load results acquired in the winter condition.

The measured inclined loads were first split into lateral and vertical uplift components and then analyzed using the following methods.

- Three lateral load analyses using Broms' Method (1965), Characteristic Load Methods (CLM) (1994), and p-y Method (LPILE), were performed and then comparisons with measured lateral load were attempted.
- Calibration factor for the lateral load analysis was then established such that the modeling analysis provides the best-fit trend with the measured lateral load results.
- Vertical uplift load models using Das and Seely (1982) and O'Neill and Poormoayde (1980), were analyzed and comparisons with the measured ultimate vertical uplift load component was made.
- Based on the comparisons, the calibration factor for the vertical uplift load analysis was established.

- A design chart for the inclined load at the 16.1° angle was then developed based on calibration factors from the horizontal and lateral load analyses for various foundation dimensions.

Uplift Force Models

When drilled shafts need to sustain the pulling force in the vertical axis or in the inclined direction, they need to be designed against pullout. In general soil types, the model used to find the uplift capacity can be applied as shown below. This study presents two different models developed by Das and Seeley (1982) and O'Neill and Poormoayed (1980). Generally, the total ultimate uplift capacity of a single shaft or pile can be expressed as shown in Eq. 23.

$$P_u = P_0 + W \quad (23)$$

where P_u = Total Ultimate Uplift Capacity.

P_0 = Net Uplift Capacity.

W = Effective Self-Weight of the Shaft.

In 1982, Das and Seeley presented the model that has been used for uplift force prediction which was developed from pipe piles located in saturated clay. The net ultimate capacity for vertical uplifting load can be given as follows.

$$P_0 = Lp\alpha'c_u \quad (24)$$

where L = depth of shaft below the ground.

p = perimeter of the shaft.

α' = adhesion factor.

c_u = undrained shear strength parameter.

Table 6.1 shows the results from the Das and Seeley model. However, this model was developed by not considering the uplift force, so it is necessary to find a model in which the uplift force was considered. In 1980, O'Neill and Poormoayed proposed Eq. 24 based on the concept that showed the process of expansion occurs slowly enough so that excess positive or negative pore water pressures are not developed. They also suggested a value of $\phi = 1.3$ and δ_r , which is the particular value for soil in Texas.

$$f_{\max} = \phi\sigma'_{ho}\tan\delta_r \quad (25)$$

where ϕ = Correlation Coefficient.

σ'_{ho} = Horizontal Swell Pressure.

δ_r = The Effective Angle of Internal Friction between Soil and Concrete.

Table 6.1 shows a summary of the results between the aforementioned models compared with the actual vertical uplift component of the field test results.

Table 6.1. Summary of Ultimate Uplift Results Compared with the Models.

Shaft No.	Diameter (ft)	Depth (ft)	Actual Vertical Uplift Force (kips)	Prediction of Uplift Force (kips)	
				Das and Seely (1982)	O'Neill and Poormoayed (1980)
1	1	6	4.17	6.77	1.85
2	1	10	4.83	13.98	2.30
3	1	14	7.22	19.10	2.76
4	2	6	5.52	14.90	5.06
5	2 ^A	10	-	30.23	6.88
6	2	10	11.36	30.23	6.88
7	2	14	11.53	41.38	8.71
8	3	6	7.72	24.40	9.64
9	3 ^B	14	-	66.85	17.84
Average Ratio (Measured/Predicted)				0.37	1.67

Note: ^A denotes concrete material failure and ^B denotes excessive channel section yielding

Table 6.1 shows that the model Das and Seely (1982) developed provides results that matched closely with the actual field test results. Even though some of the field test results cannot be compared with the models, an average of the ratio between actual results and the predicted values helped in the creation of the design chart with the average ratio between the actual and the predicted results being 0.37 at ultimate load. This means that the model provides overestimated results when compared with the actual field test results. The first model with side friction was chosen since most of the uplift was traced to the tension mobilized in the cable due to low temperature, which lifted the shaft as uplift contribution at overburden depths is small. Otherwise, the shafts would have failed during rainfall events, which were not the case. Cold temperature conditions triggered the failures more than the uplift being fully mobilized at the site. Hence, the first model that uses the side friction to the total vertical force was considered for the design chart development. The second model might have provided a closer match with

measured results, but that is unrealistic, considering the water saturation during winter events may not reach larger depths.

Lateral Deflection and Lateral Capacity Models Consideration

Lateral Deflection Criteria. To develop a design chart, an appropriate criterion for lateral allowable deflection should be selected at which the loads are construed as ultimate loads. Many researchers and organizations, such as Broms, Czerniak, Kinney, Ivey and Hawkins, International Building Code (IBC), and local DOTs use different deflection values for defining the ultimate loads on the shafts. Generally, deflections vary with types of structures. For example, 0.25 in. deflection at the top of the shaft is used to estimate loads for foundations supporting high-rise structures. However, for structures such as transmission towers, sign posts, and noise barriers, 0.5 in. or larger deflection (can be several inches) criterion are followed to define ultimate loads in load tests (Chen 2000).

Broms (1964), Czerniak (1958), Kinney (1959), Ivey and Hawkins (1966) assumed that 0.5 in. lateral deflection at ground surface is the deflection limitation for several conditions and structures. Based on the 2003 International Building Code (IBC) requirements, the ultimate inclined load at 0.5 in. (12.5 mm) or 0.75 in. (19.0 mm) is considered as a failure load. For DOTs, Colorado Department of Transportation (CDOT) (2004) presented study of permissible lateral deflections, 0.6 in., 1.0 in., and 1.5 in., relating to various factor of safety values. The results show that all proposed deflections are safe and provide factor of safety ranging from 1.20 to 4.70. However, in some cases, 1.5 in. deflection may not be able to work for wall constructions because the top of the wall may exceed the deflection requirement. Thus, they concluded that 1 in. permissible deflection at the drilled shaft head is an appropriate criterion for such walls.

As aforementioned, the criterion of lateral movement varies from 0.25–1.5 in. depending on the uses of those structures. In this section, both importance of the structure and efficiency of the cable barrier systems located in expansive soil area are considered so that the loads inducing a maximum deflection of 0.5 in. are considered as ultimate loads. This criterion can keep the cables from becoming slack, thereby maintaining the integrity of the cables in sustaining any applied or impact loads that can negate the full efficiency of the cable barrier system to protect the travelling public. However, lateral deflection at ground surface close to 1 in. can be applied

in areas where expansive soils are not located. Hence, in the present analysis, ultimate loads are established at deflection criteria of 0.5 and 1.0 in., respectively. Using lower deflection will result in increased drilled shaft dimensions and costs which may not be the most cost-effective way of designing these foundations. The graphs or design charts developed for both criteria of 0.5 in. and 1 in. are shown in the later section. In addition, the charts for lesser deflection criterion of 0.25 in. are also included for more conservative designs.

Lateral Capacity Models. Several methods are typically used in the prediction analysis of lateral capacities of the drilled shafts and these methods include Broms' Method (1965), Characteristic Load Method (CLM) by Duncan (1994), Strain Wedge Method by Ashour et al. (1998), and p-y Method (LPILE). In the present study, Broms' Method, Characteristic Load Method, and the p-y Method using the LPILE program to find the best-fit trend leading to an appropriate design chart were considered. The Broms and Characteristic Load methods can provide the ultimate load values which correspond to the 0.5 in. deflection criterion. The results from the LPILE program can be compared with the load-deflection curve from the field test results as shown in Figure 6.1. The load-deflection from the LPILE program can be compared through the ultimate load at various deflections, and these results are primarily used for establishing ultimate loads at various deflection criteria. These deflections include 0.25 in, 0.5 in., and 1 in. Table 6.2 shows the results from the field tests and the models, and Figure 6.2 compares the field test results and the models.

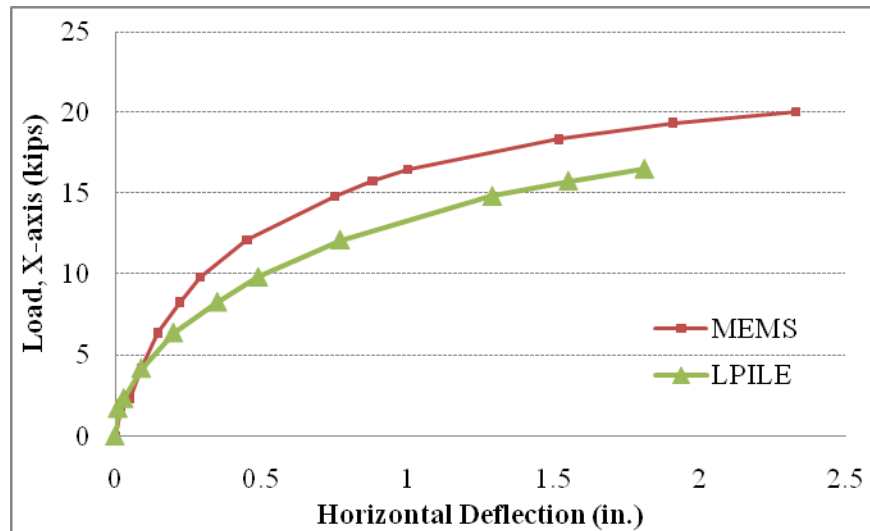


Figure 6.1. Example of Comparison between Field Test Results and LPILE Model of the 2 ft (0.6 m) Diameter × 6 ft (3 m) Depth.

Table 6.2. Summary of Ultimate Lateral Results Compared with the Models at 0.5 in.

Shaft No.	Diameter (ft)	Depth (ft)	Field Test (kips)	Predictions of Lateral Load (kips)		
				Broms (1965)	CLM (1994)	LPILE
1	1	6	8.04	6.98	7.62	6.72
2	1	10	14.51	14.74	7.31	11.66
3	1	14	14.41	21.15	6.94	13.64
4	2	6	12.11	6.34	20.33	9.9
5 ^A	2	10	-	18.38	19.50	19.2
6	2	10	25.84	18.38	19.50	19.2
7	2	14	25.84	31.59	18.50	31.7
8	3	6	20.27	5.71	39.21	11.9
9 ^B	3	14	-	37.28	35.68	41.2

Note: ^A denotes concrete material failure and ^B denotes excessive channel section yielding

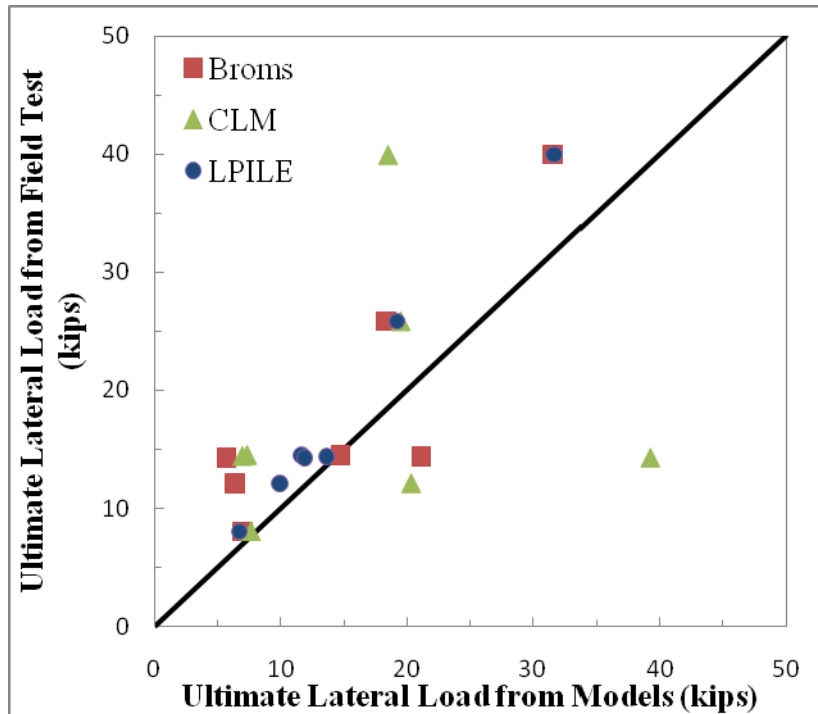


Figure 6.2. Comparisons between Ultimate Load of Field Results and Models (Deflection=0.5 in.).

From Figure 6.2, the predicted results from LPILE show the trend close to the 1:1 line with the predicted results from the Broms and Characteristic Load Methods being more scattered. The reason that LPILE provided the results close to the field test results is a fundamental factor of this method developing the p-y curves representing the true behavior of soils by considering the non-linearity of the soil modulus. For the Broms' Method, the limitation is the soil along the depth of the drilled shaft being assumed as cohesive soil only. However, the

undrained shear strength used in the calculations came from the average of the soil along with the depth.

The Characteristic Load Method has more limitations than the other methods. One limitation is that the shaft must be long enough so that the behavior is not affected to any significant degree by its length. Another limitation is that the ultimate load could not be analyzed directly. However, to find the ultimate load at 0.5 in. (12.5 mm), a back calculation is required to be done. In short, the LPILE provides the predicted results closest to the actual field test results and the ratio between the actual results to the predicted results is 1.21, which means the models provided slightly overpredicted results for present test shafts. The reason that LPILE provides overpredicted results is the undrained shear strength parameters used in the LPILE program as input data for all the layers are from the saturated condition, which is very difficult to be true in the real field condition.

Table 6.3. Calibration Factor at Different Lateral Deflection.

Lateral Deflection Consideration	Calibration Factor (Ratio of Measured Results to LPILE Results)
at 0.50 in.	1.21
at 1.00 in.	1.20

Finite Element Modeling (FEM Model)

In this research, finite element modeling (FEM) of the drilled shaft is performed by using the ABAQUS program. The results from this model are primarily used to compare with the field monitoring result; also, force distribution from shaft to surrounding soil was considered. In Figure 6.3, the FEM model simulated the 2 ft diameter \times 6 ft long drilled shaft; soil properties of adjacent soil strata are given by using the laboratory data based on tests performed on saturated soil conditions of winter. Figures 6.4 and 6.5 present the result from the ABAQUS program.

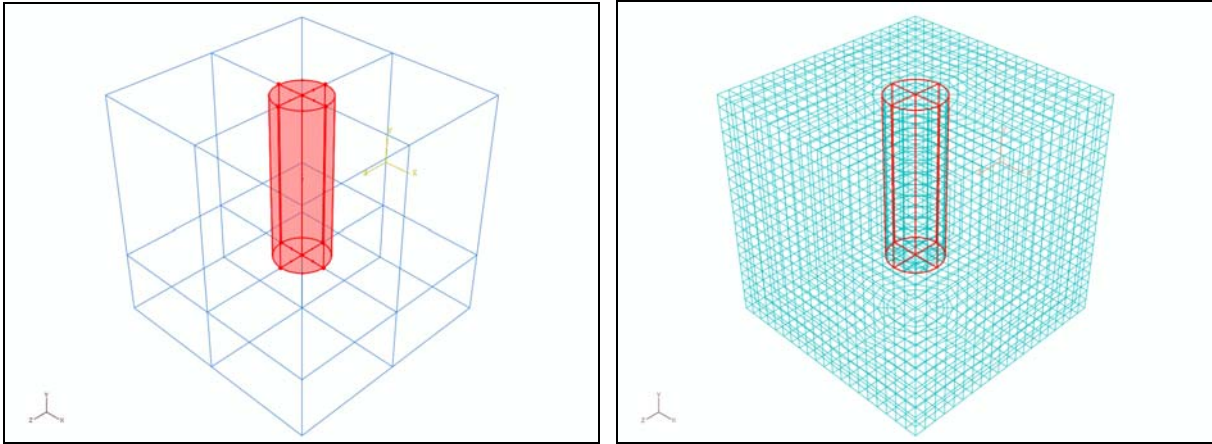


Figure 6.3. Model Developed in FEM Model.

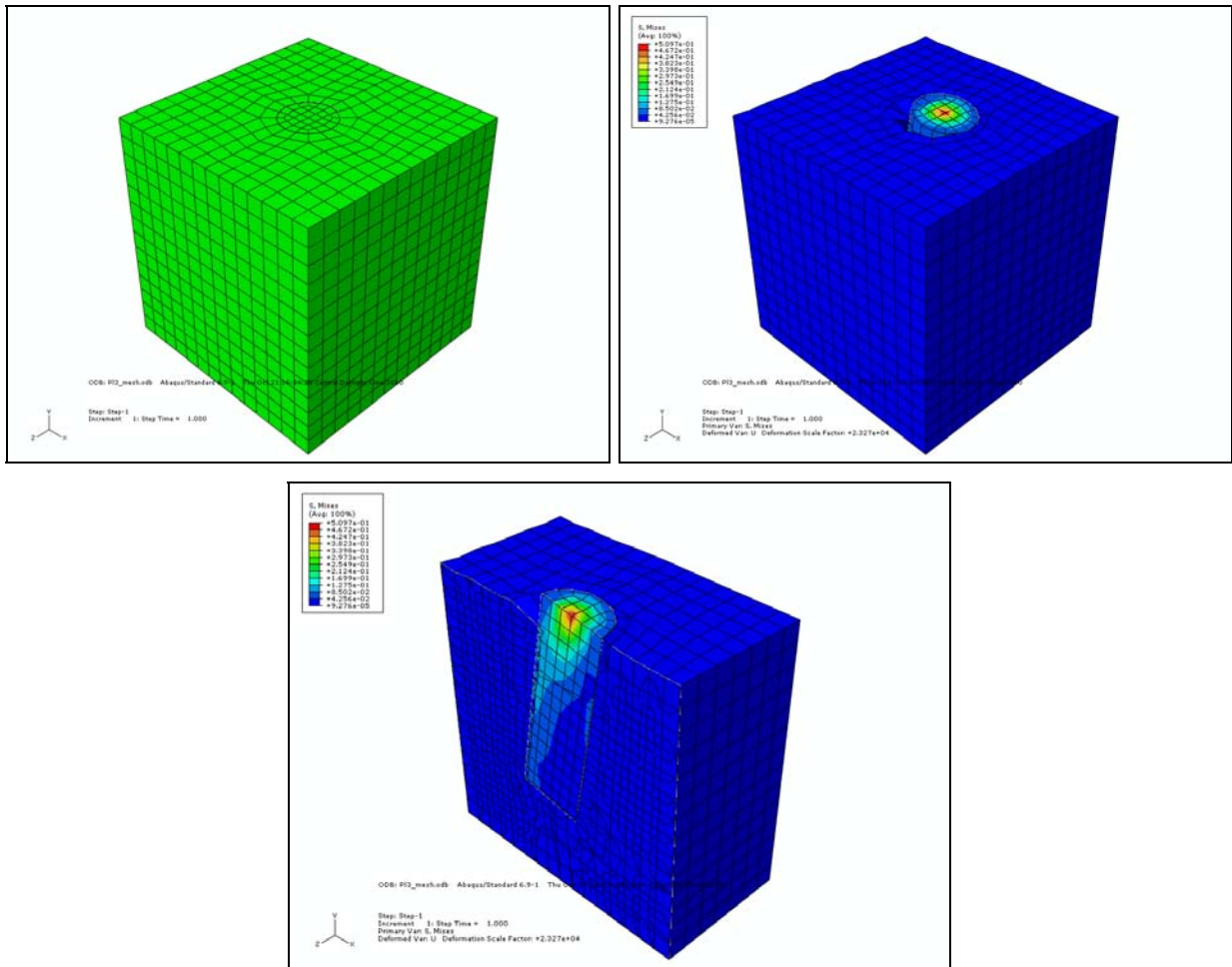


Figure 6.4. Stress in Shaft after Loading.

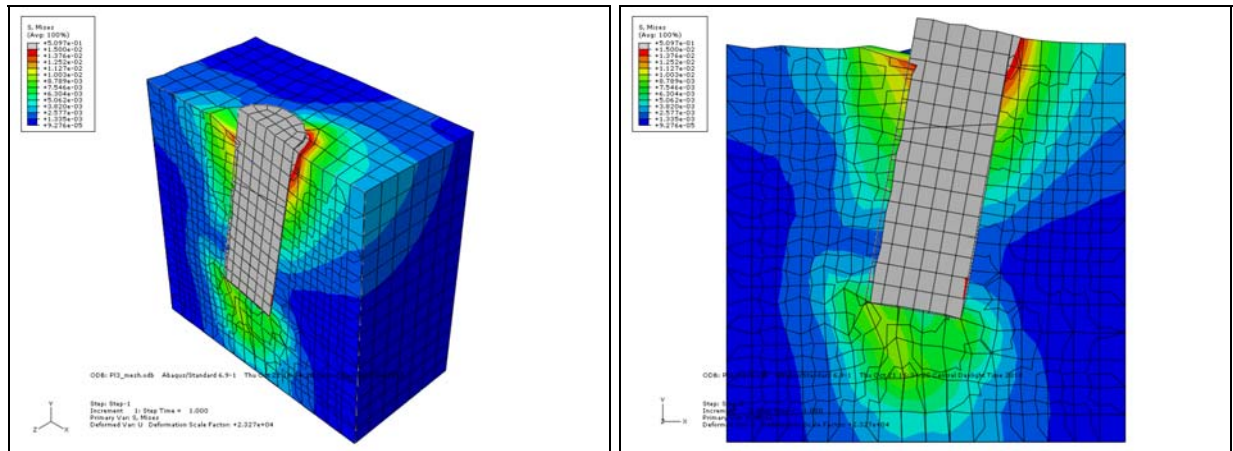


Figure 6.5. Stress in the Surrounding Soil after Loading.

From the Figure 6.4 results, when the shaft was pulled by tensile load acting at an angle of 16.1° with the horizontal plane, stress at the top of the shaft is directly increased and transferred to the adjacent node and to the lower component until the end of the shaft. In addition, Figure 6.5 shows that surrounding soils are affected from this loading. The highest stress is noted around the top of ground surface closed to the head shaft. Then, the stress increased in the soil is distributed to outer surrounding soil. Moreover, there is some additional stressing at the end of the shaft due to the soil resisting the movement at the bottom of the shaft.

Figure 6.6 compares the FEM model results with the field results and with the finite difference based model, LPILE. All the results from field results and FEM model were separated into horizontal components. Overall, the ABAQUS and LPILE program provide close results. Also, the results show that the ABAQUS model provides closer matching with field load test results than LPILE. However, the ABAQUS results still did not match exactly with the field results due to variations in soil parameters.

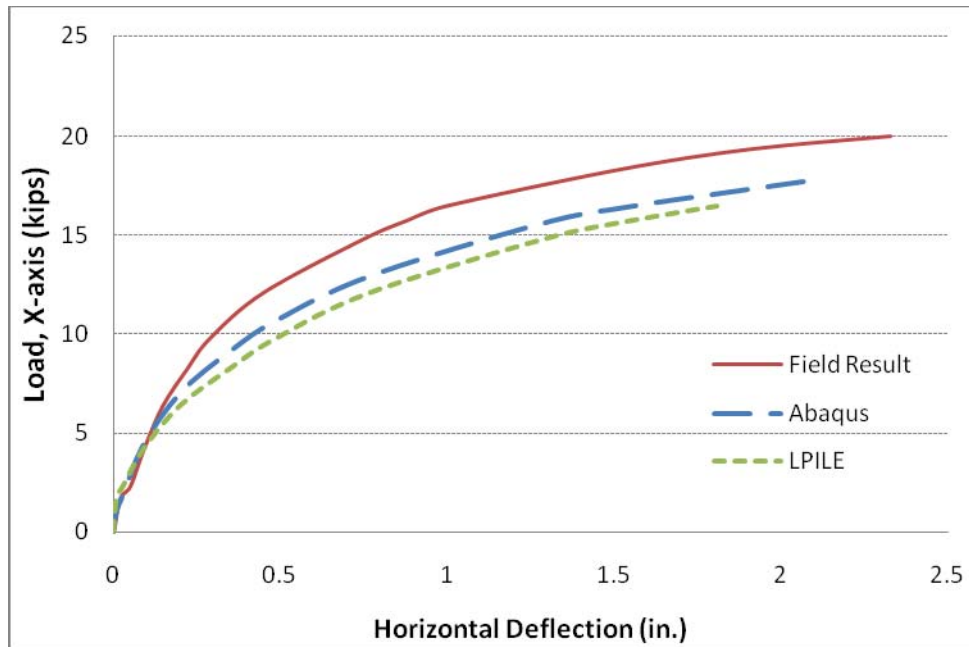


Figure 6.6. Comparison among Field Test Result, FEM Model by ABAQUS Program and LPILE Model of the 2 ft (0.6 m) Diameter × 6 ft (3 m) Depth.

Hence, in the proposed design chart development, researchers used the LPILE method for the design charts since this method's predictions are very close to measurements.

DEVELOPMENT OF DESIGN CHARTS

The following assumptions are used in the design chart development: all soil layers are assumed to be saturated and hence only undrained shear strength properties are considered in the design chart development. Predominantly two types of soil layers with clay layer of high plasticity are being underlain with another clay layer of mixed plasticity. Undrained shear strength of the upper clay layer is around 5.5 psi; for the lower layer, 3.3 psi. Factors for correcting lateral and uplift loads developed from the present research are also assumed to be valid for other soil strata conditions. This assumption is needed as load tests on drilled shafts of other soil strata are difficult to perform with various hypothetical soil layer conditions. From the previous section, the ultimate uplift force prediction model by Das and Seely and the ultimate lateral load prediction from LPILE are used in the design chart development. In the model validation, the trends from the uplift force predictions are overestimated when compared to the field test results; hence, the uplift predictions are reduced using factors of 0.22 and 0.28 for lateral movements of 0.5 and 1.0 in. criteria, respectively. The Das and Seely method does not

require the use of swell pressures of soil layers for uplift capacity analysis. Also, the lateral load predictions are underestimated when compared to the lateral component of the field test results and so, another factor higher than 1 (1.21 and 1.20 for lateral deflections of 0.5 and 1.0 in. criteria, subsequently) is used to correct the LPILE predictions.

After corrections of the predicted load data, both uplift force and lateral loads are combined to correspond to a resultant inclined load acting at a 16.1° angle to estimate the inclined load as shown in Eq. 26. Two soil layers with different types and depths of clay layers are considered in the analysis. Design chart results for ultimate inclined loads of drilled shafts of various diameters (1–3 ft [0.3–0.9 m]) and depths (6–14 ft [1.8–4.3 m]) are calculated as shown in Figures 6.7 and 6.8 for 0.5 and 1.0 in. permissible deflection criteria.

$$\text{Inclined load at } 16.1^\circ = \sqrt{(U^2 + L^2)} \cos(\tan^{-1} \frac{U}{L} - 16.1^\circ) \quad (26)$$

where U = Uplift force.

L = Lateral force.

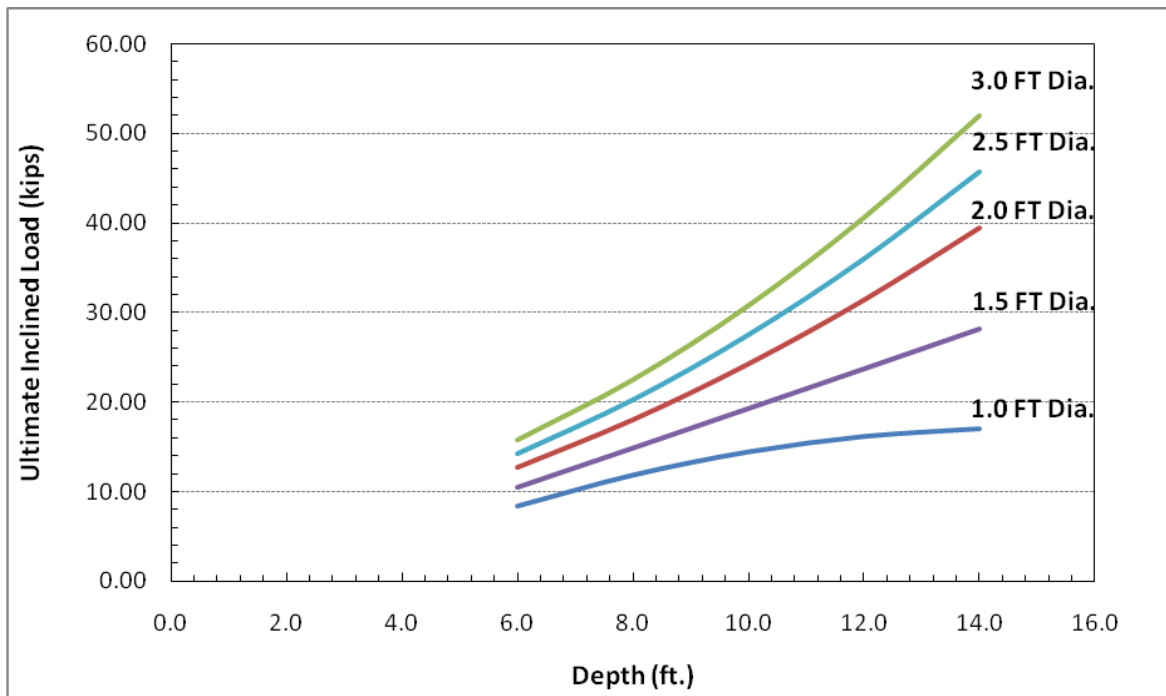


Figure 6.7. Design Chart on Field Results for Finding the Appropriate Size of Drilled Shaft in the Cable Barrier Systems by Using 0.5 in. Lateral Deflection Criterion.

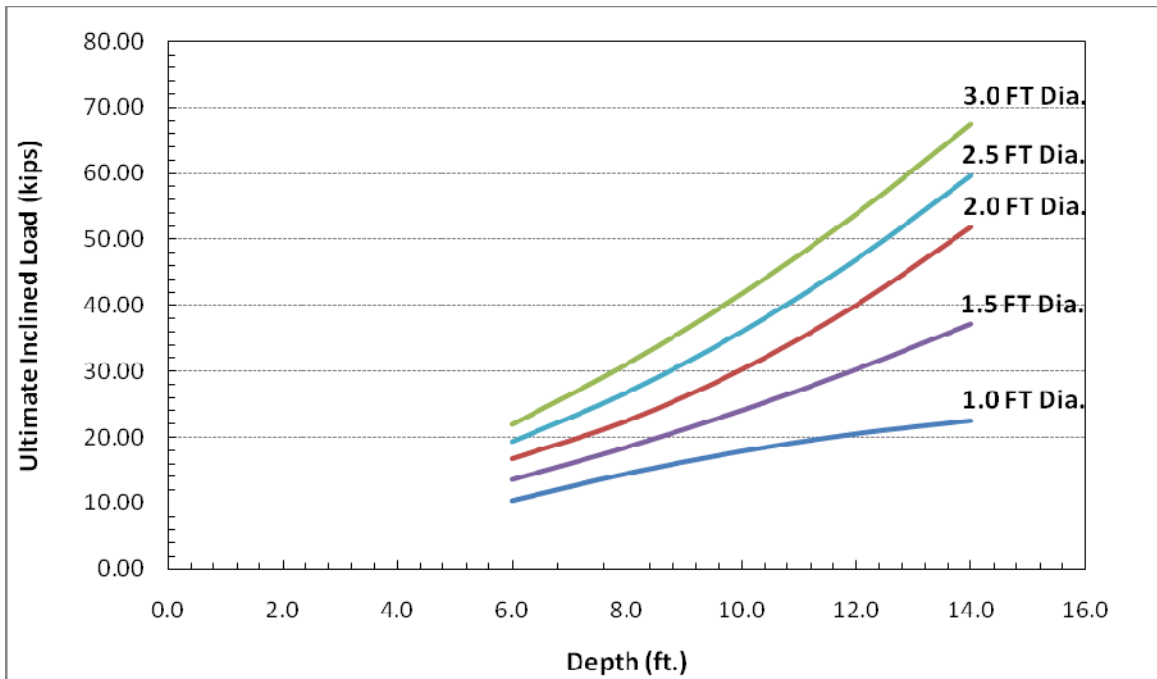


Figure 6.8. Design Chart Based on Field Results for Finding the Appropriate Size of Drilled Shaft in the Cable Barrier Systems by Using 1.0 in. Lateral Deflection Criterion.

Researchers conducted further analysis to develop design charts that could be used for different soil conditions. In this analysis, the top 3 ft clay layer of undrained shear strength of 250 psf is considered constant for the entire analysis. The bottom two clay layers with undrained shear strength properties (S_u) varying between 250–500 psf, 500–1000 psf, 1000–1500 psf, and 1500–2000 psf, are considered and average undrained shear strengths for these layers are calculated. Figure 6.9 shows the average undrained shear strength calculations.

The final selection of the design charts are based on several LPILE analyses with various soil strength properties in the bottom layer. Figure 6.10 presents the LPILE results for various layers. For each range (e.g., 250–500, 500–250 psf, and others), the lower bound of the predicted capacity is considered for conservative and safe designs of foundations. This will not only lead to safer design of drilled shafts, but will also simplify the use of design charts.

Overall, four design chart categories are introduced, based on the average undrained shear strengths of the bottom layer. These charts are termed as Design Charts A, B, C, and D; they are valid for four ranges of average undrained shear strength of bottom layer (between 3 and 12 ft) varying from 250–500 psf, 500–1000 psf, 1000–1500 psf, and 1500–2000 psf, respectively (Figure 6.11). Soils that exhibit undrained shear strengths more than 2000 psf are not considered

here as such soils are considered strong; in such cases, Design Chart D will be recommended for usage in such cases.

Design Charts A, B, C, and D with 0.5 and 1.0 deflection criteria are shown in the Figures 6.12–6.19. Overall, 16 scenarios of various soils layers are considered in this analysis, which is expected to capture various soil strata and their strength properties.

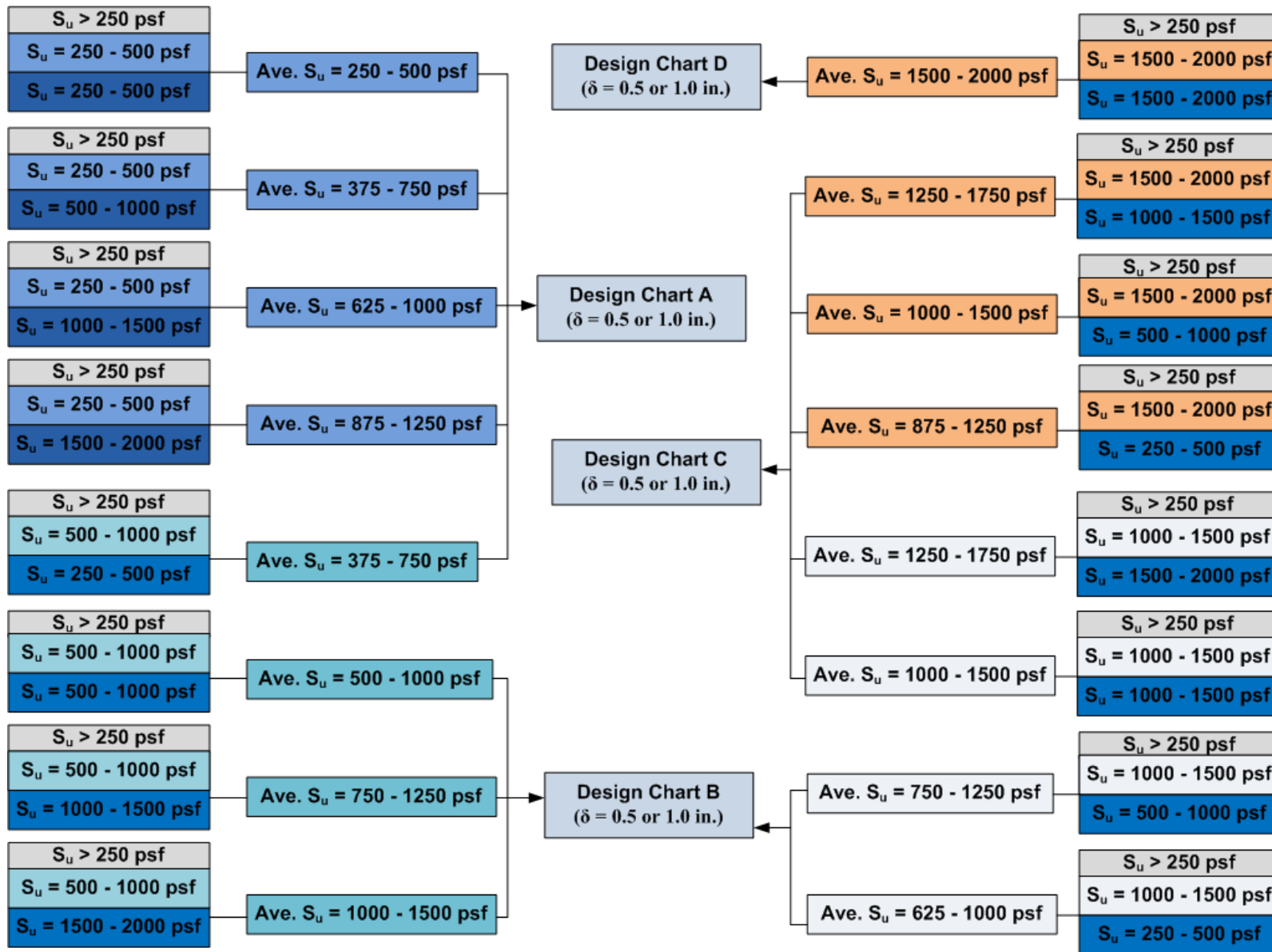


Figure 6.9. Flow Chart for Choosing the Design Chart for Bottom Layer Consideration.

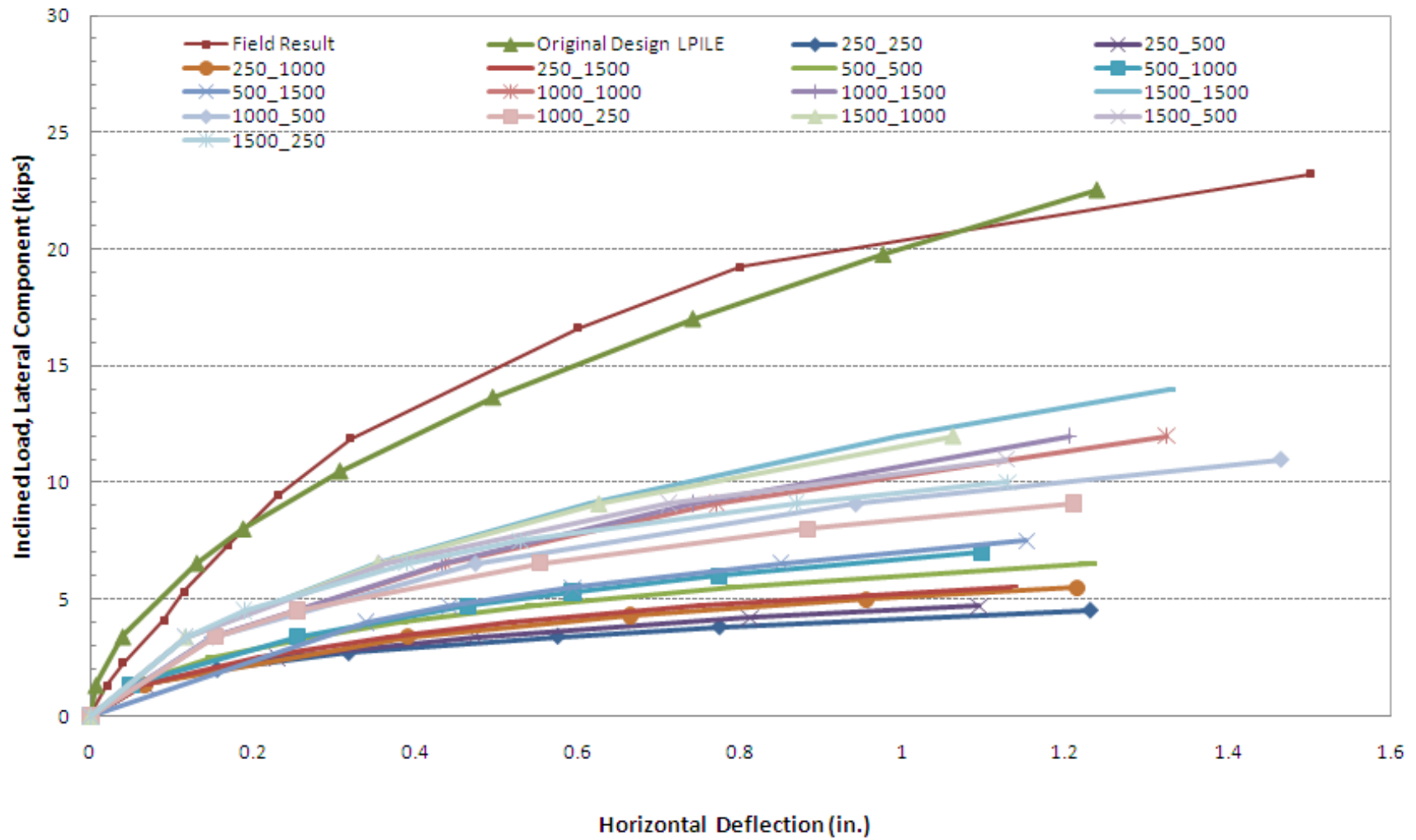


Figure 6.10. An Example of LPILE Results under Different Undrained Shear Strengths.

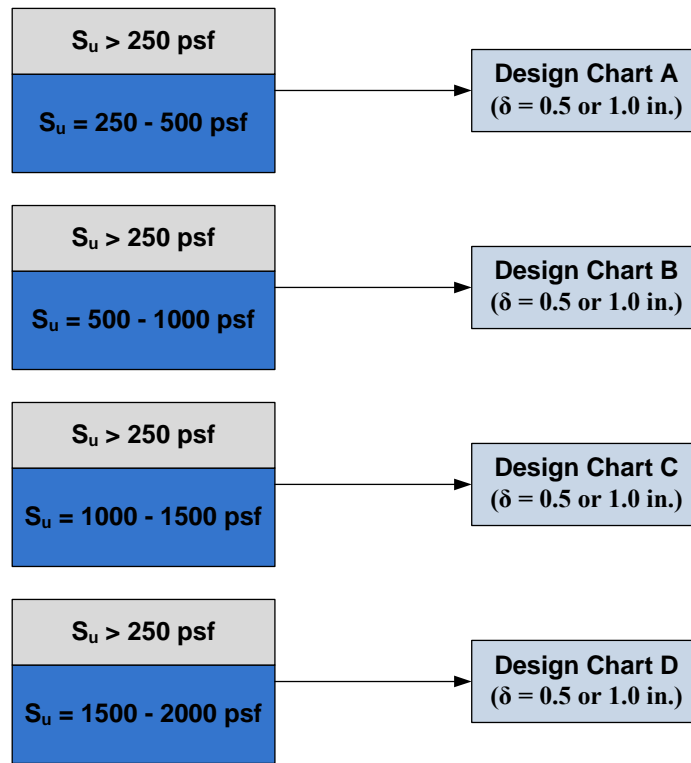


Figure 6.11. Flow Chart for Choosing the Design Chart for 1 Bottom Layer Consideration.

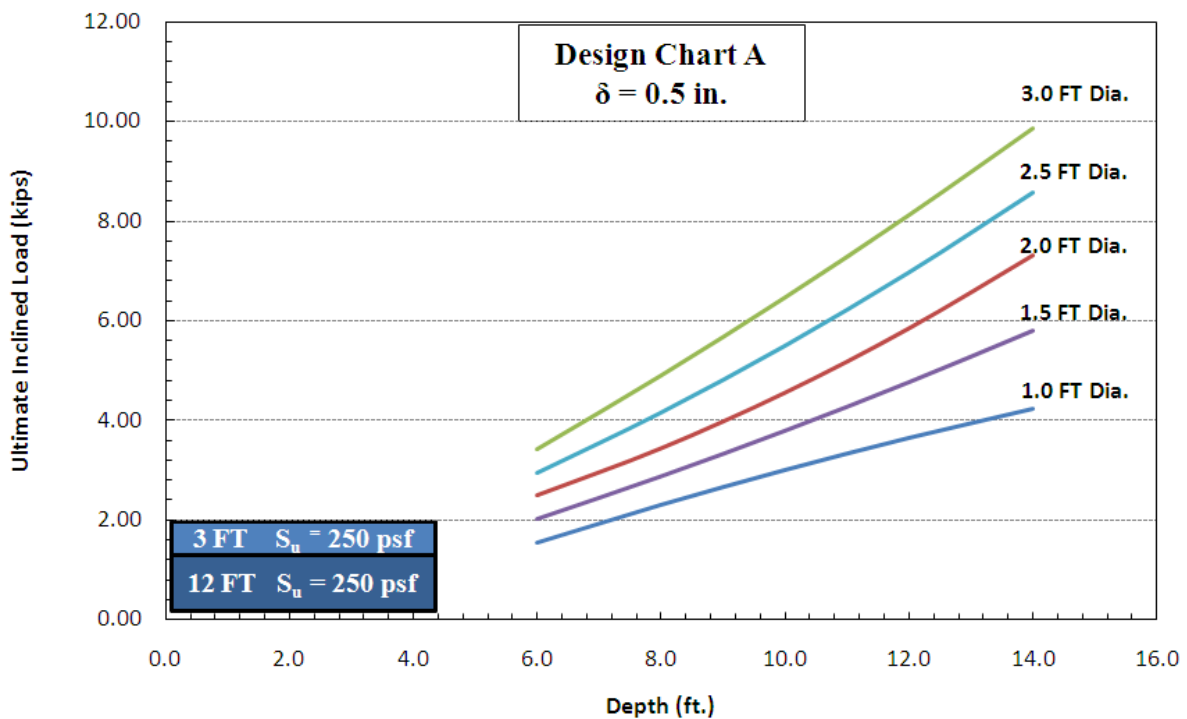


Figure 6.12. Design Chart A with 0.5 in. Deflection Criteria (δ).

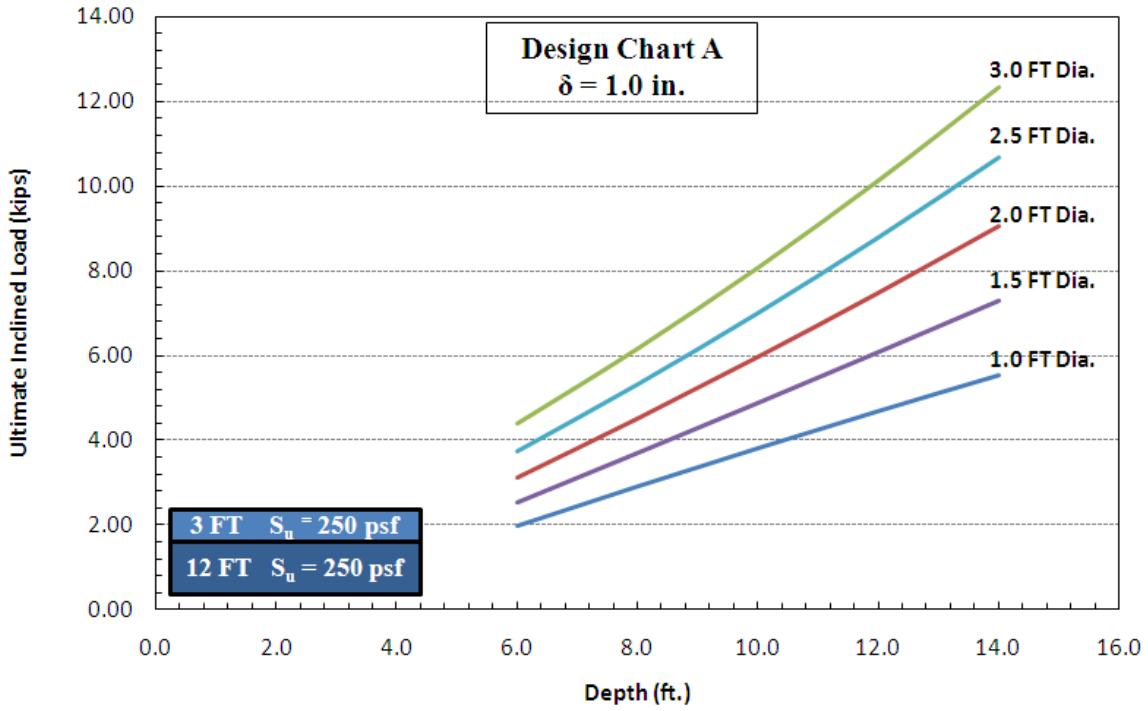


Figure 6.13. Design Chart A with 1.0 in. Deflection Criteria (δ).

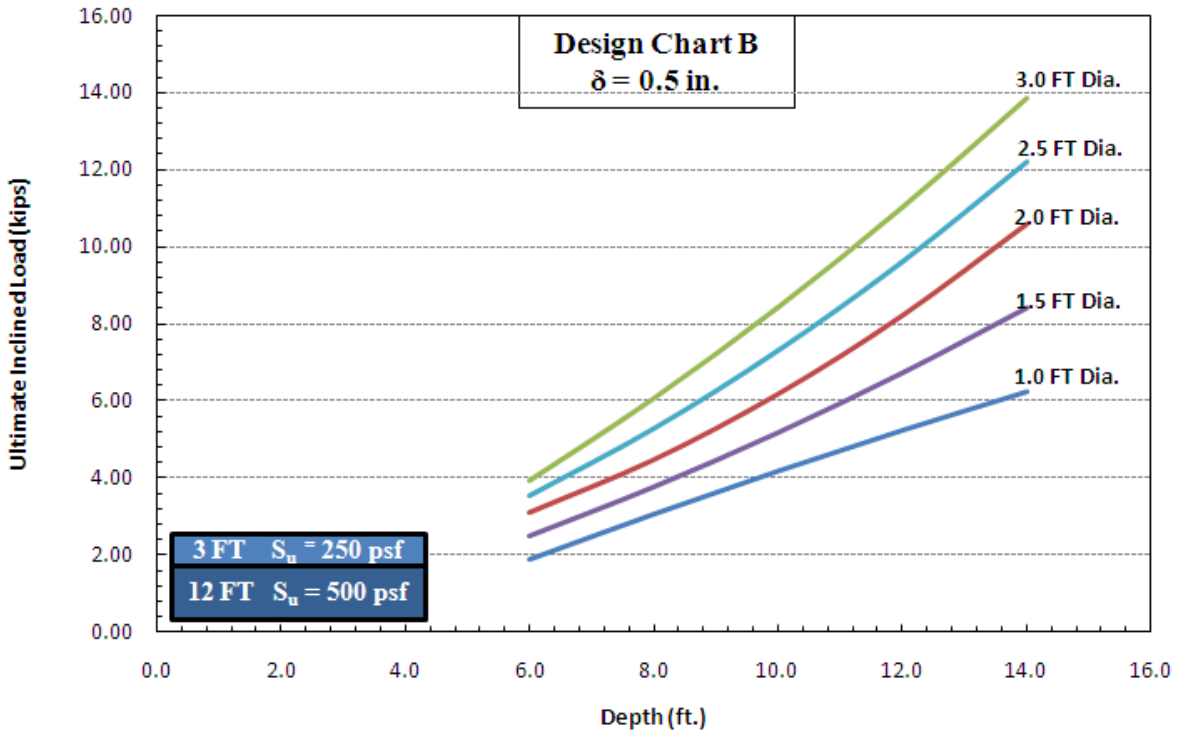


Figure 6.14. Design Chart B with 0.5 in. Deflection Criteria (δ).

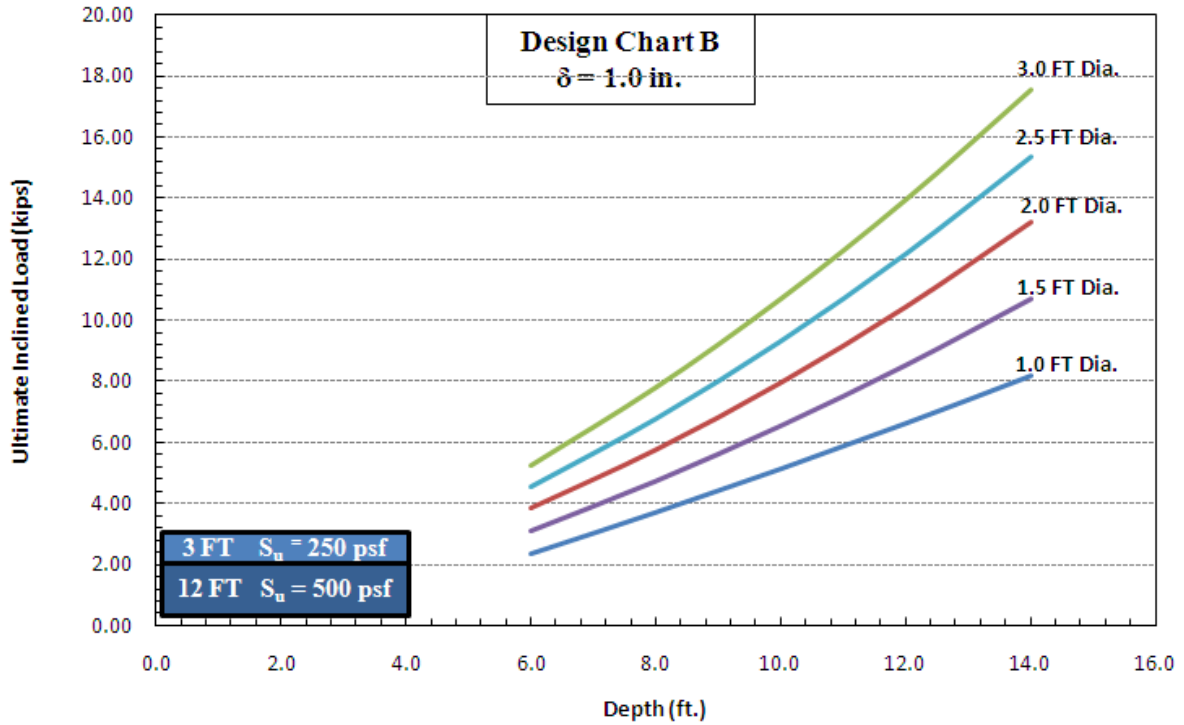


Figure 6.15. Design Chart B with 1.0 in. Deflection Criteria (δ).

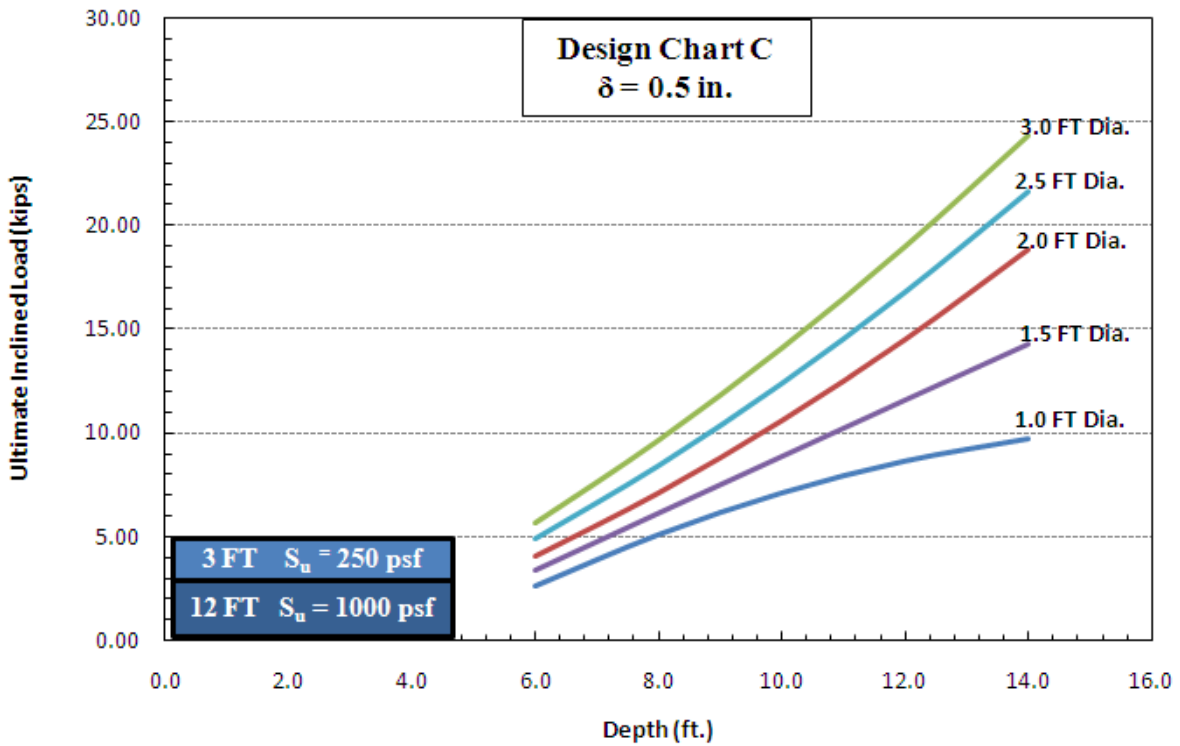


Figure 6.16. Design Chart C with 0.5 in. Deflection Criteria (δ).

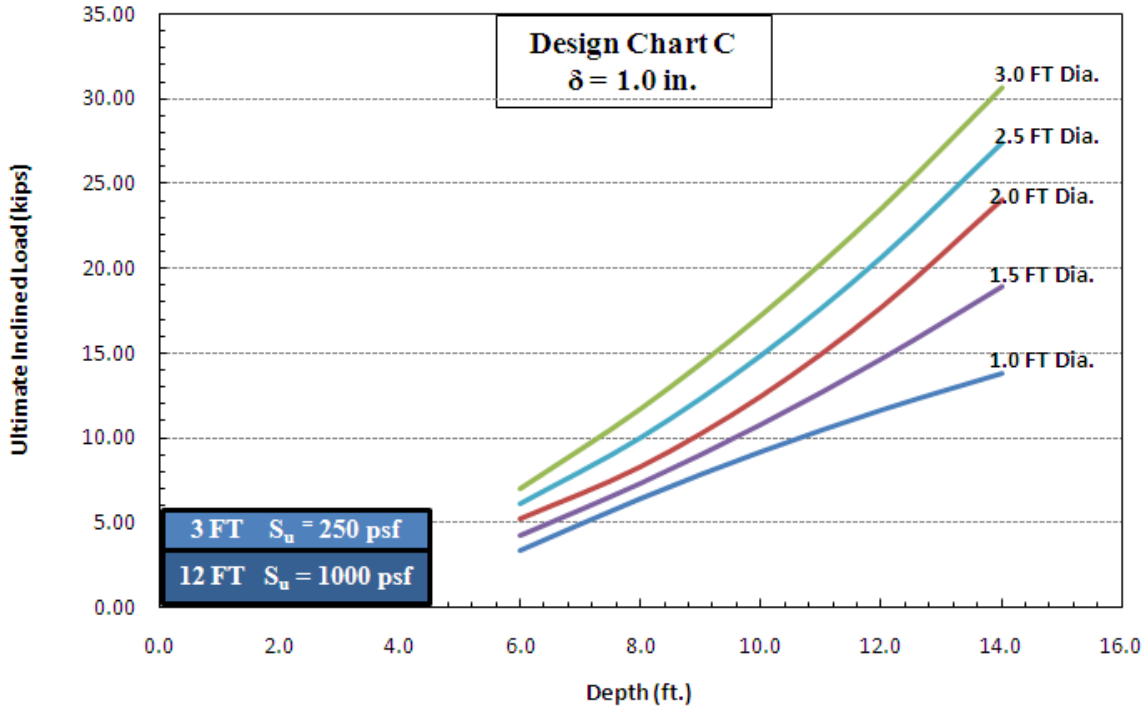


Figure 6.17. Design Chart C with 1.0 in. Deflection Criteria (δ).

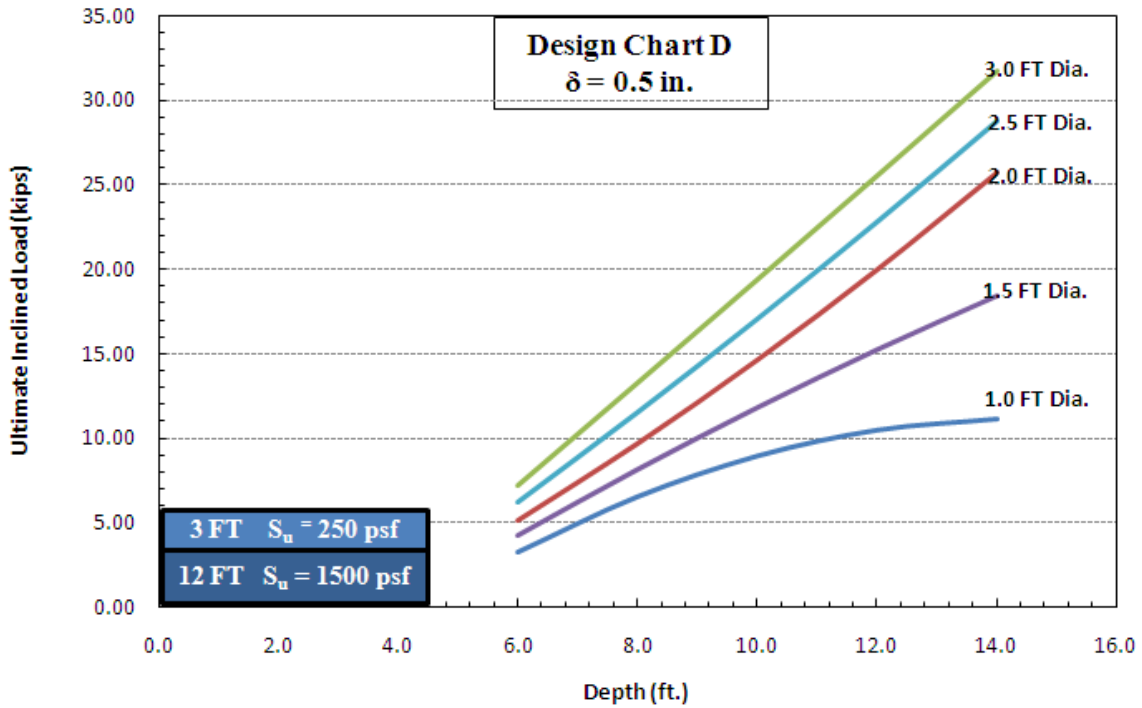


Figure 6.18. Design Chart D with 0.5 in. Deflection Criteria (δ).

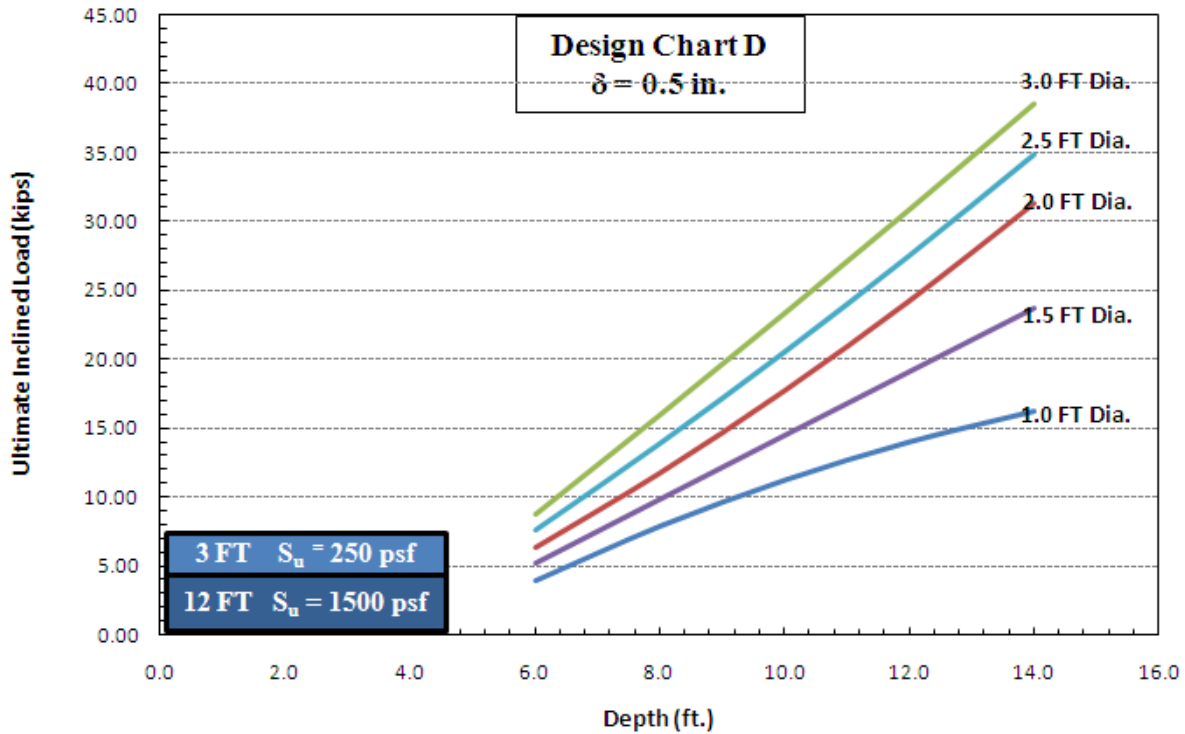


Figure 6.19. Design Chart D with 1.0 in. Deflection Criteria (δ).

To use a specific design chart, the undrained strengths of soils below 3 ft of the ground surface are needed. A simple arithmetic average of the undrained shear strengths is recommended for this step to choose the appropriate chart for designing the drilled shaft. The next section describes the steps involved in using the design chart to determine the sizes of the drilled shaft.

The design tensile strength of the cables used in the cable barrier systems can vary between 3000 lb for hot temperature conditions (around 100°F) to 8000 lb for cold temperature conditions (below 0°F). Before selecting the number of cables from the present design charts, it is imperative to ensure that the tensile strength of the cables used can withstand the design tension that will be mobilized due to cold temperature conditions. If needed, more cables can be used to avoid material failure during the field operation conditions.

The present design charts are developed for a three-cable barrier system. However, in the case of the two-cable barrier system, users should check the cable material strength failure as an additional design step. If the present design principles do not result in two or three cable barrier

system due to deficiencies in material strength or extreme soil and environmental conditions, the researcher recommends the use of single shaft for each cable barrier.

Example Illustrating the Use of the Design Chart

When using the Design Chart to find the appropriate sizes of drilled shafts for supporting cable barriers, there are three main factors that need to be considered. The first one is determining the undrained soil strength properties in the region. The second is establishing the tensile load generated in the cable based on the assumed coldest temperature that the systems might experience. The last is finding available space for the drilled shaft installation. From the manufacturer’s design specifications, the load experienced by the cable at the ambient temperature condition is used to determine the tension in the cable, which is the proven load to prevent cross-over collisions. An example design problem is given here:

Step 1: Cable barrier system needs to be constructed in the area where most of the soil is clay. Site investigation shows the soil located is on clayey subsoil and the undrained shear strength of soil layers are given in the Table 6.4.

Table 6.4. Example of Undrained Shear Strength for Choosing the Design Chart.

Depth (ft)	Undrained Shear Strength (S_u), psf
0–4	700
4–9	1000
9–15	750

The Flow Chart shown in Figure 6.19 identifies Design Chart B for 0.5 or 1.0 deflection criteria as the best design chart suitable for the above soil condition. The 1.0 in. deflection criterion is used here for the design and construction. Hence, the Design Chart B with 1.0 in. deflection criterion is selected (Figure 6.13).

Step 2: In a 3-cable barrier system, the tension of each cable at 10°F (−12.2°C) should be 7200 lb. A cold temperature condition of 10°F (−12.2°C) is considered here as the worst case field temperature. Since all three cables are anchored into one single drilled shaft, the ultimate load acting on the drilled shaft is $7,200 \text{ lb} \times 3 \text{ cables} = 21,600 \text{ lb}$ (21.6 kips).

Step 3: Typically the factor of safety values against overturning (lateral failure) or pullout (uplift) failures of the drilled shaft are around 1.5 to 2.0. A value of 2 is assumed here for

conservative design. Therefore, the ultimate load that the shaft needs to resist is $21,600 \text{ lb} \times 2.0 = 43,200 \text{ lb}$ (43.2 kips).

Step 4: Figure 6.13 shows that a load estimated from the previous step is beyond the boundary provided in the graph. Hence, the number of cables connected to the drilled shaft should be changed to two cables connected to one drilled shaft plus another cable to a drilled shaft or three cables separated and connected to one single drilled shaft. Here, one cable connected to a drilled shaft is chosen.

Step 5: The ultimate load acting on one cable attached to one drilled shaft is recalculated as $7200 \text{ lb} \times \text{F.S. of } 2$ and this value is equivalent to $14,400 \text{ lb}$ (14.4 kips). Thus, from Figure 6.13, the appropriate sizes to withstand this load are 3.0 ft diameter \times 12 ft depth and 2.5 ft diameter \times 14 ft depth, respectively, as shown in Figure 6.20. The final size of the shaft chosen from this group is based on construction considerations.

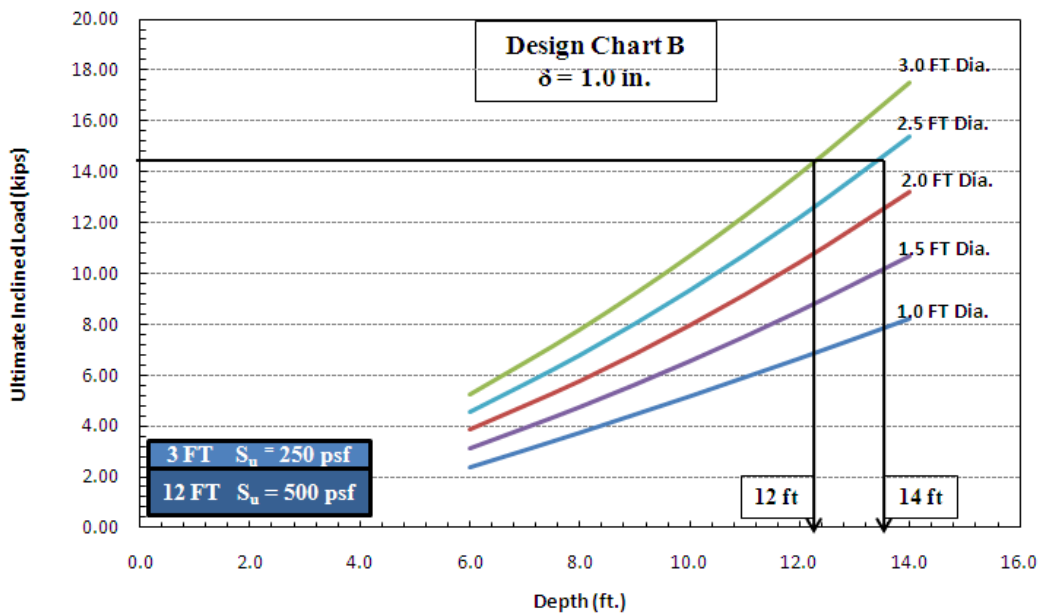


Figure 6.20. Example of Using the Design Chart.

Another variable that influenced the use of design chart is the assumed factor of safety value. Based on the limited number of field inclined load test data, currently the researchers recommended the FS value of about 1.5 to 2.0, which is quite high. However, this high value is needed as this design is related to safety issues involving human lives or to limit the number of crossover accidents. This FS value may be reduced in the future with the improved performance of these cables barriers with minimal distress.

CONSTRUCTION GUIDELINE AND RECOMMENDATION

The drilled shaft foundations for the cable barrier systems can be installed with general construction; however, there are a few additional recommendations for construction in high PI soils. During a wet season, water is the main issue that can make expansive soils swell. Thus, before construction starts, drainage should be provided at the areas close to the ends of each cable barrier system until the construction is finished. Another consideration: after excavation is finished, the lateral expansion of the expansive soil underneath the ground should be visually investigated to ensure that the cross-section of the drilled shafts is consistent along the depth of that shaft. If there is some lateral soil expansion in the hole, the solution is drilling again and using casings in that area.

Due to the potential swelling and shrinkage of the soil, a concrete pad or mow strip (Figure 6.11) should be placed on the ground surface at the top of the end drilled shaft plus around the first post next to the drilled shaft to keep soils surrounding the shaft from having low volume changes. Also, this pad or strip can prevent the surficial soil from cracking during the dry season. Appendix A gives the full details of the mow strip. Current TxDOT contracts usually require a concrete pad poured as a mow strip continuously for the entire run of the cable system. Researchers recommend that this practice continue with the additional requirement of pouring concrete 1–2 ft (0.3–0.6 m) past the end shaft.

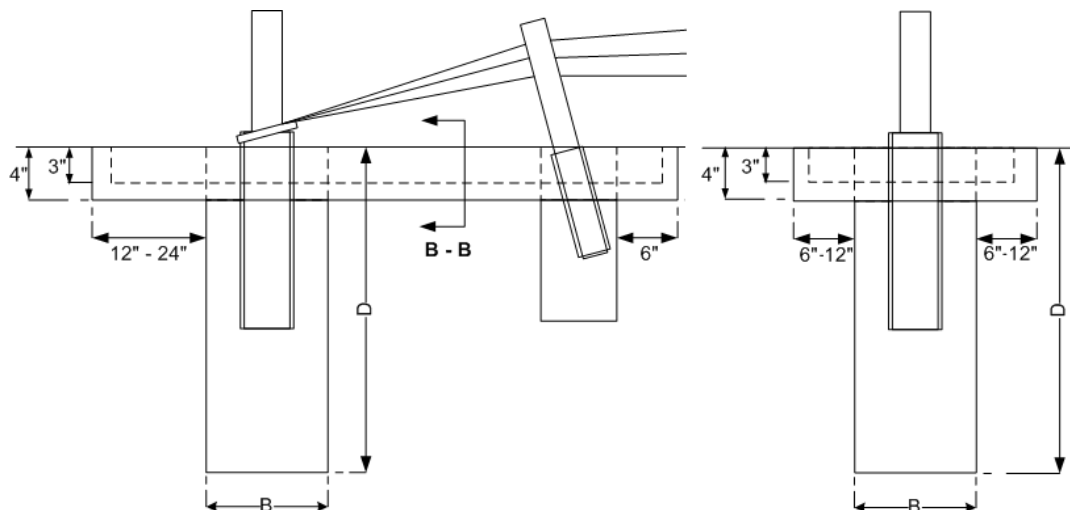


Figure 6.21. Details of Concrete Pad Placed on the Top of the Drilled Shaft at the End of Cable Barrier Systems.

During a dry season, construction can be performed normally. However, curing any concrete above ground is needed to retain water in the mix to propagate the hydration process as long as possible, thus yielding the highest strength.

Another recommendation for the maintenance program is monitoring and re-tensioning of cables. In one year, there are two major changes of the weather condition—hot to cold and cold to hot—that has a big impact on the absence of tensile force in cables. Therefore, monitoring should be performed at least twice a year (winter and summer), and re-tensioning cables is necessary if the cable tension does not match the tension chart based on the current temperature provided by different manufacturers.

CHAPTER 7

SUMMARY AND CONCLUSIONS

The failure occurred in 2007 when the area south of Terrell in Kaufmann County, Texas, had received an abundance of rain and experienced unusually cold weather for an extended period. Researchers hypothesized that soil expansion caused uplift and tensile forces in the cables created by the colder weather and, in turn, caused the failures. They then developed a plan to confirm or reject this hypothesis. This research effort focused mainly on site selection, site soil characterization, load test facility design and construction, and discussion of the load test results. The following narrative describes some of the major findings and summary results from this thesis research effort.

A test site was located on IH 20 at Rose Hill Road, which is near the site of the two previous failures, in an area that would readily accommodate the construction equipment, provide unrestricted access, and provide safety from the travelling public.

Preconstruction field investigation and laboratory testing yielded soil that was classified as silty sand, high-plasticity clay, and lean clay. The two clay soils were of significant interest to the researchers for this study. From these test results, researchers deemed that the selected site was very satisfactory for continuing the installation of the design test sets in the field. Additionally, weather conditions during the past nine months from June 2009 to February 2010 allowed the researchers to perform load tests under summer- and winter-like conditions that contributed to the two actual cable barrier systems failures three years earlier.

In September 2009, field testing for the summer condition (dry and hot) occurred. This consisted of testing one test shaft from each of the three reaction shafts. As the hypothesis focused on soil expansion and cold weather, these three tests were used only for comparison purposes here. In February 2010, the additional nine shafts were subjected to load tests under ideal field winter conditions (totally saturated soil and cold temperatures). The area also unexpectedly received a record 24-hour snowfall of 12 in. (300 mm) adding to the continuance of the soil being totally saturated. Ice lenses were seen on the water that was ponded on the ground surface, indicating freezing temperatures during the night. The 1 ft (0.3 m) and 2 ft (0.6 m) test shafts experienced large lateral and vertical displacements due to the load testing during this winter condition. Cracking of the concrete, both horizontally and vertically, was

observed on several of the test shafts. The 3 ft (0.9 m) shafts did not experience displacement nor material failure. The following summarizes a few major conclusions from this research.

- Site selection and soil characterization showed that the upper strata contained soils that can be characterized as expansive in nature. The volumetric swell strains of Soil Layers 2 and 3 are 11.1 percent and 7.7 percent and the linear/volumetric shrinkage strains are 12.1/6.8 percent and 8.4/5.22 percent, respectively. These results indicate that the present soils close to the surface are indeed expansive.
- The load test design includes a design of the reaction and the test shaft configuration and spacings between them. Preliminary LPILE analyses conducted on these reaction and test shafts using the hypothetical lateral loads estimated from tensile loads in the cables showed that a spacing of 20 ft between each reaction and test shaft for the given testing condition resulted in lesser influence of the reaction shaft movements on the test results.
- The load tests in the inclined configuration were successful and the field load testing went smoothly as per the design. Ultimate inclined loads were successfully obtained for the majority of the tests conducted. Though the channel section to which the Dywidag bar was connected had yielded in one test, this incident was quickly corrected with additional splicing, resulting in the completion of the test. Subsequent tests on all of the other test shafts were conducted by providing the same additional splicing at each of the steel channel pieces. Overall, the inclined load tests were conducted successfully in these north Texas soil conditions.
- Tests under inclined loads showed different failure modes at different seasonal periods. These include large lateral and vertical movements for smaller diameter shafts to breaking of the shafts near the ground surface zones due to high tensile stresses being developed from the loadings.
- Tests conducted on the shafts of identical dimensions in the summer and winter conditions showed that the load-displacement response in the hot and dry season condition (summer) was close to the brittle failure condition. In the wet and cold season condition (winter), however, the response was close to the flexible failure condition.
- Ultimate loads on the smaller test shafts appear not to be influenced by the weather condition. However, the 2 ft diameter shafts yielded higher ultimate loads in the summer condition tests than in the winter condition tests.

This research also presents models to be used for the analysis, design, and construction of drilled shafts used as foundations for cable barrier systems. A few models for the ultimate uplift capacity and the lateral load are used to compare and generate the graph helping in design selection. A few conclusions based on the test results of the various sizes of the drilled shafts, model comparisons, and the design charts are summarized in the following:

- Models that were used in this study are separated into two axes. The ultimate uplift capacity was used for the vertical direction and the ultimate lateral load was used for the horizontal direction. From the comparisons between the field test results and the developed models, the uplift capacity of Das and Seely's model provided reasonable results with an average ratio between the field test and the predicted results at 0.22 and 0.28 for 0.5 in. and 1.0 in. criteria. For the ultimate lateral load, the p-y Method using the LPILE program provided the best-fit results against the field test results with over-predicted results at 1.21 and 1.20 for 0.5 in. and 1.0 in. criteria, respectively.
- The Design Chart was developed based on the exact soil sampled and tested in that area and the combination between the validated models in the vertical and horizontal axes. The load shown in the graph is the ultimate load. Therefore, prior to taking the considered load to the Design Chart, a factor of safety (F.S.) of 1.5–2.0 applied for against pulling-out (uplift) and overturning (lateral load) should be used for that load. When choosing an appropriate drilled shaft size, the available space for the drilled shaft construction, the depth that can be drilled, and financial costs must be taken into consideration.

A construction guideline is provided in this paper. It shows the schematic of drilled shaft construction located in expansive soil used at the ends of the cable barrier systems. In addition, a few recommendations used for construction in dry and wet seasons and maintenance program are explained.

REFERENCES

Abendroth, R. E., Greimann, L. F., and Ebner, P. B. (1989). "Abutment pile design for jointless bridges." *Journal of Structural Engineering, ASCE*, 115 (11), pp. 2914–2929.

Alberson, D. C. (2006). Update on guidelines for the selection of cable barrier systems. *NCHRP Project, 20-7 (210)*.

Albin, R. B., Bullard D. L., Jr., and Menges, W. L. (2001). Washington State cable median barrier. *Transportation Research Record*, (1743), pp. 71–79.

Al-Khafaf and Hanks, R. J. (1974). "Evaluation of the Filter Paper Method for Estimating Soil Water Potential." *Soil Science*, Vol. 117, pp. 194–199.

Al-Saoudi, N. K. S. and Salim, H. M. (1998). "The behavior of groups of reinforced concrete model piles in expansive soil." *Proceedings of the 2nd International Conference on Unsaturated Soils, Beijing, August, Technical Committee of the 2nd International Conference on Unsaturated Soils*. Eds., Vol. 1, pp. 321–326.

Ashour, M., Norris, G., and Pilling, P. (1998). "Lateral Loading of a Pile in Layered Soil Using the Strain Wedge Method." *Journal of Geotechnical and Geoenvironmental Engineering, ASCE*, Volume 124, No. 4, pp. 303–315.

Ashour, M., Norris, G. M., and Pilling, P., (2002). "Strain Wedge Model Capability of Analyzing Behavior of Laterally Loaded Isolated Piles, Drilled Shafts, and Pile Groups." *Journal of Bridge Engineering*, Volume 7, No. 4, July 2002, pp. 245–254.

ASTM C31 / C31M – 09, (2009), "Standard Practice for Making and Curing Concrete Test Specimens in the Field." ASTM International, West Conshohocken, PA., 2009, DOI: 10.1520/C0031_C0031M-09, www.astm.org.

ASTM C39 / C39M – 05e2, (2005), "Standard Test Method for Compressive Strength of Cylindrical Concrete Specimens." ASTM International, West Conshohocken, PA., 2005, DOI: 10.1520/C0039_C0039M-05E01, www.astm.org.

ASTM C617 – 09a, (2009), "Standard Practice for Capping Cylindrical Concrete Specimens." ASTM International, West Conshohocken, PA., 2009, DOI: 10.1520/C0617-09A, www.astm.org.

ASTM Standard D698-00a. (2003). "Standard Test Method for Laboratory Compaction Characteristics of Soil Using Standard Effort (12,400 ft-lbf/ft³ (600 kN/m³))." *Annual Book of ASTM Standards*, Soil and Rock (I), 4(8), ASTM International, West Conshohocken, PA.

ASTM Standard D2487-00. (2003). "Standard Classification of Soils for Engineering Purposes (Unified Soil Classification System)." *Annual Book of ASTM Standards*, Soil and Rock (I), 4(8), ASTM International, West Conshohocken, PA.

ASTM Standard D2850-95 (2003), “Standard Test Method for Unconsolidated-Undrained Triaxial Compression Test on Cohesive Soils.” *Annual Book of ASTM Standards*, 4(8), ASTM International, West Conshohocken, PA.

ASTM Standard D3080-98, (2003), “Standard Test Method for Direct Shear Test of Soils Under Consolidated Drained Conditions.” *Annual Book of ASTM Standards*, 4(8), ASTM International, West Conshohocken, PA.

ASTM Standard D 3966-90, (2003), “ASTM, Standard Test Method for Piles Under Lateral Loads.” *Annual Book of ASTM Standards*, 4(8), ASTM International, West Conshohocken, PA.

ASTM Standard D4318-05. (2003). “Standard Test Methods for Liquid Limit, Plastic Limit, and Plasticity Index of Soils.” *Annual Book of ASTM Standards*, Soil and Rock (I), 4(8), ASTM International, West Conshohocken, PA.

ASTM Standard D4546-96, (2003), “Standard Test Methods for One-Dimensional Swell or Settlement Potential of Cohesive Soils,” *Annual Book of ASTM Standards*, 4(8), ASTM International, West Conshohocken, PA.

ASTM Standard D5298-03, (2003), “Standard Test Method for Measurement of Soil Potential (Suction) Using Filter Paper,” *Annual Book of ASTM Standards*, 4(8), ASTM International, West Conshohocken, PA.

Aung, K. K. Rahardjo, H. Leong, E. C. and Toll, D. G. (2001). “Relationship between porosimetry measurement and soil water characteristic curve for an unsaturated residual soil.” *Geotechnical and Geological Engineering*, 19, pp. 401–416.

Bhushan, K., Haley, S.C., and Fong, P. T. (1979). “Lateral Load Tests on Drilled Piers in Stiff Clays.” *Journal of Geotechnical Engineering Division, ASCE*, 105 (GT 8), pp. 969–985.

Brinch Hansen, J. (1961). “The ultimate resistance of rigid piles against transversal forces.” *Geoteknisk Institutionel Bulletin*, (12). Copenhagen, Denmark.

Broms, B. B. (1964a). “Lateral resistance of piles in cohesive soils.” *Journal of the Soil Mechanics and Foundation Division*, 90 (SM2), pp. 27–63.

Broms, B. B. (1964b). “Lateral resistance of piles in cohesionless soils.” *Journal of the Soil Mechanics and Foundation Division*, 90 (SM3), pp. 123–157.

Broms, B. B. (1965). “Design of Laterally Loaded Piles.” *Journal of the Soil Mechanics and Foundation Division*, 91 (SM3), pp. 77–79.

Cameron, D. A. and Walsh, P. F. (1981). “Timber piles for residential foundations in expansive soil.” *1st National Local Government Engineering Conference, Adelaide*, August. pp. 165–169.

Casagrande, A. (1932b). Discussion of “A New Theory of Frost Heaving” In A.C. Benkelman and F.R. Ohlmstead (Eds), Proceedings of the Highway Research Board, 11 pp. 168–172.

Chapel, T. A. and Nelson, J.D. (1998). “Field investigation of helical and concrete piers in expansive soil”. *Proceedings of the 2nd International Conference on Unsaturated Soils, Beijing*, August, 1998, Technical Committee of the 2nd International Conference on Unsaturated Soils Eds., Vol. 1, pp. 206–211.

Chen, F. H. (1988). *Foundations on expansive soils*, 2nd Edition. New York, USA: Elsevier Science Publications.

Chen, F. H. (2000). *Soil Engineering: Testing, Design, and Remediation*, Florida, USA: CRC Press LLC.

Craig, R. R. (1999). *Mechanics of Materials*, 2nd edition. New York, USA: John Wiley & Sons, Inc.

Czerniak, E. (1958), “Design Criteria for Embedment of Piers,” Consulting Engineer, March 1958.

Das, B. M., and Seeley, G. R. (1982). “Uplift Capacity of Pipe Piles in Saturated Clay,” *Soils and Foundations*, The Japanese Society of Soil Mechanics and Foundation Engineering, Vol. 22, No. 1, pp. 91–94.

Davisson, M. T., and Robinson, K. E. (1965). “Bending and buckling of partially embedded piles.” *Proceedings, 6th International Conference on Soil Mechanics and Foundation Engineering*, 2, pp. 243–246.

Day, R. W. (2006). *Foundation Engineering Handbook*. New York, NY: McGraw-Hill.

Duffy, D. and Charania, E. (1984). ”Study of pile uplift characteristics in swelling clays using a newly developed test”. *Proceedings of the 5th International Expansive Soils Conference*, Adelaide, May, 1984, Vol. 1, pp. 75–79.

Duncan, J. M., Evans, L. T., Jr., and Ooi, P. S. K. (1994). “Lateral load analysis of single piles and drilled shafts.” *Journal of Geotechnical Engineering, ASCE*, 120 (6), pp. 1018–1033.

Dunnavant, T. W., and O’Neill, M. W. (1989). Experiment p-y Model for Submerged, Stiff Clay. *Journal of Geotechnical Engineering, ASCE*, 115(1), pp. 95–114.

Federal Highway Administration Publication No. FHWA-IP-84-11, *Handbook on Design and Construction of Drilled Shafts Under Lateral Load*, 1984.

Fredlund, D.G. and Rahardjo (1993). *Soil Mechanics for Unsaturated Soils*. New York, USA: John Wiley & Sons, Inc.

Fredlund, D.G., Xing, A., Huang, S. (1994). "Predicting the permeability function for unsaturated soils using the soil-water characteristic curve." *Canadian Geotechnical Journal*, Vol. 31, No. 4, August 1994, pp. 533–546.

Greimann, L. F., Abendroth, R. E., Johnson, D. E., and Ebner, P. E. (1987). *Pile design and tests for integral abutment bridge, Final Report*. Ames, Iowa: Iowa DOT Project HR-273, ISU-ERI-Ames 88060.

Hetenyi, M., (1946). *Beams on Elastic Foundations*. Ann Arbor: University of Michigan Press.

Hibbeler, R. C. (2008). *Mechanics of Materials 7th edition*. New Jersey, USA: Pearson Prentice Hall, Pearson Education.

Holtz, R. D., and Kovacs, W. D. (1981). *An Introduction to Geotechnical Engineering*. Eaglewood Cliffs, NJ: Prentice Hall.

Houston, W. N., Walsh, K. D., Harraz, A.M., Perry, C.R, and Houston, S.L. (2004). "Lateral Load Tests on Drilled Shafts in Cemented Soil." *Geotechnical Special Publication (Geo-Trans)*, ASCE, 126 (2), pp. 1258–1269.

Hussein E. A. (2001). "Viscoplastic Finite Element Model for Expansive Soils." *EJGE paper 2001-0122*.

International Building Code. (2003). "Presumptive Load-Bearing Values," International Code Council (ICC).

Ivey, D. L. and Hawkins, L. (1966), "Footing Design for Wind-Resistant Highway Sign Boards." *Texas Transportation Researcher, Texas Transportation Institute*, 2 (2), pp. 3–5.

Johnson, L. D., and Stroman, W. R. (1976). "Analysis of Behavior of Expansive Soil Foundations." *U.S. Army Engineer Waterways Experiment Station Technical Report S-76-8*.

Jones, D. E., and Holtz, W. G. (1973). "Expansive Soils—The Hidden Disaster." *Civil Engineering (ASCE)*, 43 (8), pp. 49–51.

Justo, J, Saura, J., Rodriguez, J, Delgado, A., Jaramillo, A. (1984). "A finite element method to design and calculate pier foundations in expansive collapsing soils." *Proceedings, 5th International Expansive Soils Conference, Adelaide 1*: pp. 119–123.

Kaplar, C. W. (1970). "Phenomenon and Mechanism of Frost Heaving." *Highway Research Record*, 304, pp. 1–13.

Kinney, E. E. (1959), "Correct Embedment for Pole Structures," *Wood Preserving News*, October, 1959.

Klaiber, F. W., White, D. J., Wipf, T. J., Phares, B. M., and Robbins, V. W. (2004). "Development of Abutment Design Standards for Local Bridge Designs." *Final Report for Iowa DOT TR-486: Volume 1 of 3, August 2004*, pp. 13–23.

- Lu, N. and Likos, W. J. (2004). *Unsaturated Soil Mechanics*. New York, USA: John Wiley & Sons, Inc.
- Marinho, F. A. M., Oliveira, O. M. (2006). “The filter paper method revisited.” *Geotechnical Testing Journal*, 29(3), pp. 1–9.
- Matlock, H., and Ripperger, E. A. (1958). “Measurement of soil pressure on a laterally loaded pile.” *Proceedings, American Society for Testing and Materials*, pp. 1245–1259.
- Matlock, H., and Reese, L. C. (1961). Foundation Analysis of Offshore Pile-Supported Structures.” *Proceedings, Fifth International Conference, International Society of Soil Mechanics and Foundation Engineering*, Paris, France, 2, pp. 91–97.
- Matlock, H. (1970). “Correlations for design of laterally loaded piles in soft clay.” *Proceedings 2nd Offshore Technical Conference*, 1, pp. 577–594.
- McClelland, B., and Focht, J.A., Jr. (1958). Soil modulus for laterally loaded piles. *Journal of Soil Mechanics Foundation Division, ASCE*, 123, pp. 1049–1086.
- McClelland, M. (1996). *History of Drilled Shaft Construction in Texas*. Paper presented before the 75th Annual Meeting of the Transportation Research Board, Washington, D.C.
- McVay, C. M., (2003). *Calibrating Resistance Factors for Load and Resistance Factor Design for Statnamic Load Testing*, Final Report BC354-42. Florida Department of Transportation.
- Meyerhof, G. G., and Adams, J. I. (1968). “The ultimate uplift capacity of foundations.” *Canada Geotechnical Journal*, 5, pp. 225–244.
- Meyerhof, G. G. (1973a). The uplift capacity of foundations under oblique loads. *Canadian Geotechnical Journal*, 10, pp. 64–70.
- Meyerhof, G. G. (1973b). “Uplift resistance of inclined anchors and piles.” *Proceedings, 8th International Conference on Soil Mechanics and Foundation Engineering*, Moscow, 2.1, pp. 167–172.
- Meyerhof, G. G. (1980). “The bearing capacity of rigid piles and pile groups under inclined loads in clay.” *Canadian Geotechnical Journal*, 18, pp. 297–300.
- Mitchell, J. K. (1976). *Fundamental of Soil Behavior*. New York, USA: John Wiley & Sons, Inc.
- Mohamedzein, Y. E. A., Mohamed, M. G. and Shareif, A. M. (1999). “Finite element analysis of short piles in expansive soils.” *Computers and Geotechnics*, Vol. 24, pp. 231–243.
- Nelson, J. D., and Miller, J. D. (1992). *Expansive Soils: Problems and Practice in Foundation and Pavement Engineering*. New York, NY: John Wiley & Sons, Inc.

Nuhfer E. B., Proctor R. J., and Moser N. (1993). *The Citizen's Guide to Geologic Hazards*. Arvada, CO: AIPG Press.

Nusairat, J., Liang, R. Y., Engel, R., Hanneman, D., Abu-Hejleh, N., and Yang, K. (2004). "Drilled Shaft Design for Sound Barrier Walls, Signs, and Signals," Final Report. Colorado Department of Transportation (CDOT). Report No. CDOT-DTD-R-2004-8.

O'Neill, M. W., and Poormoayed, N. (1980). "Methodology for Foundations on Expansive Clays." *Journal of the Geotechnical Engineering Division, ASCE*, Vol. 106, No. GT12, December 1980, pp. 1345–1367.

O'Neill, M. W., Reese, L. C., and Cox, W. R. (1990). "Soil behavior for piles under lateral loading." *22nd Annual Offshore Technology Conference*, Houston, TX, pp. 279–287.

O'Neill, M. W., and Reese, L. C. (1999). "Drilled shaft: Construction procedure and design methods." *Publication No. FHWA-IF-99-025*, 2, pp. 1–21.

Penner, E., and Burn, K. N. (1970). "Adfreezing and Frost Heaving of Foundations." *Canadian Building Digest*, National Research Council, Ottawa, Ontario: Institute for Research in Construction. *CBD-128*, 8.

Perez-Ruiz, D. D. (2009). "A Novel Servo-Controlled True Triaxial Apparatus for Modeling Unsaturated Soil Response under Suction-Controlled Stress Paths," Dissertation. Texas, USA: University of Texas at Arlington.

Petry, T. M., and Armstrong, J. C. (1989). "Stabilization of Expansive Soils." *Transportation Research Record*, (1219), pp. 103–112.

Power, K. C., Vanapalli, S. K. and Garga, V. K. (2008). "A Revised Contact Filter Paper Method." *Geotechnical Testing Journal*, 31 (6), pp. 1–9.

Punthutaecha, K., Puppala, A. J., Vanapalli, S. K., and Inyang, H. (2006). "Volume change behaviors of expansive soils stabilized with recycled ashes and fibers." *Journal of Materials in Civil Engineering*, 18 (2), pp. 295–306.

Puppala, A. J., B. Katha, and L. R. Hoyos. (2004). "Volumetric Shrinkage Strain Measurements in Expansive Soils Using Digital Imaging Technology." *ASTM Geotechnical Testing Journal*, Vol. 27, No. 6, 2004, pp. 547–556.

Reese, L. C., and Matlock, H. (1956). "Non-dimensional solutions for laterally loaded piles with soil modulus assumed proportional to depth." *Proceedings, 8th Texas Conference on Soil Mechanics and Foundation Engineering*. The University of Texas, Austin, Texas: Bureau of Engineering Research.

Reese, L. C., Cox, W. R., and Koop, R. D. (1975). "Field testing and analysis of laterally loaded piles in stiff clay." *Proceedings 7th Offshore Technical Conference*, 2, pp. 473–483.

- Reese, L. and Welch, R. (1975). "Lateral Loading of Deep Foundations in Stiff Clay." *Journal of Geotechnical Engineering Division, ASCE*, 101 (GT 7), pp. 633–649.
- Reese, L. C., and Allen, J. D. (1977). *Drilled shaft design and construction guidelines manual, Vol.2. Structural analysis and design for lateral loading*. U.S. Department of Transportation, FHWA, Office of Research and Development.
- Reese, L. C. (1984) "Handbook on Design of Piles and Drilled Shafts Under Lateral Loads," Report No. FHWA-IP-84-11.
- Reese, L. C. (1986) "Behavior of Piles and Pile Groups Under Lateral Loads," Report No. FHWA/RD-85/106 (NTIS PB86-238466).
- Robinson, B., Suarez, V., Robalino, P., Kowalsky, M., and Gabr, M. (2006). Pile Bent Design Criteria. *NC DOT Research Project 2005-19*. Report No. FHWA/NC/2006-14.
- Rollins, M., K., Weaver, T. J., and Peterson, K. T. (1997). "Statnamic lateral load testing of a full-scale fixed-head pile group," Report. UDOT, FHWA.
- Sinha, J. and Poulos, H. G. (1999). "Piled raft systems and free standing pile groups in expansive soils". *Proceedings, 8th Australia New Zealand Conference on Geomechanics*, Hobart, February, Vol. 1, pp. 207–212.
- Soil Moisture Equipment Corp. (2003). TRASE Operating Instruction.
- Sridharan, A., Sreepada R. A., Sivapullaiah, P. V. (1986). "Swelling Clays." *Geotechnical Testing Journal*, Vol. 9, No. 1, Mar, 1986, pp. 24–33.
- Terzaghi, K. (1955). "Evaluation of Coefficient of Subgrade Reaction." *Geotechnique* 5, pp. 297–326.
- Tex-107-E, (2002). "Determination the Bar Linear Shrinkage of Soils." *Manual of Material Testing Procedure*, Texas Department of Transportation (TxDOT), Austin, Texas.
- Ubanyionwu, G. I., (1985). *Uplift Capacity of Rigid Piles in Clay under Inclined Pull, Thesis*. Texas, USA: The University of Texas at El Paso.
- Welch, R. C., and Reese, L. C. (1972). "Laterally Loaded Behavior of Drilled Shafts." Research Report (89-10). The University of Texas at Austin: Center for Highway Research.
- Westman, E. C. (1993). "Evaluation of pier uplift in expansive soils." Master Thesis, Department of Civil Engineering, The University of Colorado at Denver.

Wiseman, G., Komornik, A., and Greenstein, J. (1985). "Experience with Roads and Buildings on Expansive Clays." *Transportation Research Record*, 103, pp. 60–67.

Yong, R. N., and Warkentin, B. P. (1975). *Soil Properties and Behavior*. New York, USA: Elsevier Science Publications.

**APPENDIX A: DESIGN AND CONSTRUCTION GUIDELINES FOR
SHAFTS SUPPORTING TRAFFIC BARRIERS (PRODUCT 1)**

DESIGN AND CONSTRUCTION GUIDELINES FOR DRILLED SHAFTS SUPPORTING MEDIAN CABLE BARRIER SYSTEMS

The design of a reliable drilled shaft foundation system was developed due to the failure of several foundations used to support highway median cable barrier systems. The failures observed when the cable barrier systems had failed in an abnormally wet and cold field condition. A subsequent factor determined in the failures revealed high plasticity soils located in the failure areas. The high plasticity soil has significant characteristics of swelling and shrinkage behavior creating many problems for pavements and structures. The actual failure mechanisms were determined to be excessive movement in both of the vertical and horizontal directions. To mitigate or negate these failures, research was performed to determine the various acceptable sizes of drilled shafts. The researchers selected drilled shaft sizes of 1 ft (0.3 m)–3 ft (0.9 m) diameter \times 6 ft (1.8 m)–14 ft (4.3 m) depth with testing in summer and winter (dry and wet condition), and using the same angle (16.1°) as the manufacturers' designs for the cable barrier systems as shown in Figure A.1

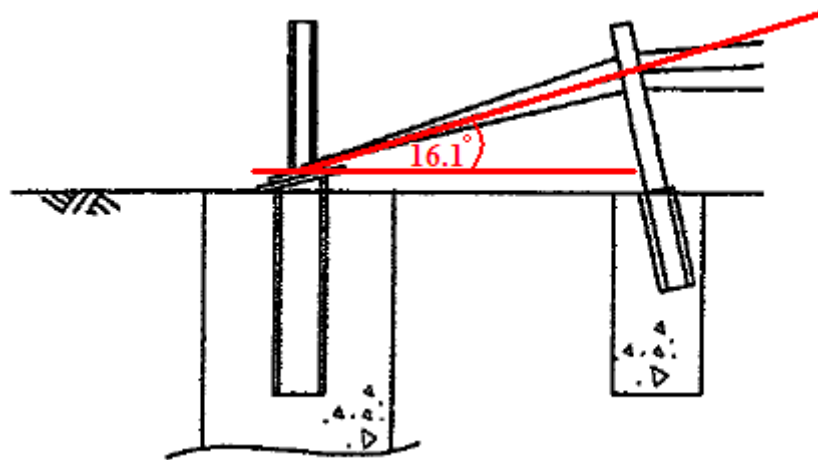


Figure A.1. Typical Cable End Slope Design.

Once the researchers selected the drilled shaft sizes to be used for testing and analysis, three test setups were constructed in the field to perform tests and collect data. A typical setup is shown in Figure A.2.



Figure A.2. View of a Reaction Shaft with Inclined Dywidag Bar.

In the field tests, each test shaft was subjected to an applied tension from a hydraulic jack mounted behind each reaction shaft and the load transferred through a high tension steel bar (Dywidag bar). The applied loads were measured by a calibrated gauge attached in-line to the jack's hydraulic pump and strain gages attached on the steel bar in order to also measure the actual force. The results collected from the field test are comprised of the inclined load acting on the test shafts, vertical and horizontal movements of the shafts through vertical inclinometers and a MEMS-SAA system, and visual observation of the surrounding soil movements. All of this data was used in the following approach.

Analysis Approach

In order to develop a design chart, consideration of lateral movements at 0.5 and 1.0 in. was selected as the optimal, acceptable criterion and step-by-step procedures are explained as following.

- Measured Inclined Loads are split into lateral and vertical uplift loads.
- Lateral load analysis and comparisons with measured lateral loads were investigated.
- Calibration factor for lateral load analysis was established.
- Vertical uplift load analysis and comparisons with measured vertical uplift load were investigated.

- Calibration factor for vertical uplift load analysis was established.
- Design charts were developed based on calibration factors from both lateral and vertical load components. The final design charts at 0.5 and 1.0 in. are presented in Figures A.3 and A.4 below.

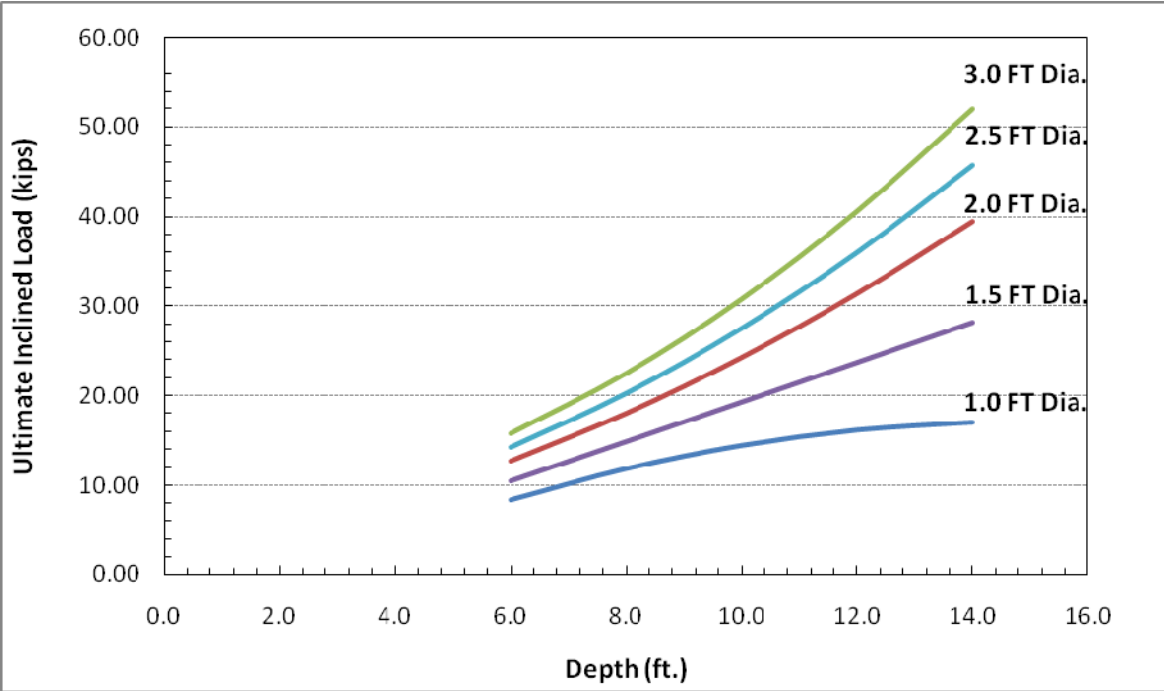


Figure A.3. Design Chart on Field Results for Finding the Appropriate Size of Drilled Shaft in the Cable Barrier Systems by Using 0.5 in. Lateral Deflection Criterion.

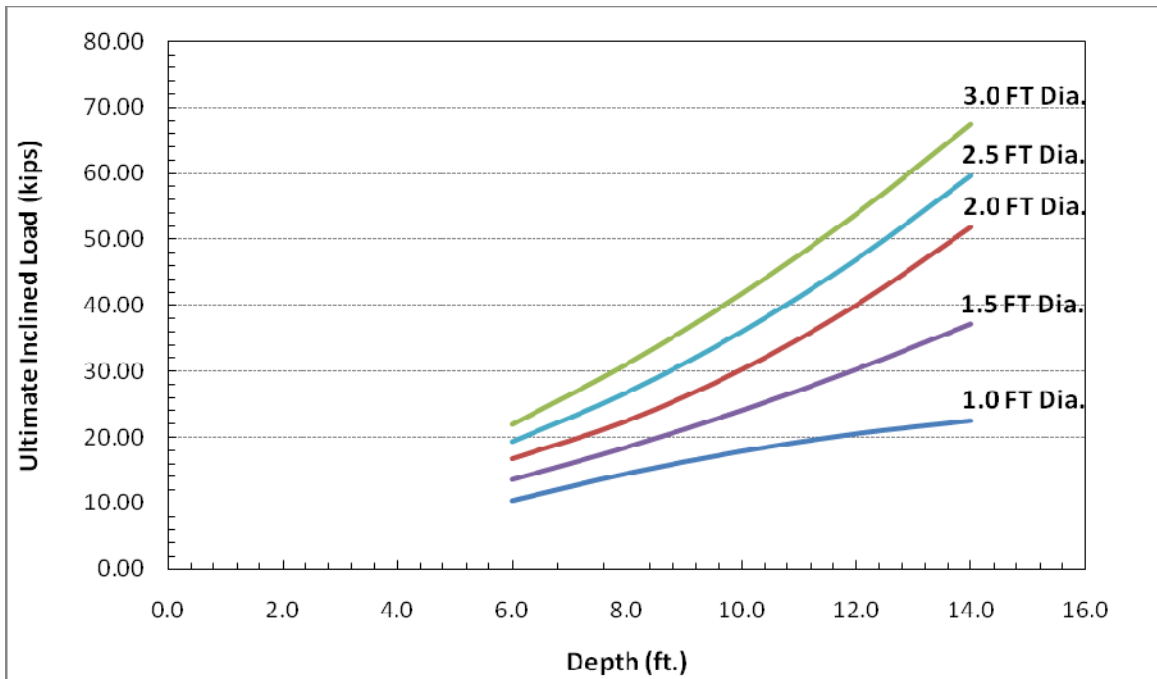


Figure A.4. Design Chart Based on Field Results for Finding the Appropriate Size of Drilled Shaft in the Cable Barrier Systems by Using 1.0 in. Lateral Deflection Criterion.

In order to provide the design charts being able to use it for different soil conditions, further analysis was carried out to develop design charts. In this analysis, the top 3 ft clay layer of undrained shear strength of 250 psf is considered constant for the entire analysis. The bottom two clay layers with undrained shear strength properties (S_u) varying between 250–500 psf, 500–1000 psf, 1000–1500 psf, and 1500–2000 psf, are considered and average undrained shear strengths for these layers are calculated. Figure A.5 shows the average undrained shear strength calculations.

It should be noted here that the final selection of the design charts are based on several LPILE analyses with various soil strength properties in the bottom layer. Figure A.6 presents the LPILE results for various layers. For each range (e.g., 250–500, 500–250 psf, and others), the lower bound of the predicted capacity are considered for conservative and safe designs of foundations. This will not only lead to safer design of drilled shafts, but will also simplify the use of design charts.

Overall, four design chart categories are introduced which are based on the average undrained shear strengths of the bottom layer. These charts are termed as Design Charts A, B, C, and D and they are valid for four ranges of average undrained shear strength of bottom layer (between 3 and 12 ft) varying from 250–500 psf, 500–1000 psf, 1000–1500 psf, and

1500–2000 psf, respectively (Figure A.7). Soils that exhibit undrained shear strengths more than 2000 psf are not considered here as such soils considered strong and in such cases, Design chart D will be recommended for usage for such cases.

Design Charts A, B, C, and D with 0.5 and 1.0 deflection criteria are shown in the Figures A.8–A.16. Overall, 16 scenarios of various soils layers are considered in this analysis, which is expected to capture various soil strata and their strength properties.

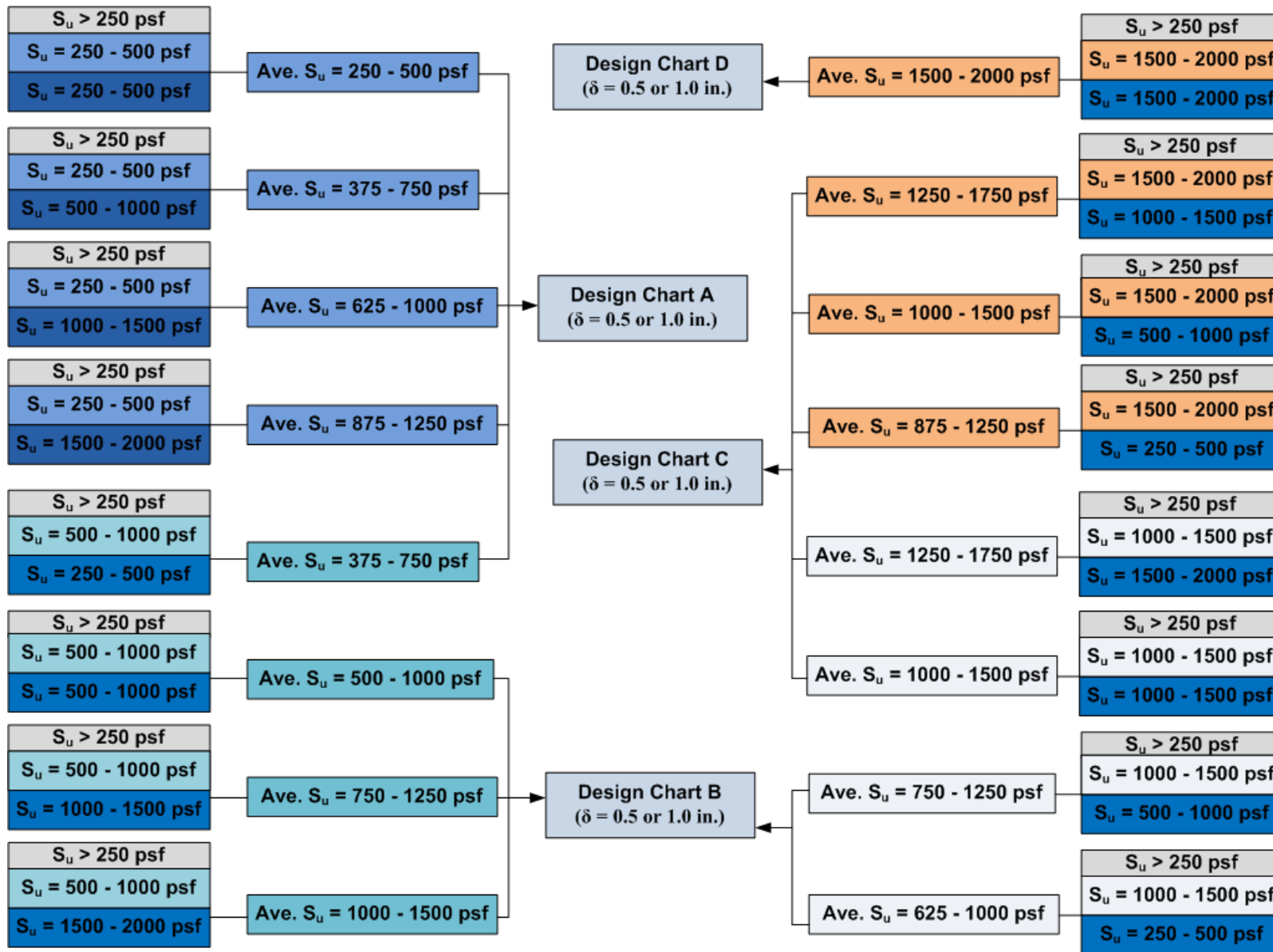


Figure A.5. Flow Chart for Choosing the Design Chart for Bottom Layer Consideration.

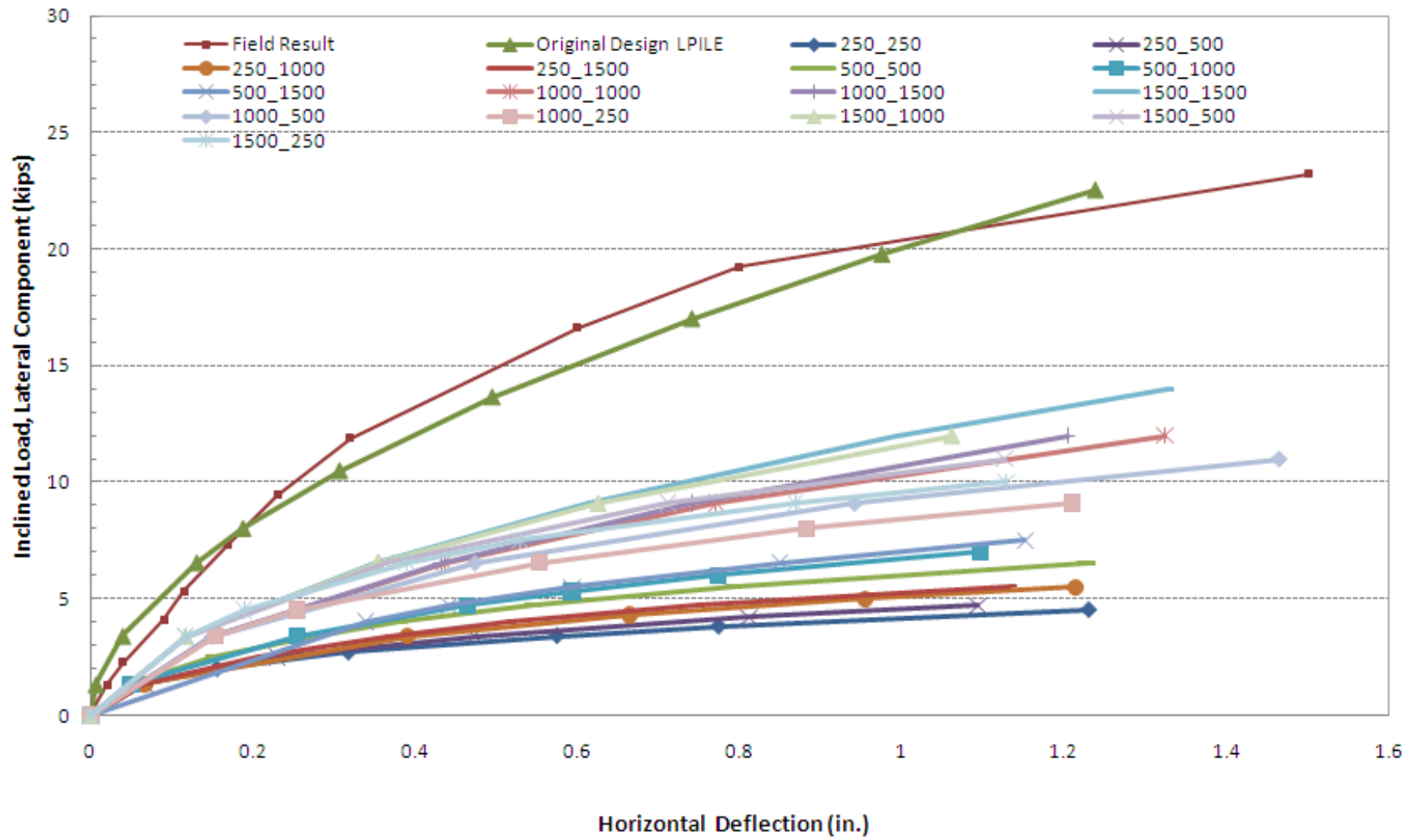


Figure A.6. An Example of LPILE Results under Different Undrained Shear Strengths.

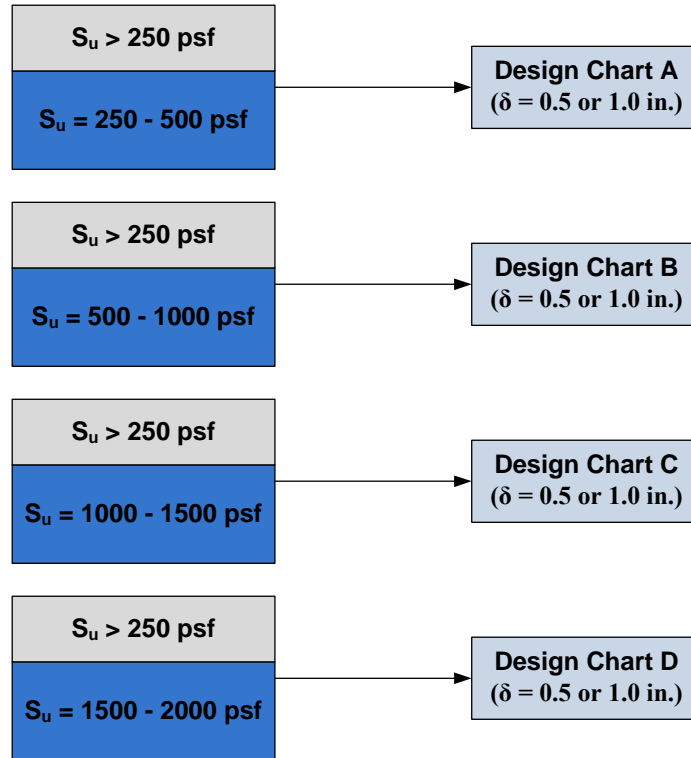


Figure A.7. Flow Chart for Choosing the Design Chart for 1 Bottom Layer Consideration.

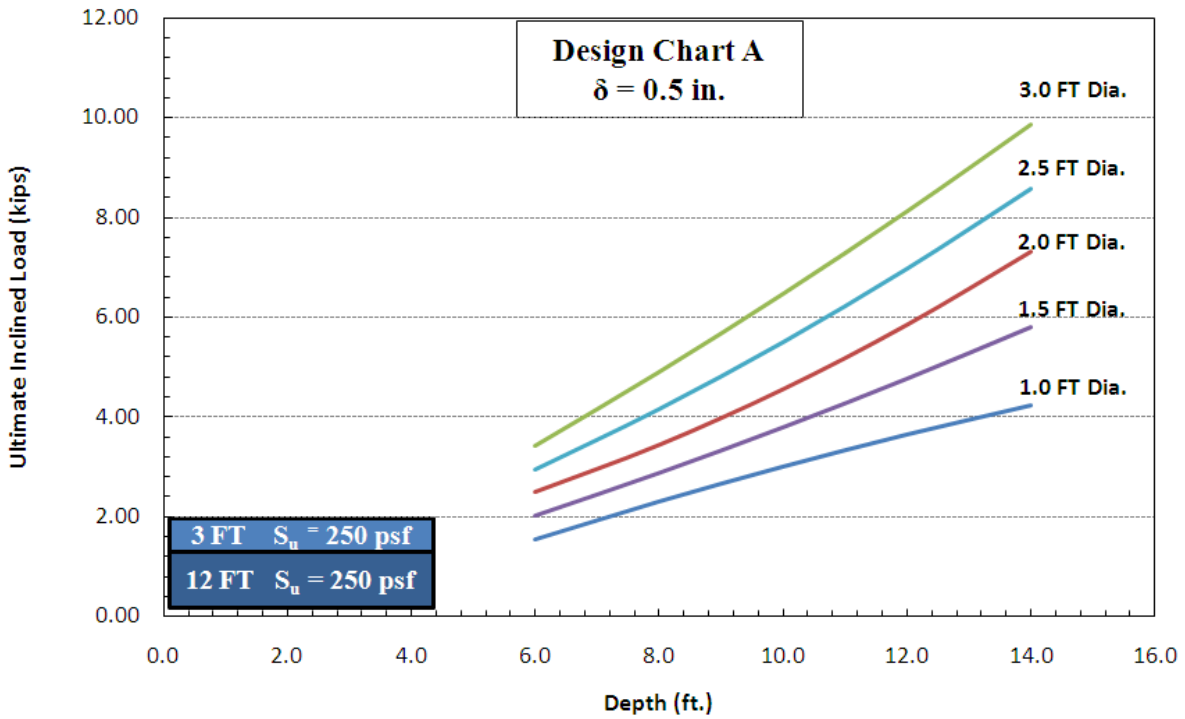


Figure A.8. Design Chart A with 0.5 in. Deflection Criteria (δ).

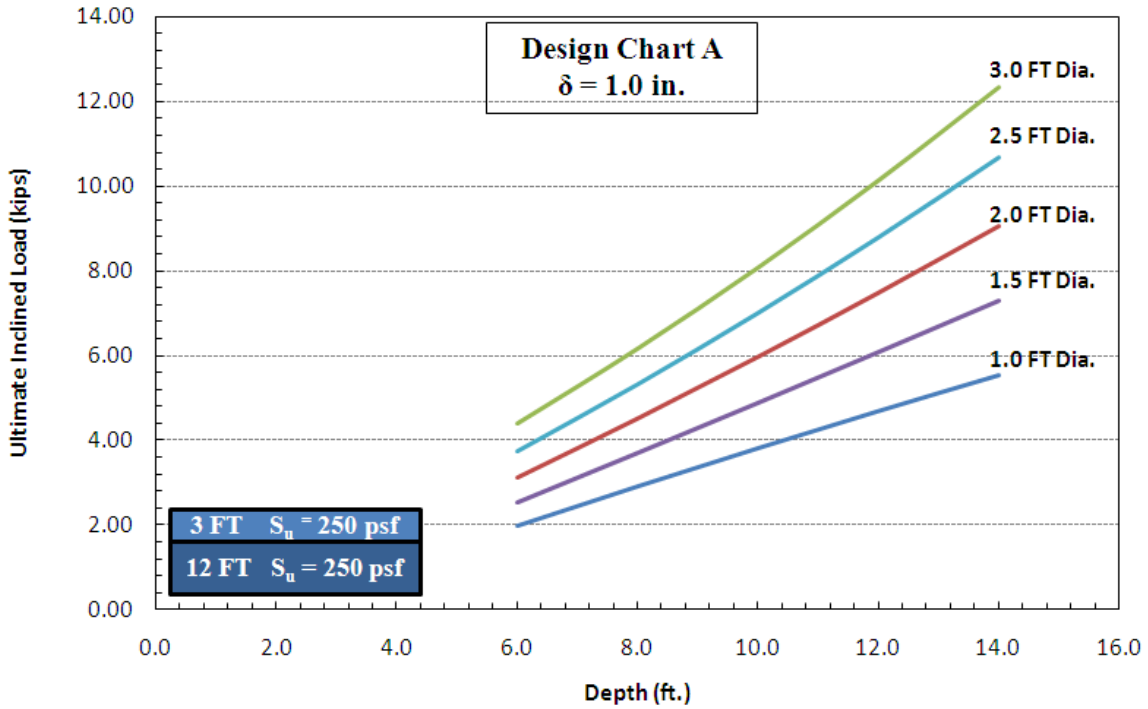


Figure A.9. Design Chart A with 1.0 in. Deflection Criteria (δ).

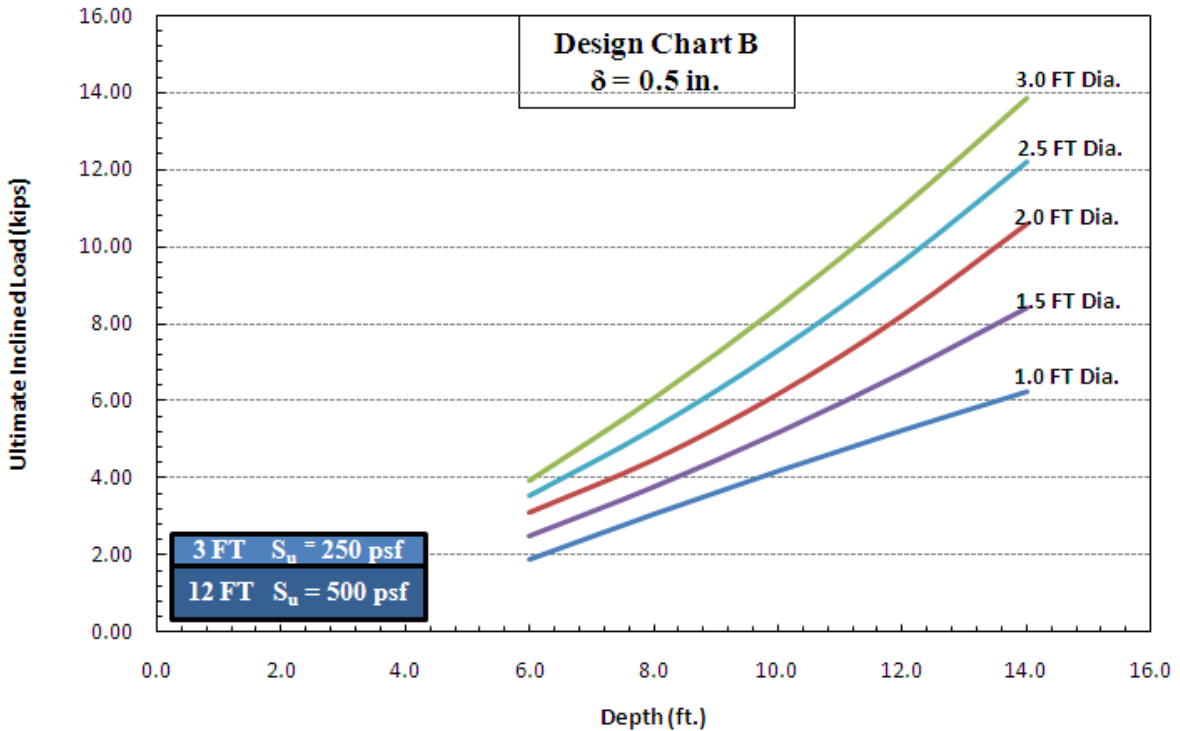


Figure A.10. Design Chart B with 0.5 in. Deflection Criteria (δ).

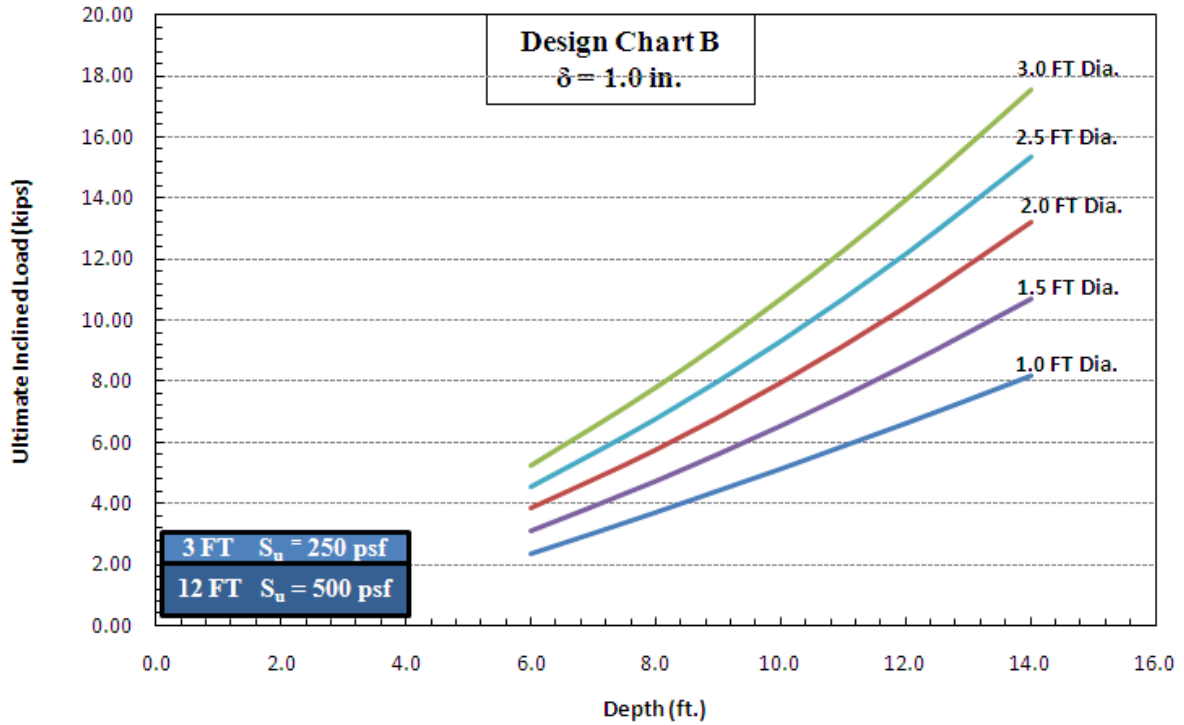


Figure A.11. Design Chart B with 1.0 in. Deflection Criteria (δ).

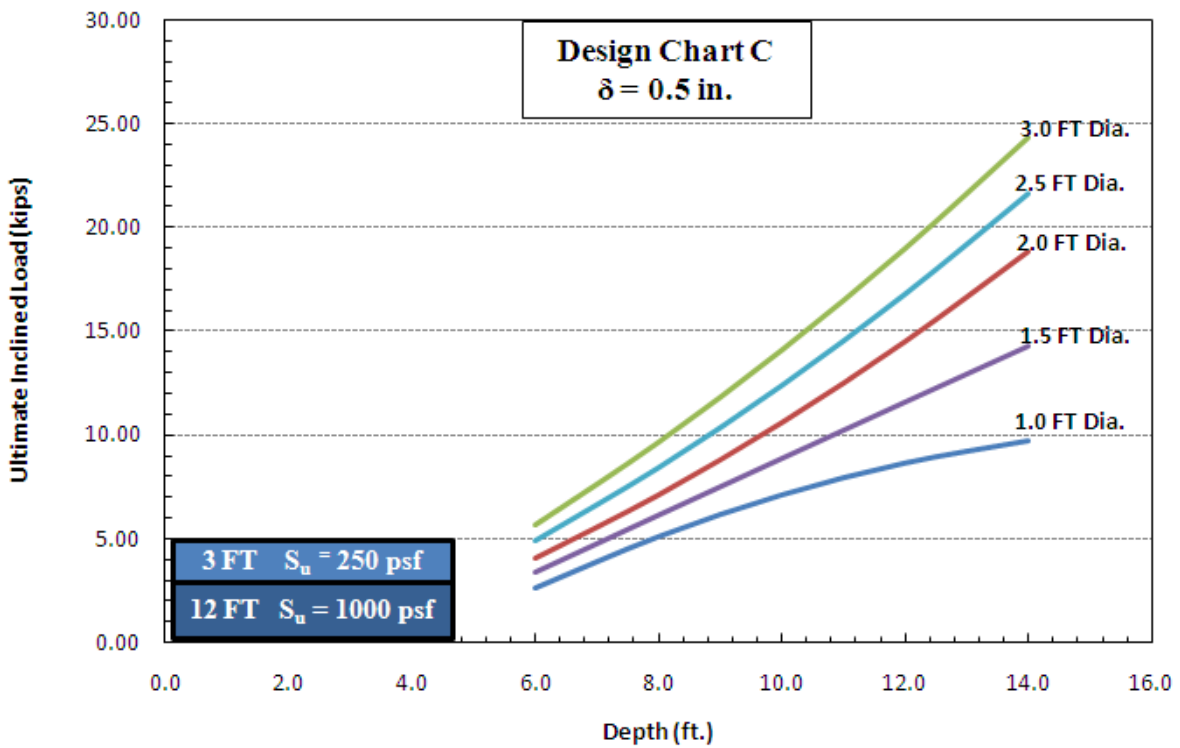


Figure A.12. Design Chart C with 0.5 in. Deflection Criteria (δ).

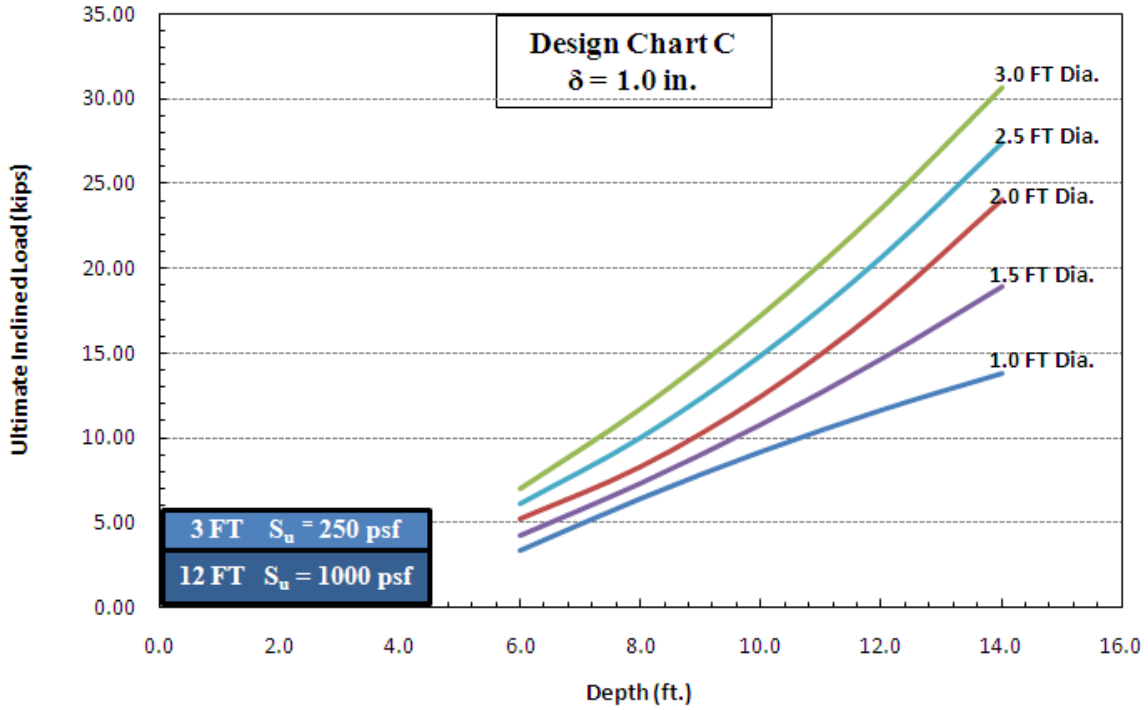


Figure A.13. Design Chart C with 1.0 in. Deflection Criteria (δ).

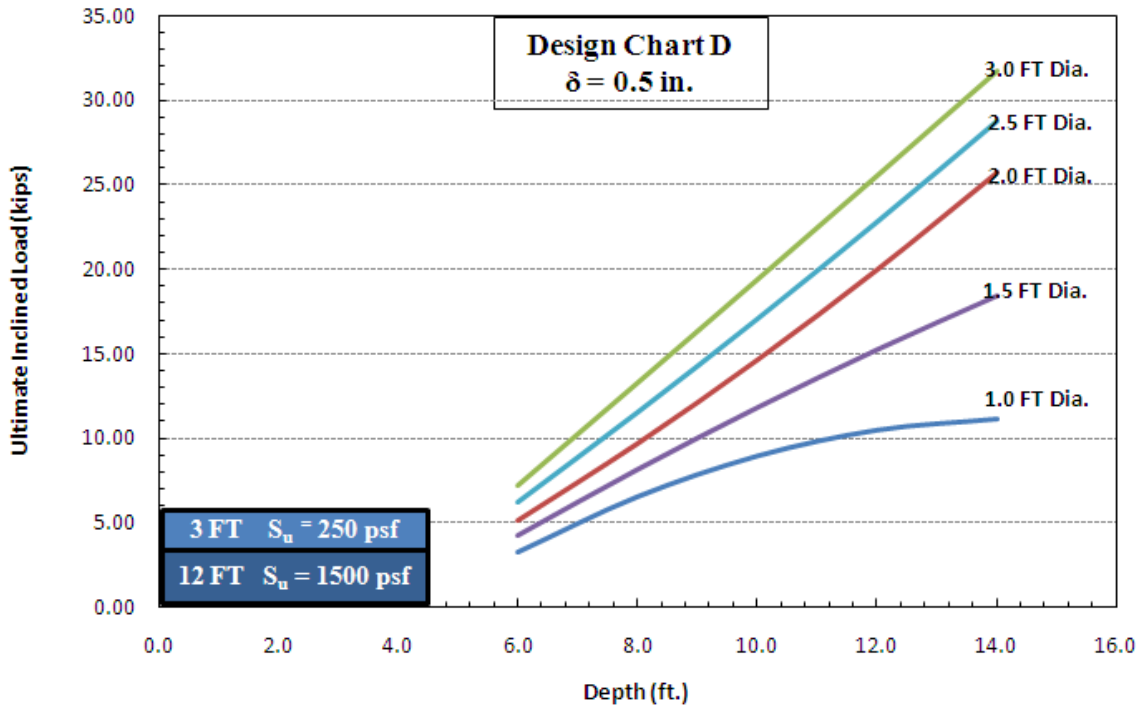


Figure A.14. Design Chart D with 0.5 in. Deflection Criteria (δ).

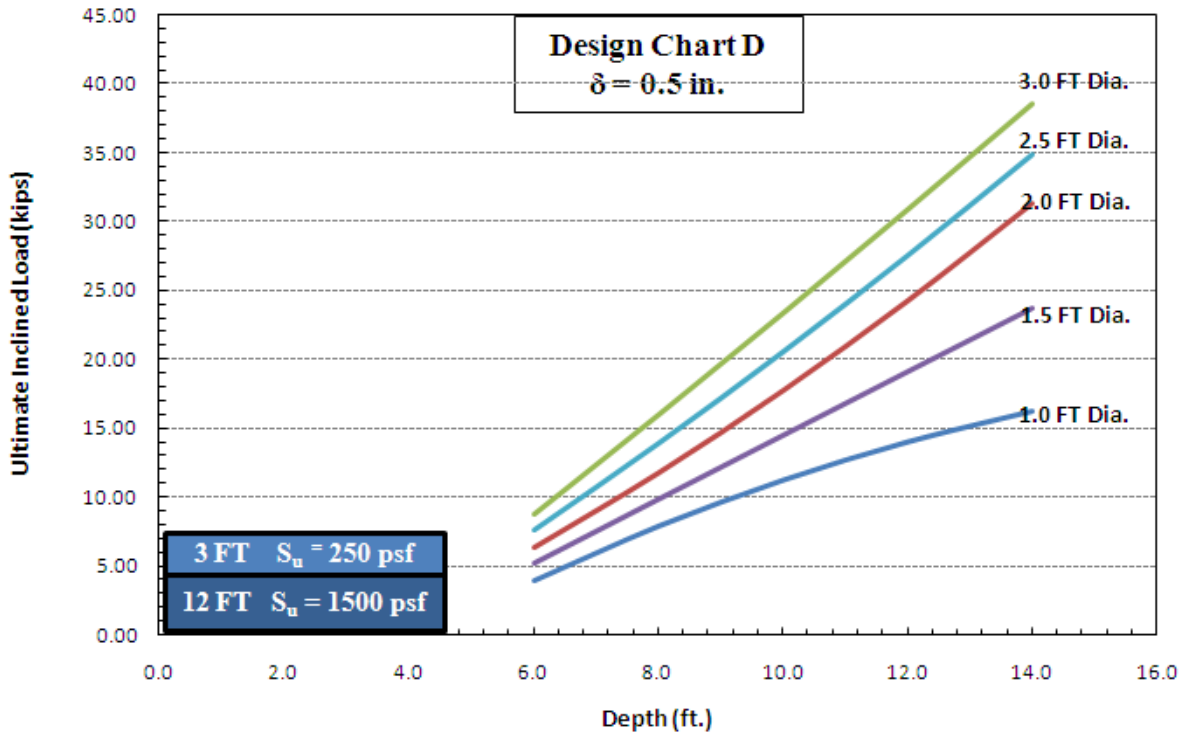


Figure A.15. Design Chart D with 1.0 in. Deflection Criteria (δ).

In order to use a specific design chart, the undrained strengths of soils below 3ft of the ground surface are needed. A simple arithmetic average of the shear strengths is sufficient for the next step to choose the appropriate design chart for designing drilled shaft. The next section describes the steps involved in the use of design chart for determining the sizes of the drilled shaft.

Chart Selection and Procedure

The soil properties in that area are needed to be discovered and then the appropriate criteria for soil properties should be matched with the given flow charts. After that, the loads shown in the design charts represent the ultimate load at the 16.1° angle used in the actual cable barrier systems. However, other criteria that must be considered and ambient temperature that cable systems will experience. In areas of highly expansive clays or showing previous distress, use the 0.5 chart. Use the 1.0 chart for less expansive clay soils. For temperature consideration, use the tensions obtained from the manufacturers' chart as shown in Table A.1.

Table A.1. Example of a Manufacturer’s Table for Cable Tensions in a Gibraltar TL-3 Cable Barrier System.

Cable Tension (lb) at Different Temperatures (°F)	
-10°F	8000
0	7600
10	7200
20	6800
30	6400
40	6000
50	5600
60	5200
70	4800
80	4400
90	4000
100	3600
110	3200

Note: Allowable Deviation from Chart $\pm 10\%$

Chart Using Procedures

Before using the chart, use the following steps:

- Calculate the ultimate load by selecting the load from each manufacturer’s cable tension table at the lowest temperature that the cable barrier systems can be expected to experience.
- The number of cables in the selected barrier system is multiplied by the ultimate load calculated from Step 1.
- Apply a Factor of Safety (FS) of 1.5–2.0 against overturning (lateral failure) and pullout (uplift).

After the ultimate load is calculated from the above steps, directly apply it to the graphs to determine the appropriate drilled shaft size (diameter and depth) to be used at both ends of each cable barrier system.

Construction and Maintenance Guidelines

Generally, installation of the drilled shaft foundations for the cable barrier systems can be performed with normal construction procedures; however, there are a few additional recommendations for construction in high PI soils:

- Before construction starts, provide proper drainage at the ends of each cable barrier system until construction is finished.
- After excavation is finished, the lateral expansion of the expansive soil underneath the ground should be visually investigated. If there is some lateral soil expansion in the hole, the second time of drilling or the use of casing in that area is needed.
- Due to the expected swelling and shrinkage of the soil, a concrete pad or mow strip should be placed on the ground surface at the top of the end drilled shaft plus the first post to keep soil moisture constant at that area and prevent soil at the top shaft crack, which leads to the loss of contact between drilled shaft and soil in dry season as shown in Figure A.16.

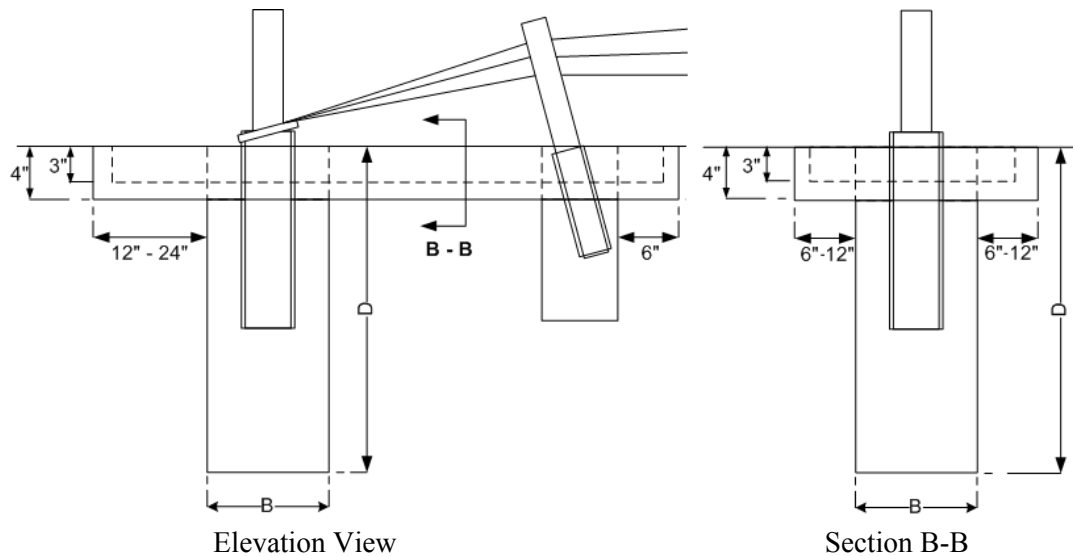


Figure A.16. Details of Concrete Pad Placed on the Top of the Drilled Shaft at the End of the Cable Barrier System.

- During a dry season, construction can be performed normally; however, proper curing of any concrete above ground is needed to retain water in the mix to propagate the hydration process as long as possible yielding the highest strength. This higher strength will provide additional support to the drilled shaft foundations against horizontal or vertical movement in a fixed-head condition.

APPENDIX B: DISTRICT SURVEY ANALYSIS

INTRODUCTION

In this Appendix, researchers prepared a survey questionnaire to seek information on how and under what circumstances the failure of drilled shaft foundations supporting cable median barriers is encountered. The questionnaire was distributed to **110** area officers of the Texas Department of Transportation (TxDOT) across the state, since this foundation failure is more likely a localized problem than a global issue. Initially, the questionnaire was distributed through electronic media; subsequently, telephonic survey was carried out as there were no responses received from any district area offices. In this process, a total of **80** area officers were contacted and **32** responses were obtained. Researchers obtained 22 responses from 25 districts. Odessa, Wichita Falls, and Yoakum District's area officers were either non-responsive or researchers could not contact the area officers after several trials. Since the respondents are more than one from each TxDOT district, in this analysis; the responses are not presented in terms of percentage. This technical memorandum discusses the analysis of these survey responses from several TxDOT area offices. The questionnaire is presented at the end of this memorandum.

RESPONSES

The first question posed to each TxDOT area official was whether the district or area uses cable median barriers. Out of 32 respondents, 13 respondents said that they do not have cable median barrier systems either in their area or in their entire district. Figure B.1 shows the responses for this question. Further analysis and results are based on 19 responses received from area offices that dealt with the cable median barriers.

For the question "How long is the cable median barrier used in your area?", the responses varied from 1 mile to 100 miles. For better understanding and presentation, the responses are reported in five categories, i.e., use of cable median barriers of length: 0–5 miles; 6–10 miles; 11–20 miles; 21–50 miles and >50 miles (see Figure B.2). Except in Huntsville, Bryan District, which has installed cable median barriers over 91 miles in their district, most of the districts/areas installed cable median barriers measuring less than 10 miles long. Two districts (Sherman area of Paris District and San Angelo District) reported that they recently installed the cable median barriers (less than a year old).

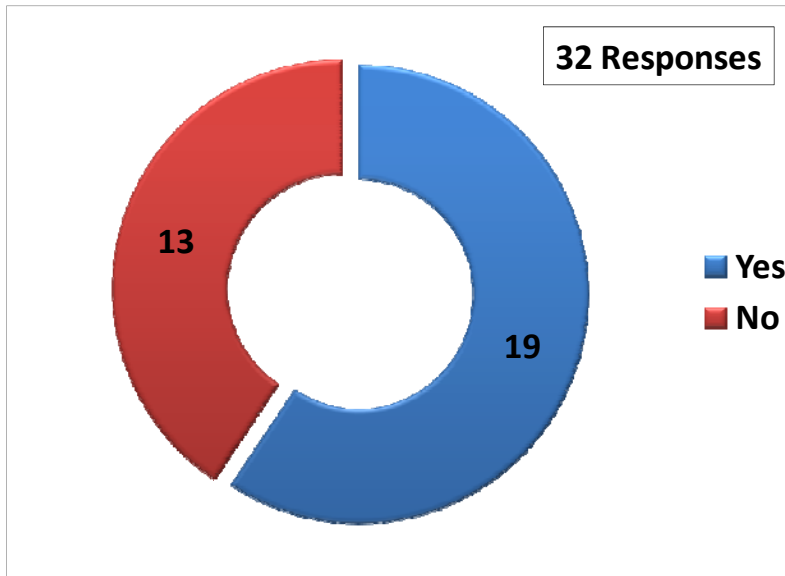


Figure B.1. Usage of Cable Median Barriers.

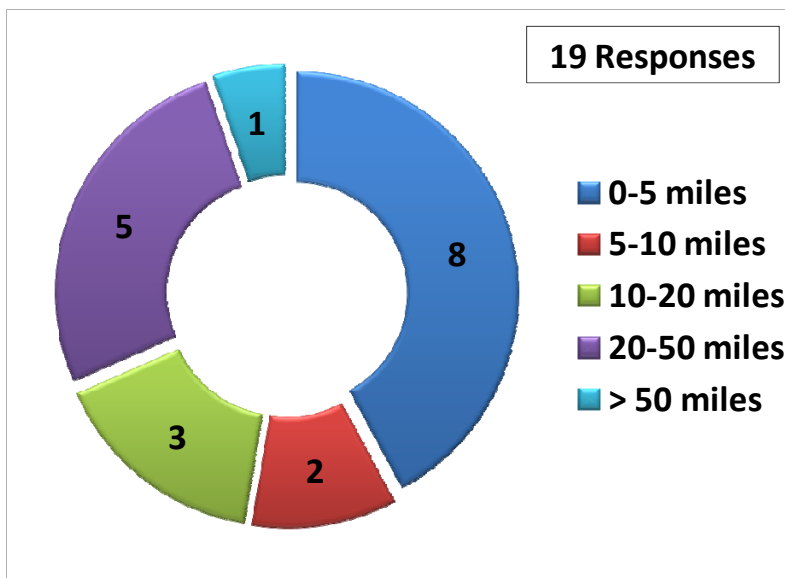


Figure B.2. Length of Cable Median Barriers Used.

Majority of the respondents stated that they use Trinity Cable Safety Systems. Some of the districts use Gibraltar Cable Barrier System and Brifen Safety Fence. None of the districts use Safence system. All these systems are classified under high-tension cable barrier systems. Figure B.3 presents the number of area offices using different types of cable barrier systems. Figure B.4 depicts the pictures of these cable barrier systems that TxDOT has adopted.

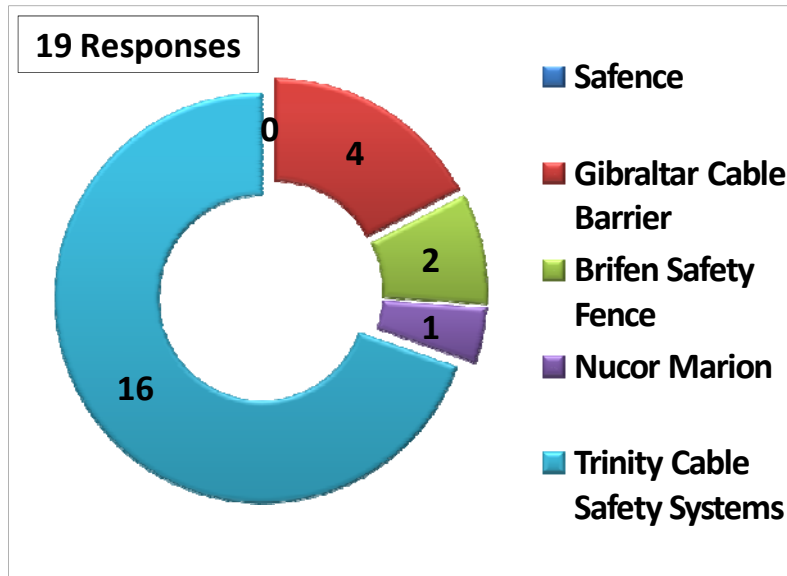


Figure B.3 Type of Cable Median Barrier Used.



a) Trinity Cable Safety Systems b) Gibraltar Cable Barrier c) Brifen Safety Fence

Figure B.4. Different Types of Cable Median Barrier Systems Used in the State of Texas.

Among the districts/area offices using cable median barrier systems, only five respondents (out of 19) reported that they have noticed failures of these cable median barriers. The reason cited for these failures is vehicle crashes only (four out of five respondents). Vehicle type was reported as 18-wheeler trailer trucks and mini trucks. Counter portion of respondents (14 out of 19) attributed the satisfactory performance of these cable barrier systems to low traffic volume of heavy vehicles and/or new installations of these barrier systems in their area. They also reported that they have only minor maintenance issues if there was any vehicle crash. Figure B.5 shows the responses related to failures of cable median barrier systems. The cable system failures observed in Kaufman County of Dallas District were not due to vehicle crashes. The type of cable barrier subjected to failure was reported as Gibraltar Cable Barrier System; however, the County uses Gibraltar, Brifen, and Trinity cable systems.

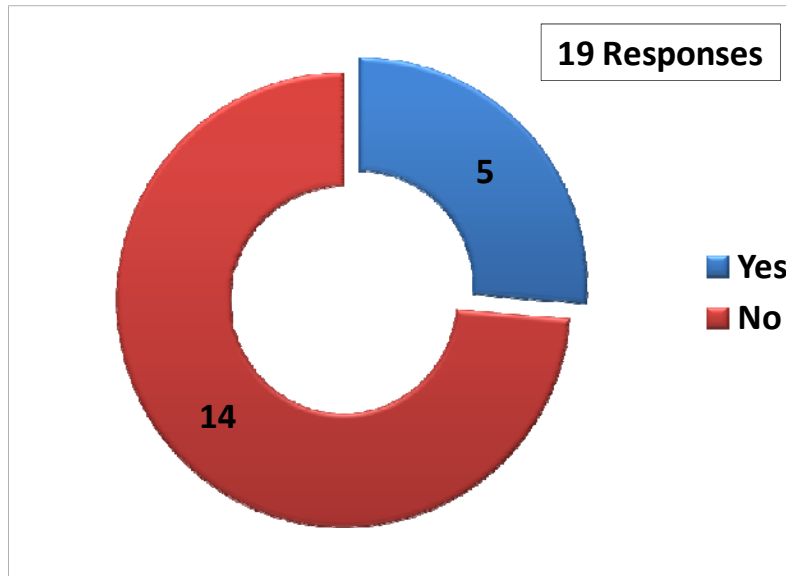


Figure B.5. Failures Related to Cable Median Barriers.

Majority of respondents stated that the most affected structural component of the cable barrier system would be a series of cable-supporting middle posts (around 10) because these are directly subjected to vehicle attack during crashes. The TxDOT personnel of Kaufman County reported that the failures were observed in drilled shafts that work as a cable release anchor post mostly during December 2006–February 2007. All these failures were identified by visual inspections and analyzed through digital photography.

Among the respondents, those who experienced failures due to vehicle crashes have high PI clays. However, the failures are not attributed to the high PI clays except in Kaufman County. Few of these failures were also in sandy clayey soils. However, Kaufman County has high PI clays along Interstate Highway 20. Further discussions with the TxDOT area officials revealed that these failures were observed only during severe winter storm periods from December 2006–February 2007. It was also noted that the failures could also be due to swell/shrink behavior of highly expansive soils in that region.

For the question on whether they have any construction related to foundation repair activity coming up in their area, none of the respondents reported that they have any such activity lined up.

The TxDOT officials were asked whether they anticipate any new cable median barrier construction activity coming up next year; only 10 out of 80 personnel contacted reported that

they do. Table B.1 summarizes the TxDOT area office involved in the construction activity and the details of prospective construction site location.

Table B.1. Summary of Proposed Cable Median Barrier Construction Site Locations.

S. No	TxDOT District/Area Office	Site Location
1	Amarillo	Amarillo
2	Austin/North Travis	US 290 and US 71
3	Austin/South Travis	Loop 1
4	Austin/Bastrop County	SH 71
5	Beaumont/Jefferson County	IH 10
6	Bryan/Huntsville (Madison Co.)	SH 30
7	El Paso/Alpine (Culberson Co.)	West of SH 118 and US 90
8	West El Paso	West of IH 10 and US 55
9	Fort Worth/Decatur	In Jack/Wise Counties
10	Fort Worth/Keene	IH 35W south of Alvarado to just north of Grandview
11	Houston/Brazoria	SH 288
12	Laredo/Carrizo	IH 35 and in Webb County
13	Pharr/San Benito	US 77; US 281(Pharr)

SURVEY QUESTIONNAIRE

Districts Survey on Cable Median Barriers for TxDOT Research Project 0-6146

NAME:

District:

Please click or check (with X) to the following questions. We thank you in advance for your input.

1. How long is cable median barrier used in your District?

_____miles

2. Which cable median barrier(s) is (are) used in your District? (Please check more than 1 choice if applicable)

- Safence Gibraltar cable barrier Brifen Safety Fence
- Nucor Marion Trinity Cable Safety Systems Others,
specify_____

3. Have you encountered failure(s) of cable median barriers in your District?

- Yes No

If the answer to the above question is **No**, then please move forward to Question No. 11.

4. Is the failure due to vehicle crashes?

- Yes No

If the answer to the above question is **Yes**, specify the type of vehicle_____, then please move forward to Question No. 11.

If the answer to the above question is **No**, specify the cause(s)_____.

5. Which cable median barrier(s) is (are) experienced failure in your District? (Please check more than 1 choice if applicable)

- Safence Gibraltar cable barrier Brifen Safety Fence
- Nucor Marion Trinity Cable Safety Systems Others,
specify_____

6. Please select the procedure followed to identify this problem in the field.

- Visual inspection/Measurements
- Others, specify_____

7. Which structure of the cable median barrier(s) experienced failure?

- Drilled shaft(s) that work as cable release anchor post Cable
 Terminal post Others, specify_____

Please explain the failure characteristic(s)

8. In which season has the cable median barrier(s) experienced failure?

- Summer Fall Winter Spring

Please specify the weather condition including temperature before 1–2 week failure

9. Have soil investigations been done in the failure area?

- Yes No

If the answer is **Yes**, is the soil plasticity index high in that area?

- Yes No

10. Do you have any construction related information for the foundation repair activity coming up?

- Yes No

If the answer is **Yes**, please specify the location: _____

11. Do you anticipate any new cable median barrier construction in your District next year?

- Yes No

If your answer is **Yes**, please specify the location: _____

12. We would like to contact you if we have any follow-up questions. Please provide your email and/or phone number where we can reach you.

Email:

Tel:

We thank you very much for your input. We request that survey responses be emailed to anand@uta.edu faxed to 817-272-2630 or mailed to: Anand J. Puppala, PhD, PE, Professor, Box 19308, Department of Civil and Environmental Engineering, The University of Texas at Arlington, Arlington, TX 76019, USA.

APPENDIX C: MANUFACTURER DESIGN PLAN SHEET

APPENDIX D: CONCRETE MIX DESIGNS

TEXAS DEPARTMENT OF TRANSPORTATION
HYDRAULIC CEMENT CONCRETE MIX DESIGN & CONTROL
Material Properties

SAMPLE ID:		SAMPLED DATE:	
TEST NUMBER:		LETTING DATE:	
SAMPLE STATUS:		CONTROLLING CSJ:	
COUNTY:		SPEC YEAR:	2004
SAMPLED BY:		SPEC ITEM:	
SAMPLE LOCATION:		SPECIAL PROVISION:	
MATERIAL CODE:		CLASS:	CLASS C
MATERIAL NAME:			
PRODUCER:			
AREA ENGINEER:		PROJECT MANAGER:	

COURSE/LIFT:		STATION:		DIST. FROM CL:	
--------------	--	----------	--	----------------	--

AGGREGATE PROPERTIES (FROM LABORATORY TESTING)

	Percentage (%)	Aggregate Type/Source	Specific Gravity (SSD)	Rodded Unit Weight (U _{DRY})	Fineness Modulus (FM)	Free (Surface) Moisture (%)	Absorption (%)
Test Method			Tex-403-A	Tex-404-A	Tex-402-A	Tex-409-A	Tex-403-A
Coarse Aggregate 1:	100	TXI Beckett Road Pea Gravel	2.65	121.20		0.3	0.1
Coarse Aggregate 2:							
Coarse Aggregate 3:							
Coarse Aggregate 4:							
Total Coarse Aggr.:	100	<= Must equal 100					
Fine Aggregate 1:	100	TXI Ferris	2.65		2.72	6.0	0.1
Fine Aggregate 2:							
Total Fine Aggr.:	100	<= Must equal 100					

CEMENTITIOUS MATERIALS

	Percentage by Weight (%)	Pozzolan Type/Source	Specific Gravity	% NA ₂ O equivalent in cement*
Hydraulic cement	80	TXI Midlothian Ty I/II	3.15	
Fly Ash	20	Boral Headwaters	2.50	
Ground Granulated Blast Furnace Slag				
Silica Fume				
UFFA				
Metakaolin				
Other Pozzolan				
Total Cementitious Matl:	100	<= Must equal 100		

* Only required if Mix Design Options 6 or 7 are used.

CHEMICAL ADMIXTURES

	Type/Source	Type	Dosage (fl oz./100 lbs. cement)	% Solids
Air entraining admixutre				
Set Retarder				
Accelerator				
Water reducer	W.R. Grace Mira 85	A	16.90	
High-range water reducer				
Water reducing retarder				
High-range water reducing retarder				
Lithium nitrate admixture				
Corrosion inhibitor				

OTHER MATERIALS

	Type/Source	Specific Gravity	Dosage (lbs/CY)
Fibers			

Figure D.1. Concrete Design Material Properties.

TEXAS DEPARTMENT OF TRANSPORTATION
HYDRAULIC CEMENT CONCRETE MIX DESIGN & CONTROL
Mix Proportions based on ACI 211.1-91®

SAMPLE ID		SAMPLED DATE	
TEST NUMBER		LETTING DATE	
SAMPLE STATUS		CONTROLLING CSJ	
COUNTY		SPEC YEAR	2004
SAMPLED BY		SPEC ITEM	
SAMPLE LOCATION		SPECIAL PROVISION	
MATERIAL CODE		CLASS	CLASS C
MATERIAL NAME			
PRODUCER			
AREA ENGINEER		PROJECT MANAGER	#VALUE!
COURSE/LIFT		STATION	
		DIST. FROM CL	

Nom. Max. Agg. Size, (inches)	0.5	Air Entrained?	No.	Slump, (inches)	6	Exposure	NA
Mix Design Option?		See Item 421.4.A.6		Mix design target strength, (psi)	4800		
Basic Water Demand, lb/CY	383	Water Adjustment Factor	0.66	Controlling w/c or w/cm	0.45		

Mix Component	lb/CY	%/CY	fl oz.	Specific Gravity	Density, lbs/ft ³	Approx. Sacks	Absolute Vol. (ft ³)	Weight (lbs/CY)	Weight [†] (lbs/CY)
Water	253			1.00	62.4		4.05	253	156
Total Cementitious	562								
Portland Cement		80		3.15	196.6	4.79	2.29	450	
Flyash		20		2.5	156.0	1.19	0.72	112	
GGBF Slag									
Silica Fume									
UFFA									
Metakaolin									
Other Pozzolan									
Air entraining admixture:									
Set retarder									
Accelerator									
Water Reducer			94.98				0.10		
High-Range Water Reducer									
Water Reducing Retarder									
Hi-Range H2O Reducing Retarder									
Lithium Nitrate Admixture									
Corrosion Inhibitor									
Paste Volume=Total (water + cm)							7.16		
Approximate Entrapped Air*		0.0					0.00		
Specified Value**		Need Exposure							
Air = Paste Volume:							7.16		
Fibers:									

	%	Sp. Gr. SSD	Unit Weight, lbs/ft ³	Bulk Vol. = b/b ₀ x 27, ft ³	Absolute Vol. (ft ³)	Weight (lbs/CY)	Weight [†] (lbs/CY)
Total Aggregate Volume, ft ³					19.84		
Coarse Aggregate Factor (CAF):	0.55						
Coarse Aggregate 1:	100	2.65	121.2	14.85	10.89	1800	1805
Coarse Aggregate 2:							
Coarse Aggregate 3:							
Coarse Aggregate 4:							
Mix vol. subtotal:					18.05		
Weighted Average FM:	2.7						
Fine Aggregate 1	100	2.65			8.95	1480	1569
Fine Aggregate 2							

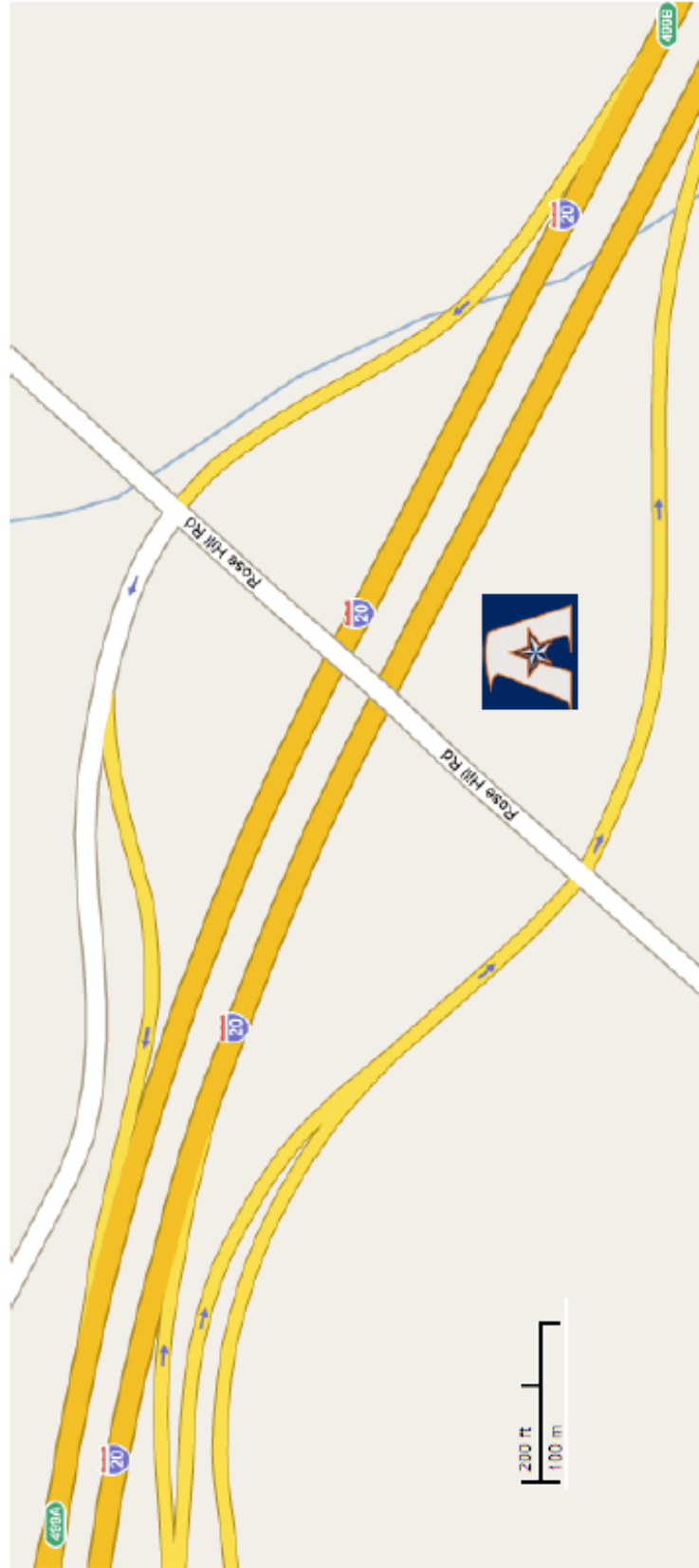
	CY	Absolute Vol. (ft ³)	Weight (lbs/CY)	lbs/ft ³
Total Weight:			4095	
Size of Truck, CY:				
Est. Total Weight / Truck :			0	
Total Absolute Volume:				
Theoretical Weight of Concrete Computed on an Air-Free Basis (see Tex-417-A):				
Design Yield (Unit Weight):				151.7

* Only applicable for non-air-entrained concrete
 ** Only applicable for air-entrained concrete
 † Weight adjusted based on aggregate moisture, aggregate absorption, and admixture water content

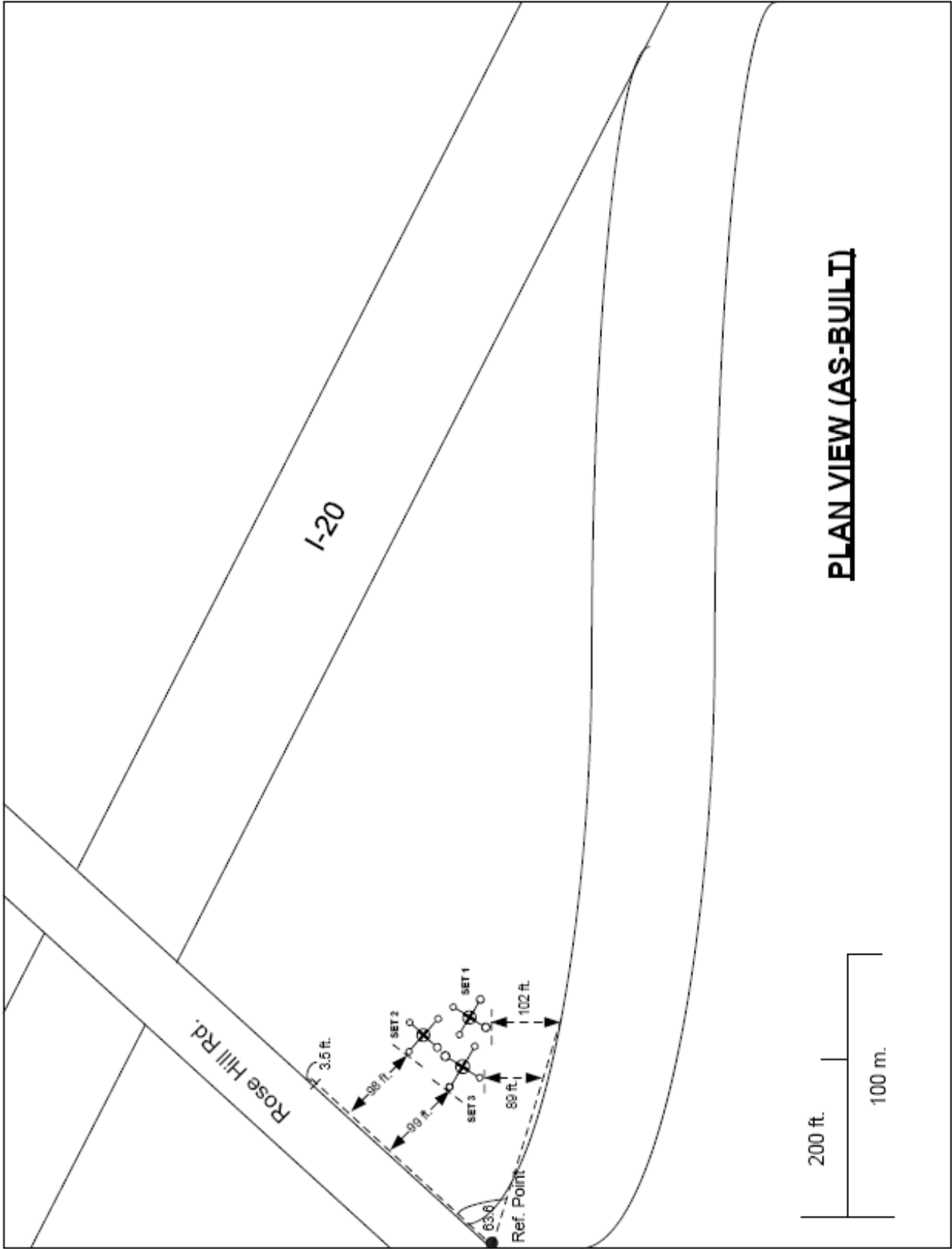
Figure D.2. Concrete Design Mix Proportions.

APPENDIX E: AS-BUILT DRAWING FOR LOAD TEST SETUP

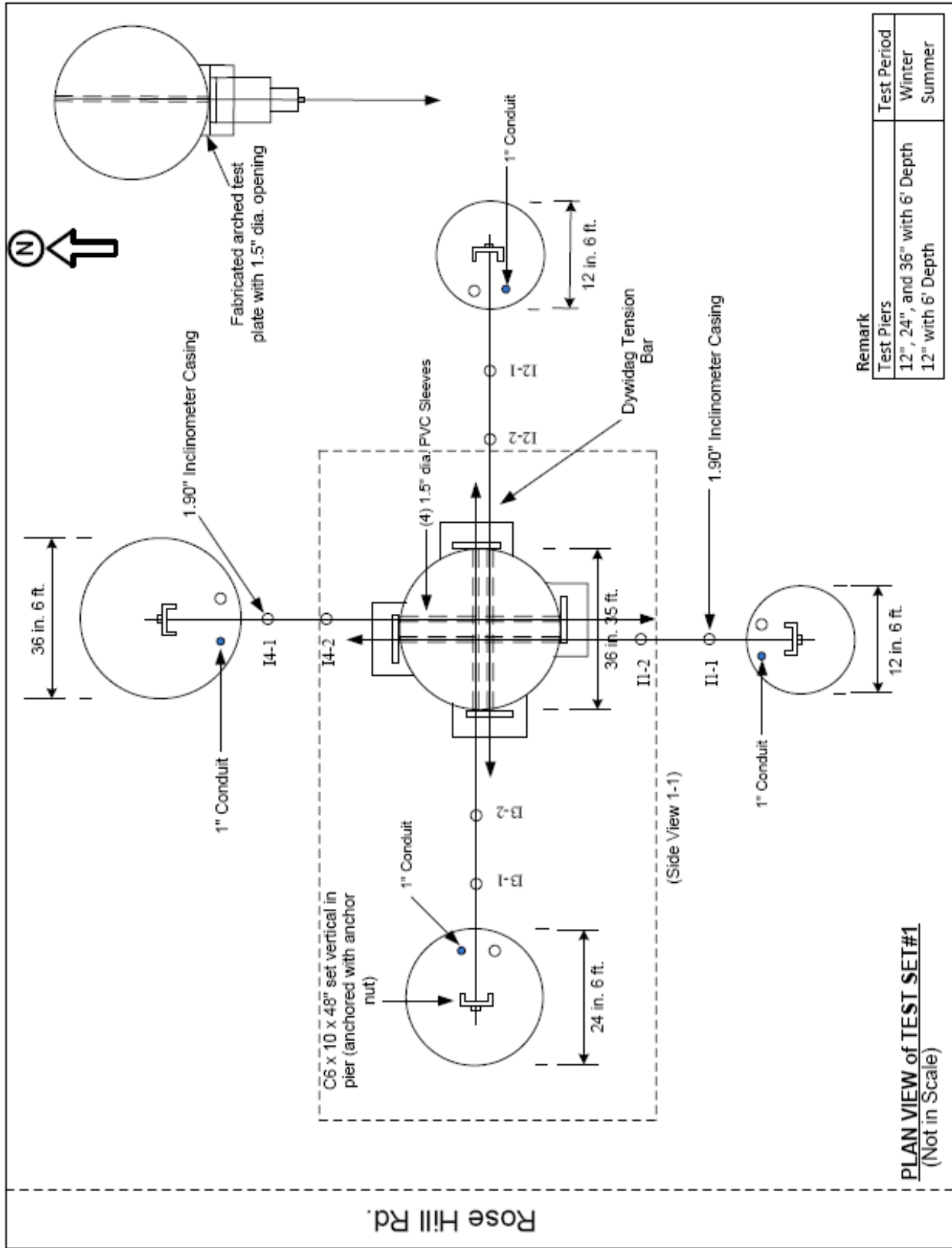
Lateral Loads on Drilled Shafts (AS-BUILT)

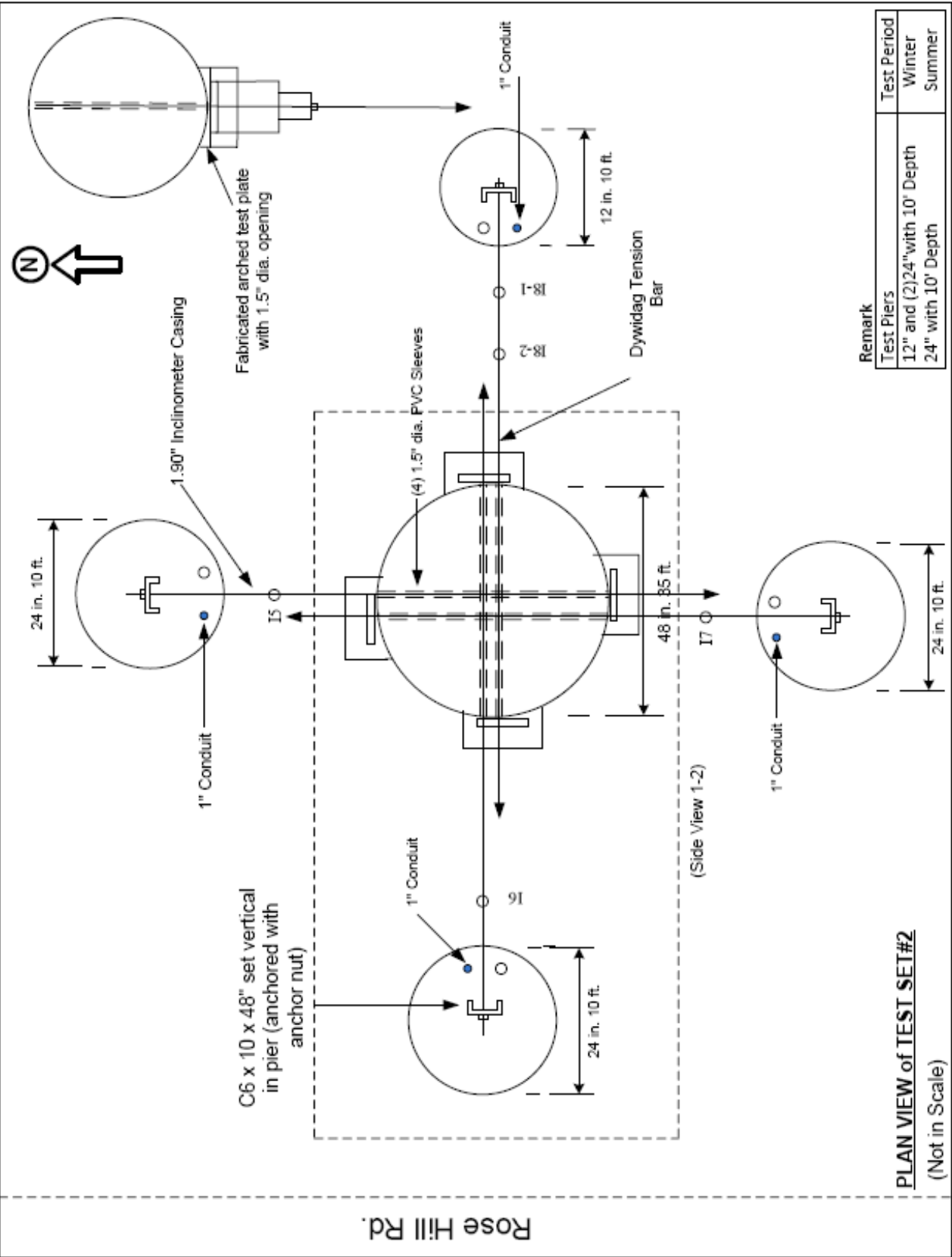


TX-DOT Project # 0-6146
Project Location located on I-20 & Rose Hill Rd.
Area \approx 280,000 sq.ft.

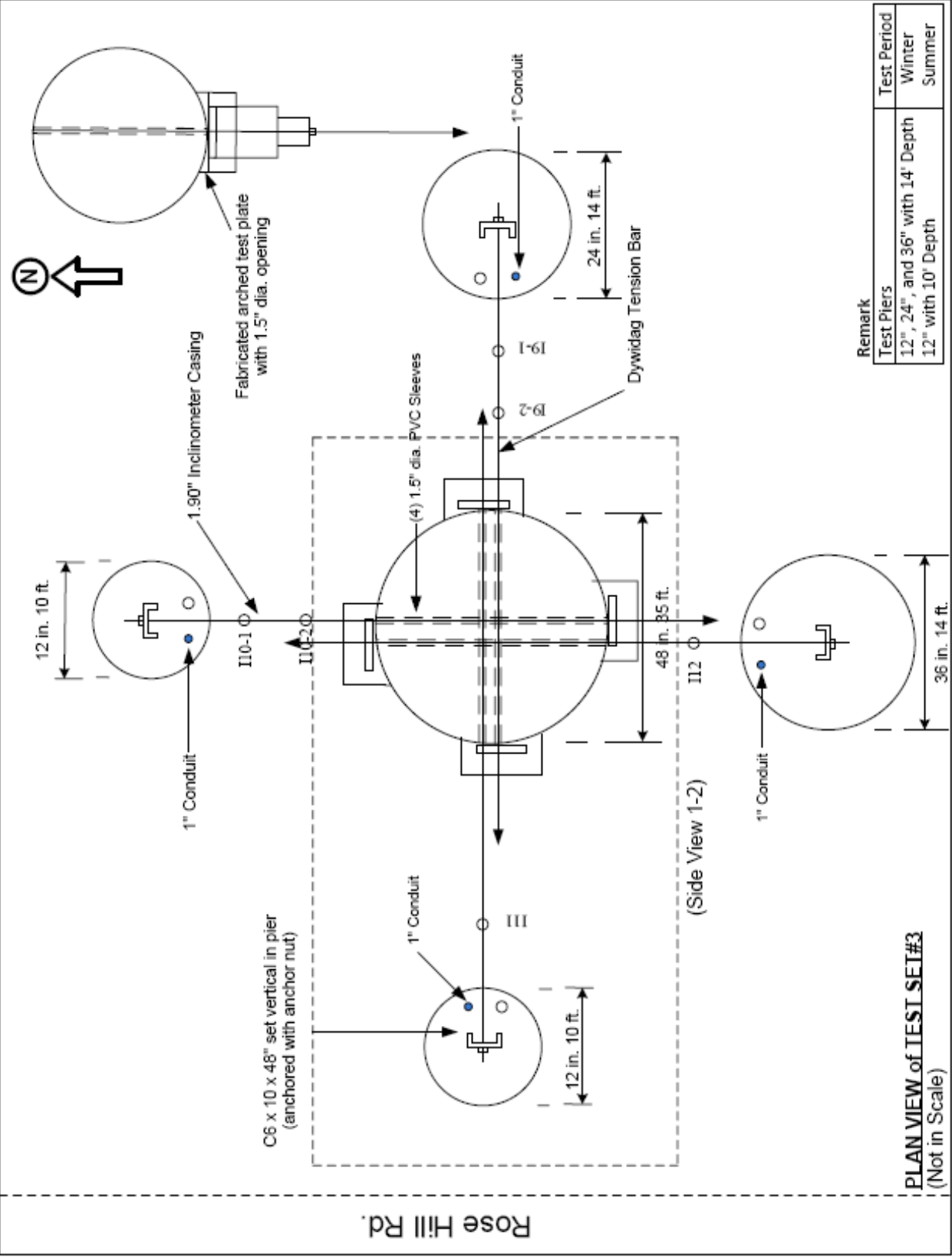


PLAN VIEW (AS-BUILT)



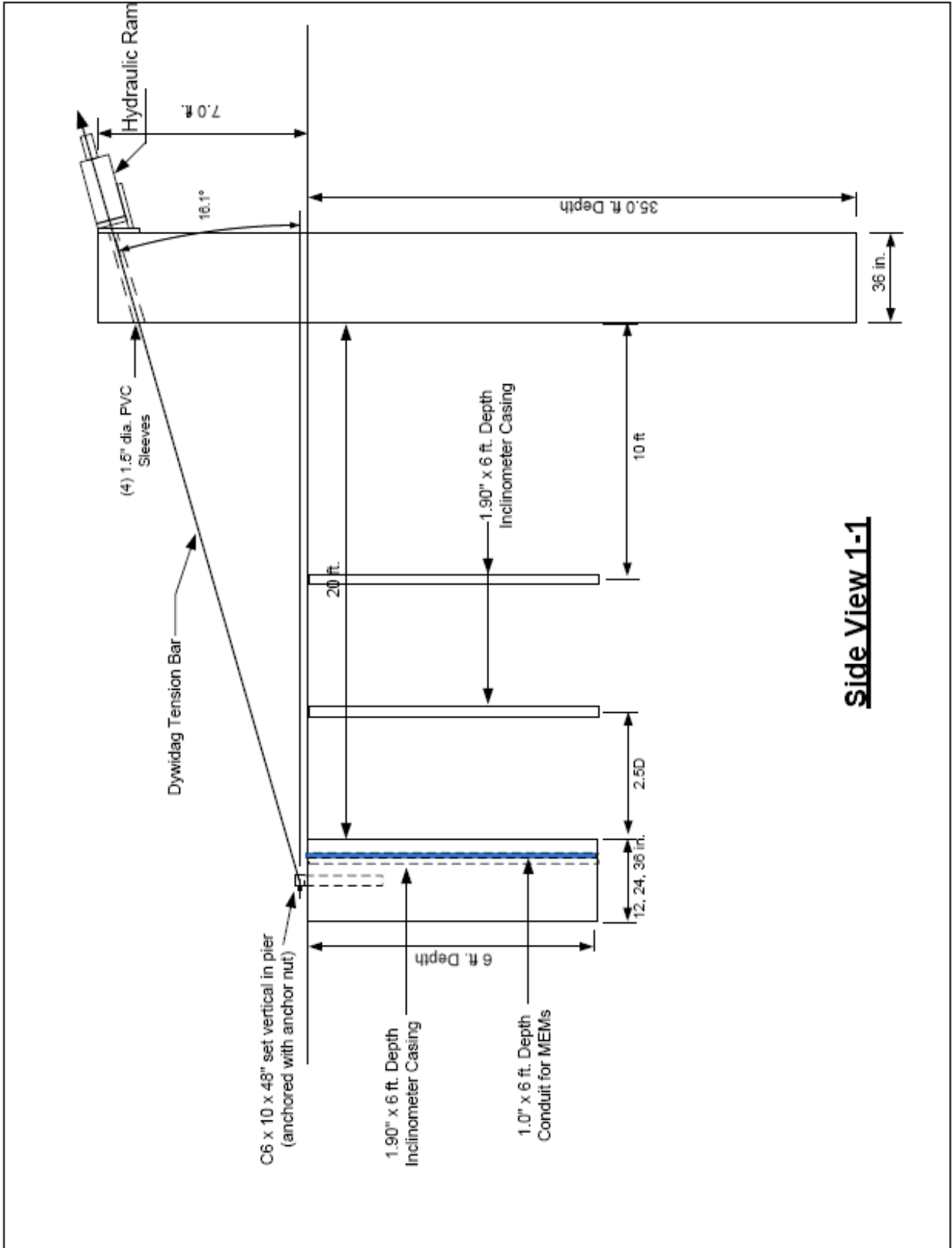


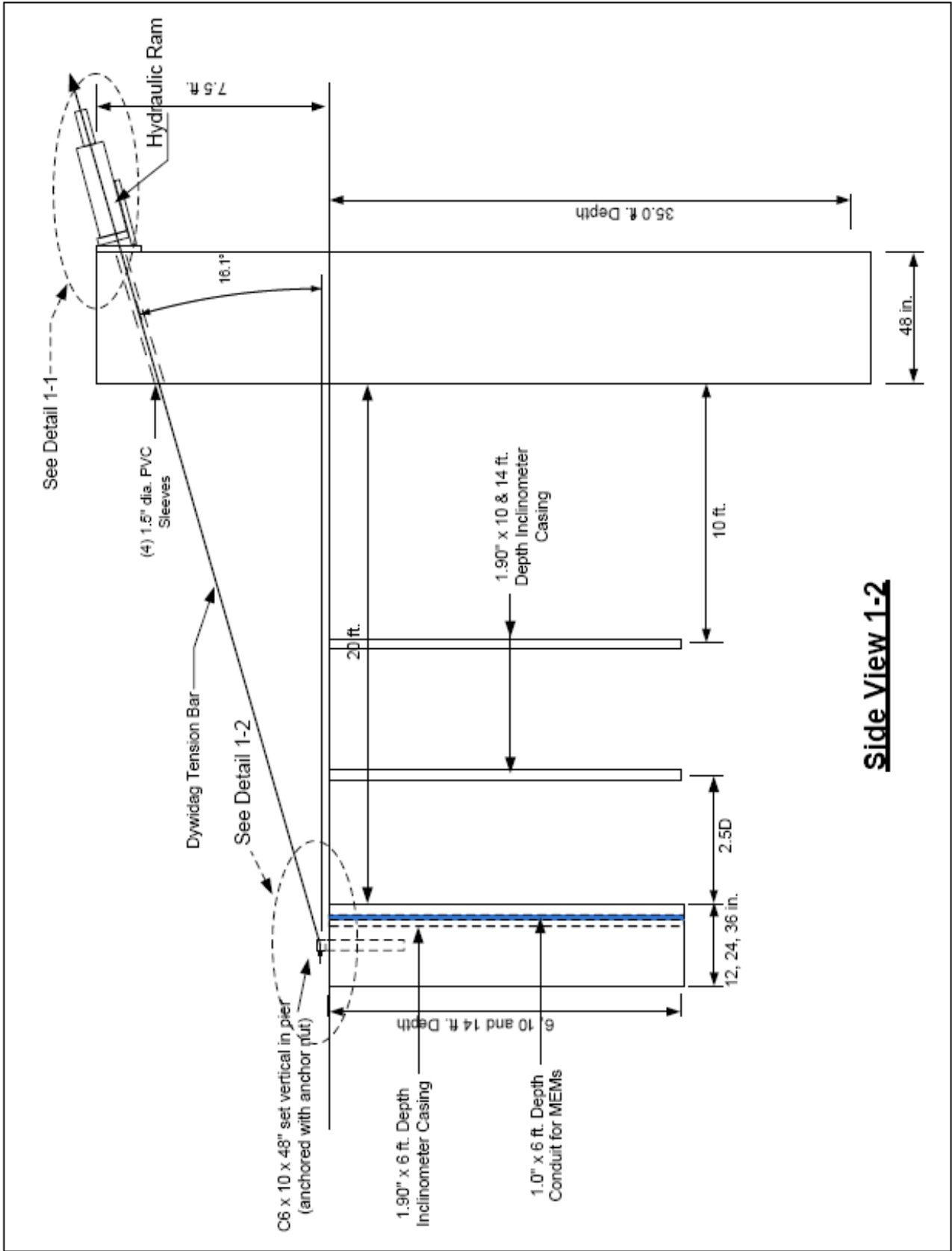
Remark	Test Period
Test Piers	Winter
12" and (2)24" with 10' Depth	Summer
24" with 10' Depth	



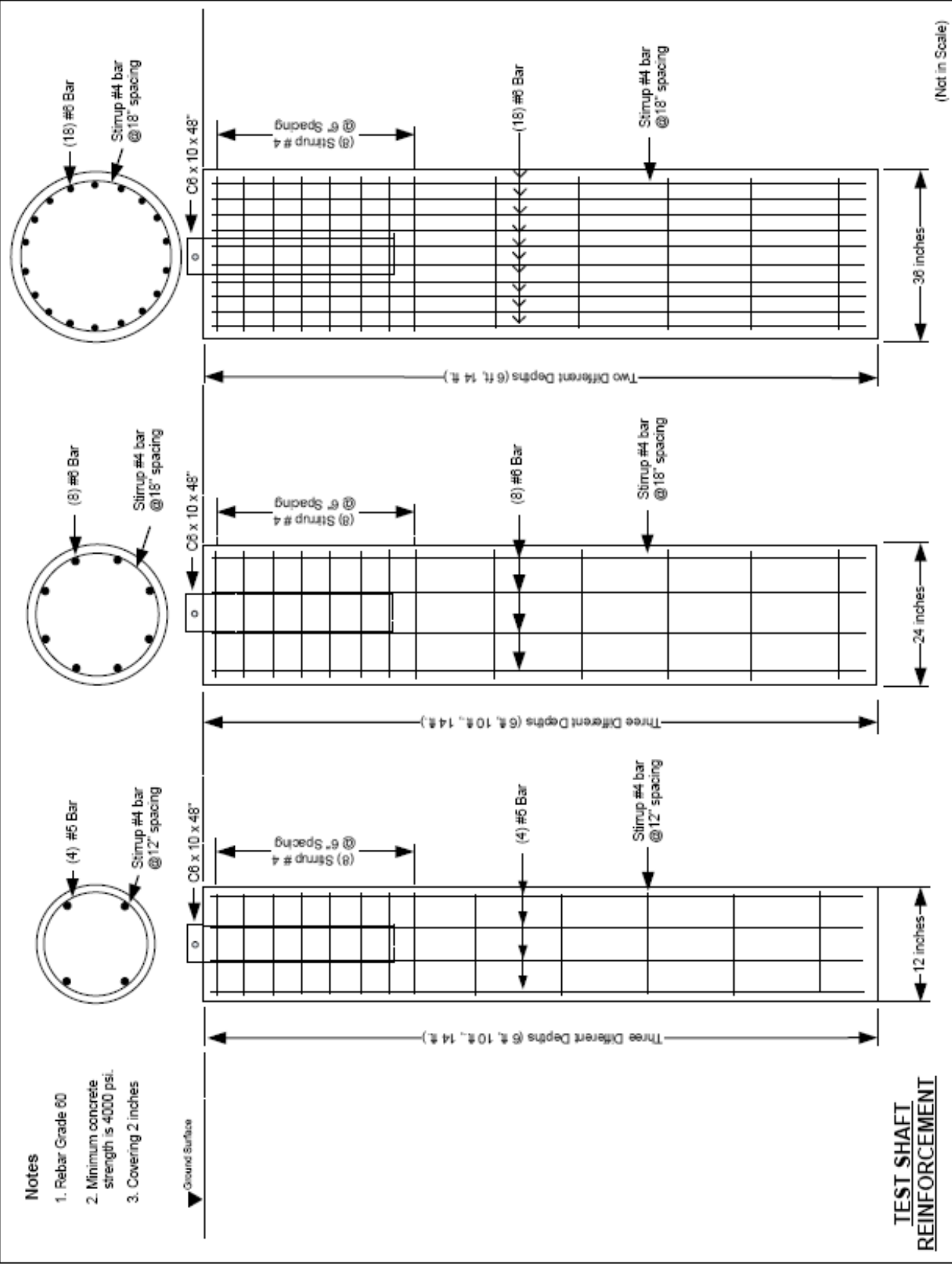
Remark	
Test Piers	Test Period
12", 24", and 36" with 14' Depth	Winter
12" with 10' Depth	Summer

PLAN VIEW of TEST SET#3
(Not in Scale)



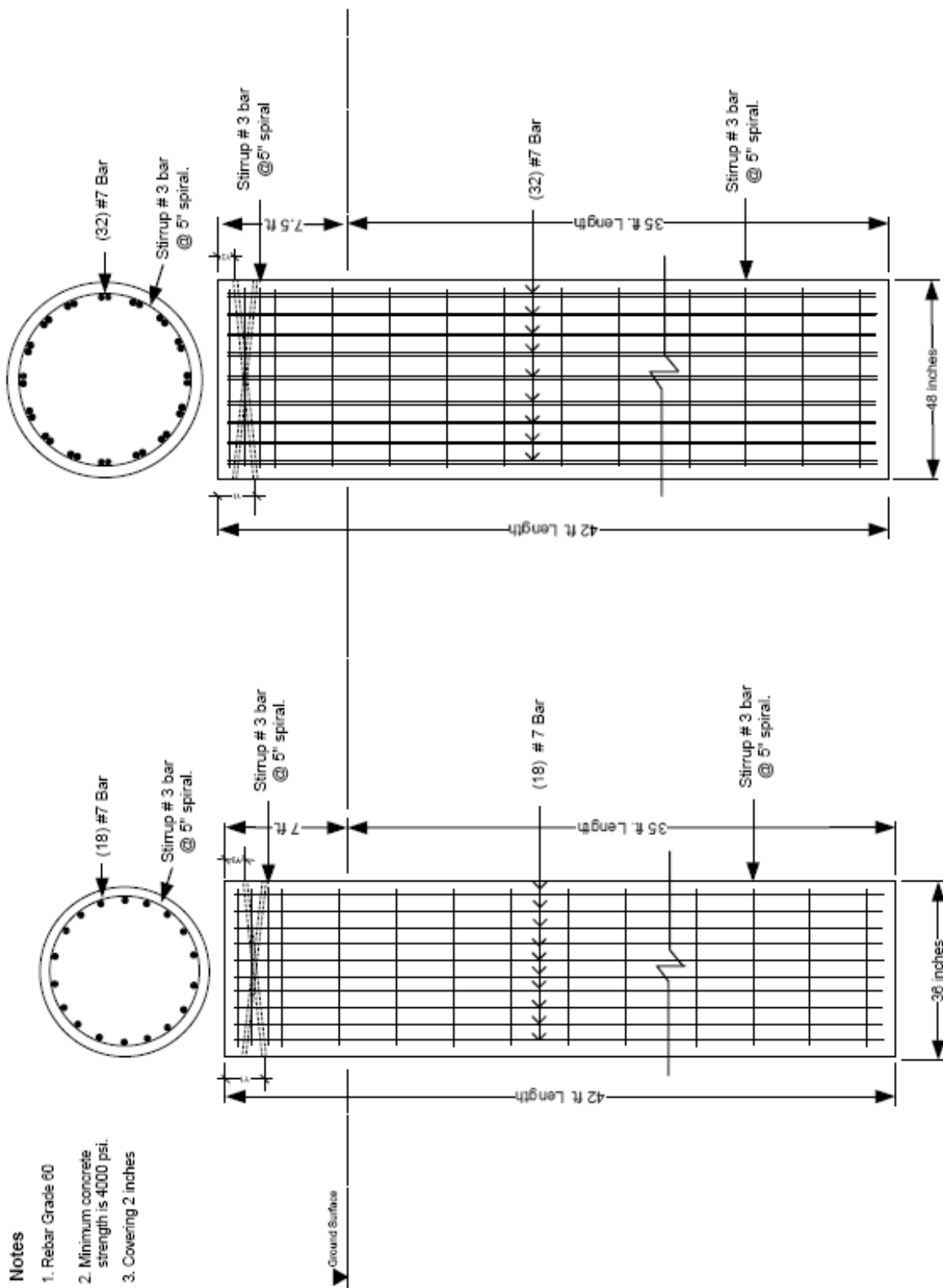


Side View 1-2

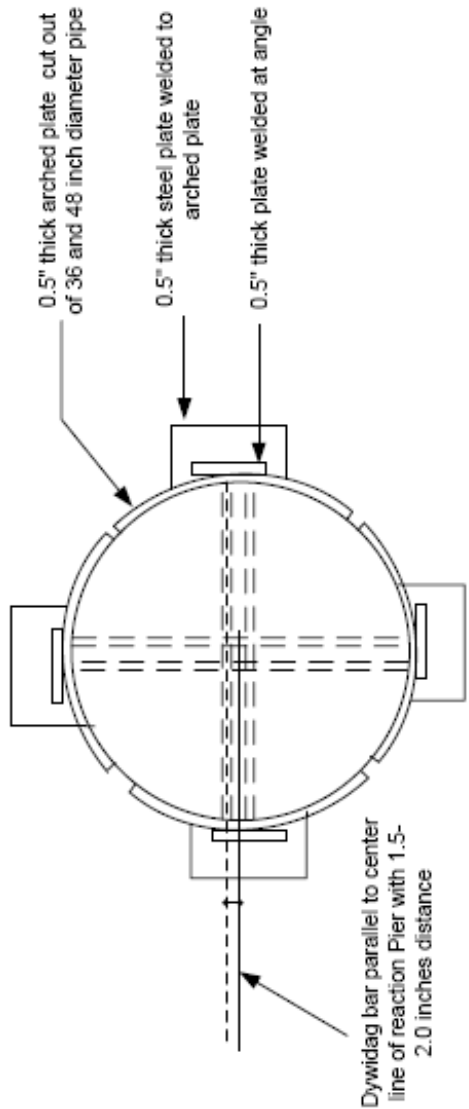


Notes

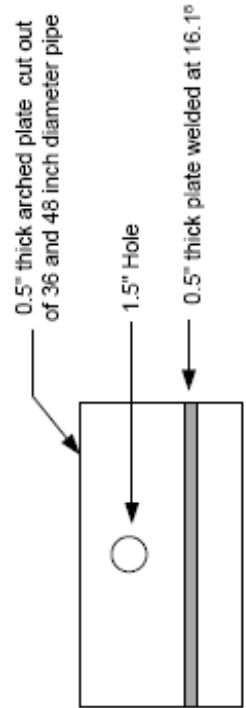
- 1. Rebar Grade 60
- 2. Minimum concrete strength is 4000 psi.
- 3. Covering 2 inches



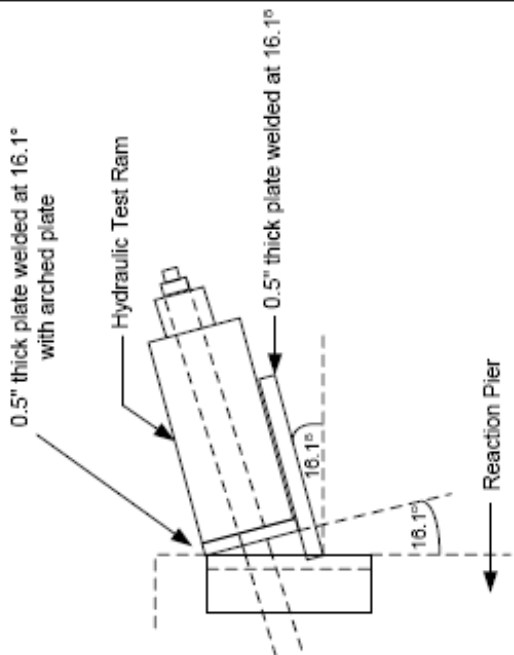
**REACTION SHAFT
REINFORCEMENT**



Cross Section

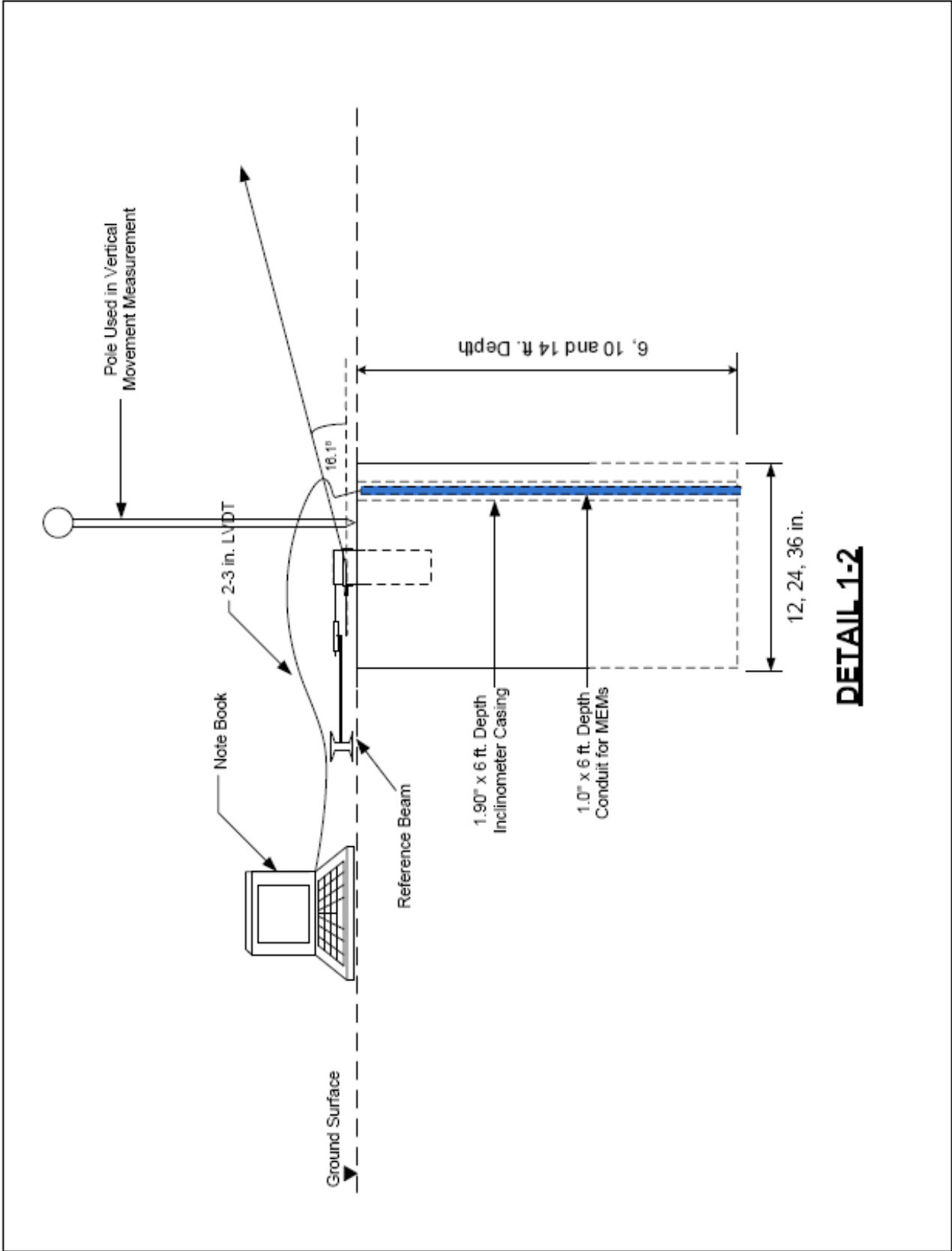


Front View



Side View

DETAIL 1-1



DETAIL 1-2

APPENDIX F: LOAD CELL CALIBRATION REPORT

CALIBRATION TEST CERTIFICATE

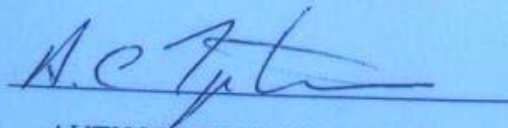
CON - TECH SYSTEMS
550 KING ST. W.
BROCKVILLE ONT.

LOAD TEST ON

S.N. CTS-J-100-2

REFERENCE GAUGE ENERPAC DGBI SN 468
CERTIFIED 06/2008 TRACEABLE TO NIST

REFERENCE	LOAD IN KIPS
1000 psi	18.46
2000 psi	35.94
3000 psi	54.80
4000 psi	73.06
5000 psi	91.13
6000 psi	109.98
7000 psi	129.43
8000 psi	146.90
9000 psi	164.39
10000 psi	181.28



AUTHORIZED SIGNATURE

DATE JUNE 1 2009

RECERTIFICATION DATE : JUNE 2010

CALIBRATION TEST CERTIFICATE

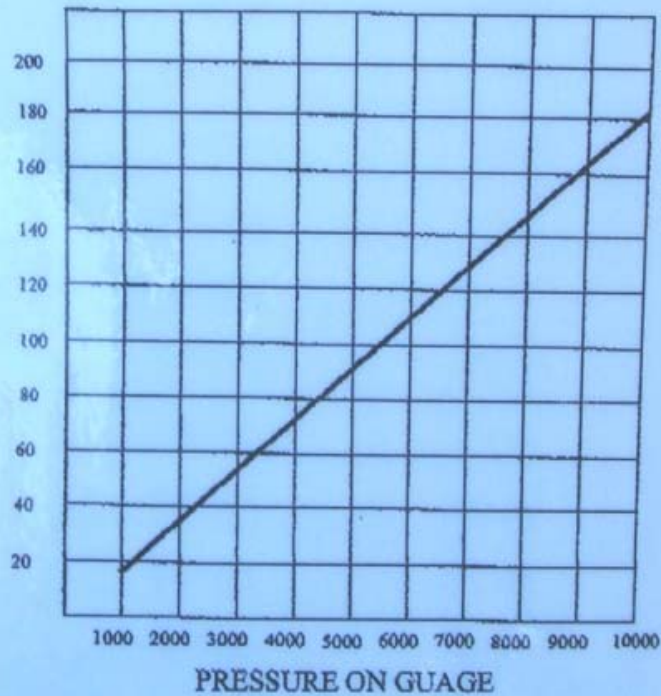
CON - TECH SYSTEMS
4502 HANNA DR.
ELIZABETH TOWN, ON.

LOAD TEST ON

S.N. CTS-J-100-2

REFERENCE GAUGE ENERPAC DGB1 SN 468
CERTIFIED 06/2008 TRACEABLE TO NIST

LOAD IN KIPS

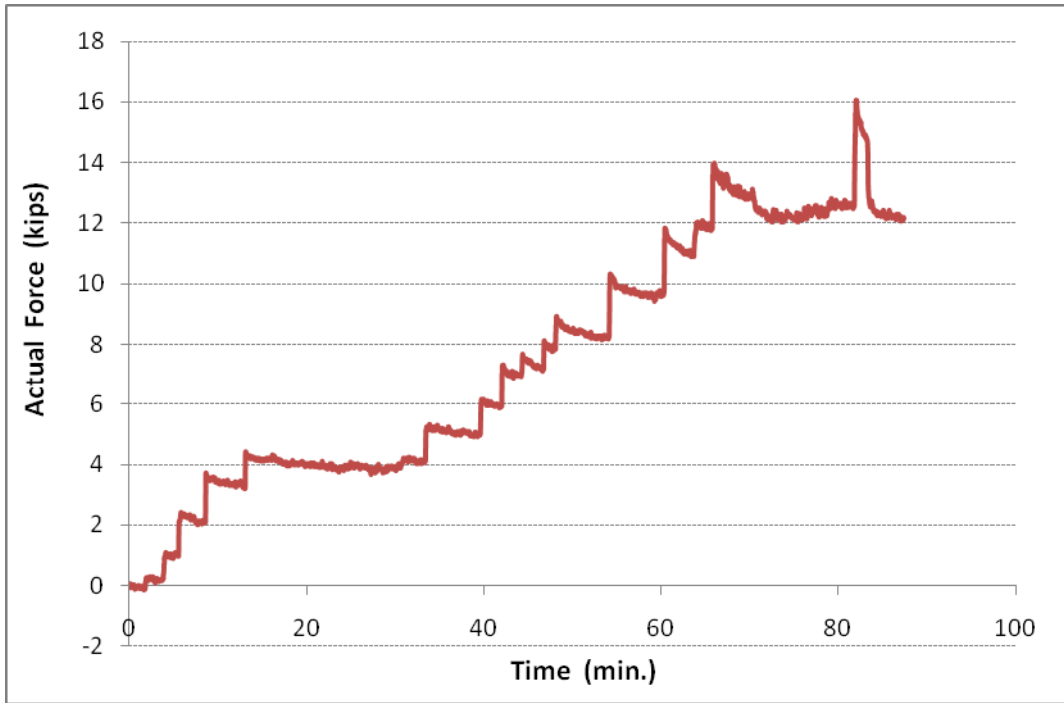


AUTHORIZED SIGNATURE

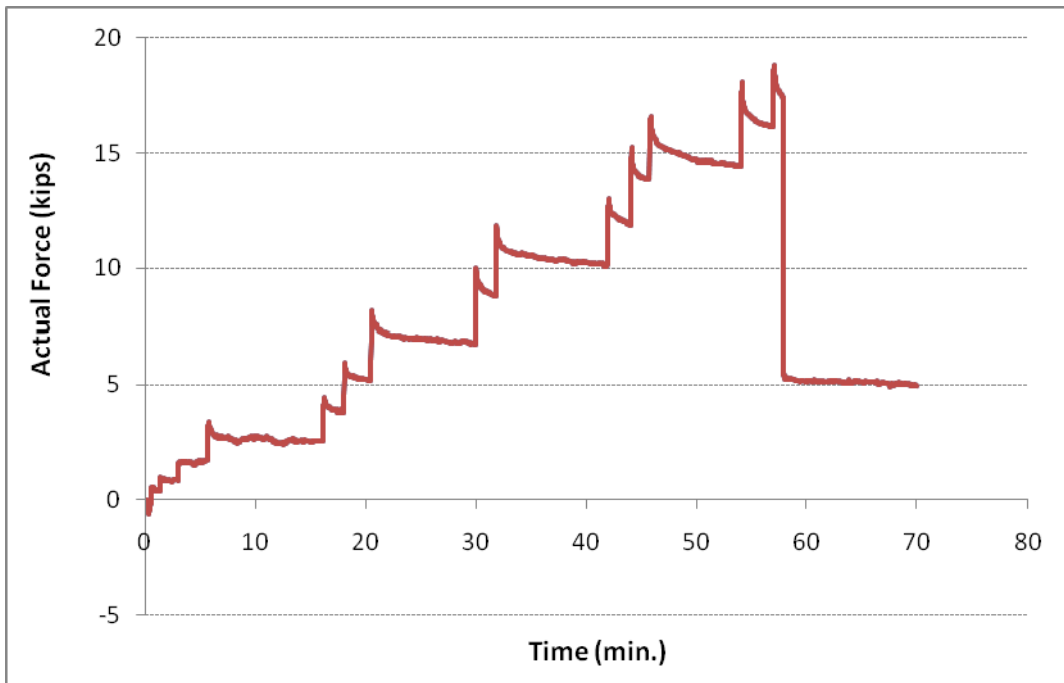
DATE JUNE 1 2009

RECERTIFICATION DATE : JUNE 2010

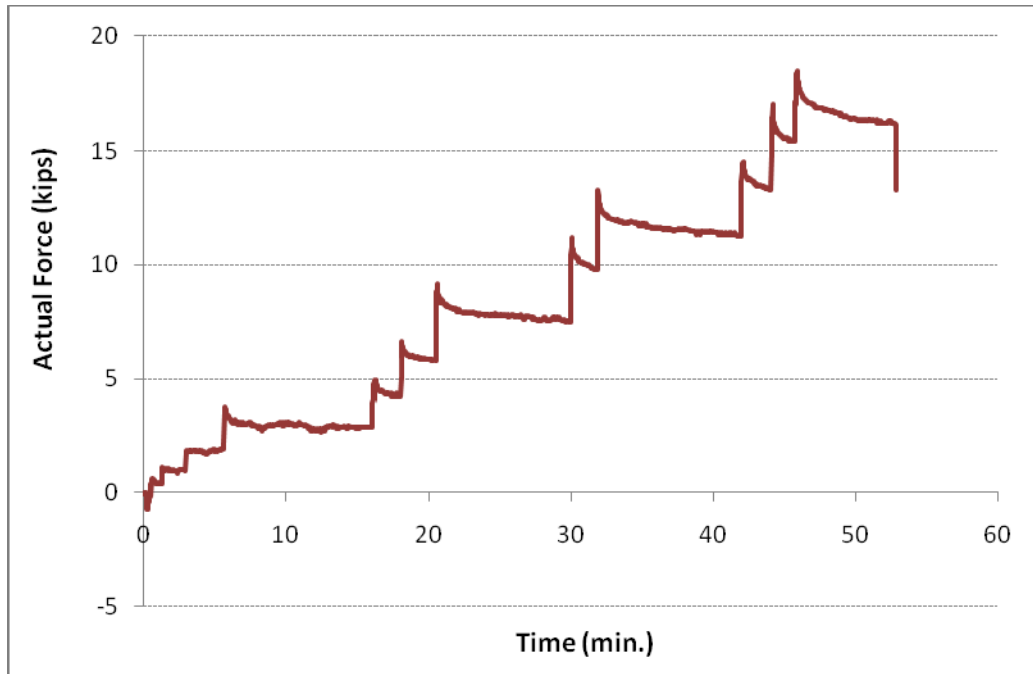
APPENDIX G: LATERAL LOAD TEST RESULTS



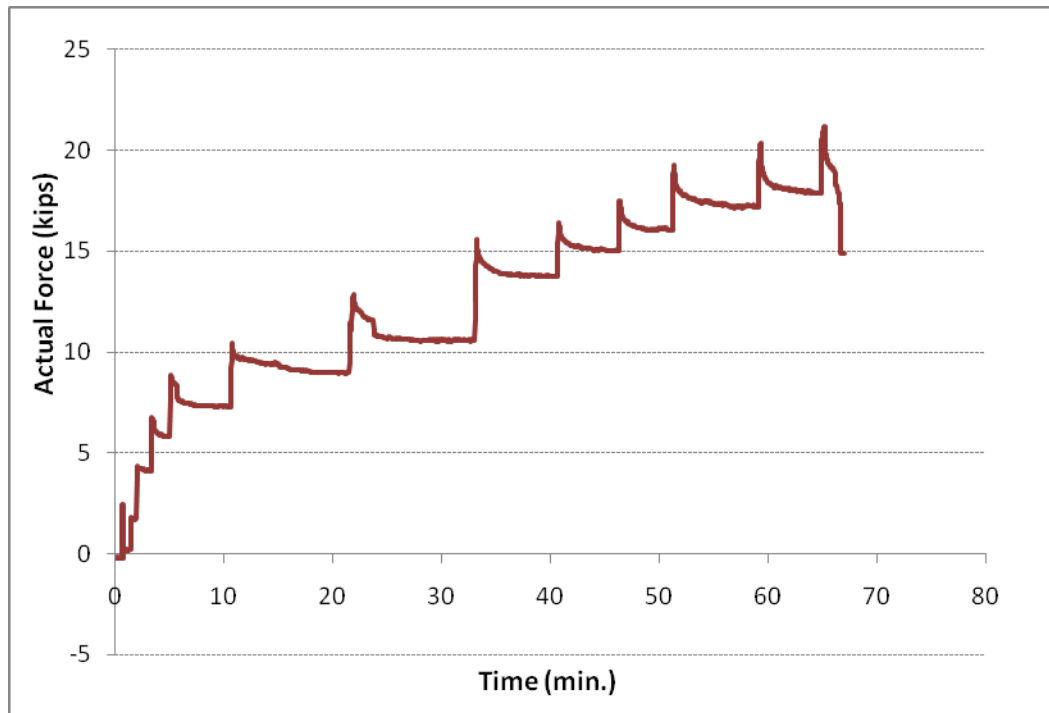
(a) 1 ft diameter × 6 ft depth shaft



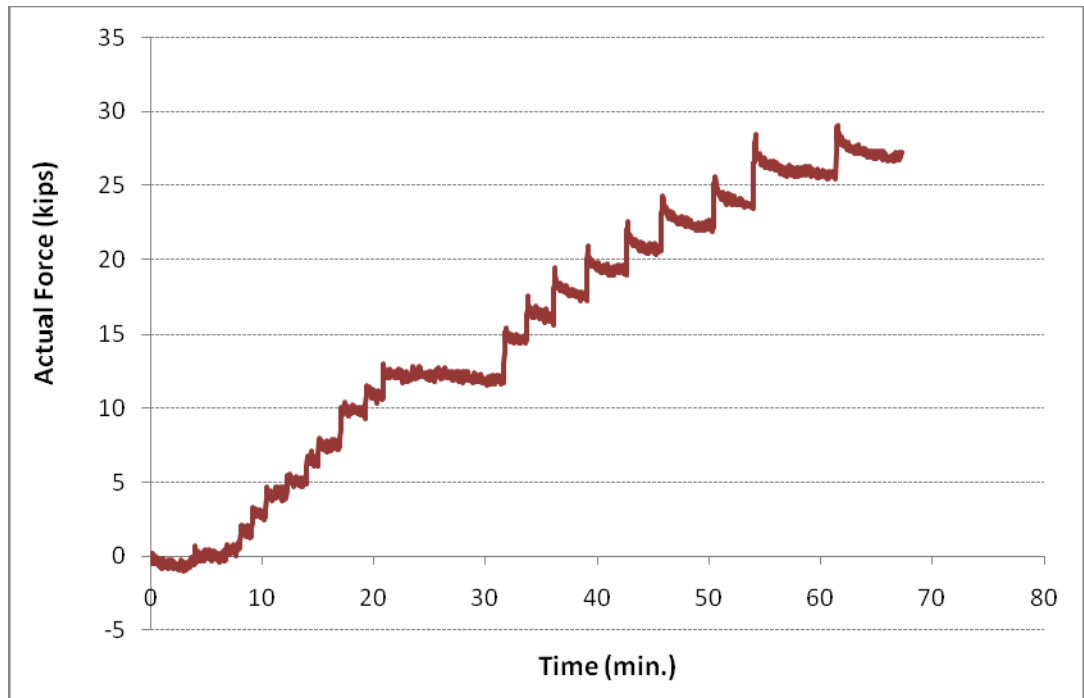
(b) 1 ft diameter × 10 ft depth shaft



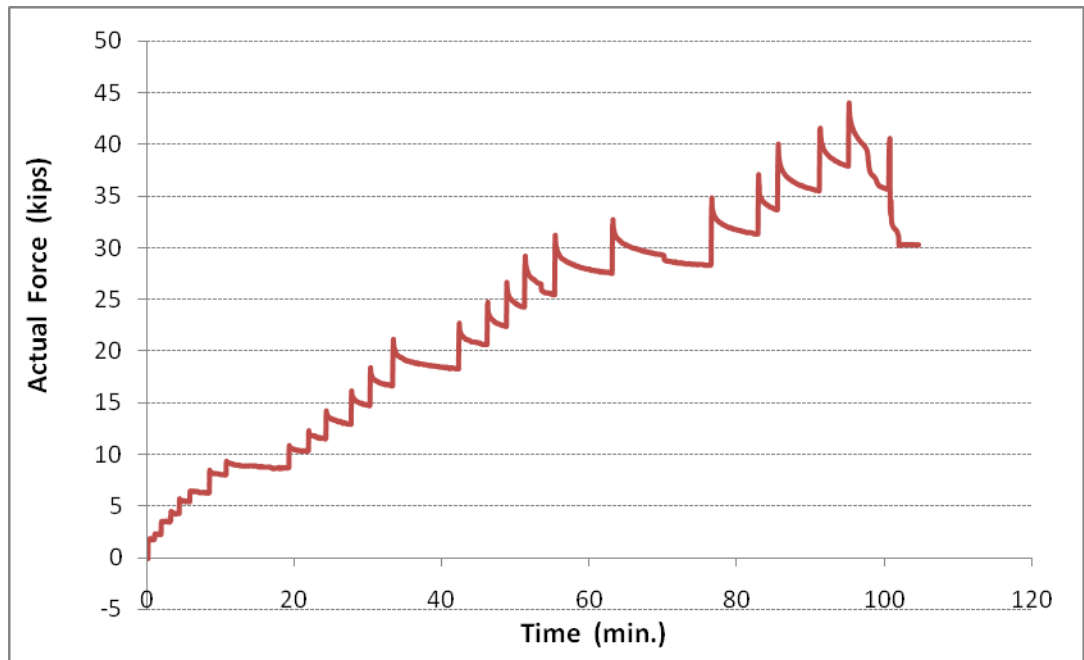
(c) 1 ft diameter × 14 ft depth shaft



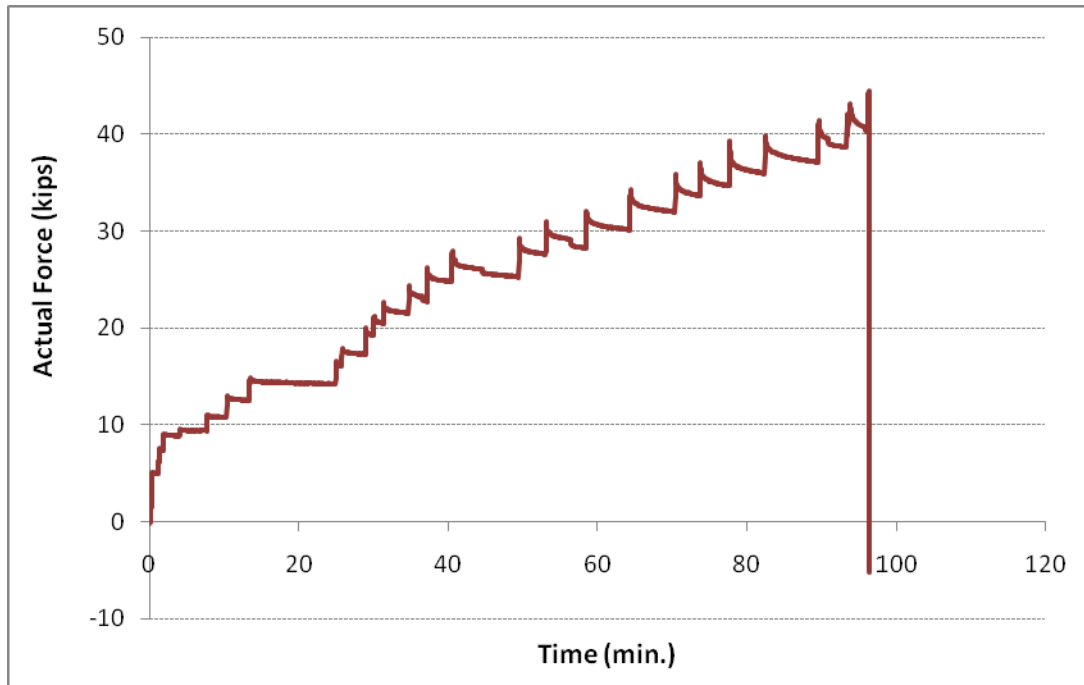
(d) 2 ft diameter × 6 ft depth shaft



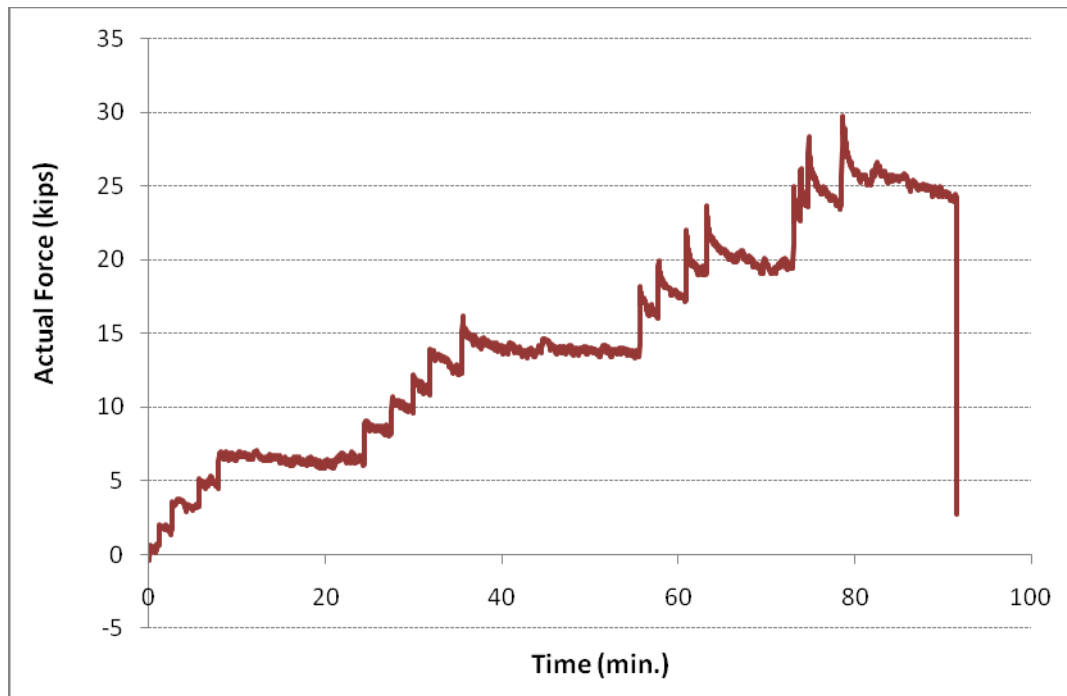
(e) 2 ft diameter × 10 ft depth (1) shaft



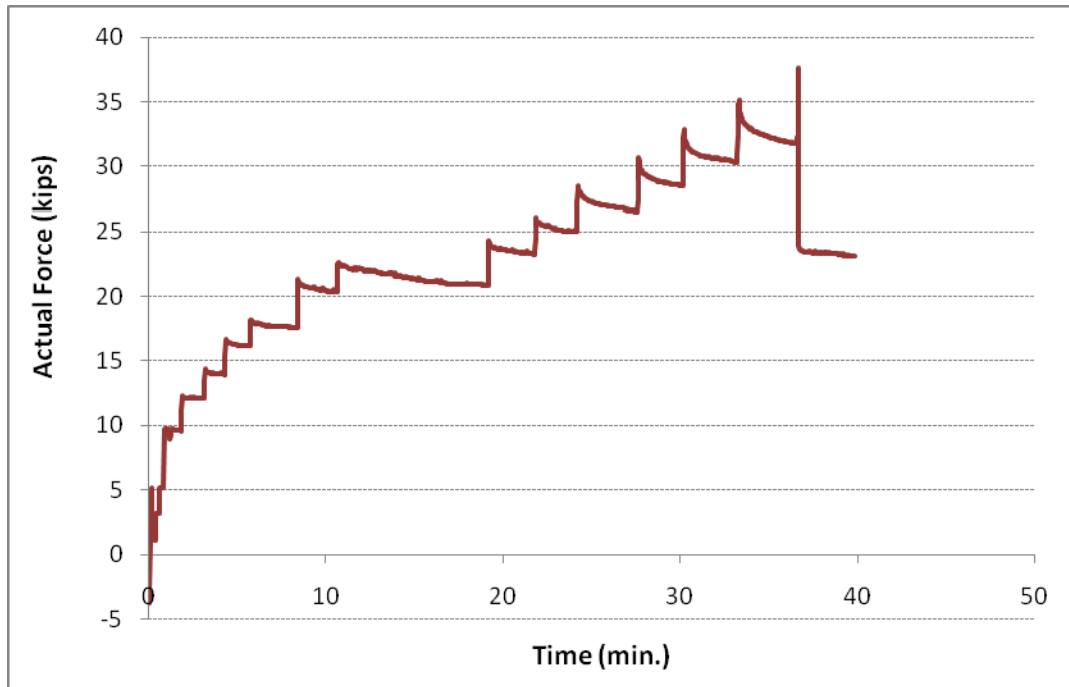
(f) 2 ft diameter × 10 ft depth (2) shaft



(g) 2 ft diameter x 14 ft depth shaft

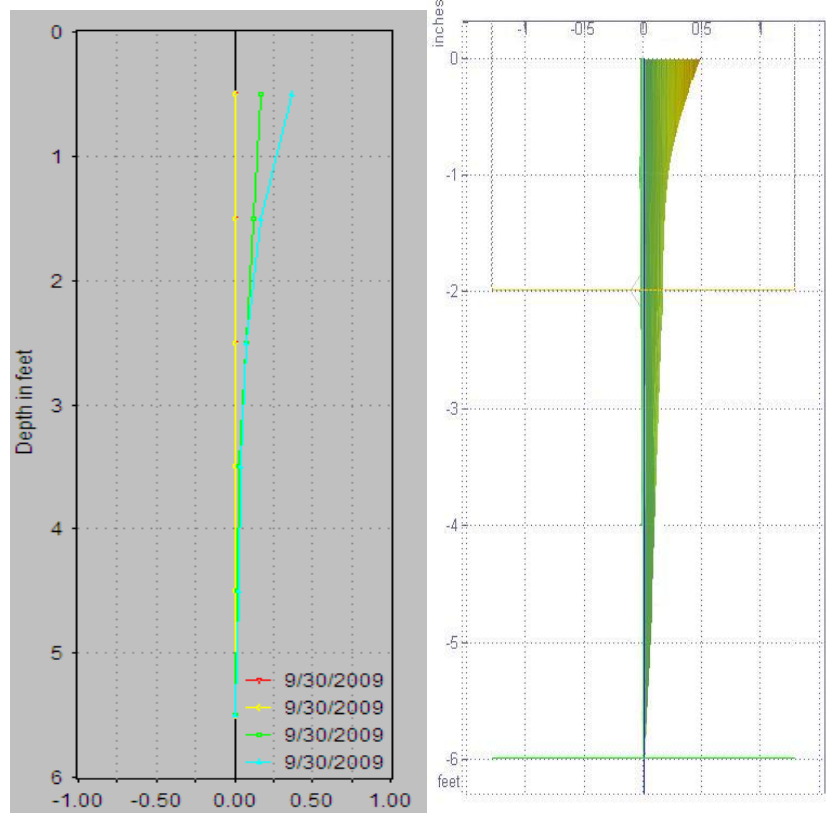


(h) 3 ft diameter x 6 ft depth shaft



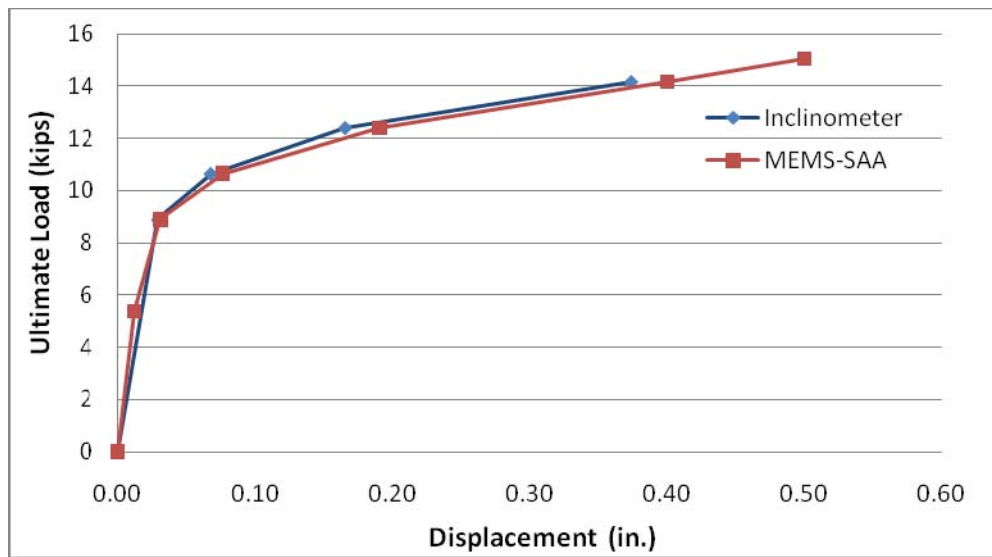
(i) 3 ft diameter × 14 ft depth shaft

Figure G.1. Full Set of Actual Force from Strain Gauge per Time.



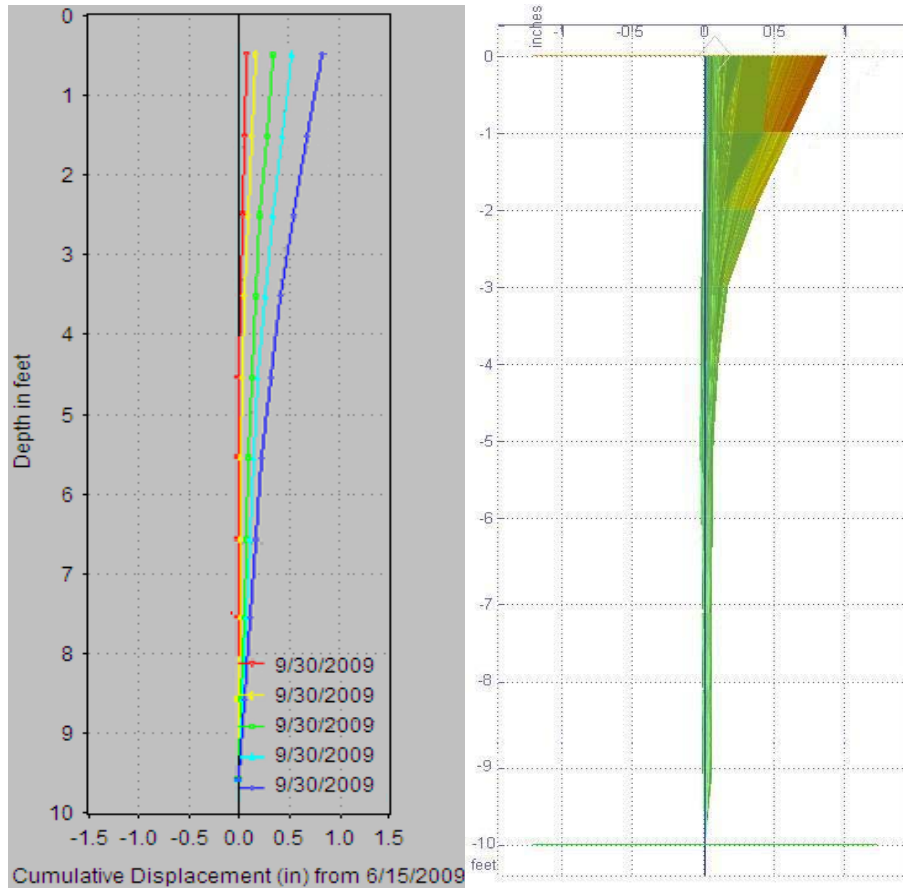
(a)

(b)



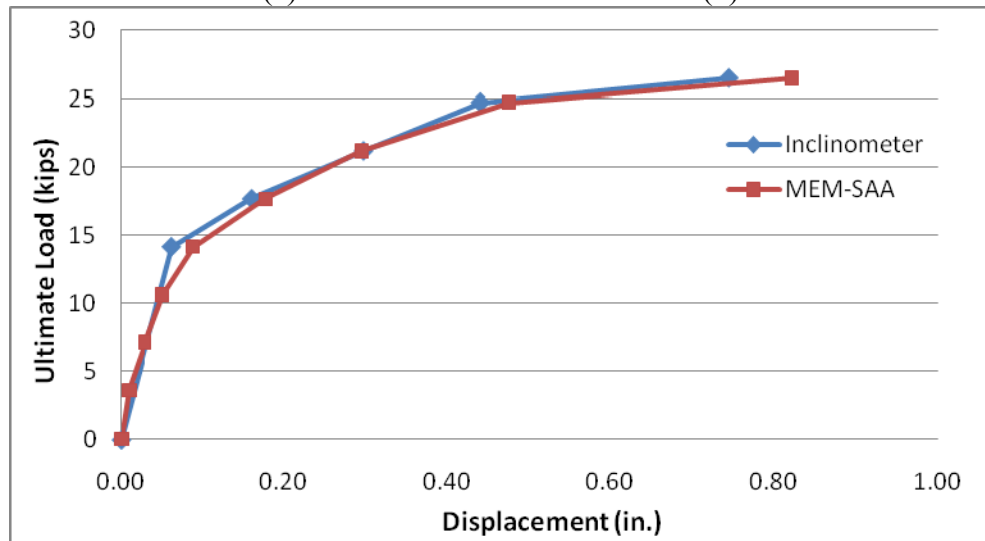
(c)

Figure G.2. Test Shaft (1 ft diameter \times 6 ft depth) Displacement Data: (a) Inclinometer, (b) MEMS-SAA, and (c) Ultimate Load versus Displacement Comparison (Summer Condition).



(a)

(b)



(c)

Figure G.3. Test Shaft (1 ft diameter \times 10 ft depth) Displacement Data: (a) Inclinator, (b) MEMS-SAA, and (c) Ultimate Load versus Displacement Comparison (Summer Condition).

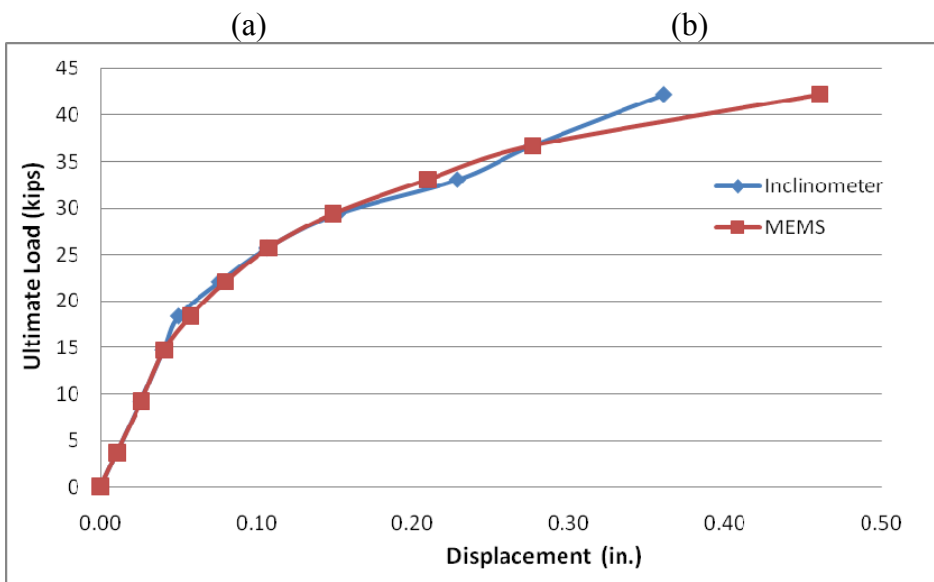
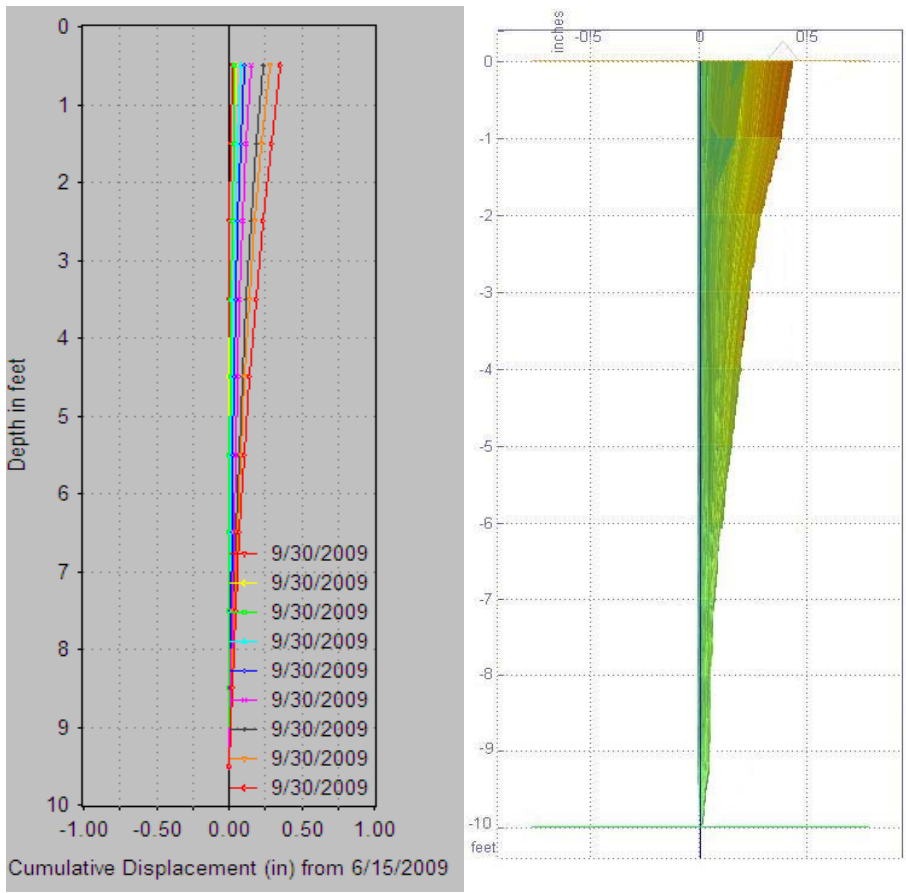
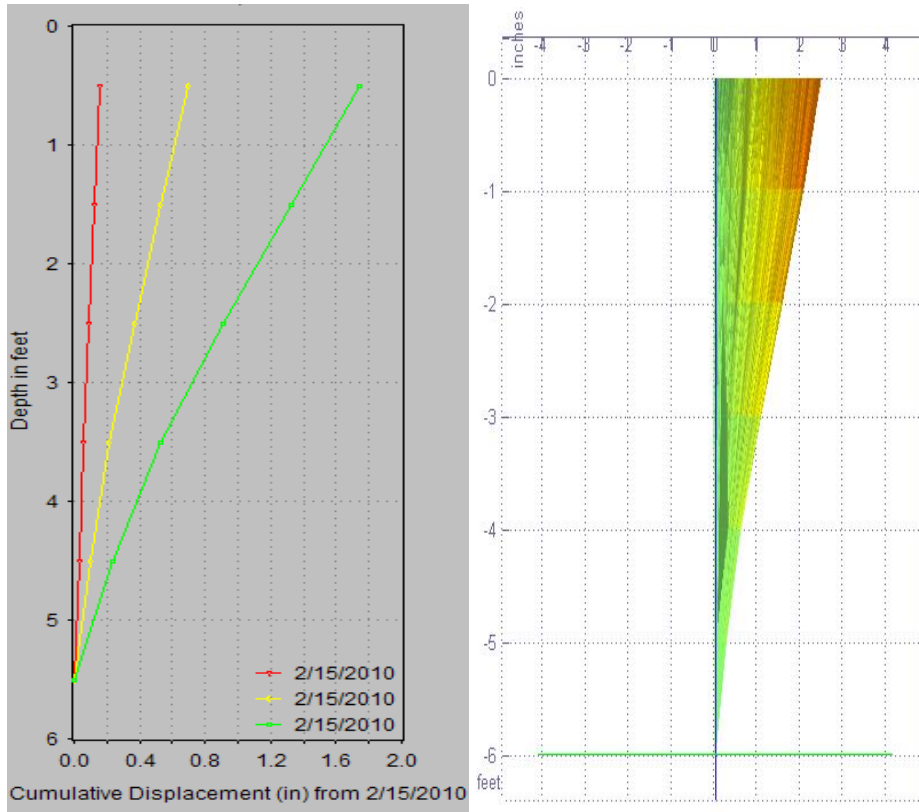
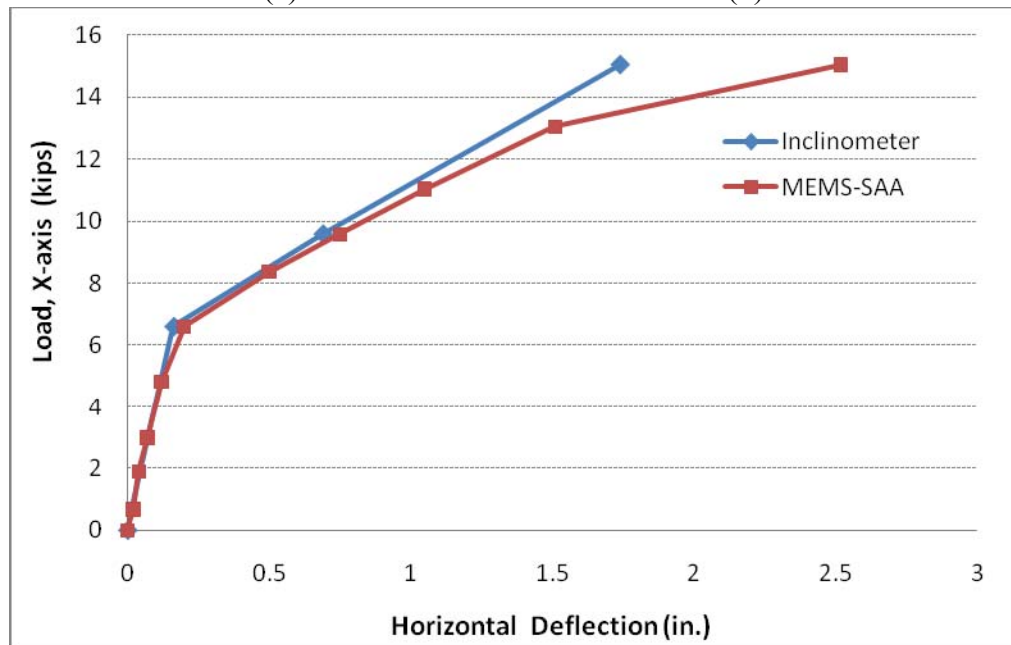


Figure G.4. Test Shaft (2 ft diameter × 10 ft depth) Displacement Data: (a) Inclinator, (b) MEMS-SAA, and (c) Ultimate Load versus Displacement Comparison (Summer Condition).



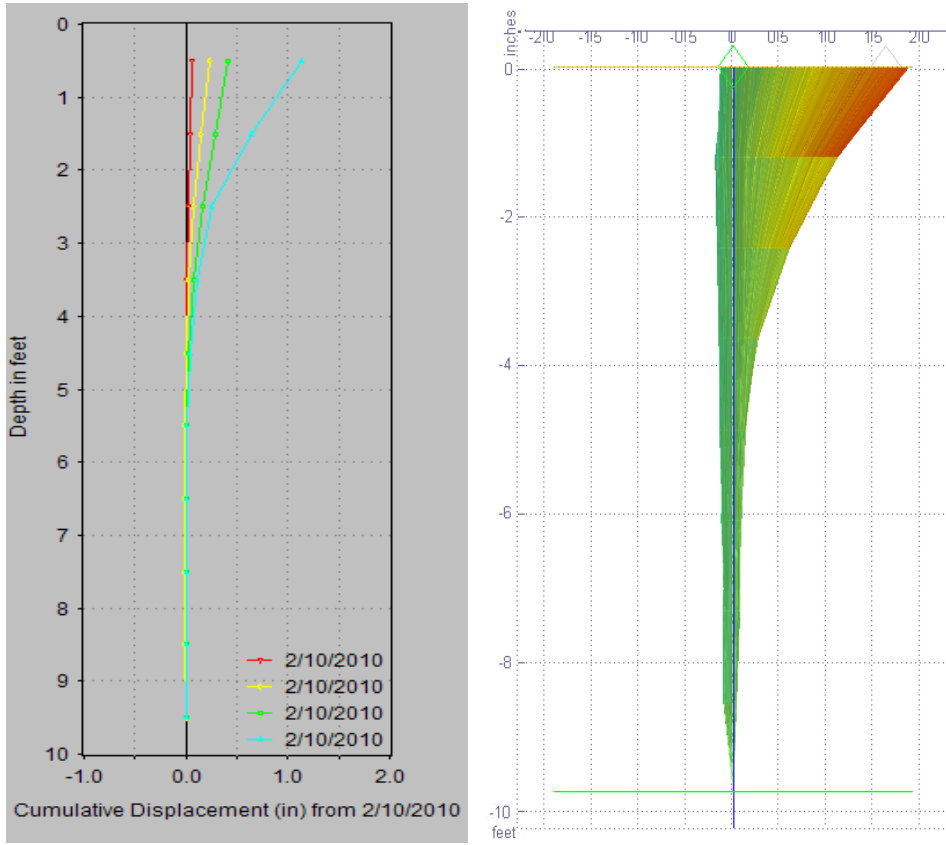
(a)

(b)



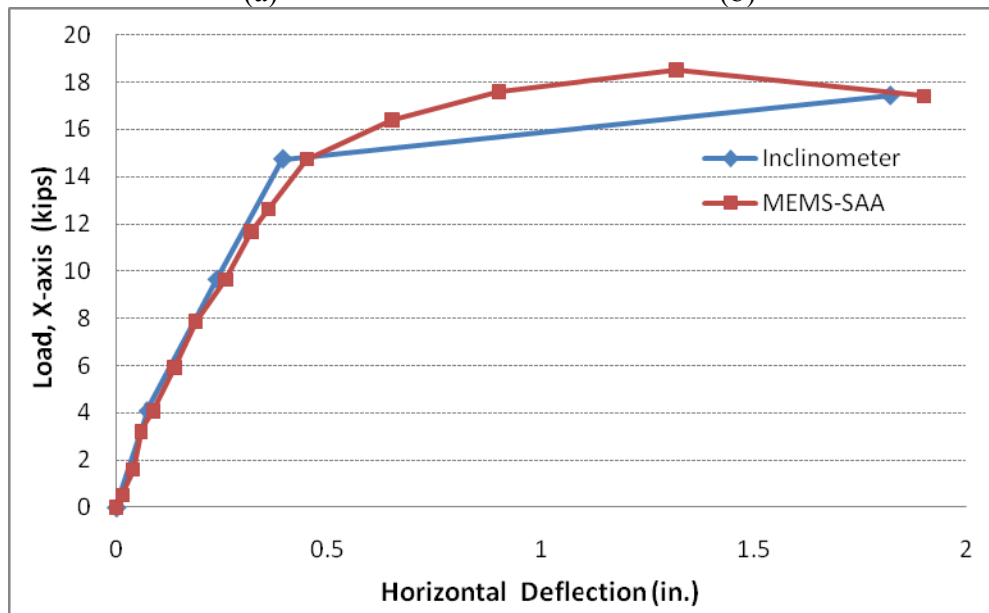
(c)

Figure G.5. Test Shaft (1 ft diameter × 6 ft depth) Displacement Data: (a) Inclinometer, (b) MEMS-SAA, (c) Ultimate Load versus Displacement Comparison (Winter Condition).



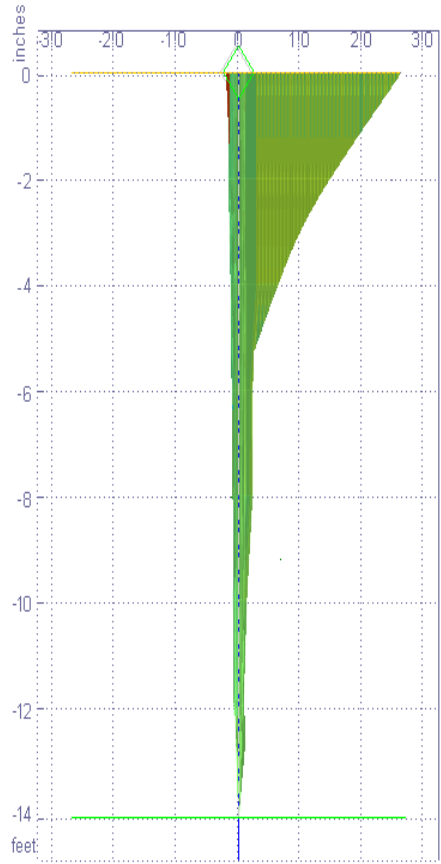
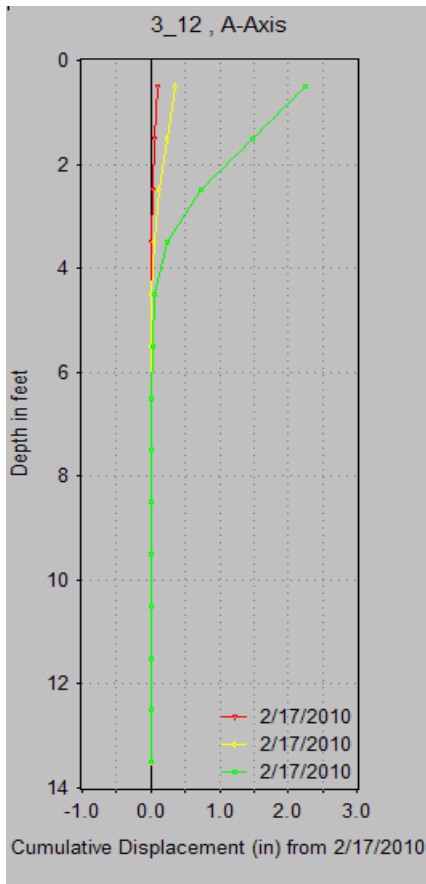
(a)

(b)



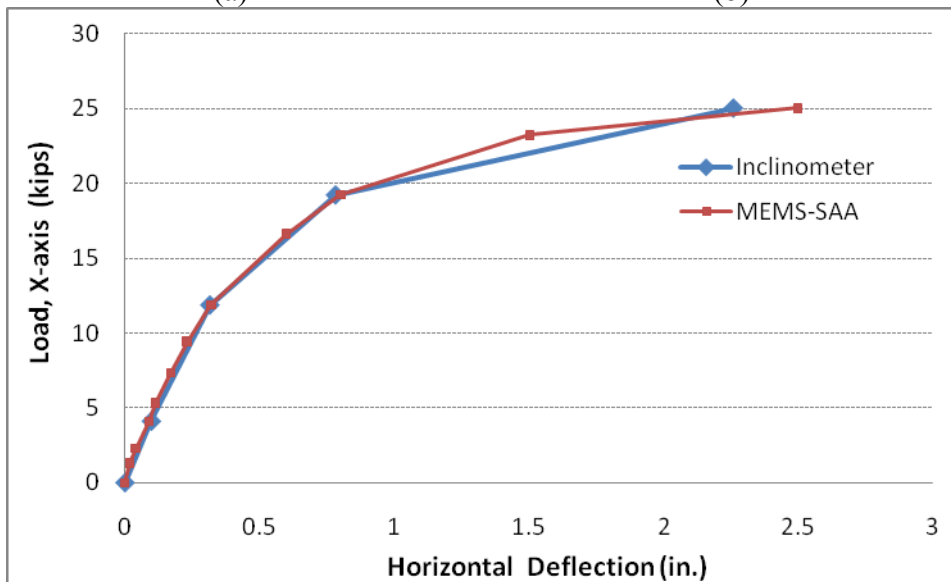
(c)

Figure G.6. Test Shaft (1 ft diameter × 10 ft depth) Displacement Data: (a) Inclinometer, (b) MEMS-SAA, (c) Ultimate Load versus Displacement Comparison (Winter Condition).



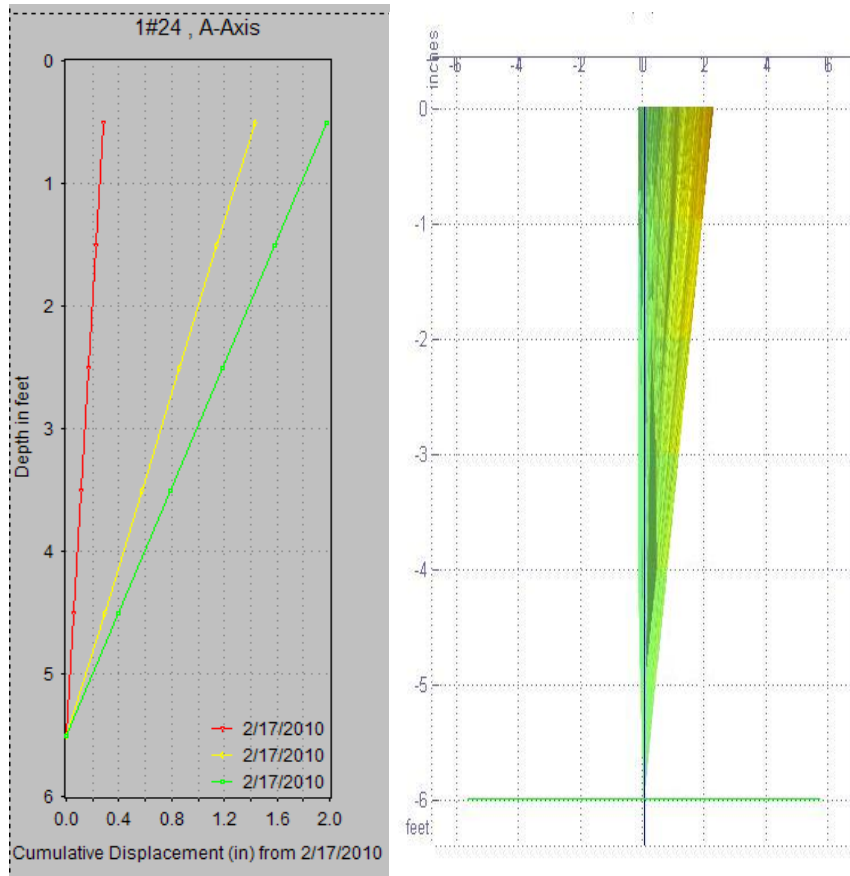
(a)

(b)



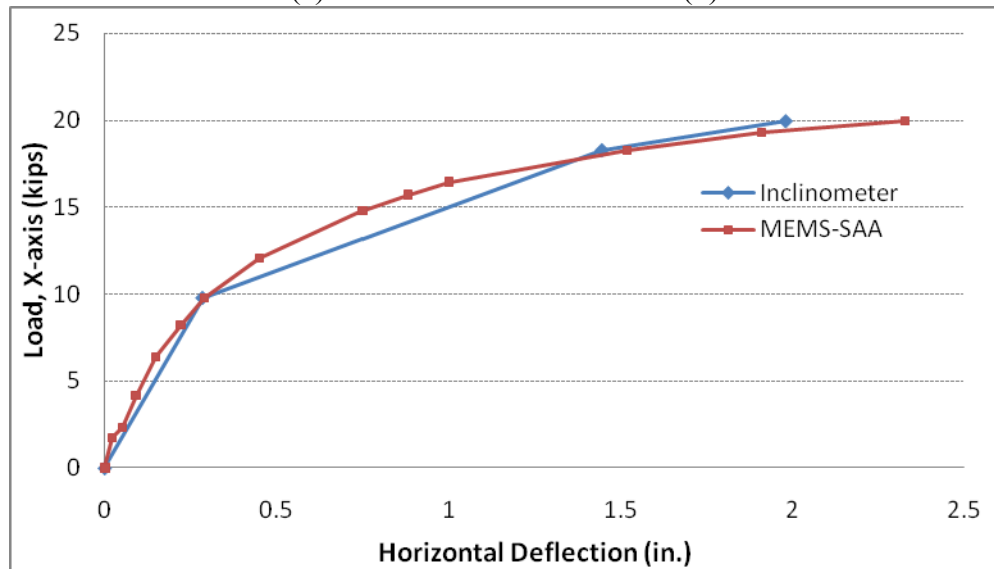
(c)

Figure G.7. Test Shaft (1 ft diameter × 14 ft depth) Displacement Data: (a) Inclinometer, (b) MEMS-SAA, (c) Ultimate Load versus Displacement Comparison (Winter Condition).



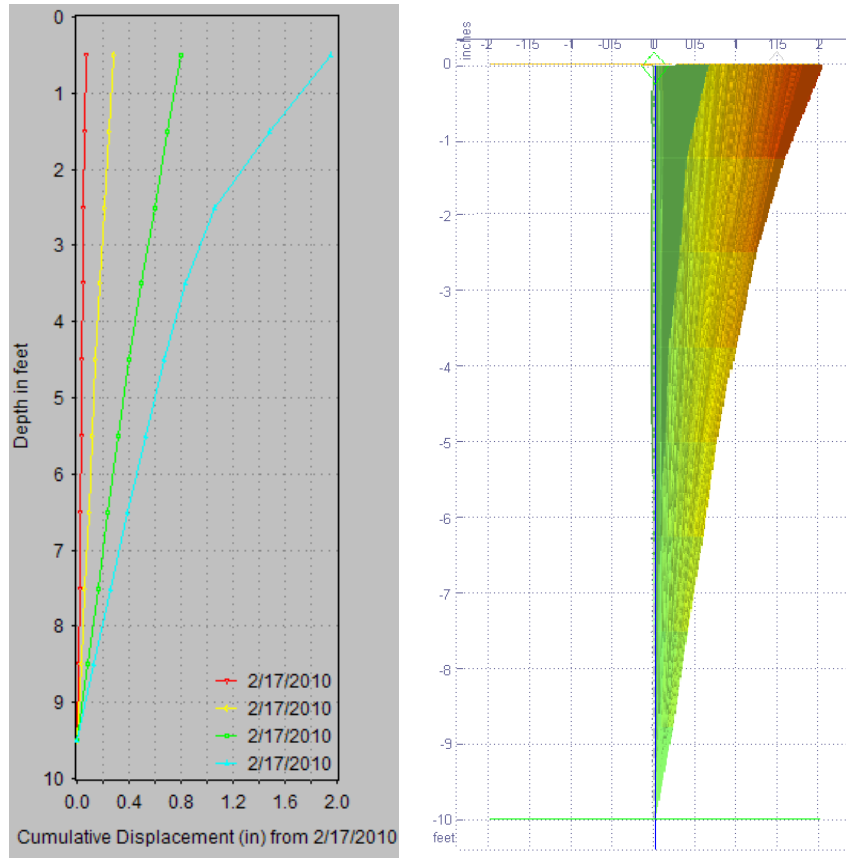
(a)

(b)



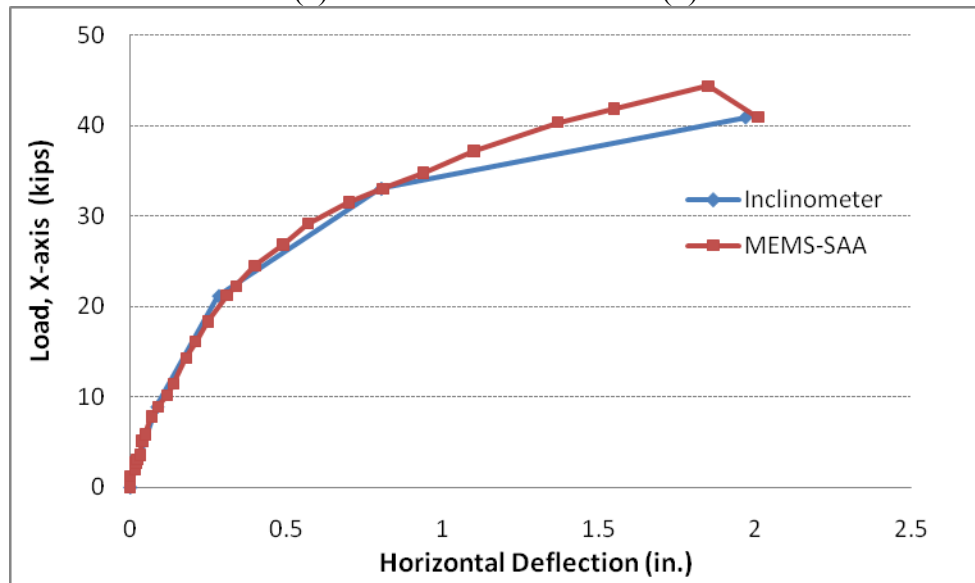
(c)

Figure G.8. Test Shaft (2 ft diameter × 6 ft depth) Displacement Data: (a) Inclinator, (b) MEMS-SAA, and (c) Ultimate Load versus Displacement Comparison (Winter Condition).



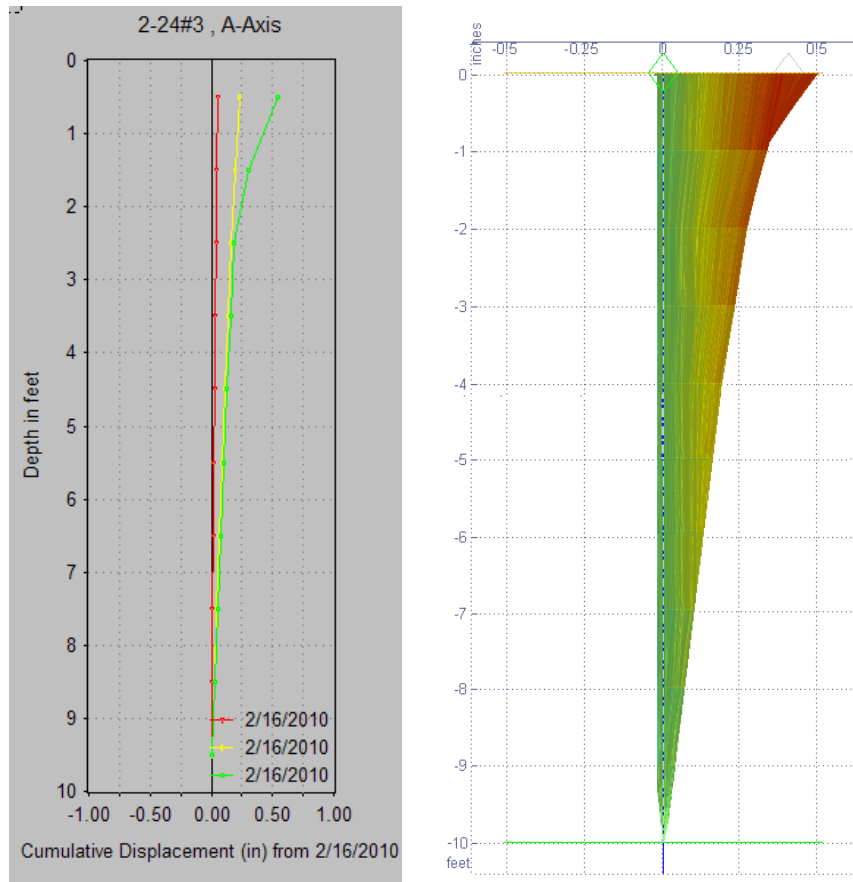
(a)

(b)



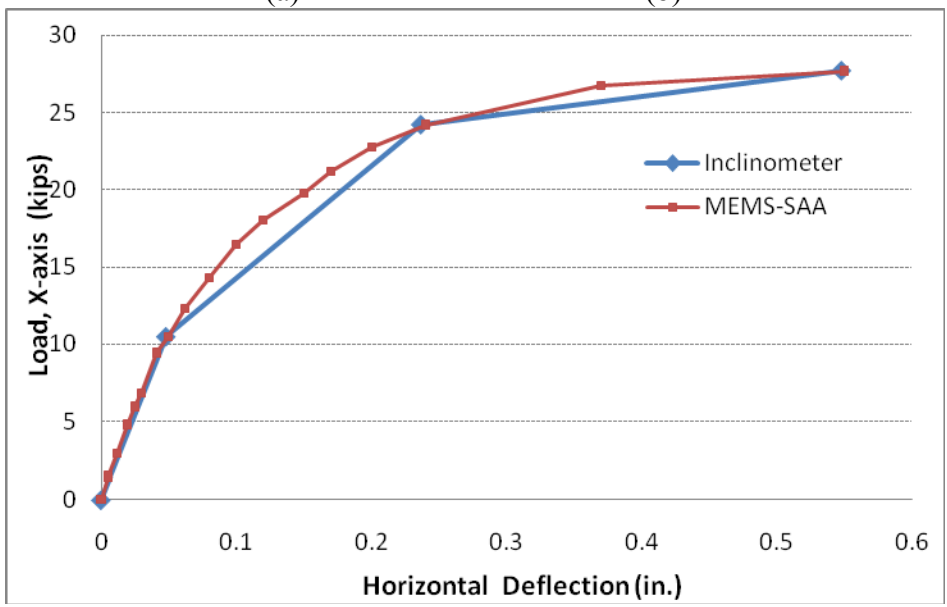
(c)

Figure G.9. Test Shaft#1 (2 ft diameter × 10 ft depth) Displacement Data: Inclinometer, (b) MEMS-SAA, and (c) Ultimate Load versus Displacement Comparison (Winter Condition).



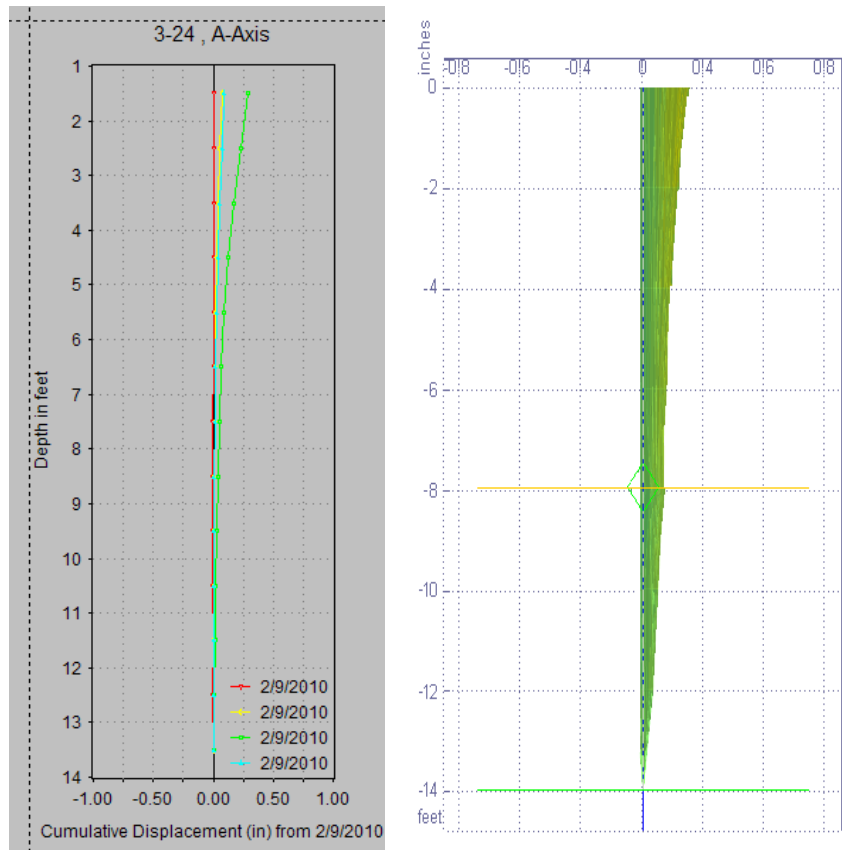
(a)

(b)



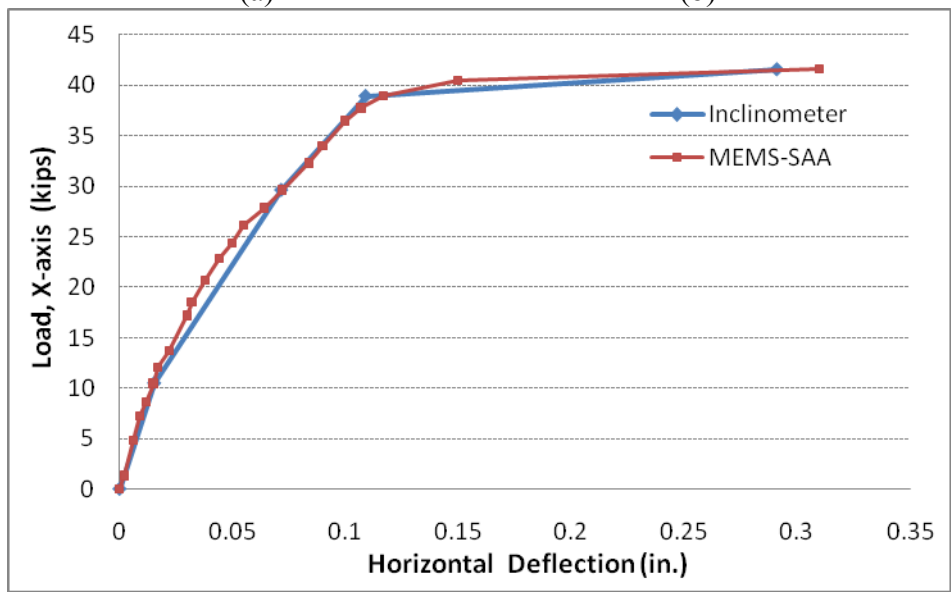
(c)

Figure G.10. Test Shaft#2 (2 ft diameter × 10 ft depth) Displacement Data: (a) Inclinometer, (b) MEMS-SAA, and (c) Ultimate Load versus Displacement Comparison (Winter Condition).



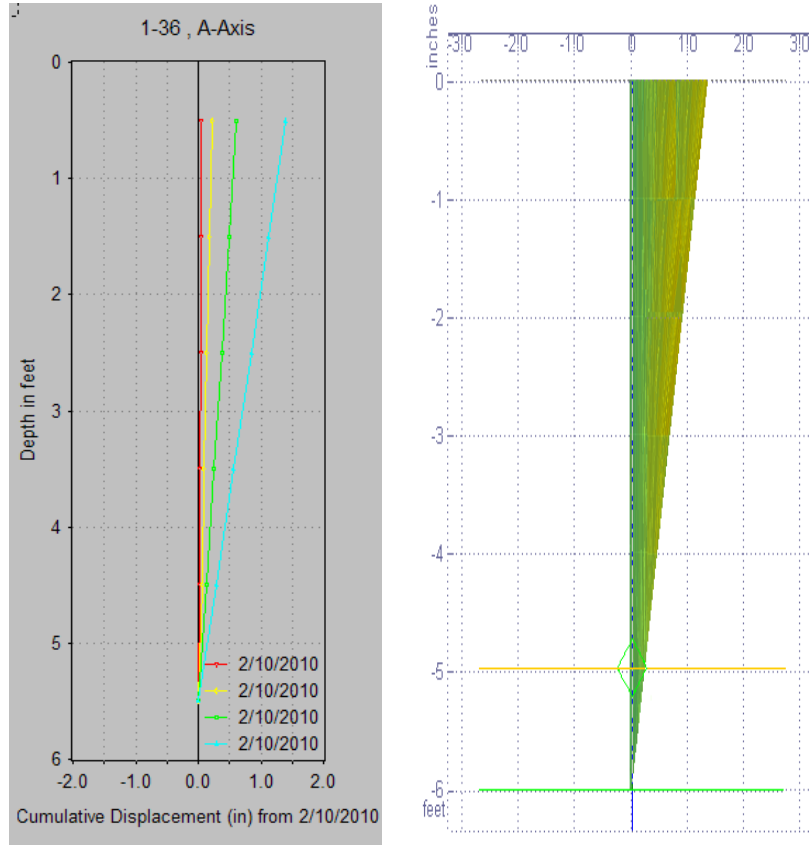
(a)

(b)



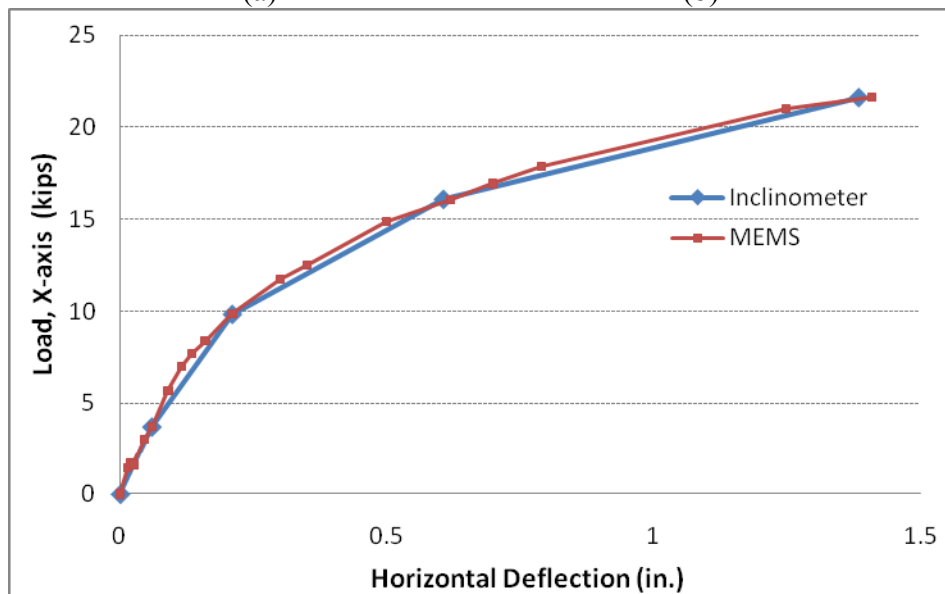
(c)

Figure G.11. Test Shaft (2 ft diameter × 14 ft depth) Displacement Data: (a) Inclinometer, (b) MEMS-SAA, and (c) Ultimate Load versus Displacement Comparison (Winter Condition).



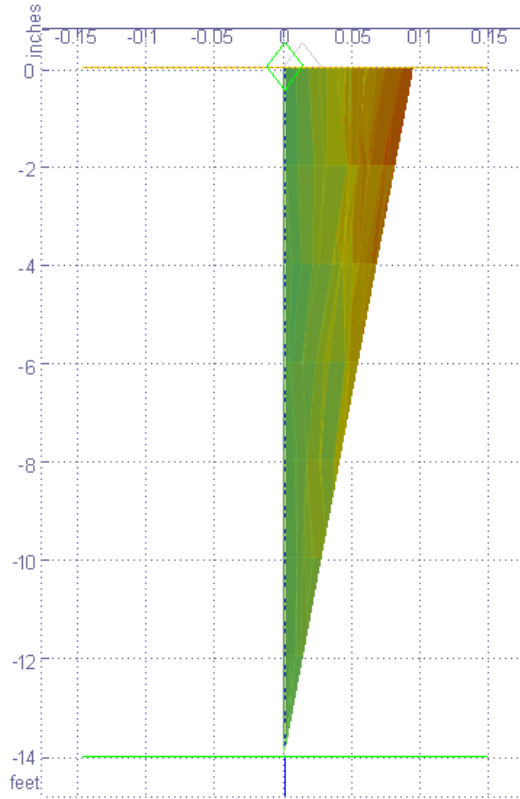
(a)

(b)

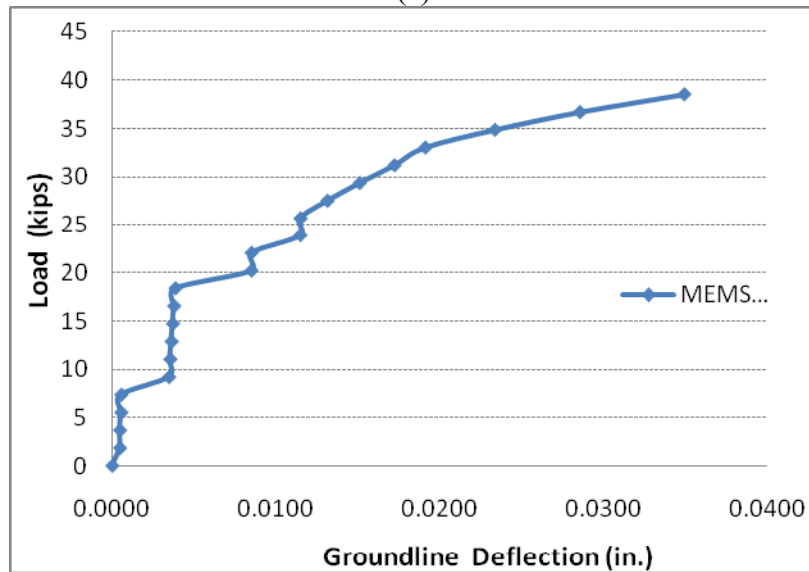


(c)

Figure G.12. Test Shaft (3 ft diameter × 6 ft depth) Displacement Data: (a) Inclinometer, (b) MEMS-SAA, and (c) Ultimate Load versus Displacement Comparison (Winter Condition).



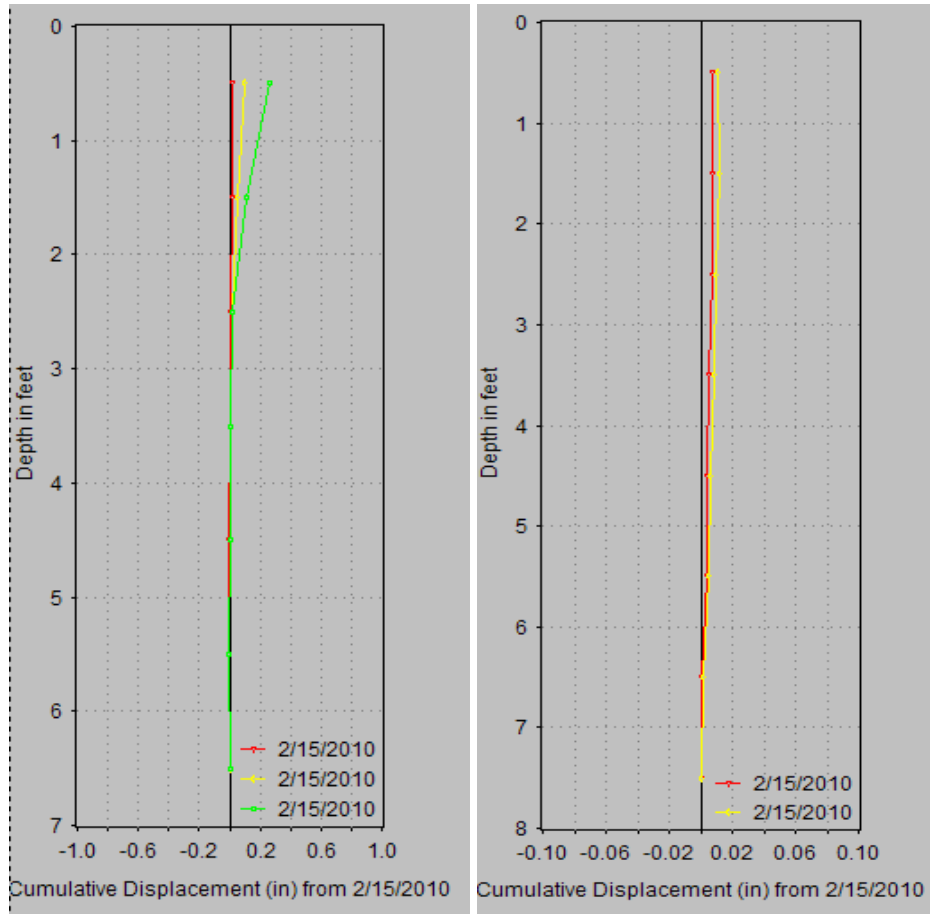
(a)



(b)

Figure G.13 Test Shaft (3 ft diameter × 14 ft depth) Displacement Data: (a) MEMS-SAA and (b) Ultimate Load versus Displacement Comparison (Winter Condition).

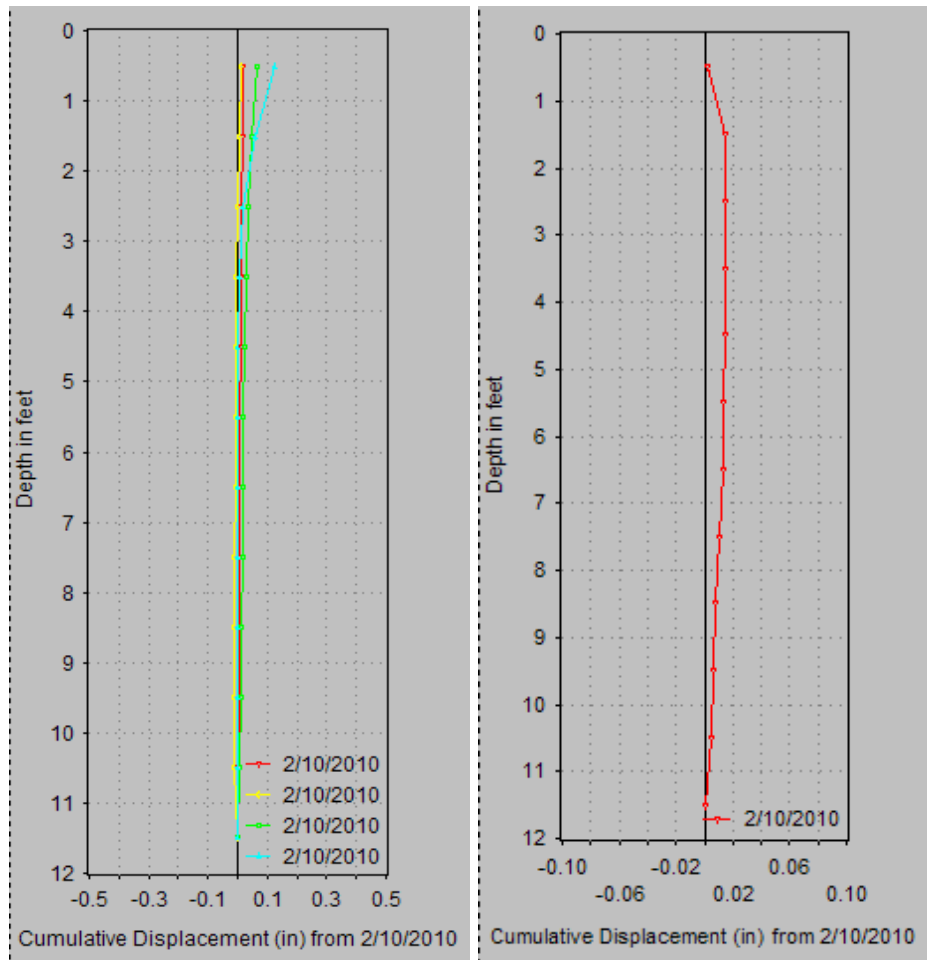
Note: Because the accuracy of inclinometer is not enough, the result can show only MEMS-SAA data



(a)

(b)

**Figure G.14. Displacement Data of Surrounding Soil of Test Shaft (1 ft diameter × 6 ft depth):
 (a) Inclinometer at 2D of Test Shaft and (b) Inclinometer at the Middle of
 Test Shaft and Reaction Shaft.**



(a)

(b)

Figure G.15. Displacement Data of Surrounding Soil of Test Shaft (1 ft diameter × 10 ft depth): (a) Inclinometer at 2D of Test Shaft and (b) Inclinometer at the Middle of Test Shaft and Reaction Shaft.

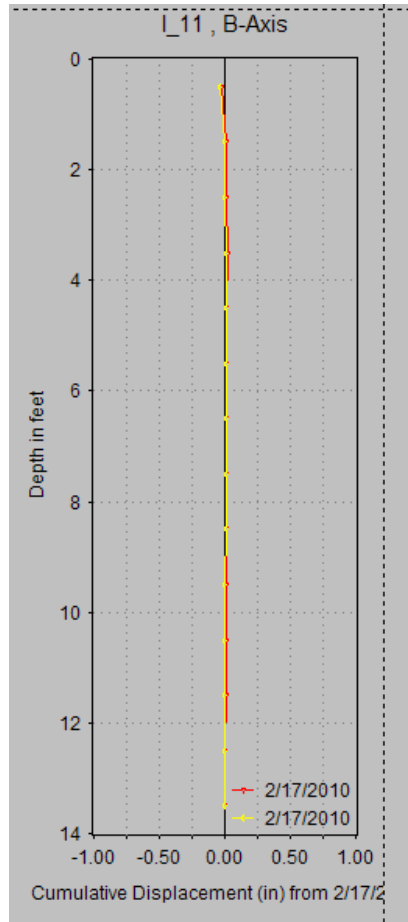
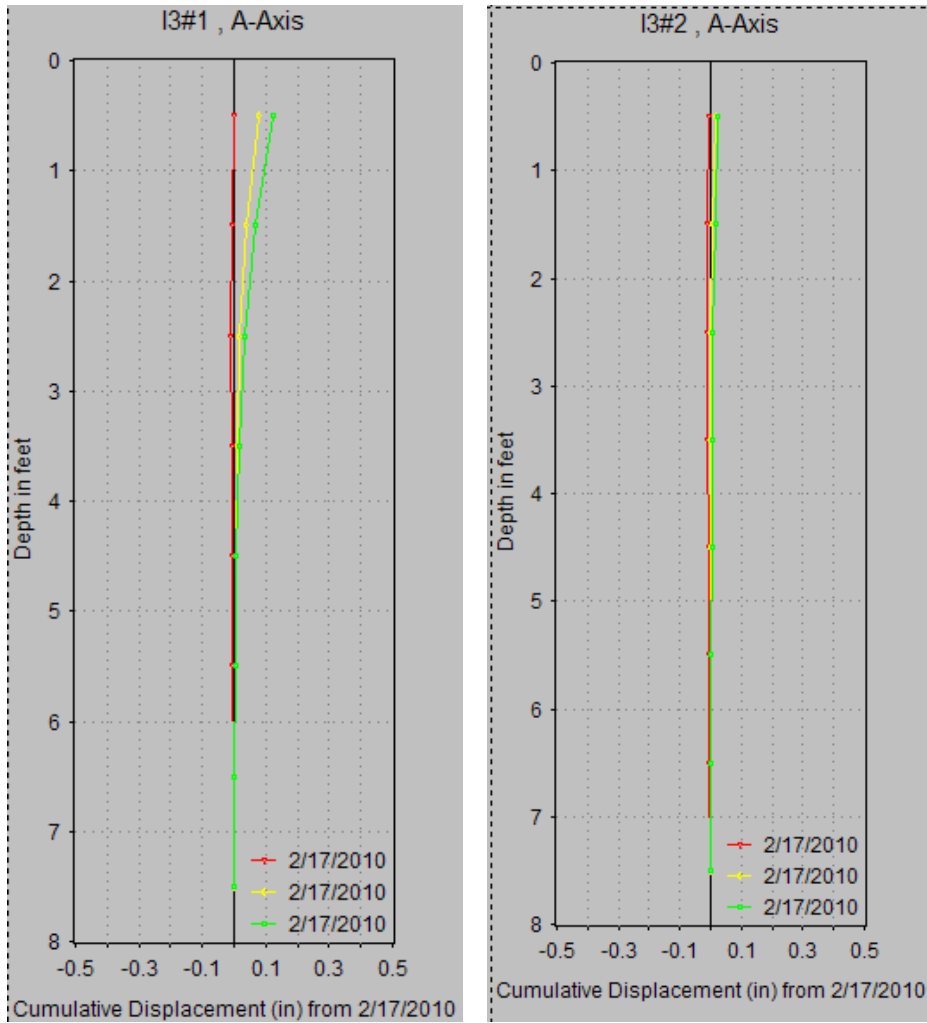


**Figure G.16. Displacement Data of Surrounding Soil of Test Shaft(1 ft diameter × 14 ft depth):
Inclinometer at 2D of Test Shaft.**



(a)

(b)

Figure G.17. Displacement Data of Surrounding Soil of Test Shaft (2 ft diameter × 6 ft depth): (a) Inclinometer at 2D of Test Shaft and (b) Inclinometer at the Middle of Test Shaft and Reaction Shaft.

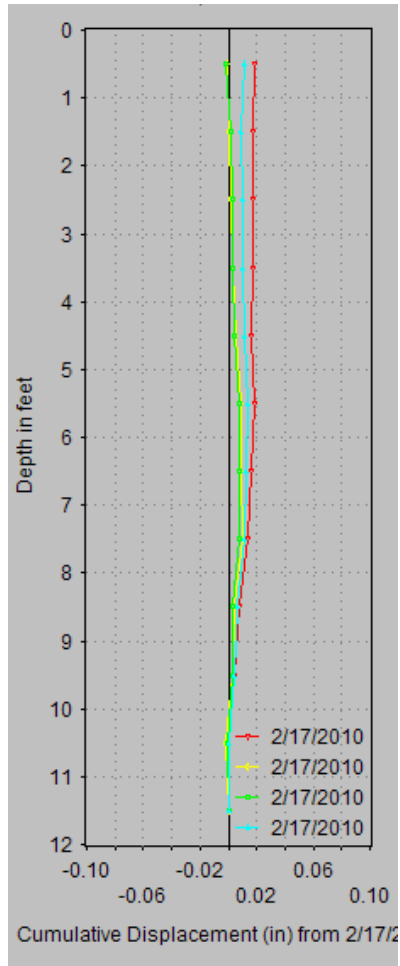


Figure G.18. Displacement Data of Surrounding Soil of Test Shaft#1 (2 ft diameter × 10 ft depth): Inclinometer at 2D of Test Shaft.

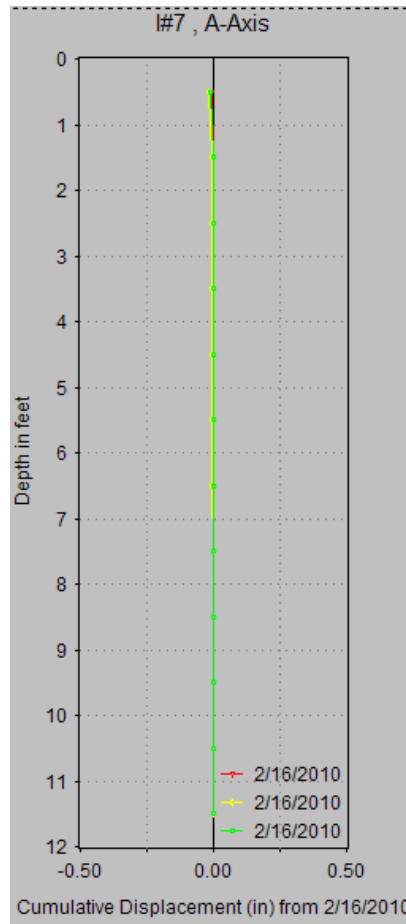
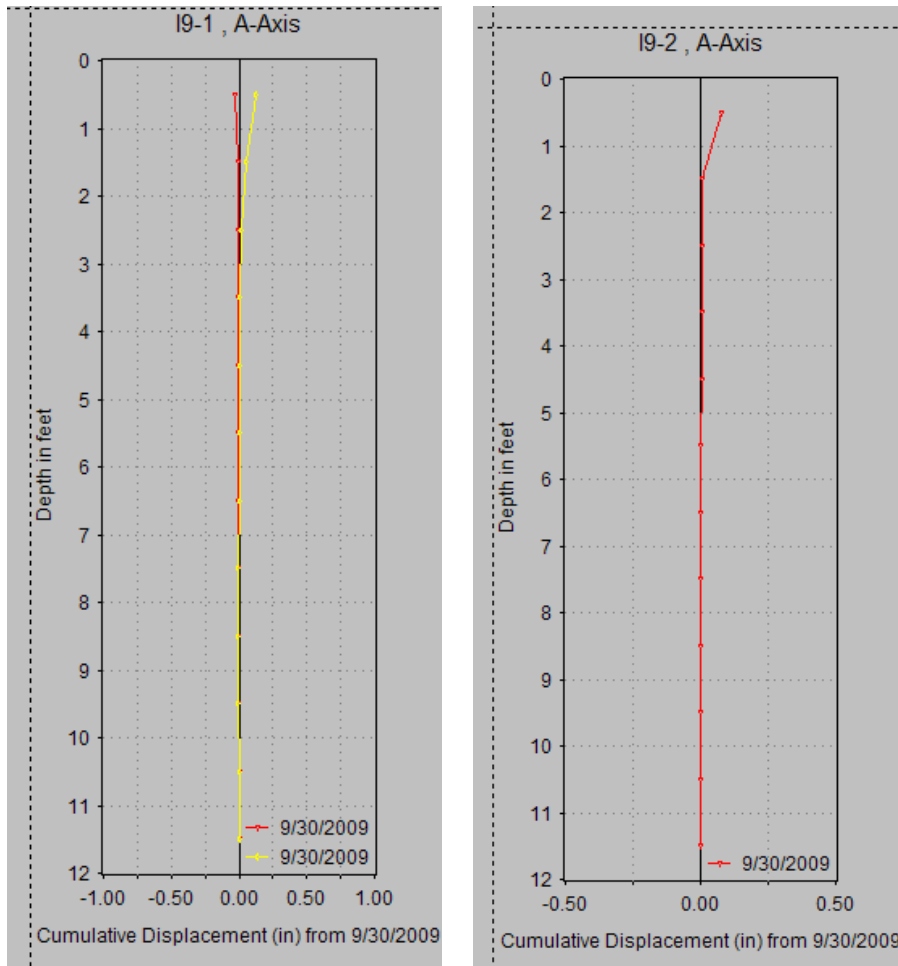


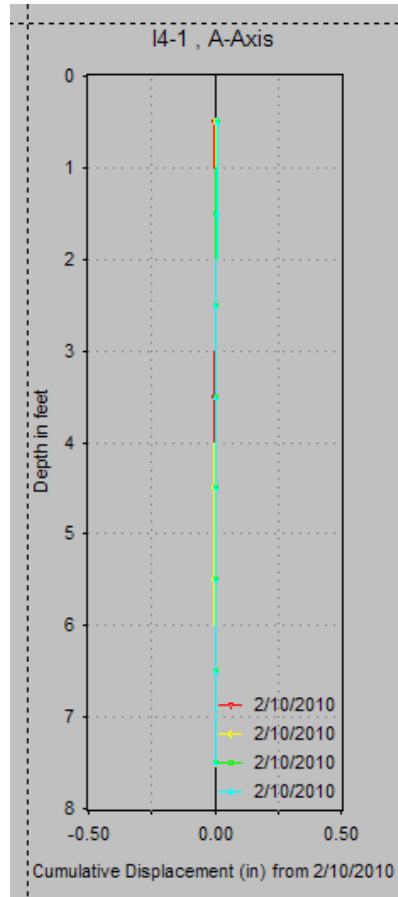
Figure G.19. Displacement Data of Surrounding Soil of Test Shaft#2 (2 ft diameter × 10 ft depth): Inclinator at the Middle of Test Shaft and Reaction Shaft.



(a)

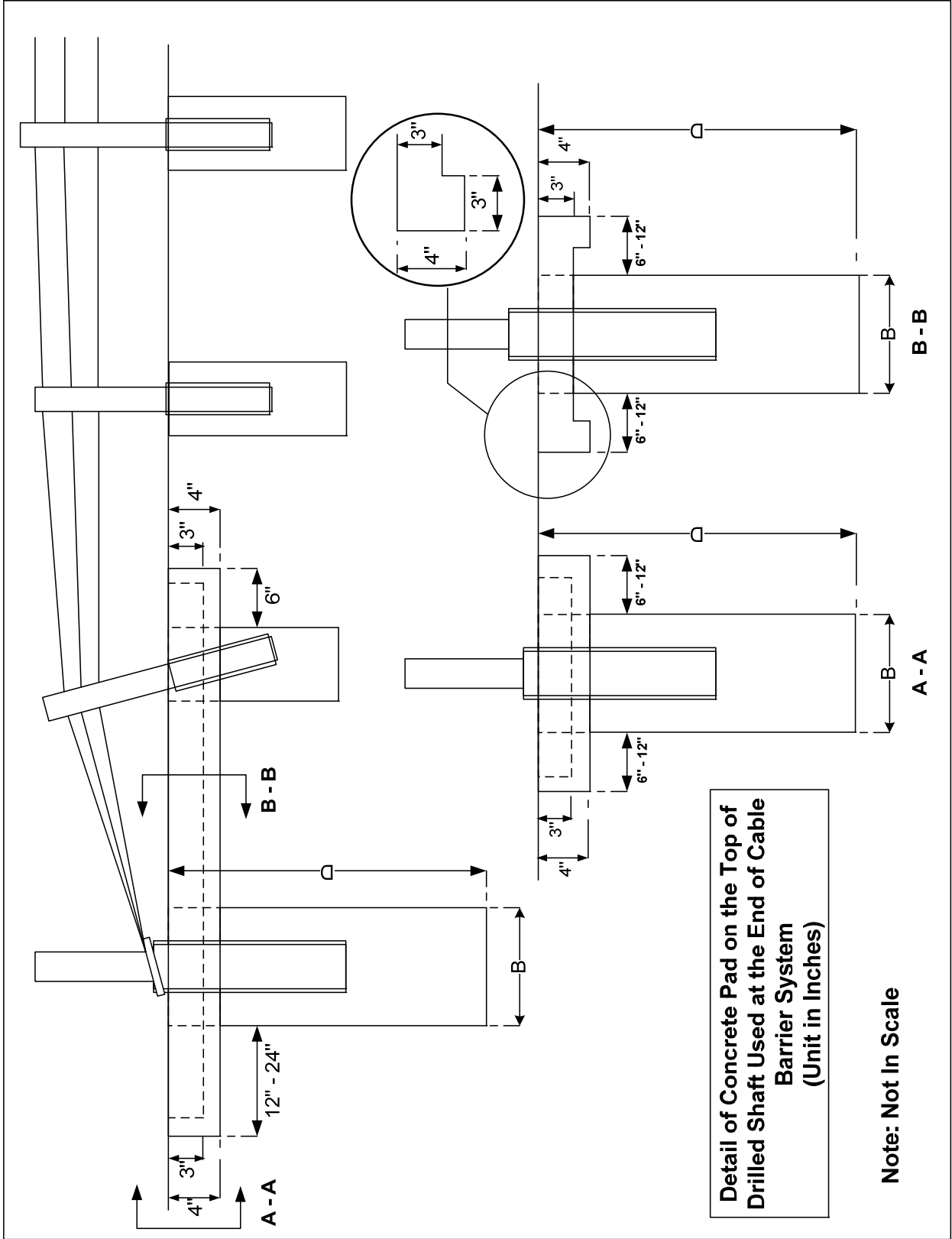
(b)

Figure G.20. Displacement Data of Surrounding Soil of Test Shaft (2 ft diameter × 14 ft depth): (a) Inclinometer at 2D of Test Shaft and (b) Inclinometer at the Middle of Test Shaft and Reaction Shaft.



**Figure G.21. Displacement Data of Surrounding Soil of Test Shaft (3 ft diameter × 6 ft depth):
Inclinometer at the Middle of Test Shaft and Reaction Shaft.**

**APPENDIX H: DETAIL OF RECOMMENDATION FOR CONCRETE PAD
USED ON TOP OF DRILLED SHAFTS AT THE END OF CABLE
BARRIER SYSTEMS**



Detail of Concrete Pad on the Top of Drilled Shaft Used at the End of Cable Barrier System (Unit in Inches)

Note: Not In Scale

